12-2014

Integration of Energy Storage into a Future Energy System with a High Penetration of Distributed Photovoltaic Generation

Arthur K. Barnes
University of Arkansas, Fayetteville

Integration of Energy Storage into a Future Energy System with a High Penetration of Distributed Photovoltaic Generation

Integration of Energy Storage into a Future Energy System with a High Penetration of Distributed Photovoltaic Generation

A dissertation submitted in partial fulfillment
of the requirements for the degree of
Doctor of Philosophy in Electrical Engineering

by

Arthur Barnes
University of Florida
Master of Science in Electrical Engineering, 2007
University of Colorado
Bachelor of Science in Electrical and Computer Engineering, 2003

December 2014
University of Arkansas

This dissertation is approved for recommendation to the Graduate Council.

_____
Dr. Juan Carlos Balda
Dissertation Director

_____
Dr. Simon Ang
Committee Member

_____
Dr. Christophe Bobda
Committee Member

_____
Dr. H. Alan Mantooth
Committee Member:

_____
Dr. Roy A. McCann
Committee Member

ABSTRACT

Energy storage units (ESU) are increasingly used in electrical distribution systems because they can perform many functions compared with traditional equipment. These include peak shaving, voltage regulation, frequency regulation, provision of spinning reserve, and aiding integration of renewable generation by mitigating the effects of intermittency.

As is the case with other equipment on electric distribution systems, it is necessary to follow appropriate methodologies in order to ensure that ESU are installed in a cost-effective manner and their benefits are realized. However, the necessary methodologies for integration of ESU have not kept pace with developments in both ESU and distribution systems. This work develops methodologies to integrate ESU into distribution systems by selecting the necessary storage technologies, energy capacities, power ratings, converter topologies, control strategies, and design lifetimes of ESU. In doing so, the impact of new technologies and issues such as volt-VAR optimization (VVO), intermittency of photovoltaic (PV) inverters, and the "smart" PV inverter proposed by EPRI are considered.

The salient contributions of this dissertation follow. A unified methodology is developed for storage technology selection, storage capacity selection, and scheduling of an ESU used for energy arbitrage. The methodology is applied to make technology recommendations and to reveal that there exists a cost-optimal design lifetime for such an ESU. A methodology is developed for capacity selection of an ESU providing both energy arbitrage and ancillary services under a stochastic pricing structure. The ESU designed is evaluated using ridge regression for price forecasting; Ridge regression applied to overcome numerical stability and overfitting issues associated with the large number of highly correlated predictors. Heuristics are developed to speed convergence of simulated annealing for placement of distributed ESU. Scaling and clustering methods are also applied to reduce computation time for placement of

ESU (or any other shunt-connected device) on a distribution system. A probabilistic model for cloud-induced photovoltaic (PV) intermittency of a single PV installation is developed and applied to the design of ESU.

ACKNOWLEDGMENTS

I would first like to thank my wife Diana for her patience, understanding, and not asking when I would graduate too many times. I would next like to thank my Advisor Juan Balda for his drive, motivation and passion for the field. Next, I would like to thank my friends and coworkers Andres Escobar, Luciano Garcia, Eliana Mérida Fernandez, Jonathan Hayes, and Corris Stewart. I would also like to thank my parents for their dedication and earnestness, and my sister Becky for her guidance and support. I would also like to thank the members of the GRAPES industry advisory board, particularly Pat Bourne, Mark Mobley and Mike Russ.

DEDICATION

This dissertation is dedicated to the good, hard-working people of the State of Arkansas, without whose support the University of Arkansas would not exist.

TABLE OF CONTENTS

CHRONOLOGICAL LIST OF PAPERS

[1] © 2011 IEEE. Reprinted, with permission, from A.K. Barnes, J.C. Balda, S.O. Geurin, and A. Escobar Mejía, "Optimal battery chemistry, capacity selection, charge/discharge schedule, and lifetime of energy storage under time-of-use pricing," in *IEEE PES Innovative Smart Grid Technologies Europe (ISGT-EU)*, 2011, pp. 1–7.

[2] © 2012 IEEE. Reprinted, with permission, from A.K. Barnes, J.C. Balda, A. Escobar Mejía, and S.O. Geurin, "Placement of energy storage coordinated with smart PV inverters," in *IEEE PES Innovative Smart Grid Technologies (ISGT)*, 2012, pp. 1–7.

[3] © 2012 IEEE. Reprinted, with permission, from A.K. Barnes, J.C. Balda, and C.M. Stewart, "Selection of converter topologies for distributed energy resources," in *IEEE Applied Power Electronics Conference and Exposition (APEC)*, 2012, pp. 1418–1423.

[4] © 2013 IEEE. Reprinted, with permission, from A.K. Barnes and J.C. Balda, "Sizing and economic assessment of energy storage with real-time pricing and ancillary services," in *IEEE International Symposium on Power Electronics for Distributed Generation Systems (PEDG)*, Fayetteville, AR, 2013, pp. 1–7.

[5] © 2014 IFAC. Reprinted, with permission, from A.K. Barnes, J.C. Balda, and J.K. Hayes, "Modeling PV clouding effects using a semi-Markov process with application to energy storage," in *International Federation of Automatic Control World Congress (IFAC)*, Cape Town, South Africa, 2014.

[6] © 2014 IEEE. Reprinted, with permission, from A.K. Barnes and J.C. Balda, "Placement of distributed energy storage via multidimensional scaling and clustering," in *International Conference on Renewable Energy Research and Applications (ICRERA)*, Milwaukee, WI, 2014.

[7] © 2014 IEEE. Reprinted, with permission, from A.K. Barnes, J.C. Balda, and A. Escobar Mejía, "A semi-Markov model for control of energy storage in utility grids and microgrids with PV generation," *IEEE Transactions on Sustainable Energy* (in review), August 2014.

[8] A.K. Barnes and J.C. Balda, "Value assessment of distributed energy storage via multidimensional scaling," *IEEE Transactions on Power Systems* (in review), December 2014.

CHAPTER ONE

INTRODUCTION AND CONTRIBUTIONS

I. INTRODUCTION

The United States currently depends on fossil fuels for about 67% of its electrical energy production [1]. Moreover, by the year 2040, the energy demand in the United States is expected to increase by 29% from 2012 values [2]. It is essential to reduce this over-reliance on fossil fuels in meeting this growing demand for energy. Doing so will avoid the detrimental environmental impacts of greenhouse gases and/or other pollutants, and reduce the dependence on foreign energy supplies. Thus, moving power generation away from fossil fuels and towards clean renewable energy sources, primarily solar and wind electric power, will greatly decelerate the adverse environmental impacts of fossil-fuel generation, while still meeting the increasing energy demand of our technology-driven society. The issues caused by proliferation of solar and wind energy sources are compounded by the projected retirements of coal and nuclear bulk power plants, which together currently make up 58% of US electrical energy production, as illustrated in Fig. 1 [1], [2].

In conjunction with adding more renewable energy sources, electric power generation and delivery can be improved further by using the electric grid more efficiently to reduce energy wasted in existing generation, transmission and distribution systems [3], and if possible, to minimize the need for adding more central power stations burning fossil fuels. The traditional power system is giving way to future energy systems as a result of this optimization. This system is characterized by large-scale bulk generation, unidirectional power flows, and sparsely distributed control. By contrast, future energy systems are characterized by distributed

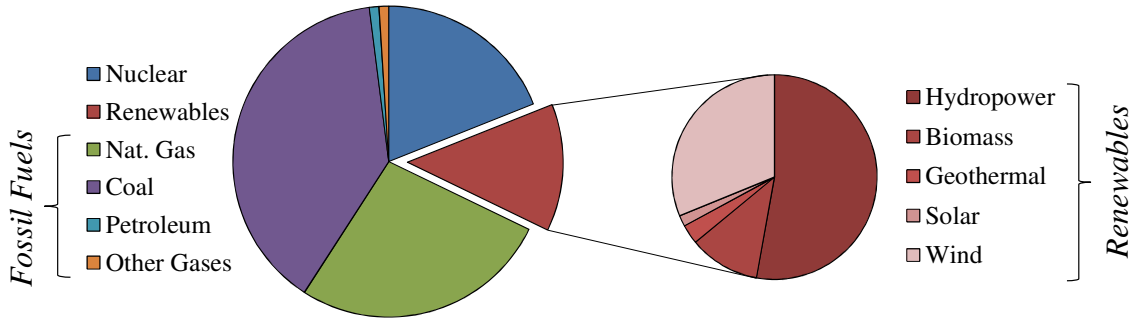

Fig. 1. Comparison of US primary electrical energy sources by type [1].

generation, bidirectional power flows, and a high number of networked, dispersed control/sensing points. It is envisioned that future energy systems will take an integrated approach to both reduce energy consumption and improve reliability, while empowering consumers to be active participants in the grid, rather than passive users of energy. This integrated approach depends on a number of enabling technologies, including combined heat-and-power, distributed generation, solar photovoltaic (PV) generation, wind generation, energy storage units (ESU), microgrids, conservation voltage reduction (CVR) and "smart" grid communications as illustrated in Fig. 2. This dissertation focuses on ESU by developing ologyologies to integrate them into future energy systems in a cost-effective manner, and to analyze their benefits. The remainder of the Section will address four technology spaces where advances are important to optimize future energy systems. Section I.A elaborates on the benefits of future energy systems. Sections I.B–I.D discuss the roles of microgrids, CVR, and ESU in future energy systems, respectively. Section I.E summarizes the issues inherent in allocating ESU into future energy systems. Last, Section I.F reviews existing software packages for distribution system analysis and their relevance to the ESU allocation problem.

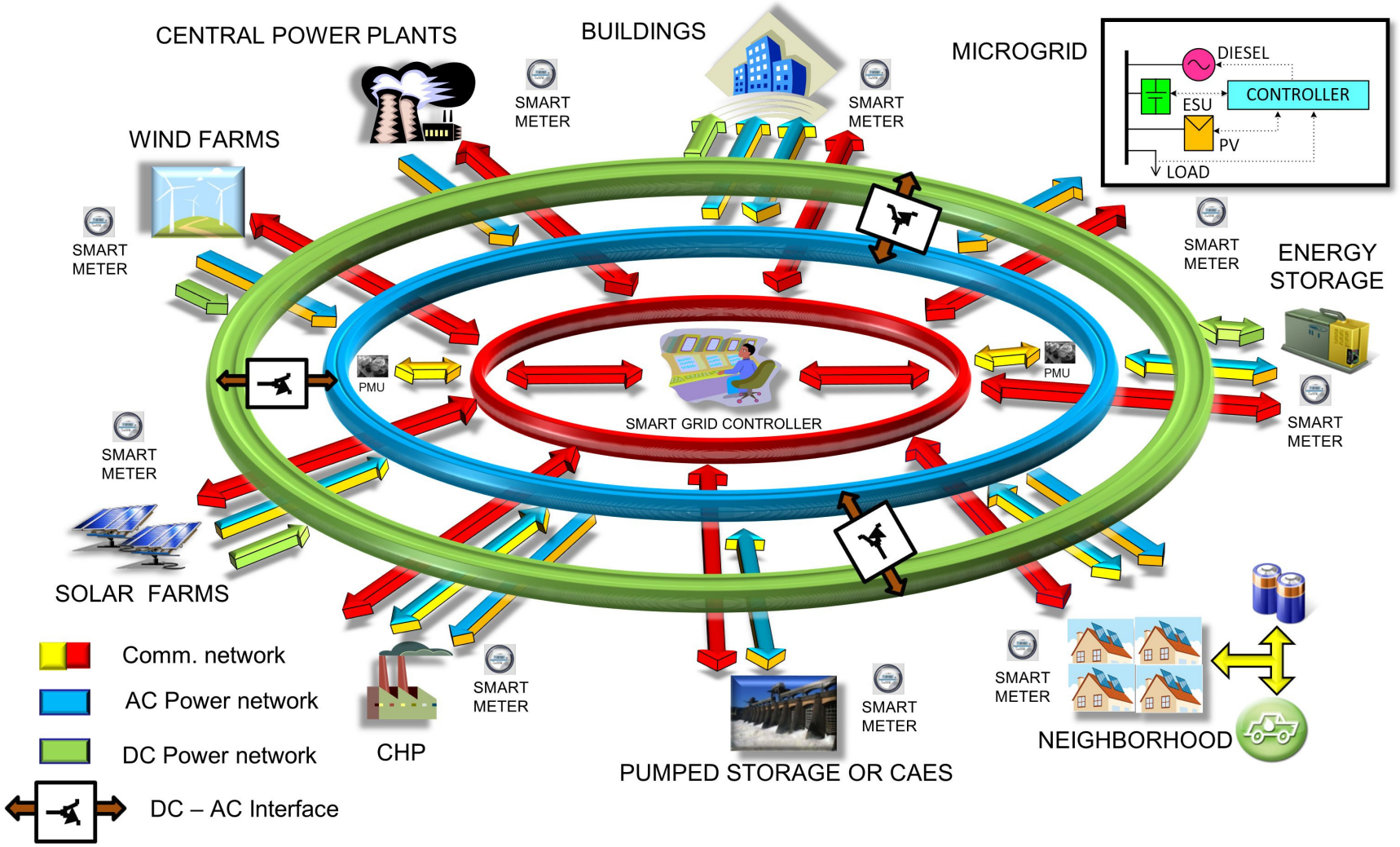

Fig. 2. Conceptual diagram of a future energy system, highlighting the bidirectional flow of information and power, used with permission of Andrés Escobar Mejía and Juan Carlos Balda [4].

I.A. Operation and Benefits of Future Energy Systems

In future energy systems, it is envisioned that a regional or area dispatcher coordinates the operation of several distribution systems in response to a wide area network optimization. On the policy side, flexibility is introduced by providing regulatory incentives such as time-of-use and peak load shaving rebates [5], [6]. Both future distribution systems and the so-called microgrids served by on those distribution systems will be operated in an optimal manner in response to (price) signals emanating from a regional transmission operator (RTO) [7]. These incentives are made possible by "smart" meters and "smart" grid communications, as illustrated in Fig. 3.

This collection of physical equipment (distributed generation, ESU, sensors, etc.), communication systems, and regulatory structures produces tangible benefits for both consumers and utilities. These include: decreasing the energy needed from (traditional) generation plants, reducing transmission and distribution power losses, recovering waste heat, and improving

Fig. 3. A wireless mesh networked energy monitoring unit displays current pricing information for a residential consumer under the Southern California Edison electrical system. "Traffic light" style indicators on the side indicate the current pricing tier.

reliability indices.

I.B. The Role of Microgrids in Future Energy Systems

One of the enabling technologies, the microgrid, deserves special mention for its promise to transform the operation of the electrical grid. Microgrids are standalone electrical grids or portions of a larger utility grid that can operate in a self-sustaining islanded mode if necessary. Microgrids typically include an aggregate of enabling technologies: local generation, ESU, and controllable loads with coordinated control, as depicted in Fig. 4 [8]. Microgrids that interact with a larger grid use the local generation, ESU and controllable loads to appear as a single generator or controllable load. While connected, they can provide services to the larger grid such as energy arbitrage, demand management, or reactive power compensation. These capabilities provide for reduced power consumption from the larger grid while improving reliability and power quality to the customers within the microgrid. As examples, a college campus or military base could benefit from microgrids. For a microgrid with intermittent renewable generation such as PV, it is necessary to make the intermittent generation dispatchable by coordinating it with the ESU and local fossil-fuel generation [9]; this is a requirement for a standalone microgrid to establish power balance. It is also necessary to make intermittent

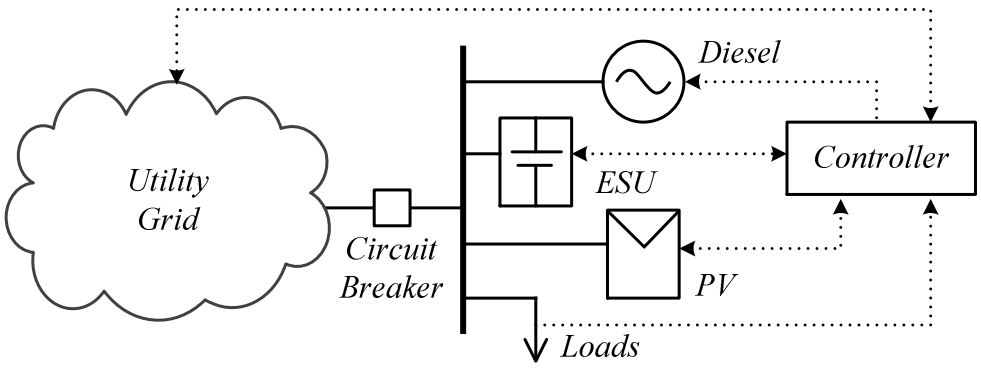

Fig. 4. Simplified schematic representation of a microgrid.

generation dispatchable for a microgrid reducing demand from (or supplying power to) a larger grid. This dispatchability requirement ensures that the microgrid can provide scheduled load reduction (or supplied power). The requirement holds true not only for PV installations within microgrids, but also for large PV installations that are permanently grid connected, either utility- or customer-owned.

I.C. The Role of CVR in Future Energy Systems

CVR is another important enabling technology in future energy systems. It is a useful tool for demand management that does not require the addition of a communications infrastructure or controllable loads, and is a key component of volt-VAR optimization (VVO), which is discussed later in Section II. Instead of employing controllable loads, it exploits tap changers on substation transformers and in-line voltage regulators to reduce the overall voltage on a distribution system. On the average, customer loads on a distribution system will draw less power if the line voltage is reduced. Currently this still applies, even with power electronic loads. For example, a typical compact fluorescent lamp (CFL) will consume less power as line voltage decreases [10]. This is because low-cost power electronic converters use a diode front-end without power factor correction (PFC), so the dc-link voltage is tied to the line voltage. The typical CFL will apply a square-wave ac voltage across the tube with a half-bridge inverter, and is unable to regulate current [11]. However, it is likely that the anticipated proliferation of PFC front-ends will result in constant-power and nearly unity power factor operation of a majority of loads; this is illustrated by the adoption of PFC in LED lighting technology [12]. Despite this trend, it will probably take years for the necessary cost reductions to take place, so CVR will continue to provide value in the near future. For a typical distribution system, a 1V drop below nominal will decrease the load by about 1%, with approximately a 3% maximum reduction in total load

possible [14]. The linearized relationship $\Delta P_{load}/\Delta|V_{load}|$ between the change in load power and change in load voltage magnitude is referred to as the CVR factor, which will be used later in this dissertation. The disadvantage of CVR is that a flatter load profile is required because the voltage drop on a feeder increases at peak load, when CVR is likely to be applied. This makes the feeder more susceptible to under-voltage conditions, such as when PV output power drops.

I.D. The Role of ESU in Future Energy Systems

ESU bring a host of benefits to future energy systems, such as load shifting, voltage regulation, and frequency regulation [13]. These benefits can be categorized in two major groups: reducing cost/maximizing profit, and improving power quality/security. The individual applications are summarized below.

Economic applications of ESU include participating on energy and ancillary service spot markets. The act of an ESU participating in an energy market or responding to a time-varying electricity price structure is referred to as energy arbitrage. An ESU performing energy arbitrage will charge (purchase power) during periods when the cost of energy is low and discharge (sell power) during periods when the cost is high [13], [14]. There are two mechanisms that result in high electricity prices, periods of high demand, and unexpected shortage of supply. Using ESU to supply power during periods of high demand is related to load leveling [15]–[17]; this displaces peaking generation. Because peaking generation operates for a fraction the time that baseload generation does, it is economic to construct peaking generation with low initial cost, such as single-cycle gas turbines. However, the demands of lower construction cost and also the higher ramp-rate requirements of peaking generation mean that by nature it is less efficient. Both arbitrage and load-leveling are energy-constrained and require the ESU to be sized to provide hours of discharge duration. ESU can also participate in ancillary service markets, either

spinning reserve, frequency regulation, or reactive power [18], [19]. Other applications which lead to economic benefits include avoidance of transmission congestion costs, deferring upgrades, and reducing distribution system losses [20]–[22].

Within the context of microgrids, ESU provide the ability to perform unit dispatch more efficiently. Reciprocating engines will consume a fixed amount of fuel even when load is negligible [9]. Additionally, such engines operating at low load (and operating temperature) can suffer carbon build-up within the engine [23]. ESU allow the microgrid to operate more efficiently at low loads by using charge/discharge scheduling [24]. A generator under charge/discharge scheduling operates as close to full power as possible (its most efficient operating condition) for a fraction of the time to both supply load and charge the ESU. The remaining fraction of the time, the ESU and any renewable generation will supply loads.

Power quality/security applications of ESU on distribution systems include providing uninterruptible power supply (UPS) functionality, compensating for voltage sags, improving the feeder voltage profile, providing black start capability, compensating for voltage flicker, and relieving overloaded network components [25]–[27]. Within the context of microgrids, the ESU provide power balance during transient events. These events include the transition to islanding mode, or sudden changes in power during operation in islanded mode (for example, when a motor load starts or local PV generation is suddenly clouded). This is critical because dispatchable generation in microgrids may have slow response times (as is the case with microturbines and fuel cells) or may require several seconds to turn on.

Last, ESU are useful for integrating intermittent renewable generation such as PV or wind into the electrical grid. For integration of PV, ESU provide a number of functions. These include

reducing voltage and frequency fluctuations caused by cloud-induced intermittency of PV output power, and improving dispatchability by reducing forecast errors [28]–[31].

I.E. Integration of ESU into Future Energy Systems

Integration of ESU into a distribution system is achieved by selecting the storage capacities, the storage technologies to use, the locations of each ESU, the power rating of the individual ESU, the power electronic interface (PEI) topology of the ESU, and the scheme to coordinate the ESU with other resources, such as PV [32]. This activity is made more challenging because the component tasks are interdependent. For example, the best storage technology depends on the charge/discharge profile [20].

Many different storage technologies are available for delivering power for a few seconds to several hours. The most common forms of storage technologies are batteries, compressed-air, electric double-layer capacitors, energy storage, pumped-hydro energy storage, vanadium redox flow batteries, and flywheels [33]. Examples of battery technologies are lithium-ion (Li-ion) or nickel-metal hydride (NiMH), though several other technologies exist [34]. The battery chemical compositions considered are presented in Fig. 5. Prices and figures-of-merit are based on 2011 values [35].

Of particular interest among these other technologies are electric double-layer capacitors, commonly known as ultracapacitors (UC). UC can be coordinated with batteries for providing frequency regulation and integration of intermittent renewable generation, as illustrated in Fig. 6. The methodology used for storage capacity selection must be able to deliver recommendations about which storage technology or combination of technologies to use.

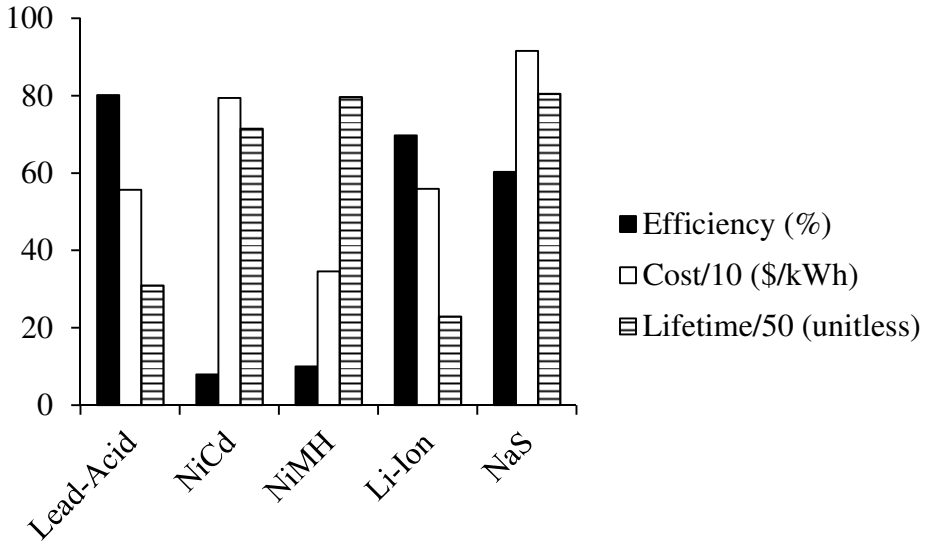

Fig. 5. Comparison of the merits of 5 common battery chemical compositions.

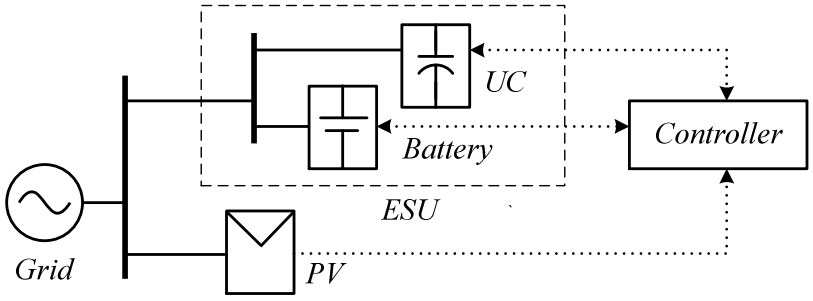

Fig. 6. Example of a hybrid battery-UC ESU applied to smooth a PV installation.

Another important consideration is that ESU will interact with other pieces of equipment and methodologies for achieving either power balance, load reduction or voltage regulation. These include demand management through controllable customer loads or through VVO, and distributed energy resources (DER) such as PV inverters. To control the ESU efficiently in conjunction with PV inverters it is necessary to model the power variability inherent to PV generation.

However, the “smart” PV inverter can mitigate some of the effects of this variability by either curtailing power output or absorbing/injecting reactive power to regulate voltage. Current grid codes do not permit DER to provide voltage regulation, but there is considerable motivation to allow this [36]–[38]. ESU must be coordinated with these DER, and the coordination must be considered when determining placement, power ratings and control of ESU. These resources will be supervised through a network as components of microgrids or future energy systems as mentioned above. Therefore, individual components will not operate independently and the predicted operation of the ESU and other equipment must be considered when determining placement and power ratings.

A PEI is necessary in order to interface the ESU storage to the electric grid. Several different topologies are available [3], [39]–[42]. The best PEI topology in terms of overall efficiency depends on the operating conditions of the storage in terms of net power flow and input/output voltages. This work demonstrates the selection of the best topologies for both battery- and UC-based ESU, which is considered separately from the storage capacity and technology selection problem. The selected topology for battery-based ESU is illustrated in Fig. 7.

I.F. Tools for Integration of ESU

Software tools are used by utility planners to determine shunt capacitor bank sizes and locations. These tools establish an economic tradeoff between distribution and transmission system losses versus the installation costs of capacitor banks. Commonly used commercial software applications include Cyme, Windmil, Synergee, and Distribution Engineering Workstation (DEW) [43]–[46]. In addition to models for shunt capacitors, commercial applications typically include or have add-on tools available for performing capacitor placement automatically.

Open-source tools are also available, notably Gridlab-D from Pacific Northwest National Laboratories (PNNL) and OpenDSS from the Electric Power Research Institute (EPRI). These have more flexible analysis capabilities, including quasi-dynamic load flow, harmonic load flow, openly documented model formats, support for interprocess communication, scripting, and the ability to create custom equipment types [47], [48].

However, support for ESU in both classes of software is in its infancy. Some include models for ESU but with limited control sophistication, restricted to either following a pre-set schedule, maintaining power flow at a setpoint, or charging/discharging when a measured quantity exceeds a threshold [46], [49], [50]. Others include a battery model, but rely on the user to generate control signals [51]. None include tools for placement or power rating selection. The absence of tools exists because the required methodologies are still in their developmental stages. These tools must be developed to aid the efficient use of ESU. A number of issues are unique to ESU, and must be taken into account when designing such tools.

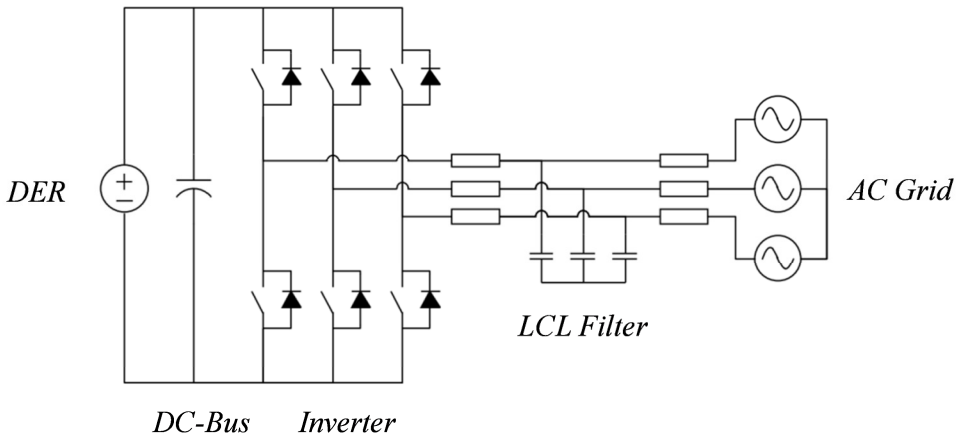

Fig. 7. A single-stage PEI (inverter with no intermediate dc-dc converter) connecting a DER to the utility grid.

II. MAIN MOTIVATION FOR THIS DISSERTATION

The main motivation for this dissertation is to solve three main problems related to integration of ESU into future energy systems:

1. ESU storage capacity, storage technology selection, and scheduling,
2. placement, power rating selection, and coordination of individual ESU with PV inverters, and
3. PEI topology selection.

In solving these problems effectively, several important deficiencies in the existing methodologies for design and analysis of ESU must be addressed. First, at the time the relevant work was performed, there was a dearth of methodologies for storage technology selection of ESU or on how to coordinate a combination of different storage technologies for utility applications [35].

Second, the state-of-the-art of DER placement had not kept pace with technical innovations currently making their way into distribution systems. The first of these innovations is the concept of VVO, in which equipment for voltage regulation and reactive power compensation on a distribution system are coordinated to reduce power consumption. The concept of VVO won success with utilities, allowing them to reduce power consumption with their existing equipment. Both major utility equipment manufacturers and upstarts have responded with their own systems, including Cooper Power Systems, PCS Utilidata, ABB, and S&C [52]. The second of these innovations is the "smart" inverter, proposed by EPRI [37], [53]. Such inverters include sensing, control, and communication functionality. These capabilities allow inverters to eliminate PV-induced overvoltage by curtailing real power injection, or by absorbing reactive power. These inverters can also inject reactive power for the purposes of up-regulating voltage or line loss

reduction. Rather than being a problem for distribution engineers to mitigate, PV could be an asset that can be exploited within the context of a VVO framework [54]. At the time the relevant work was completed, the existing state-of-the art in DER and ESU placement addressed distribution systems operating with traditional equipment and control methodologies [16]-[18].

A third problem is the choice of the PEI impacts the overall efficiency of ESU. Although the necessary analysis was carried out in previous work [55], no "best-practice" topology recommendations existed for grid-connected ESU that considered typical battery/UC configurations, grid voltages, and operating conditions (battery/UC voltages and currents).

Last, there is a deficiency in work characterizing and modeling intermittency of PV generation, particularly when compared to wind generation. This characterization and modeling is necessary for forecasting, evaluating any deleterious effects on utility equipment, designing ESU to mitigate such effects, and scheduling PV with a combination of other generation sources, ESU, dispatchable loads, and critical loads [56].

III. CASE STUDIES FOR INTEGRATING ESU

The research presented here focuses primarily on distribution systems with a high penetration of DER, notably PV generation, that make use of ESU to reduce the RTO's need for scheduling inefficient peaking generation, as well as to reduce the amount of excess generation capacity needed for load following and reserve (spinning) capacity [19]. It is assumed the distribution systems are owned by single, large commercial or institutional customers participating in a real-time pricing program, but are still intended to be representative of a range of radial electrical systems [12]. The primary purpose of the ESU is to perform energy arbitrage in response to the cost of electricity.

However, the ESU could also be used for ancillary services such as spinning reserve, frequency regulation, voltage regulation, and reactive power compensation. The last two capabilities are assisted with the ability of the PV inverters to provide reactive power. Voltage regulation is particularly helpful if CVR is also used for demand management.

Several distribution systems are selected in order to assess the efficacy of the methodologies proposed across a range of representative systems. These include:

1. a 17-bus radial system from rural Italy [57],
2. an 11-bus radial system from rural Arkansas [58],
3. an 18-bus radial system [32], [59],
4. a 41-bus radial system from southern California [54], and
5. a large radial system with 1699 customers [60].

Note that not all proposed methodologies are tested across all systems. For example, the last distribution system listed serves to validate the scalability of the methodologies on a large system model.

IV. SUMMARY OF WORK PERFORMED

The work performed in this dissertation was divided into four main areas: (1) calculating storage capacity and scheduling of an individual ESU connected to the grid, (2) determining placement and power ratings of multiple ESU on a distribution system, (3) topology selection for the PEI connecting an ESU to the grid, and (4) modeling of PV clouding applied to the design and control of ESU. The remainder of this section describes these areas in more detail.

IV.A. Storage Capacity Selection and Scheduling of ESU

For the case of storage capacity selection and scheduling of individual ESU, the case of a customer-owned ESU operating under a TOU pricing model is considered. Both two-level and three-level TOU pricing models are analyzed [35]. Multiple battery chemical compositions are studied: lead-acid, NiCd, NiMH, Li-ion and NaS. The cycle life of the battery is taken into account as a constraint. The ESU is evaluated over a range of possible lifetimes, and the optimal size, schedule, and mixture of battery technologies are calculated.

To reflect projected changes in how electrical energy is billed, the analysis is extended to the case of an ESU that operates under a pricing structure linked to the day-ahead electricity market. The ESU provides not only energy, but also ancillary services in the form of regulation and spinning reserve. This scenario could also correspond to an ESU operating as a price taker on the day-ahead electricity market. In the analysis, it is assumed that a Li-ion battery is selected, based on the results of previous work [33]. The battery is sized using linear programming and a set of historical pricing data [61]. Because the pricing structure is not deterministic, it is required to validate that the battery design meets lifetime requirements. Additionally, the validation verifies if the actual profitability matches the projected profitability using perfect information. To perform validation, it is necessary to design a forecaster for the price of providing energy, regulation, and spinning reserve services. A linear forecaster with ridge regression is selected for this purpose [62], [63]. To account for lifetime issues, the conditions under which the optimal scheduling will charge and discharge are analyzed. The lifetime constraints are added indirectly to the validation scheduler for the ESU by including upper/lower thresholds for charging/discharging the ESU, respectively. The predicted prices are then used to schedule the

ESU over a one-week lookahead interval over every hour. This is done over four three-week periods during each season of one year to calculate the actual profitability of the ESU.

IV.B. Placement and Power Rating of ESU

For the case of placement and power rating selection of multiple ESU on a distribution system, the economic value of placing the ESU is determined along with the solution for ESU allocation. The problem is formulated in terms of a positive-sequence representation of a radial distribution system in which customers on the system are billed according to a three-level time-of-use (TOU) pricing structure that varies depending on season. The feeder also includes "smart" PV inverters, which are able to inject reactive power under either local or coordinated control to reduce losses and regulate voltage [37]. The allocation of these inverters is included as part of the ESU allocation problem. The allocation problem considers a 20-year design lifetime, balance-of-system costs, maintenance costs, battery costs, and the cost of electricity consumed.

Placement and power rating selections are performed using simulated annealing to select the individual buses for placement [58], [64]. An inner optimal power flow (OPF) solver calculates the necessary power ratings of the individual ESU [65]. For the placement objective, only the peak loading of the feeder is considered. The placement is validated by calculating the optimal economic dispatch of the ESU considering only the TOU pricing structure. It is then verified that under all loading conditions, the ESU can both charge and discharge at the locations specified without violating voltage constraints.

The analysis with simulated annealing revealed that the OPF selects candidate buses for ESU placement in sets of discrete, well-spaced groups. Within groups, the candidate locations tend to be placed at adjacent or nearly adjacent buses. This observation motivated a follow-up analysis which developed a heuristic methodology to speed placement of ESU and "smart" PV [66]. In

the follow-up analysis, ESU candidate locations are also selected via an OPF under peak load conditions. The actual ESU locations are then selected with a clustering algorithm that groups nearby candidate locations into a single ESU. To allow the use of clustering, multidimensional scaling (MDS) is employed to convert the matrix of impedances between different buses into points in a space [67]. The performance of the methodology is compared against an existing genetic algorithm (GA) approach, both in terms of speed of computation and quality of the solution [32]. To validate the final ESU placement, a set of worst-case feeder load and ESU charge/discharge conditions were selected, rather than a daily charge/discharge profile. Based on the worst-case conditions, the maximum flicker from the ESU providing frequency regulation is calculated. Additionally, it is verified that the ESU will not introduce steady-state over- or under-voltage conditions.

Based on the verification that "smart" PV inverters proved helpful in regulating voltage, an additional follow-up study evaluates the benefit of ESU also providing reactive power specifically in terms of power savings. The key question to be answered is whether an ESU with a practical (lossy) PEI can still provide advantages in terms of reducing losses and energy consumption on a distribution system, particularly one that already has an economic deployment of shunt capacitor banks. Also of interest is whether the CVR factor will impact the power savings gained by ESU deployment. Based on this focus, the study omits the "smart" PV inverters and economic analysis, instead focusing exclusively on the use of ESU for reducing feeder energy consumption. Again, an OPF is used to select candidate locations for ESU placement, but an inverter loss model is added [68]. As with the previous study, with the ESU allocated, the ability of the ESU to operate under worst-case loading and charge/discharge conditions is validated. Additionally, the flicker introduced by the ESU providing regulation

services is quantified. In this analysis, two new feeders are studied. Moreover, the impacts of inverter efficiency and CVR factor on feeder power reduction are analyzed.

IV.C. PEI Topology Selection

The study of PEI topology selection for an ESU is motivated by the observation that the most efficient topology for interfacing DER to the grid depends on the operating conditions. The analysis only considers the single- and double stage inverter topologies, as it was observed that practical battery and UC string voltages are on the order of 300 V to 1 kV, negating the motivation for multilevel topologies that provide voltage sharing capability [56]. Being able to draw power from individual cells (as is the case with cascade topologies) is not deemed necessary, as the UPS industry demonstrates that cell balancing can be accomplished with good battery lifetimes by periodic overcharging [70]. The key observation, however, is that under certain design parameters for the same DER, either a single-stage or double-stage topology can be more efficient. Therefore, the preferred topology could depend on the distribution of operating conditions over time. The existing analytical models of inverter and boost converter losses are employed to compare their overall performance across a parameter sweep in terms of input voltage / power [55].

IV.D. Modeling of Cloud-Induced PV Intermittency

The last area of work applies probabilistic modeling of cloud-induced PV intermittency to the design and control of ESU. The methodology is applicable to large, centralized PV installations. The decision to study intermittency of centralized PV is motivated by the observation that PV intermittency at short time-scales decreases sharply with geographical separation [71], [72]. Therefore, the case of interest when addressing PV intermittency is that of

the large, centralized installations for which this methodology is applicable. To develop the PV modeling methodology, solar irradiance data is collected at a high time resolution (1s sampling period). The irradiance data is then classified in terms of clear sky or shaded conditions by the following steps. The clear sky irradiance profile is predicted with a polynomial curve fit [56]. The normalized error between the actual and predicted irradiance profiles is then clustered to classify the data. Given the classified data, the durations of clear and shaded periods are then inferred. The distributions of the clear and shaded durations provide sufficient information to characterize the intermittency of the PV. A generalized Pareto distribution is empirically shown to fit the data. In order to make use of the distributions, they are discretized and employed as hold times for a semi-Markov discrete-time random process model (SMDTRP) [73]. Several useful properties of the model are demonstrated, including the ability to generate simulated clouding data, perform short-term probabilistic forecasting, and calculate the expectation of ESU controller performance for mitigating PV intermittency. This last property is applied to the case of an ESU smoothing PV output power in order to reduce the number of operations for the tap-charger regulating voltage on the feeder that the PV serves.

A follow-on study replaces the clustering-based classification with a traditional Bayes classifier that is easier to analyze [68]. Another property of the model is demonstrated, the ability to calculate the distribution of PV power over a time interval consisting of several sample periods. An analytical expression for the cumulative distribution function (CDF) of the clear-sky state occupancy distribution is derived to do so. The CDF is then used to create a quantized five-level approximation of the distribution of PV energy in 1 hour. This approximation is employed as an input to a microgrid scheduling algorithm with dynamic programming [68], [74]. The algorithm operates in 1-hour intervals over a week, coordinating a PV inverter, diesel generator,

and battery-based ESU. The PV power can be curtailed, but the load power cannot be controlled. The dynamic programming algorithm requires that the battery state-of-charge also be quantized in six levels. To overcome this quantization issue and to ensure efficient operation of the diesel generator, the dynamic programming selects between either a load-following or cycle-charging coordination algorithm at each time step. By selecting between two coordination algorithms, the dynamic programming ensures the diesel generator operates at its most efficient loading.

V. CONTRIBUTIONS OF THIS DISSERTATION

This dissertation has the following novel contributions:

V.A. Storage Capacity Selection and Scheduling of ESU

Two methodologies were developed. The first methodology uses linear programming to select storage technologies, capacities, and charge/discharge schedule in an integrated manner when operating under a deterministic electricity pricing structure [35].

The methodology was applied to produce the following novel conclusions:

1. Under plausible pricing conditions, the Li-ion battery is most cost-effective because it has the highest efficiency of the technologies compared, allowing the ESU to produce a profit even during small differences between peak and off-peak pricing.
2. The cost of Li-ion in terms of lifetime energy throughput (measured in cumulative kWh output from the battery) is competitive with cheaper technologies such as lead-acid.
3. The overall profitability of the ESU is sensitive to the design lifetime. This is a particularly relevant observation, as there are incentives to design ESU to last 20 years [75]. The motivation for this lifetime is so that the time to failure of ESU will match that of other distribution system equipment. Unfortunately, such long design lifetimes do not

result in using the batteries in the most cost-effective manner possible. This is because a long lifetime requires oversizing the battery and/or restricting the number of times it discharges. When accounting for the time value of money, oversizing the battery is a poor choice. A lifetime on the order of 10 years is shown to be more reasonable.

The second methodology calculates battery size and profitability for a Li-ion-based ESU providing both energy arbitrage and ancillary services. The ESU operates under a dynamic pricing scheme linked to the day-ahead electricity market (though the same problem formulation could also correspond to it operating as a price-taker on a day-ahead electricity market). The lifetime limitations of the battery are included as constraints [61]. The methodology is based on linear programming for scheduling and employs forecasting to handle pricing uncertainty. It has the novel characteristic of applying ridge regression for price forecasting, which overcomes numerical issues caused by the high degree of correlation between the predictor variables. It was applied to reach the novel conclusion that the scheduling of ESU is relatively insensitive to forecasting error. This is because the most cost-effective use of the ESU is to provide frequency and regulation services throughout most of the day, and to charge during off-peak nighttime hours. During these nighttime hours, the pricing variability is lower, so it is easy to predict when to charge accurately.

V.B. Placement and Power Rating of ESU

Two methodologies were developed. The first one applies simulated annealing to place the ESU on a future distribution system with PV in order to minimize power consumption through the use of VVO/CVR [58].

The first methodology has the following novel characteristics:

1. It accounts for the projected proliferation of VVO in conjunction with “smart” PV inverters.
2. It applies heuristics to speed convergence of simulated annealing by weighting certain buses to encourage ESU placement at those buses. The weights are based on the bus voltage, real power draw, and reactive power draw.

The methodology was applied to reach the following novel conclusions:

1. The presence of “smart” PV inverters actually reduces the amount of energy storage required to decrease the voltage regulation on the feeder (necessary to perform CVR).
2. Placing the ESU to assist with CVR does not negatively impact their use for energy arbitrage, as peak feeder load and electricity prices are highly correlated.

The second methodology is a heuristic for ESU placement using MDS and clustering [66]. The methodology employs a nonlinear constrained optimization engine to solve an initial OPF in order to select candidate ESU buses.

The methodology has the following novel characteristics:

1. Buses are mapped into points on a continuous-valued space with MDS.
2. Clustering is applied to aggregate candidate buses for ESU into ESU locations

While the placement problem remains combinatorial in the new space, it can now be solved using clustering, a well-developed subset of machine learning. Highly efficient implementations of the well-known k-means algorithm exist, which can then be applied [76].

Additionally, the following novel analysis was performed:

1. It is shown that a set of points in the MDS space can accurately represent the system in terms of its connectivity and positive sequence impedances.

2. The reduction in ESU benefits resulting from clustering is quantified.

The methodology was applied to reach the following novel conclusions:

1. The heuristic significantly reduces computation time over a GA approach while producing a solution with only a small reduction in benefits.
2. The methodology quantifies the impact of the converter losses affect upon the benefits yielded by dispersing ESU across a distribution system (as opposed to placing them adjacent to the substation). With current converter efficiencies it shows that reactive power injection gained by oversizing the ESU PEI can still reduce overall feeder power consumption.
3. The methodology quantifies the effect on benefits of distributed ESU by the projected migration to constant-power power electronic loads (and the resulting decrease in CVR factor to 0). It is shown that benefits sharply decrease (but remain positive) as the CVR factor approaches 0.

V.C. PEI Topology Selection for ESU

A methodology was developed to select the PEI topology for ESU based on a typical battery configuration, operating voltage range, and operating current range. The analysis is based on existing analytical formulas for PEI losses [77]. The methodology is applied to reach the following novel conclusions: A single-stage PEI topology is the most efficient under all operating conditions for a battery-ESU, while a double-stage PEI topology is the most efficient under all operating conditions for a UC-ESU.

V.D. Modeling of Cloud-Induced PV Intermittency

A novel methodology was designed to classify measured irradiance (or PV power) data according to whether or not the sensor (or PV array) is obscured by clouds. The data produced by this classifier is applied to produce a model for cloud-induced PV intermittency. It is shown the model can be used in forecasting, simulation, controller design, and scheduling problems [56].

The methodology has the following novel characteristics:

1. It applies clustering to classify irradiance (or PV power measurements) according to whether or not the sensor (or PV array) is shaded.
2. The methodology employs a SMDTRP model whose hold times are based on a discretized general Pareto distribution to modeling PV clouding.
3. The methodology applies the SMDTRP state occupancy distribution to a microgrid scheduler based on dynamic programming. The scheduler chooses between load-following and cycle-charging operation at each stage.

The methodology was applied to reach the following novel conclusions:

1. The model is well-suited for generating simulated PV clouding data for simulation studies.
2. The model can perform short-term probabilistic forecasting without any additional sensors.
3. The model can be applied to design an optimal rule-based controller for grid equipment interacting with PV (e.g., ESU, generators, tap changers, shunt capacitors) by using it to calculate the expectation of a cost function (e.g., total battery output energy, generator fuel use, number of switching events) over a performance period.

4. The model can be used within stochastic scheduling methodologies for either grid-connected or standalone equipment (e.g., ESU, generators, dispatchable loads).

VI. ORGANIZATION OF THIS DISSERTATION

This dissertation is organized as follows: First, Chapter 2 presents the case of storage capacity and technology selection of an ESU under a deterministic, cyclical TOU pricing structure. Chapter 3 extends the methodologies of Chapter 2 to the case of a stochastic real-time pricing structure with multiple services provided by the ESU. Chapter 4 illustrates the use of randomized search for the placement of ESU on a distribution system. Chapters 5 and 6 demonstrate how heuristics are used to speed up the placement while still finding a good sub-optimal solution. Chapter 7 addresses the selection of the PEI topology. Chapters 8 and 9 study the modeling of cloud-induced PV intermittency and its application to ESU. Chapter 10 presents conclusions and recommendations for future work.

REFERENCES

[1] U.S. Energy Information Administration, "What is U.S. electricity generation by energy source?," *What is U.S. electricity generation by energy source?*, 13-Jun-2014. [Online]. Available: http://www.eia.gov/tools/faqs/faq.cfm?id=427&t=3. [Accessed: 14-Aug-2014].

[2] J.J. Conti, P.D. Holtberg, J.R. Diefenderfer, S.A. Napolitano, A.M. Schaal, J.T. Turnure, and L.D. Westfall, "Annual energy outlook 2014 with projections to 2040," U.S. Energy Information Administration, Washington DC, Report DOE/EIA-0383(2014).

[3] F. Blaabjerg, Z. Chen, and S.B. Kjaer, "Power electronics as efficient interface in dispersed power generation systems," *IEEE Transactions on Power Electronics*, vol. 19, no. 5, pp. 1184–1194, September 2004.

[4] A. Escobar Mejía, "SSEES Research Group." [Online]. Available: http://energy.uark.edu/. [Accessed: 15-Aug-2014].

[5] Southern California Edison, “Residential Rate Plans.” [Online]. Available: https://www.sce.com/wps/portal/home/residential/rates/residential-plan/tou. [Accessed: 20-Sep-2014].

[6] Southern California Edison, “Save Power Days.” [Online]. Available: https://www.sce.com/wps/portal/home/residential/rebates-savings/save-power-day. [Accessed: 20-Sep-2014].

[7] F. Meng, D. Haughton, B. Chowdhury, M.L. Crow, and G.T. Heydt, “Distributed generation and storage optimal control with state estimation,” *IEEE Transactions on Smart Grid*, vol. 4, no. 4, pp. 2266–2273, December 2013.

[8] M.M.. Abdelaziz, H.E. Farag, and E.F. El-Saadany, “Optimum droop parameter settings of islanded microgrids with renewable energy resources,” *IEEE Transactions on Sustainable Energy*, vol. 5, no. 2, pp. 434–445, April 2014.

[9] L. Guo, W. Liu, B. Jiao, B. Hong, and C. Wang, “Multi-objective stochastic optimal planning method for stand-alone microgrid system,” *IET Generation, Transmission Distribution*, vol. 8, no. 7, pp. 1263–1273, July 2014.

[10] K.P. Schneider, F.K. Tuffner, J.C. Fuller, and R. Singh, “Evaluation of conservation voltage reduction (CVR) on a national level,” Pacific Northwest National Laboratory, Report PNNL-19596, 2010.

[11] C. Contenti, “Reference design IRPLCFL5E,” 14-May-2004. [Online]. Available: http://www.irf.com/technical-info/refdesigns/irplcfl5e.pdf. [Accessed: 19-Aug-2014].

[12] B. Lehman and A.J. Wilkins, “Designing to mitigate the effects of flicker in LED lighting,” *IEEE Power Electronics Magazine*, September 2014.

[13] S.O. Geurin, A.K. Barnes, and J.C. Balda, “Smart grid applications of selected energy storage technologies,” in *IEEE PES Innovative Smart Grid Technologies (ISGT)*, 2012, pp. 1–8.

[14] B.C. Flach, L.A. Barroso, and M.V.. Pereira, “Long-term optimal allocation of hydro generation for a price-maker company in a competitive market: latest developments and a stochastic dual dynamic programming approach,” *IET Generation, Transmission & Distribution*, vol. 4, no. 2, pp. 299–314, February 2010.

[15] C.H. Lo and M.D. Anderson, “Economic dispatch and optimal sizing of battery energy storage systems in utility load-leveling operations,” *IEEE Transactions on Energy Conversion*, vol. 14, no. 3, pp. 824–829, September 1999.

[16] Tsung-Ying Lee and Nanming Chen, "Optimal capacity of the battery energy storage system in a power system," *IEEE Transactions on Energy Conversion*, vol. 8, no. 4, pp. 667–673, December 1993.

[17] Yang Jin-Shyr and Chen Nanming, "Short term hydrothermal coordination using multi-pass dynamic programming," *IEEE Transactions on Power Systems*, vol. 4, no. 3, pp. 1050–1056, August 1989.

[18] H. Bludszuweit and J.A. Dominguez-Navarro, "A probabilistic method for energy storage sizing based on wind power forecast uncertainty," *IEEE Transactions on Power Systems*, vol. 26, no. 3, pp. 1651–1658, August 2011.

[19] S.J. Kazempour, M. Hosseinpour, and M.P. Moghaddam, "Self-scheduling of a joint hydro and pumped-storage plants in energy, spinning reserve and regulation markets," in *IEEE Power and Energy Society General Meeting (PES GM)*, Calgary, Canada, 2009, pp. 1–8.

[20] Rong-Ceng Leou, "An economic analysis model for the energy storage systems in a deregulated market," in *IEEE International Conference on Sustainable Energy Technologies (ICSET)*, 2008, pp. 744–749.

[21] M. Sedighizadeh, M. Fallahnejad, M.R. Alemi, M. Omidvaran, and D. Arzaghi-haris, "Optimal placement of distributed generation using combination of PSO and clonal algorithm," in *IEEE International Conference on Power and Energy (PECon)*, 2010, pp. 1–6.

[22] F. Geth, J. Tant, E. Haesen, J. Driesen, and R. Belmans, "Integration of energy storage in distribution grids," in *Power and Energy Society General Meeting (PES GM)*, pp. 1–6.

[23] GenPower Products, Inc., "Wet stacking and how to avoid it." [Online]. Available: http://genpowerproducts.com/files/Wet-Stacking-Prevention.pdf. [Accessed: 03-Sep-2014].

[24] M. Kolhe, K.M.I. Ranaweera, and A.B.S. Gunawardana, "Techno-economic optimum sizing of hybrid renewable energy system," in *Annual Conference of the IEEE Industrial Electronics Society (IECON)*, 2013, pp. 1898–1903.

[25] J. Mitra, "Reliability-based sizing of backup storage," *IEEE Transactions on Power Systems*, vol. 25, no. 2, pp. 1198–1199, May 2010.

[26] A. Oudalov, D. Chartouni, C. Ohler, and G. Linhofer, "Value analysis of battery energy storage applications in power systems," in *IEEE Power Systems Conference and Exposition (PSCE)*, 2006, pp. 2206–2211.

[27] C. Venu, Y. Riffonneau, S. Bacha, and Y. Baghzouz, "Battery storage system sizing in distribution feeders with distributed photovoltaic systems," in *IEEE PowerTech*, Bucharest, 2009, pp. 1–5.

[28] J. Garcia-Gonzalez, R.M.. de la Muela, L.M. Santos, and A.M. Gonzalez, "Stochastic joint optimization of wind generation and pumped-storage units in an electricity market," *IEEE Transactions on Power Systems*, vol. 23, no. 2, pp. 460–468, May 2008.

[29] T.K.. Brekken, A. Yokochi, A. von Jouanne, Z.Z. Yen, H.M. Hapke, and D.A. Halamay, "Optimal energy storage sizing and control for wind power applications," *IEEE Transactions on Sustainable Energy*, vol. 2, no. 1, pp. 69–77, January 2011.

[30] Y. Riffonneau, S. Bacha, F. Barruel, and S. Ploix, "Optimal power flow management for grid connected PV systems with batteries," *IEEE Transactions on Sustainable Energy*, vol. 2, no. 3, pp. 309–320, July 2011.

[31] K. Yoshimoto, T. Nanahara, and G. Koshimizu, "New control method for regulating state-of- charge of a battery in hybrid wind power/battery energy storage system," in *IEEE Power Systems Conference and Exposition (PSCE)*, 2006, pp. 1244–1251.

[32] G. Carpinelli, G. Celli, S. Mocci, F. Mottola, F. Pilo, and D. Proto, "Optimal integration of distributed energy storage devices in smart grids," *IEEE Transactions on Smart Grid*, vol. 4, no. 2, pp. 985–995, June 2013.

[33] D.W. Trowler, "Sizing community energy storage systems to reduce transformer overloading with emphasis on plug-in electric vehicle loads," M.S. Thesis, Department of Electrical Engineering, University of Arkansas, Fayetteville, AR, 2011.

[34] J. Eyer and G. Corey, "Energy storage for the electricity grid: Benefits and market potential assessment guide," Sandia National Laboratories, Tech. Rep. SAND2010-0815, 2010.

[35] A.K. Barnes, J.C. Balda, S.O. Geurin, and A. Escobar Mejía, "Optimal battery chemistry, capacity selection, charge/discharge schedule, and lifetime of energy storage under time-of-use pricing," in *IEEE PES Innovative Smart Grid Technologies Europe (ISGT-EU)*, 2011, pp. 1–7.

[36] K. Turitsyn, P. Sulc, S. Backhaus, and M. Chertkov, "Local control of reactive power by distributed photovoltaic generators," in *IEEE SmartGridComm*, 2010, pp. 79–84.

[37] J.W. Smith, W. Sunderman, R. Dugan, and B. Seal, "Smart inverter volt/var control functions for high penetration of PV on distribution systems," in *IEEE PES Power Systems Conference and Exposition (PSCE)*, 2011, pp. 1–6.

[38] S.J. Steffel, P.R. Caroselli, A.M. Dinkel, J.Q. Liu, R.N. Sackey, and N.R. Vadhar, "Integrating solar generation on the electric distribution grid," *IEEE Transactions on Smart Grid*, vol. 3, no. 2, pp. 878–886, June 2012.

[39] M. Calais, J. Myrzik, T. Spooner, and V.G. Agelidis, "Inverters for single-phase grid connected photovoltaic systems – an overview," in *IEEE Power Electronics Specialists Conference (PESC)*, 2002, vol. 4, pp. 1995–2000.

[40] H. Al-Nasseri and M.A. Redfern, "Solid-state converter topologies for interfacing dc sources with utility power systems," in *Universities Power Engineering Conference*, 2004, vol. 2, pp. 629–633.

[41] S.B. Kjaer, J.K. Pedersen, and F. Blaabjerg, "A review of single-phase grid-connected inverters for photovoltaic modules," *IEEE Transactions on Industry Applications*, vol. 41, no. 5, pp. 1292–1306, 2005.

[42] A.K. Barnes and J.C. Balda, "Implementation of a three-phase multilevel boosting inverter using switched-capacitor converter cells," in *IEEE Energy Conversion Congress and Exposition (ECCE)*, 2010, pp. 2141–2147.

[43] "CYME - CYMDIST, Distribution System Analysis." [Online]. Available: http://www.cyme.com/software/cymdist/. [Accessed: 20-Aug-2014].

[44] "Engineering and Analysis Solutions – WindMil Software." [Online]. Available: http://www.milsoft.com/utility-solutions/upgrades/milsoft-engineering-analysis-ea-windmil. [Accessed: 20-Aug-2014].

[45] "SynerGEE® Electric - GL - Power Generation." [Online]. Available: http://www.gl-group.com/en/powergeneration/SynerGEE_Electric.php. [Accessed: 20-Aug-2014].

[46] "DEW & ISM Overview." [Online]. Available: http://www.edd-us.com/ISM_Overview.html. [Accessed: 20-Aug-2014].

[47] "GridLAB-D Simulation Software." [Online]. Available: http://www.gridlabd.org/. [Accessed: 20-Aug-2014].

[48] "OpenDSS | Free Science & Engineering software downloads at SourceForge.net." [Online]. Available: http://sourceforge.net/projects/electricdss/. [Accessed: 20-Aug-2014].

[49] R.C. Dugan, "Reference Guide: The Open Distribution System Simulator (OpenDSS)," Jun-2013. [Online]. Available: http://svn.code.sf.net/p/electricdss/code/trunk/Distrib/Doc/OpenDSSManual.pdf. [Accessed: 11-Sep-2014].

[50] "Advanced DG modeling with CYMDIST." [Online]. Available: http://www.cyme.com/company/media/highlights/CYMDIST%20DG%20Highlights.pdf. [Accessed: 11-Sep-2014].

[51] "GridLAB-D / Discussion / Technical support:Charge/Discharge strategy for Batteries." [Online]. Available: http://sourceforge.net/p/gridlab-d/discussion/842562/thread/571fdfb3/. [Accessed: 11-Sep-2014].

[52] K.P. Schneider and T.F. Weaver, "A method for evaluating volt-VAR optimization field demonstrations," *IEEE Transactions on Smart Grid*, vol. 5, no. 4, pp. 1696–1703, July 2014.

[53] B. Seal, "Specification for smart inverter interactions with the electric grid using international electrotechnical commission 61850," Electric Power Research Institute (EPRI), Knoxville, TN, Standard 1021674, October 2010.

[54] M. Farivar, C.R. Clarke, S.H. Low, and K.M. Chandy, "Inverter VAR control for distribution systems with renewables," in *SmartGridComm*, 2011, pp. 457–462.

[55] S. Ponnaluri, G.O. Linhofer, J.K. Steinke, and P.K. Steimer, "Comparison of single and two stage topologies for interface of BESS or fuel cell system using the ABB standard power electronics building blocks," in *European Conference on Power Electronics and Applications (EPE)*, 2005.

[56] A.K. Barnes, J.C. Balda, and J.K. Hayes, "Modeling PV clouding effects using a semi-Markov process with application to energy storage," in *International Federation of Automatic Control World Congress (IFAC)*, Cape Town, South Africa, 2014.

[57] G. Celli, S. Mocci, F. Pilo, and M. Loddo, "Optimal integration of energy storage in distribution networks," in *IEEE PowerTech*, Burcharest, 2009, pp. 1–7.

[58] A.K. Barnes, J.C. Balda, A. Escobar Mejía, and S.O. Geurin, "Placement of energy storage coordinated with smart PV inverters," in *IEEE PES Innovative Smart Grid Technologies (ISGT)*, 2012, pp. 1–7.

[59] W.M. Grady, M.J. Samotyj, and A.H. Noyola, "The application of network objective functions for actively minimizing the impact of voltage harmonics in power systems," *IEEE Transactions on Power Delivery*, vol. 7, no. 3, pp. 1379–1386, July 1992.

[60] A. Maitra, "Effects of transportation electrification on the electricity grid," presented at the Plug-In Hybrid and Electric Vehicle Working Group, 24-Sep-2009.

[61] A.K. Barnes and J.C. Balda, "Sizing and economic assessment of energy storage with real-time pricing and ancillary services," in *IEEE International Symposium on Power Electronics for Distributed Generation Systems (PEDG)*, Fayetteville, AR, 2013, pp. 1–7.

[62] A.E. Hoerl and R.W. Kennard, "Ridge regression: Biased estimation for nonorthogonal problems," *Technometrics*, vol. 12, no. 1, pp. 55–67, 1970.

[63] "Ridge regression - MATLAB." [Online]. Available: http://www.mathworks.com/help/stats/ridge.html. [Accessed: 23-Oct-2012].

[64] T. Sutthibun and P. Bhasaputra, "Multi-objective optimal distributed generation placement using simulated annealing," in *2010 International Conference on Electrical Engineering/Electronics Computer Telecommunications and Information Technology (ECTI-CON)*, 2010, pp. 810–813.

[65] D.P. Kothari and I.J. Nagrath, *Modern Power System Analysis*. New Delhi: Tata McGraw-Hill, 2003.

[66] A.K. Barnes and J.C. Balda, "Placement of distributed energy storage via multidimensional scaling and clustering," in *International Conference on Renewable Energy Research and Applications (ICRERA)*, Milwaukee, WI, 2014.

[67] G.A.F. Seber, *Multivariate observations*. John Wiley and Sons, 2004.

[68] A.K. Barnes, "Value assessment of distributed energy storage via multidimensional scaling," *IEEE Transactions on Power Systems*, October 2014.

[69] ABB, "Energy Storage Modules (ESM)." [Online]. Available: http://new.abb.com/medium-voltage/modular-systems/energy-storage-modules/distributed-energy-storage-(des)-modules.

[70] APC, "EPS 8000 555–1125 kVA technical specifications," APC, Technical Specifications 990–5236A-001, June 2014.

[71] J. E. C. Kern and M. C. Russell, "Spatial and temporal irradiance variations over large array fields," in *IEEE Photovoltaic Specialists Conference (PVSC)*, 1988, pp. 1043–1050 vol.2.

[72] M. Lave, J. Stein, A. Ellis, C. Hansen, E. Nakashima, and Y. Miyamoto, "Ota City: Characterizing output variability from 553 homes with residential PV systems on a distribution feeder," Sandia National Laboratories, Tech. Rep. SAND2011-9011, 2011.

[73] R.A. Howard, "System analysis of semi-Markov processes," *IEEE Transactions on Military Electronics*, vol. 8, no. 2, pp. 114–124, April 1964.

[74] F.S. Hillier and G.J. Lieberman, *Introduction to Operations Research*. McGraw-Hill, 2001.

[75] L. Mears, H. Gotschall, and H. Kamath, "EPRI-DOE handbook of energy storage for transmission and distribution applications," EPRI, Tech. Rep. 1001834, December 2003.

[76] R.O. Duda, P.E. Hart, and D.G. Stork, *Pattern Classification*. Wiley, 2001.

[77] A.K. Barnes, J.C. Balda, and C.M. Stewart, "Selection of converter topologies for distributed energy resources," in *IEEE Applied Power Electronics Conference and Exposition (APEC)*, 2012, pp. 1418–1423.

CHAPTER TWO

OPTIMAL BATTERY CHEMISTRY, CAPACITY SELECTION, CHARGE/DISCHARGE SCHEDULE, AND LIFETIME OF ENERGY STORAGE UNDER TIME-OF-USE PRICING

Arthur Barnes, Juan Carlos Balda, Scott O. Geurin, and Andrés Escobar-Mejía

A.K. Barnes, J.C. Balda, S.O. Geurin, and A. Escobar Mejía, "Optimal battery chemistry, capacity selection, charge/discharge schedule, and lifetime of energy storage under time-of-use pricing," in *IEEE PES Innovative Smart Grid Technologies Europe (ISGT-EU)*, 2011, pp. 1–7.

***Abstract* — Energy storage units (ESU) can reduce the cost of purchased electricity when used in conjunction with time-of-use (TOU) pricing. To maximize the cost reduction, the chemistries, capacities, and charge/discharge schedules of the batteries used in the ESU must be selected appropriately. The batteries must have sufficient capacities to supply the energy demanded by the charge/discharge profiles and to meet the project lifetime. The ESU responds to a TOU price structure. The ESU output power is limited by the rating of the power electronic interface. The cost of the ESU is assumed to increase linearly with battery capacity. A method using linear optimization is developed that determines the battery chemistries, capacities, and charge/discharge schedules simultaneously. The method shows that the Li-Ion battery chemistry is the most cost effective technology due to its high efficiency and that an 11-year project lifetime is most profitable.**

***Index Terms* — Distributed energy storage, battery energy storage, battery chemistries, power systems economics**

Manuscript received April 30, 2011. This work was supported in part by Grid-Connected Power Electronic Systems (GRAPES), an NSF I/UCRC).

A. K. Barnes is with the Department of Electrical Engineering, University of Arkansas, Fayetteville, AR 72701 USA (phone: 479-575-2715; e-mail: artbarnes@ieee.org).

J. C. Balda is the interim Department Head of the Department of Electrical Engineering, University of Arkansas, Fayetteville, AR 72701 USA (e-mail: jbalda@uark.edu).

S. O. Geurin is with the Department of Electrical Engineering, University of Arkansas, Fayetteville, AR 72701 USA (e-mail: sgeurin@uark.edu).

A. Escobar Mejía is with the Department of Electrical Engineering, University of Arkansas, Fayetteville, AR 72701 USA (e-mail: axe011@uark.edu).

I. INTRODUCTION

Energy Storage (ES) is a technology becoming increasingly important because it allows for a number of benefits to both electric utilities and customers alike. These include load shifting, voltage regulation, frequency regulation, energy arbitrage, and UPS capability among others [1], [2]. ES offers benefits over traditional generation, including ability to provide or change output power on a moment's notice and the lack of emissions restrictions such as those faced by diesel generators [3], [4]. This work focuses on the application of ES for energy arbitrage. The application of ES considered is a commercial customer that purchases electricity using a TOU pricing. The customer uses the ES in order to reduce its cost of electricity or generate profit in conjunction with TOU pricing.

In order to maximize profit however, it is necessary to select the chemistries, capacities, charge/discharge schedules of the batteries; these quantities are interrelated. For example, the best type of ES technology depends on the charge/discharge schedule [5], [6]. It is important to

select these values well in order to ensure that the batteries will last for the desired project lifetime, and that a suitable tradeoff is made between battery efficiency lifetime, and cost. Most ES work treats the problems of sizing and scheduling separately. One approach calculates schedules with given sizing [7–9]. Another approach determines the optimal size given a schedule [10], [11]. To date, relatively little work has been done on ES chemistry selection or coordination of different battery chemistries for utility applications. Current work on this topic focuses on coordination of ES technologies with high power density and high energy density [10], [12]. By contrast, the proposed method coordinates and allocates multiple battery chemistries using linear optimization.

This paper is organized as follows: Section II presents the optimization methodology; Section III addresses the setup of the linear optimization problem; Section IV describes the numerical results; and Section V provides the conclusions.

II. LINEAR OPTIMIZATION METHODOLOGY

The objective of the proposed method is to determine the optimal capacities and schedules for an ESU, given a set of battery chemistries and pricing structure. Revenue from ancillary services is not considered, the constant-Ah battery lifetime model is used [13], and the cost of electricity increases at a fixed rate during the project lifetime. The distribution and transmission system connecting the customer and ESU have sufficient capacity to handle peak loads, so the ESU or load power need not be curtailed, and scheduling is performed based on purely economic criteria. Furthermore, the method makes the assumptions addressed below.

II.A. Assumptions

The ESU uses a double-stage converter topology, which consists of an inverter and a bidirectional dc-dc converter, shown in Fig. 1 [14]. A common dc bus is used with a single output inverter. Each battery string connects to the dc bus through its own dc-dc converter and can use different battery chemistry. The sign of the current for each battery string is always the same, so that no battery will be used to charge any other battery. Therefore, the efficiencies of the inverter and dc-dc converter can be lumped together.

The constant-Ah model specifies that the lifetime of a battery, in terms of Ah or Wh throughput, is roughly independent of the depth-of-discharge [13]. This is accomplished by considering a battery with energy capacity E_r. At each measured depth of discharge D and cycle life N_f, the lifetime energy throughput is given by

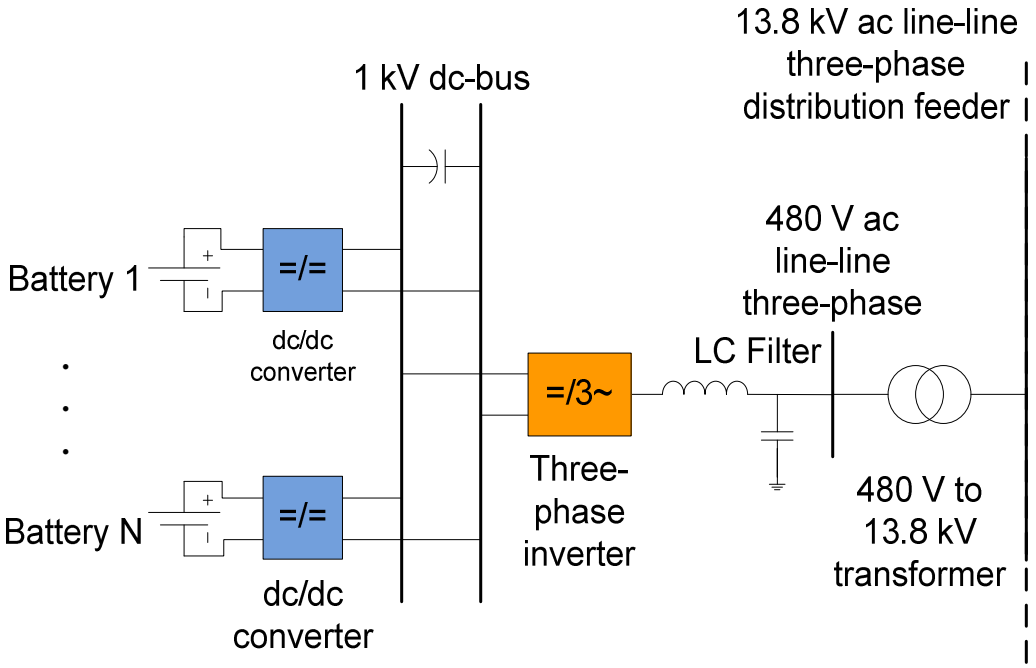

Fig. 1. ESU converter topology.

$$E_f = DN_f. \tag{1}$$

The lifetime energy throughput E_f measured at each depth of discharge D is approximately constant. Dividing E_f by E_r gives the normalized energy throughput E_{f0}

$$E_{f0} = E_f/E_r. \tag{2}$$

Fig. 2 illustrates the constant-Ah model applied for the case of the East Penn 8G8D lead-acid battery [15]. Throughout the range of D, E_f varies by only a small amount.

II.B. Optimization Objective

Net present value (NPV) is a method for measuring the value of a project that takes into account the time value of money [16]. It is useful for comparing the benefit of pursuing different project options. The project is assumed to last Y years. The cash flow from the project at each year y is a_y. The minimum acceptable return rate (MARR) is i.

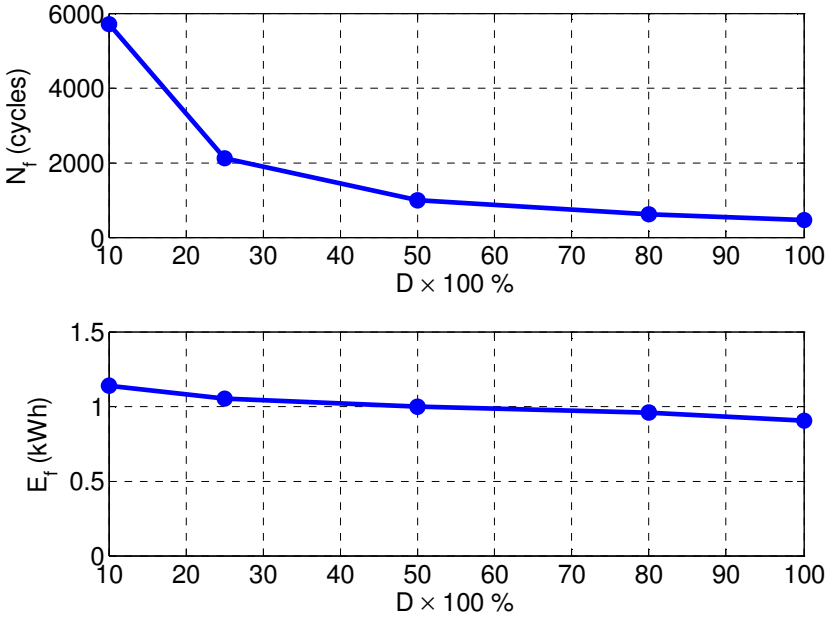

Fig. 2. Cycle life and energy throughput vs. depth of discharge for the East Penn 8G8D lead-acid battery.

The NPV of the project is then given by

$$NPV = \sum_{y=0}^{Y} \frac{a_y}{(1+i)^y}. \tag{3}$$

The cost of electricity increases at rate α each year, thus

$$a_y = (1+\alpha)^{y-1} r_1^{yearly}, \tag{4}$$

where $r_1^{yearly}$is the revenue generated by the ESU at the end of the first year. Additionally, the denominator of the summation for year 0 is 1. Therefore, the NPV can be broken up for either the case of fixed rate or increasing rate into two terms a_0 and a_r

$$NPV = a_0 + a_r, \tag{5}$$

where $a_0 = c_0$, the initial cost of the ESU, and

$$a_r = \sum_{y=1}^{Y} \frac{c_{om} + (1+\alpha)^{y-1} r_1^{yearly}}{(1+i)^y}, \tag{6}$$

where c_{om} is the yearly operation and maintenance (O&M) cost of the ESU. Separating terms and substituting yields

$$NPV = -c_0 + k_r r_1^{yearly} - k_c c_{om}, \text{ where} \tag{7}$$

$$k_r = \sum_{y=1}^{Y} \frac{(1+\alpha)^{y-1}}{(1+i)^y} \tag{8}$$

$$k_c = \sum_{y=1}^{Y} \frac{1}{(1+i)^y}. \tag{9}$$

This is used to construct the following cost function for the optimization problem

$$c = c_0 + k_r r_1^{yearly} - k_c c_{om} \tag{10}$$

$$c_0 = c_{conv} + c_{siting} + \sum_{n=1}^{N} c_n' E_n^r. \tag{11}$$

Here, c_{conv} is the converter cost and c_{siting} is the siting cost. This case considers N different battery chemistries, so c_n' is the cost per unit energy of chemistry n and E_n^r is the rated capacity allocated of that chemistry. Different pricing structures are considered depending on the season k. In this case, there are $K = 2$ different seasons, one for winter and one for summer pricing. Each season has M_k different time periods for each day. The daily profit for season k is

$$r_k^{daily} = \sum_{m=1}^{M_k} \left(c_i + c_{k,m}^{elec}\right) \Delta t_{k,m} p_{k,m}, \tag{12}$$

where c_i is the value in \$/kWh of a feed-in tariff. For each time period m and season k, $c_{k,m}^{elec}$ is the cost of electricity, $\Delta t_{k,m}$ is the length of the time period, and $p_{k,m}$ is the ESU output power. The yearly profit is then

$$r_1^{yearly} = \sum_{k=1}^{K} d_k r_k^{daily}, \tag{13}$$

where d_k is the number of days per year that the particular pricing structure applies. For the purpose of the optimization, the output power is broken up into the discharge power and charging power, respectively, so $p_{k,m} = p_{k,m}^d - p_{k,m}^c$. The discharging and charging powers for each chemistry n are

$$p_{k,m}^d = \sum_{n=1}^{N} p_{n,k,m}^d \tag{14}$$

$$p_{k,m}^c = \sum_{n=1}^{N} p_{n,k,m}^c. \tag{15}$$

II.C. Method Constraints

Taking into account the round-trip efficiency of the battery chemistry η_n, the state of charge (SoC) of each battery is [7]

$$E_{n,k,m+1} = E_{n,k,m} + \Delta t_{k,m}\left(\eta_n p^c_{n,k,m} - p^d_{n,k,m}\right). \tag{16}$$

At each time step, the battery SoC $E_{n,k,m}$ is constrained to be less that the rated capacity of the battery, so

$$0 \le E_{n,k,m} \le E_n^{rated}. \tag{17}$$

Last, the lifetime of the battery must not be violated

$$Y \sum_{k=1}^{K} d_k \sum_{m=1}^{M} \Delta t_{k,m} p^d_{n,k,m} \le E_n^{f0} E_n^{rated}. \tag{18}$$

Here, for battery chemistry n, E_n^{f0} and E_n^{rated} are the normalized energy throughput and rated capacity, respectively. This can be set up as a linear optimization problem [16].

III. LINEAR OPTIMIZATION PROBLEM SETUP

This section illustrates the design of an ESU using the method described above. The first design step is to select the battery chemistries under consideration. Battery chemistries can be characterized by a number of different qualities [17–19], including:

1. Cost per unit energy
2. Cost per unit power
3. Round trip efficiency
4. Mass per unit energy
5. Mass per unit power
6. Standby losses

7. Cycle life
8. Operating temperature range.

For stationary, grid-connected applications, only cost per unit energy, round-trip efficiency, and cycle life are considered. This is justified as follows:

For utility applications, neither volume nor mass are typically a priority. However, for certain applications this could be a consideration, such as distributed energy storage for residential applications. An example is AEP's community energy storage, which needs to fit within a pad-mount transformer enclosure in order to meet consumer acceptance [20]. For cases such as these, volumetric density could be added as a constraint. Standby losses are measured in terms of percent of SoC lost per month. Given that the system is designed to cycle on a daily basis, this does not significantly affect the efficiency of the system. Cost per unit power is not considered for this application. This is because energy, rather than power is the constraining quantity. Typically, the ratio of energy in kWh to power in kW demanded for energy arbitrage is about 7:1 [5]. By contrast, the power to energy ratio for most battery technologies ranges from about 2.6 to 5 [18]; thus, energy is by far the limiting factor. Last, the energy storage unit is assumed to be installed within a substation enclosure, so temperature range is not a consideration.

A large number of battery chemistries and other technologies for energy storage exist either on the market or in various stages of development. A small subset of these technologies is selected for this study based on their estimated technology readiness level and availability of data. The considered battery chemistries are: Li-Ion, NiMH, Lead-acid, NaS, and NiCd. These are shown in Fig. 3, where lifetime is measured in terms of normalized throughput [1], [17], [18], [21–24].

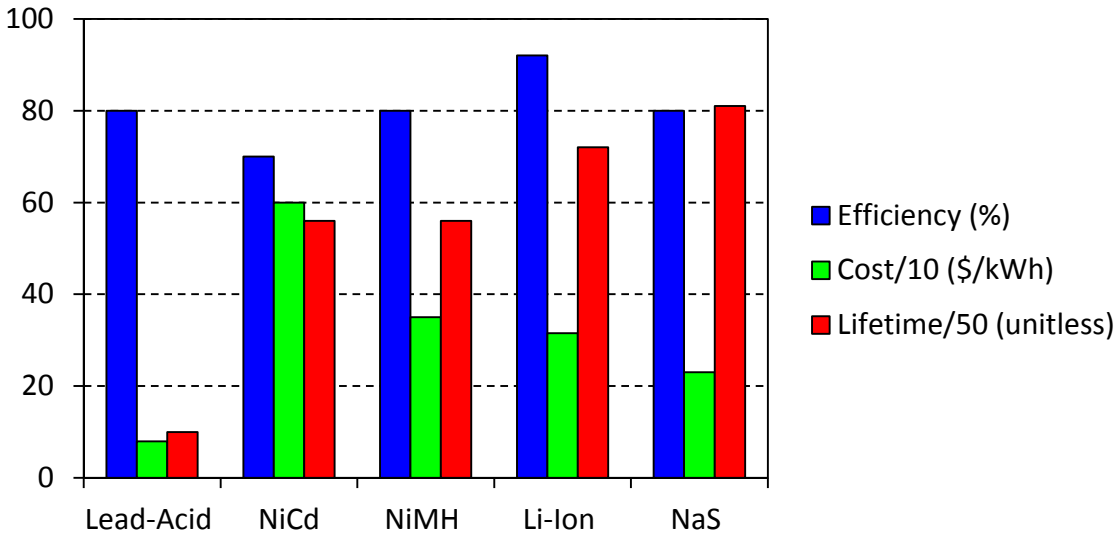

Fig. 3. Comparison of battery chemistry figures of merit.

TABLE 1. CHEMISTRY FIGURES OF MERIT

Chemistry	Efficiency (%)	Cost ($/kWh)	Cycle Life at D (cycles/%)
Lead-Acid	80	80	1000/50
NiCd	70	600	3500/80
NiMH	80	350	3500/80
Li-Ion	92	315	4500/80
NaS	80	230	4500/90

The TOU pricing used in this work is employed by the Independent Electricity System Operator (IESO) [25]. Note that since the work described in this document was performed, the pricing structure has changed, and the parameters described here no longer match the published rate. It is a "castle structure", which has separate rates for nighttime, morning/evening, and midday periods. The costs of electricity are shown in Table 2 and Table 3. The summer and winter pricing structures are significantly different. This is because the summer and winter *demand* curves are significantly different, as noted in [6]. For the rate used, weekends are off-peak. Therefore, it is assumed that the ESU does not operate on weekends. The winter rate

applies from November 1 to April 30, 184 days in total, where the summer rate applies from May 1 to October 31, 181 days in total.

As a number of utilities also use a simpler two-level pricing structure, this is also considered [26].

In order that the results for the three-level and two-level rate structures are compared fairly, a two-level pricing structure is created that results in the same average cost in ¢/kWh given the Ontario load profile [27]. This modified pricing structure is shown in Table 4 and Table 5.

The problem parameters are shown in Table 6 [5], [24], [28]. The efficiencies of the dc-dc converters and inverter are assumed constant across their operating range [14], [29]. However, the same is not true for batteries, as efficiency decreases with respect to current [30]. This is overcome by noting that the scheduled charge and discharge powers in Section IV are relatively constant, so a fixed efficiency is justified.

TABLE 2. THREE-LEVEL TOU RATE FOR WINTER.

Time	Period	Cost (¢/kWh)
7 am to 11 am	On-peak	9.9
11 am to 5 pm	Mid-peak	8.1
5 pm to 9 pm	On-peak	9.9
9 pm to 7 am	Off-peak	5.1

TABLE 3. THREE-LEVEL TOU RATE FOR SUMMER.

Time	Period	Cost (¢/kWh)
7 am to 11 am	Mid-peak	8.1
11 am to 5 pm	On-peak	9.9
5 pm to 9 pm	Mid-peak	8.1
9 pm to 7 am	Off-peak	5.1

TABLE 4. TWO-LEVEL TOU RATE FOR WINTER.

Time	Period	Cost (¢/kWh)
7 am to 9 pm	On-peak	9.0
9 pm to 7 am	Off-peak	5.1

TABLE 5. TWO-LEVEL TOU RATE FOR SUMMER.

Time	Period	Cost (¢/kWh)
7 am to 7 pm	On-peak	8.9
7 pm to 7 am	Off-peak	5.1

TABLE 6. PARAMETERS FOR THE PROBLEM SETUP

Parameter	Value
Converter power rating	2.5 MW
Converter cost	$150/kW
Siting	$100/kW
Subsidization of initial cost	30%
O&M	1%
Converter efficiency	97 %
Project lifetime	20 years
MARR	8 %
Price increase rate	2.8%/year

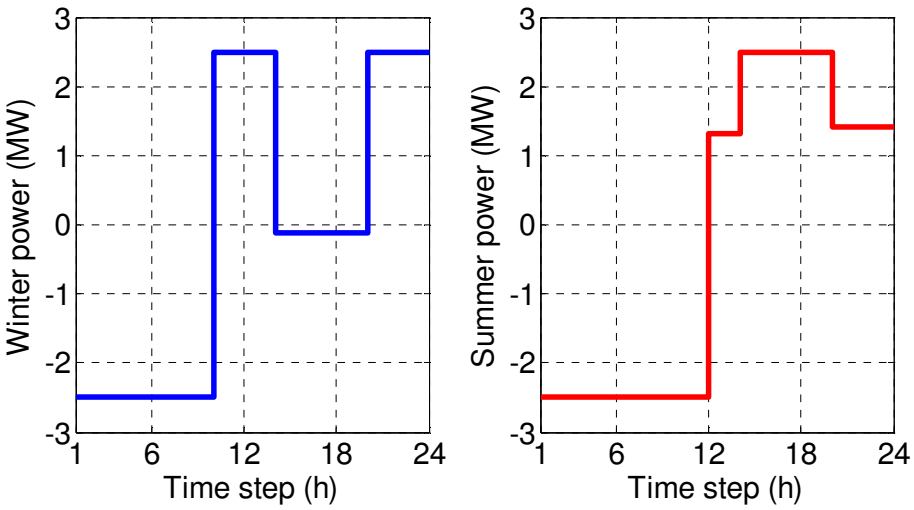

Fig. 4. Scheduled power for NaS with 8¢/kWh incentive and yearly O&M cost of 1%.

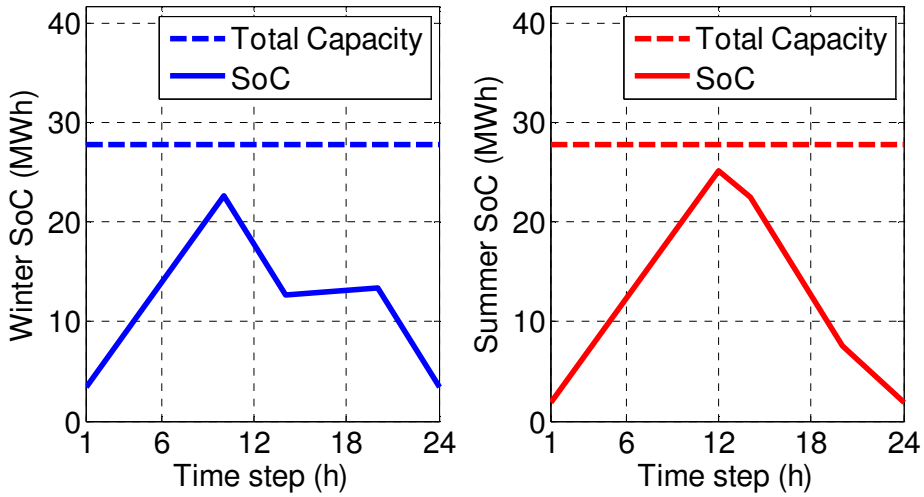

Fig. 5. Scheduled SoC and capacity for NaS with 8¢/kWh incentive and yearly O&M cost of 1%.

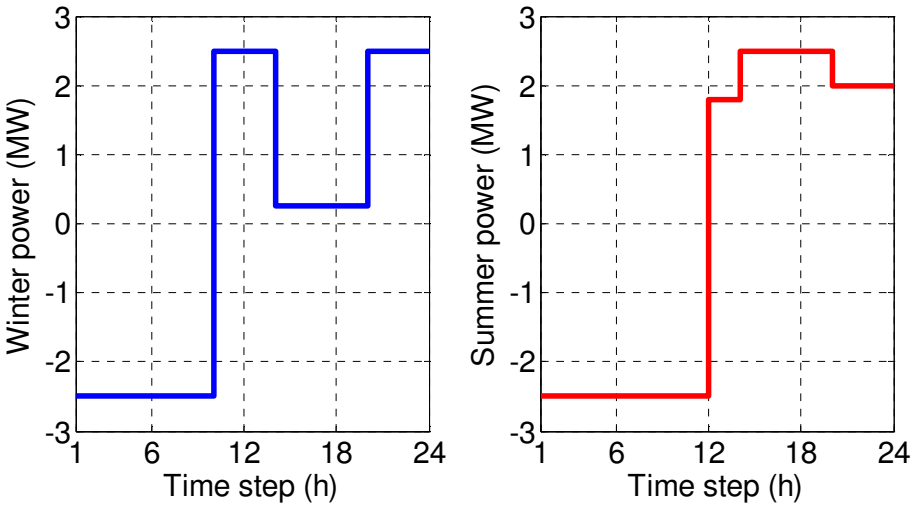

Fig. 6. Scheduled power for Li-Ion with 50¢/kWh incentive and yearly O&M cost of 1%.

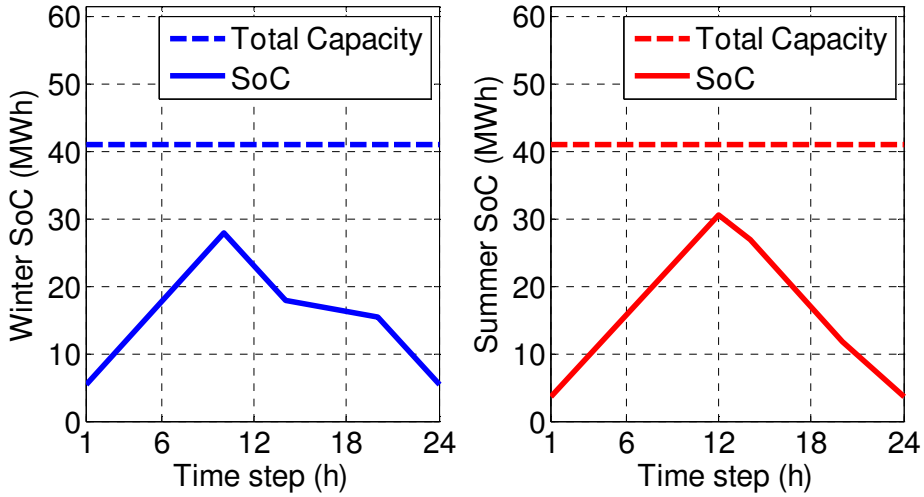

Fig. 7. Scheduled SoC and capacity for Li-Ion with 50¢/kWh incentive and yearly O&M cost of 1%.

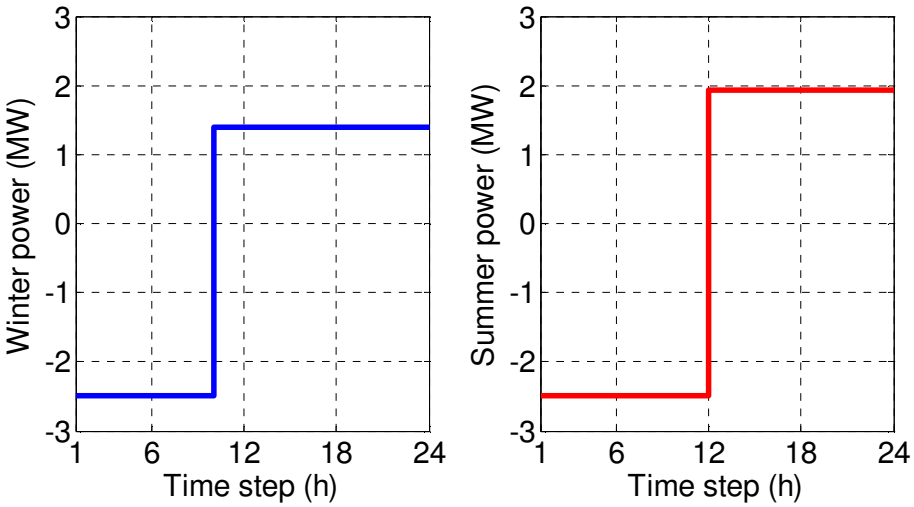

Fig. 8. Scheduled power for NaS using two-level price structure with 8/kWh incentive and yearly O&M cost of 1%.

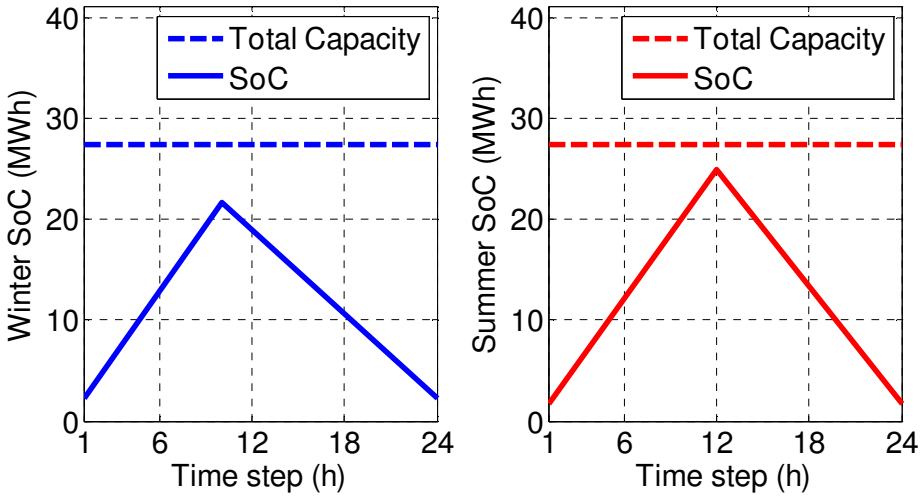

Fig. 9. Scheduled SoC and capacity for NaS using two-level price structure with 8¢/kWh incentive and yearly O&M cost of 1%.

The O&M cost is defined in terms of a percentage of c_0. The initial cost is reduced by a government subsidy. Last, a feed-in tariff in terms of discharged energy serves as an additional incentive.

Table 7 to Table 9 summarize the results. For the Li-Ion ESU, the higher efficiency allows for profit at lower price differences, resulting in higher discharge power during mid-peak in summer. The NaS ESU is predicted to have a higher operation and maintenance cost because it is required to operate at high temperatures. Four scenarios were carried out in order to see what effect this had on profitability, shown in Table 7. The O&M cost used for NaS determines whether it is the more cost-effective chemistry or not.

Table 8 compares the profitability of the different storage technologies under the same pricing structures. Both three-and two-level structures are considered. This reveals that only the Li-Ion and NaS technologies are profitable.

Fig. 10 shows how the return-on-investment (ROI) varies as function of the project lifetime using a Li-Ion ESU. The ROI is defined as in [31]:

$$ROI = \frac{NPV}{c_0} \cdot 100\%. \tag{19}$$

The highest ROI is obtained at 11 years, when the size of the battery very closely matches the daily energy demand resulting from the inverter processing rated power during peak and off-peak periods. For longer lifetimes, the battery will be oversized, resulting in a higher initial expenditure and O&M costs compared with revenue, reducing *NPV* and *ROI.* For shorter lifetimes, the battery will be also discharged during the mid-peak region, increasing daily profit but consuming the battery lifetime less wisely. This is an important consideration to take into account when designing or evaluating an ESU to maximize profitability. Table 9 shows how the sensitivity of the results to changes in the cost of batteries for Li-Ion and NaS. Given the higher efficiency and lower O&M cost of Li-Ion, it is more profitable and favored by the method even at higher costs per kWh than NaS. The infeasible region shown in red represents the point at which neither technology is profitable.

TABLE 7. SUMMARY OF RESULTS FOR ALL CHEMISTRIES CONSIDERED, 1% O&M FOR NAS

Feed-in Tariff (¢/kWh)	NaS O&M (%)	Capacities (MWh)	ROI (%)
8	**1**	**27.8 NaS**	**6.39**
50	**1**	**40.1 Li-Ion**	**221**
2	**5**	**0**	**N/A**
13	**5**	**40.1Li-Ion**	**2.42**

TABLE 8. SUMMARY OF RESULTS FOR SINGLE TECHNOLOGY ONLY, 5% O&M FOR NAS, WITH 10-YEAR LIFETIME, 15 CENTS/KWH FEED-IN TARIFF

Battery Chemistry	Capacities (MWh)		ROI (%)	
Price Structure	3-level	2-level	3-level	2-level
Lead-acid	0	50	N/A	N/A
NiCd	0	0	N/A	N/A
NiMH	0	0	N/A	N/A
Li-Ion	20.5	20.5	32.9	15.2
NaS	16.9	16.9	49.6	20.9

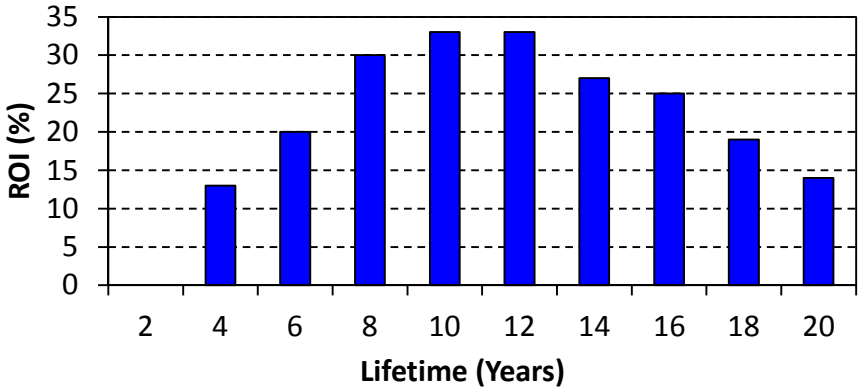

Fig. 10. ROI vs. project lifetime for Li-Ion with 15¢/kWh.

TABLE 9. SENSITIVITY OF RESULTS TO BATTERY COSTS, 5% O&M FOR NAS, WITH 10-YEAR LIFETIME, 15 CENTS/KWH FEED-IN TARIFF

Li-Ion Price ($/kWh) \ NaS Price ($/kWh)	50	100	150	200	250	300
50	363	363	363	363	363	363
100	175	175	175	175	175	175
150	316	91.5	91.5	91.5	91.5	91.5
200	316	141	46.2	46.2	46.2	46.2
250	316	141	61.5	17.6	17.6	17.6
300	316	141	61.5	17.6	Infeasible Region	

Li-Ion ROI (%) | NaS ROI (%)

IV. CONCLUSIONS

A method is developed to select battery chemistries, capacities and schedules for an ESU under TOU pricing. The outcome of this method showed that for the case of TOU pricing, a hybrid ESU with multiple chemistries was not justified. With regard to lifetime, the most cost-effective battery capacity is one that will last for exactly the design lifetime. Alternately, assuming the labor and other additional costs of replacing batteries to be negligible, the best lifetime is one where the battery capacity is exactly that of the energy supplied daily. It is shown that the best battery chemistries were not necessarily the cheapest, but those that provided the best tradeoff between cycle life and efficiency vs. cost. The determination of the best battery is particularly sensitive to O&M costs.

V. ACKNOWLEDGEMENTS

Mr. Arthur Barnes is grateful for the financial support by the Grid-Connected Power Electronic Systems (GRAPES), an NSF I/UCRC. Mr. Andrés Escobar Mejía is grateful for the financial support by the Fulbright Program and the Universidad Tecnólogica de Pereira. Mr. Scott Geurin acknowledges the financial support from the National Science Foundation under a Graduate Research Fellowship.

REFERENCES

[1] L. Mears, H. Gotschall, and H. Kamath, "EPRI-DOE handbook of energy storage for transmission and distribution applications," EPRI, Tech. Rep. 1001834, Dec. 2003.

[2] J. Eyer and G. Corey, "Energy Storage for the Electricity Grid: Benefits and Market Potential Assessment Guide," Sandia National Laboratories, Tech. Rep. SAND2010-0815, Feb. 2010.

[3] M. Black, V. Silva, and G. Strbac, "The role of storage in integrating wind energy," in *Future Power Systems, 2005 International Conference on*, 2005, p. 6 pp.-6.

[4] Caterpillar Inc., "EPA Tier 4 and the Electric Power Industry." [Online]. Available: http://www.cat.com/cda/files/595504/7/EPA%20Tier%204%20and%20the%20Electric%20Power%20Industry%20-%20LEXE0036-01.pdf. [Accessed: 20-Jun-2010].

[5] S. M. Schoenung and W. Hassenzahl, "Long vs. short-term energy storage: Sensitivity analysis," Sandia National Laboratories, Tech. Rep. SAND2007-4253, Jul. 2007.

[6] D. W. Trowler, "Sizing community energy storage systems to reduce transformer overloading with emphasis on plug-in electric vehicle loads," M.S. Thesis, Department of Electrical Engineering, University of Arkansas, Fayetteville, AR, 2011.

[7] M. Korpas and A. T. Holen, "Operation planning of hydrogen storage connected to wind power operating in a power market," *Energy Conversion, IEEE Transactions on*, vol. 21, no. 3, pp. 742-749, 2006.

[8] Y. Xu, L. Xie, and C. Singh, "Optimal scheduling and operation of load aggregator with electric energy storage in power markets," in *North American Power Symposium (NAPS)*, 2010, pp. 1-7.

[9] P. Mokrian, "Modeling and assessment of electricity market initiatives," Ph.D. Dissertation, Department of Management Science and Engineering, Stanford University, Palo Alto, CA, 2009.

[10] A. M. Tankari, B. Dakyo, and C. Nichita, "Improved sizing method of storage units for hybrid wind-diesel powered system," in *Power Electronics and Motion Control Conference, 2008. EPE-PEMC 2008. 13th*, 2008, pp. 1911-1917.

[11] Y. Makarov, P. Du, M. C. W. Kintner-Meyer, C. Jin, and H. Illian, "Optimal size of energy storage to accommodate high penetration of renewable resources in WECC system," in *Innovative Smart Grid Technologies (ISGT)*, 2010, pp. 1-5.

[12] M. E. Glavin, P. K. W. Chan, and W. G. Hurley, "Optimization of autonomous hybrid energy storage system for photovoltaic applications," in *Energy Conversion Congress and Exposition*, 2009, pp. 1417-1424.

[13] H. Binder, T. Cronin, P. Lunsager, J. F. Manwell, U. Abdulwahid, and I. Baring-Gould, "Lifetime Modeling of Lead-Acid Batteries," Risø National Laboratory, Tech. Rep. Risø-R-1515(EN), Apr. 2005.

[14] S. B. Kjaer, J. K. Pedersen, and F. Blaabjerg, "A review of single-phase grid-connected inverters for photovoltaic modules," *Industry Applications, IEEE Transactions on*, vol. 41, no. 5, pp. 1292-1306, Oct. 2005.

[15] "Deka solar photovoltaic batteries," Mar-2009. [Online]. Available: http://www.dekabatteries.com/assets/base/0919.pdf.

[16] F. S. Hillier and G. J. Lieberman, Introduction to Operations Research. McGraw-Hill, 2001.

[17] D. Ton, C. J. Hanley, G. H. Peek, and J. D. Boyes, "Solar energy grid integration systems – energy storage (SEGIS-ES)," Sandia National Laboratories, Tech. Rep. SAND2008-4247, Jul. 2008.

[18] R. M. Schupbach, "Design of an energy storage unit for fuel-cell and hybrid-electric vehicles," Ph.D. Dissertation, Department of Electrical Engineering, University of Arkansas, Fayetteville, AR, 2004.

[19] J. M. Miller, "Energy storage technology markets and applications: ultracapacitors in combination with lithium-ion," in *Power Electronics, 2007 7th Internatonal Conference on*, 2007, pp. 16-22.

[20] D. Rastler, "Energy Storage Technology Options: A White Paper Primer on Applications, Costs and Benefits," Electric Power Research Institute, Tech. Rep. 1020676, Dec. 2010.

[21] T. E. Upman, R. Ramos, and D. M. Kammen, "An assessment of battery and hydrogen energy storage systems integrated with wind energy resources in California," California Energy Commission Public Interest Energy Research Program, Tech. Rep. CEC-500-2005-136, Sep. 2005.

[22] D. Rastler and B. Kaun, "Lithium-ion Energy Storage Market Opportunities: Application Value Analysis and Technology Gap Assessment," EPRI, Tech. Rep. 1020074, Dec. 2010.

[23] D. J. L. Brett et al., "Concept and system design for a ZEBRA battery–intermediate temperature solid oxide fuel cell hybrid vehicle," *Journal of Power Sources*, vol. 157, no. 2, pp. 782-798, Autumn 2006.

[24] N. Lu, M. R. Weimar, Y. V. Makarov, and C. Loutan, "An evaluation of the NaS battery storage potential for providing regulation service in California," in *Power Systems Conference and Exposition (PSCE)*, 2011 IEEE/PES, pp. 1-9.

[25] IESO, "Time-of-Use Prices." [Online]. Available: http://www.ieso.ca/imoweb/siteshared/tou_rates.asp?sid=ic. [Accessed: 21-Jul-2011].

[26] APS, "Time-of-Use Rate Plans." [Online]. Available: http://www.aps.com/aps_services/residential/rateplans/ResRatePlans_33.html. [Accessed: 22-Jul-2011].

[27] IESO, “Market Data.” [Online]. Available: http://www.ieso.ca/imoweb/marketdata/marketData.asp. [Accessed: 21-Jul-2011].

[28] Satcon, “Satcon Solstice 500 kW System Solution,” Satcon Solstice 500 kW System Solution. [Online]. Available: http://www.satcon.com/uploads/products/en/500kW-Solstice-US.pdf. [Accessed: 08-Jun-2011].

[29] S. Ponnaluri, G. O. Linhofer, J. K. Steinke, and P. K. Steimer, “Comparison of single and two stage topologies for interface of BESS or fuel cell system using the ABB standard power electronics building blocks,” in *Power Electronics and Applications*, 2005 European Conference on.

[30] Saft, “Medium-power lithium-ion cells: VL M cells,” Doc. No. 5042-2-0305, Mar. 2005.

[31] T. Au and T. P. Au, Engineering Economics for Capital Investment Analysis. Prentice Hall, 1992.

APPENDIX A: CERTIFICATION OF FIRST AUTHOR

I hereby certify that Arthur K. Barnes is first author of the article this chapter is based on and has completed at least 51% of the work described in the article.

Juan Carlos Balda

Signature _____

Date _____

APPENDIX B: RELEASE FOR USE IN DISSERTATION

Thesis / Dissertation Reuse

The IEEE does not require individuals working on a thesis to obtain a formal reuse license, however, you may print out this statement to be used as a permission grant:

Requirements to be followed when using any portion (e.g., figure, graph, table, or textual material) of an IEEE copyrighted paper in a thesis:

1) In the case of textual material (e.g., using short quotes or referring to the work within these papers) users must give full credit to the original source (author, paper, publication) followed by the IEEE copyright line © 2011 IEEE.

2) In the case of illustrations or tabular material, we require that the copyright line © [Year of original publication] IEEE appear prominently with each reprinted figure and/or table.

3) If a substantial portion of the original paper is to be used, and if you are not the senior author, also obtain the senior author's approval.

Requirements to be followed when using an entire IEEE copyrighted paper in a thesis:

1) The following IEEE copyright/ credit notice should be placed prominently in the references: © [year of original publication] IEEE. Reprinted, with permission, from [author names, paper title, IEEE publication title, and month/year of publication]

2) Only the accepted version of an IEEE copyrighted paper can be used when posting the paper or your thesis on-line.

3) In placing the thesis on the author's university website, please display the following message in a prominent place on the website: In reference to IEEE copyrighted material which is used with permission in this thesis, the IEEE does not endorse any of [university/educational entity's

name goes here]'s products or services. Internal or personal use of this material is permitted. If interested in reprinting/republishing IEEE copyrighted material for advertising or promotional purposes or for creating new collective works for resale or redistribution, please go to http://www.ieee.org/publications_standards/publications/rights/rights_link.html to learn how to obtain a License from RightsLink.

If applicable, University Microfilms and/or ProQuest Library, or the Archives of Canada may supply single copies of the dissertation.

CHAPTER THREE

SIZING AND ECONOMIC ASSESSMENT OF ENERGY STORAGE WITH REAL-TIME PRICING AND ANCILLARY SERVICES

Arthur Barnes, and Juan Carlos Balda

A.K. Barnes and J.C. Balda, "Sizing and economic assessment of energy storage with real-time pricing and ancillary services," in *IEEE International Symposium on Power Electronics for Distributed Generation Systems (PEDG)*, Fayetteville, AR, 2013, pp. 1–7.

***Abstract* – Energy storage units (ESU) can generate profit through providing multiple services. In order to maximize profit while meeting battery lifetime constraints, it is necessary to select the capacity and charge/discharge schedule of the battery. This paper proposes a methodology to calculate the necessary ESU battery capacity for a given power rating and the lifetime profitability of the ESU. Because the price of electricity is not known more than 24 hours in advance, forecasting is necessary when scheduling the ESU. The reduction in profitability of the ESU because of forecasting errors must be taken into account. The methodology applies ridge regression for price forecasting to overcome the problem of having many highly correlated inputs, which lead to poor performance of the forecaster. The methodology demonstrates the encouraging result that the profitability of an ESU is not highly sensitive to forecaster error, as the scheduler is insensitive to the types of errors introduced by the forecaster. This is because of the nature of the variance in electricity market price.**

***Index Terms* – Energy storage sizing, scheduling, linear programming, receding-horizon**

control, electricity price forecasting, regularization, ridge regression.

I. INTRODUCTION

Energy Storage (ES) generates profit through the provision of energy, regulation and reserve services via a real-time pricing structure. In order to maximize the profit while meeting lifetime constraints, it is necessary to select the capacity and charge/discharge schedule of the batteries; these quantities are interrelated in that the charge/discharge schedule is constrained by the capacity of the battery, while the lifetime of the battery is affected by the charge/discharge schedule. Most ES work treats the problems of sizing and scheduling separately. One approach calculates schedules with a given battery capacity [1], [2], [3]. Another approach determines the optimal battery capacity given a schedule [4], [5]. By contrast, this paper proposes a method to allocate the batteries, considering lifetime while creating a predicted schedule using linear optimization. Because a real-time pricing structure is used, the price of services provided is not known beyond 24 hours in advance, so forecasting is necessary beyond this period. To account for the corresponding reduction in profit caused by imperfect forecasting, the results using forecasted pricing data are compared with those using perfect information. Separate forecasters are necessary for each service [6].

This paper is organized as follows. First, section II presents the optimization methodology for the sizing. Second, section III presents the scheduling problem that is used to evaluate the performance of the ESU designed in section II, how forecasting is performed to solve the scheduling problem, and how price thresholding is used in order to limit the amount of cycles that the battery is subjected to. Section IV introduces the problem that is used to test the proposed methods. Section V presents the results of the methodology on the test problem in

terms of battery capacity and schedule for the cases of both perfect knowledge and forecasting. Last, section VI discusses the conclusions.

II. OPTIMIZATION-BASED SIZING

The problem framework allows the scheduling of ES to be treated as a linear optimization problem [2], [3], [7], [8], [9]. Receding horizon control (RHC) is used for control. In RHC the optimal series of control inputs is calculated for a window of fixed size into the future, based on the estimated future state of the plant and inputs [2], [7], [10], [11], [12]. Linear optimization methods can be extended or modified in order to size the ES [13], [14]. This paper considers an energy storage unit (ESU) owned by a large consumer of power. The consumer purchases power through a real-time pricing structure that is indexed to the day-ahead electricity market. The real-time pricing structure includes compensation for provision of ancillary services. The services provided are spinning reserve and regulation. A constraint is that the batteries must last for a specified project lifetime. The Li-ion chemistry is selected a priori, based on earlier studies performed [15], [16]. The lifetime must be accounted for by implementing an aging model [17]. This battery technology is demonstrated in other work for use individually in the services performed, including frequency regulation [18].

The outcome of the proposed method is the optimal battery capacity. Revenue from ancillary services is considered, the constant-Ah battery lifetime model is used [19], and the cost of electricity increases at a fixed rate during the project lifetime. The distribution and transmission system connecting the customer and ESU have sufficient capacity to handle peak loads, so the ESU or load power need not be curtailed, and scheduling is performed based on purely economic criteria.

II.A. Assumptions

The constant-Ah model specifies that the lifetime of a battery, in terms of Ah throughput, is roughly independent of the depth-of-discharge (DoD) [19]. For the case of a Li-Ion battery where the battery voltage only varies by a small amount [20], the concept can be extended to a constant-Wh model. This is accomplished by considering a battery with energy capacity E_{rated}. At each measured DoD D and cycle life N_f, the lifetime energy throughput E_f is given by

$$E_f = DN_f. \tag{1}$$

Dividing E_f by E_{rated} gives the normalized energy throughput

$$E_{f0} = E_f/E_{rated}. \tag{2}$$

Fig. 1 illustrates the relationship of D vs. E_f [21]. Unlike the case of a lead-acid battery, which has approximately an inverse relationship between N_f and D [14], the Li-ion battery has a N_f vs. D relationship of

$$N_f = 30D^{-2.12}. \tag{3}$$

The above expression is derived empirically by assuming a power-law relationship of the form

$$y = Ax^b. \tag{4}$$

This is linear when plotted on a log-log scale

$$\log y = \log Ax^b \tag{5}$$

$$= \log A + b \log x. \tag{6}$$

The coefficients can then be extrapolated by means of a least-squares fit [22]. It is observed that the corresponding relationship between E_f and D is approximately inverse:

$$E_f = D \cdot 30D^{-2.12} \tag{7}$$

$$= 30D^{-1.12}. \quad (8)$$

This result indicates that Li-ion is a good option for applications that require a large number of small charge/discharge cycles, such as frequency regulation. The downside is that lifetime calculation is more complicated, as unlike the case of the lead-acid battery, the constant-Wh model is not valid across a wide range of D. This difficulty is overcome by counting throughput due to frequency regulation separately from large cycles that occur on a daily basis and reflect the battery charging during periods of low demand and low electricity prices.

II.B. Optimization Objective

The objective is to maximize the net present value (NPV), a method for measuring the value of a project that takes into account the time value of money [14]. It is useful for comparing the benefits of pursuing different project options. The project is assumed to last Y years. The cash flow from the project at each year y is a_y. The depreciation rate, also referred to as the minimum acceptable return rate (MARR) is i. The NPV of the project is then given by

$$NPV = \sum_{y=0}^{Y} \frac{a_y}{(1+i)^y}. \quad (9)$$

The cost of electricity increases at rate α each year, thus

$$a_y = (1+\alpha)^{y-1} r_1^{yearly}. \quad (10)$$

The denominator of the NPV after 0 years have passed is 1. This quantity represents the initial cost of the project. Therefore, the NPV can be broken up for either the case of fixed rate or increasing rate into three terms a_0, a_{rc}, and a_f such that

$$NPV = -a_0 + a_r - a_c - a_f. \quad (11)$$

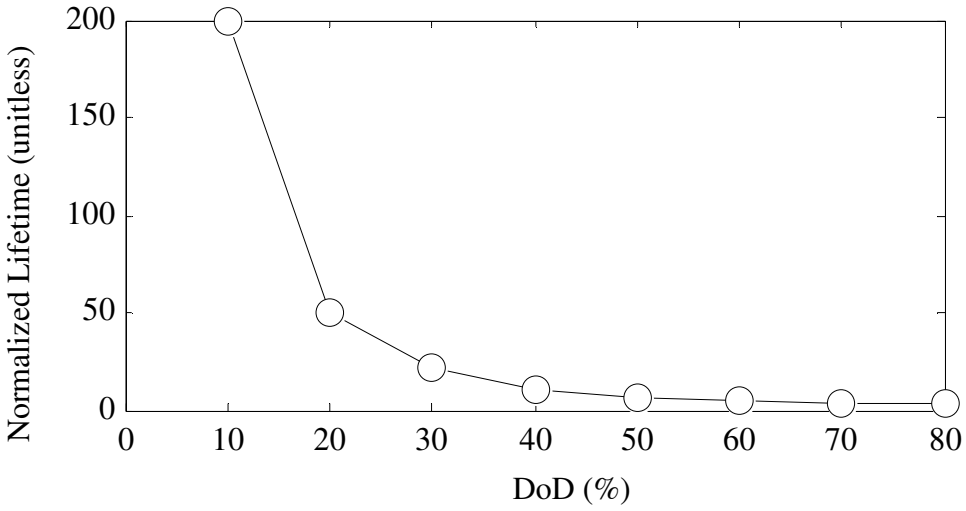

Fig. 1. Normalized lifetime throughput (unitless) vs. DoD.

In the above, $a_0 = c_0$, the cost of purchasing and installing the ESU. This is expressed in terms of the cost of the power electronic converter, siting, and battery

$$c_0 = \left(c'_{conv} + c'_{siting}\right)P_{rated} + \left(1 - k_{subsidy}\right)c'E_{rated}. \tag{12}$$

In the above, the converter and siting costs are proportional to the ESU power rating P_{rated} by the factors c'_{conv} and c'_{siting}, respectively. The battery cost is proportional to the ESU energy rating E_{rating} by the factors c' and $(1 - k_{subsidy})$, where c' is the cost per kWh of the batteries and $(1 - k_{subsidy})$ represents a government subsidy of the battery cost.

The second term a_r is the revenue gained by operating the ESU, while a_c is the operation and maintenance cost of the ES. The last term a_f is the net revenue from decommissioning the ESU at the end of the design lifetime. These terms are defined as follows:

$$a_r = \sum_{y=1}^{Y} \frac{(1+\alpha)^{y-1} r_1^{yearly}}{(1+i)^y} \tag{13}$$

$$a_c = \sum_{y=1}^{Y} \frac{c_1^{yearly}}{(1+i)^y} \tag{14}$$

$$a_f = \frac{c_f}{(1+i)^Y}. \tag{15}$$

The quantity r_1^{yearly} is the revenue produced by the ESU at the end of year one, while c_1^{yearly} is the operation and maintenance costs accrued at the one of year one. The net cost c_f from decommissioning the ESU is the disposal cost of the batteries. The operation and maintenance cost is defined as follows

$$c_1^{yearly} = c_{fixed} + \left(\frac{T}{24 \cdot 365}\right) c_T. \tag{16}$$

This includes a fixed portion that is proportional to the energy capacity of the ESU

$$c_{fixed} = E_{rated} c'_{fixed} \tag{17}$$

as well as a variable portion c_T that increases with the usage of the ESU

$$c_T = c'_{var} \Delta t \sum_{t=1}^{T} p_t^d, \tag{18}$$

where c_{var} is the incremental maintenance cost of providing a kWh of energy, Δt is the time step considered in the analysis, p_t^d is the discharge power at time period t, and T is the number of time periods. A remaining cost is the end of life disposal cost of the batteries. For the case of Li-Ion, the cost of recycling is reported as \$2.25/lb [23]. Given that the energy density of Li-Ion is approximately 100 W/kg [24], [25], the cost of recycling is approximately $c'_f = \left(\frac{1000\ Wh}{1\ kWh}\right)\left(\frac{1\ kg}{100\ Wh}\right)\left(\frac{2.2\ lb}{1\ kg}\right)\left(\frac{\$2.25}{1\ lb}\right) = \$49.5$/kWh. Although this figure sounds high, because it occurs at end-of life, the discount factor is also high, so it does not impact the profitability of the ESU significantly. The disposal cost is then

$$c_f = c_f{}' E_{rated}. \tag{19}$$

The factors in (13)–(15) can be re-expressed as scaling factors

$$NPV = -c_0 + k_r r_1^{yearly} - k_c c_1^{yearly} - k_f c_f, \text{ where} \tag{20}$$

$$k_r = \sum_{y=1}^{Y} \frac{(1+\alpha)^{y-1}}{(1+i)^y} \tag{21}$$

$$k_c = \sum_{y=1}^{Y} \frac{1}{(1+i)^y} \tag{22}$$

$$k_f = \frac{1}{(1+i)^Y}. \tag{23}$$

This is used to construct the following cost function for the optimization problem

$$c = c_0 - k_r r_1^{yearly} + k_c c_1^{yearly} + k_f c_f. \tag{24}$$

The yearly revenue is defined in terms of the revenue r_T over the test data

$$r_1^{yearly} = \left(\frac{24 \cdot 365}{T}\right) r_T. \tag{25}$$

The revenue over the test data is

$$r_T = \Delta t \sum_{t=1}^{T} c_t^e \left(p_t^d - p_t^c + K_s p_t^s\right) + c_t^r p_t^r + c_t^s p_t^s. \tag{26}$$

In the above, the quantity c_t^e is the cost of electricity at time period t, while c_t^r is the compensation for providing regulation, and c_t^s is the compensation for providing spinning reserve. The output power p_t is broken up into the discharge power p_t^d and charging power p_t^c, so $p_t = p_t^d - p_t^c$. This is necessary because of the solution method employed. The quantity p_t^s represents the power commited to spinning reserve, and p_t^r represents the power commited to

regulation. An important consideration is that the objective will result in the scheduler attempting to maximize profit by setting the initial State-of-Charge (SoC) to fully charged and the terminal SoC to fully discharged. If the number of periods T is small, this skews results, making the ES appear more profitable than it really is. Additionally, reliable conclusions cannot be drawn about what time periods are best to charge and discharge. To overcome this, existing work places the constraint that the initial and final SoC must be equal for each scheduling period [2], [7], [10]. This constraint is employed in here. However, the constraint instead can make ES appear less profitable than it should. For example if the cost of electricity at the end of a scheduling window is unusually high, it may be desirable to end the window at a lower overall state of charge. To allow this, a sufficiently long window of three weeks is used so that overall the endpoint constraints do not result in significant error.

II.C. Constraints

The constraints on the sizing/scheduling of the battery fall into three categories: power constraints, SoC constraints, and lifetime constraints. The power constraints follow:

$$p_t^s + p_t^d - p_t^c \leq P_{rated} \tag{27}$$

$$p_t^r + p_t^d + p_t^c \leq P_{rated}. \tag{28}$$

The SoC constraints take into account the round-trip efficiency of the battery chemistry η_n, the SoC of the battery, the discharge power, charging power, and the power reserved for ancillary services [7]. This resulting equality is

$$E_{t+1} = E_t + \Delta t\left(\eta p_t^c - p_t^d\right) + \Delta t(\eta - 1)K_r p_t^r - \Delta t K_s p_t^s \tag{29}$$

At each time step, the battery SoC E_t is constrained to be less that the rated capacity of the battery, as well as greater than a minimum SoC

$$E_{min} \leq E_t \leq E_{rated}. \tag{30}$$

Additionally, the battery must be able to provide UPS capability or reserve power for a minimum time duration T_s without falling below a minimum power level so

$$E_t + T_s\left(\eta p_t^c - p_t^d - p_t^s\right) \geq E_{min}. \tag{31}$$

Last, the lifetime of the battery must not be violated:

$$YE_{yearly} \leq E_{f0}E_{rated} \tag{32}$$

$$E_{yearly} = \left(\frac{T}{24 \cdot 365}\right) E_T \tag{33}$$

$$E_T = \sum_{t=1}^{T} \Delta t\left(p_t^d + K_r^E p_t^r + K_s p_t^s\right). \tag{34}$$

This can be set up as a linear optimization problem [26]. The scaling factor K_r^E presents a solution to the issue of the nonlinear E_f vs. D curve. This factor incorporates two components. The first component is the increased amount of lifetime energy throughput that the battery can withstand at very small D. The ratio of the amount of lifetime energy throughput in Wh consumed per Wh of discharge around a typical regulation cycle compared to the nominal 80% DoD discharge is K_r^E [18]. The second component accounts for the fact that the actual energy throughput experienced by the battery is significantly less than the Wh of regulation capacity it is scheduled to provide. In [18], a 5 MW ESU provides regulation based on the actual grid frequency. This results in the battery being subjected to 20.4 MWh of throughput each week. The corresponding fraction of lifetime reduction that occurs each hour is $9.943 \cdot 10^{-4}$. This is converted to units of lifetime MWh per MWh of regulation service provided as follows, assuming that the relationship between fraction of battery lifetime MWh consumed is related

approximately linearly to the battery capacity and battery power rating. The second component is therefore

$$K_r^E \left(\frac{MWh}{MWh}\right) = (9.943 \cdot 10^{-4}) \frac{(5\ MW)}{(7 \cdot 24\ h)} (1\ h) = 2.959 \cdot 10^{-5} \left(\frac{MWh}{MWh}\right).$$

III. SCHEDULING AN ESU WITH RHC

For the case of a practical ESU scheduler, the actual price of electricity is not perfectly known. Several methods have been devised to account for this. These include RHC [2], [7], [11], stochastic programming [27], stochastic dynamic programming, and rule-based methods [28].

RHC makes use of a forecasted state of the system for a window extending a fixed number of intervals into the future. This forecast and the optimal control inputs are recalculated at each time step. Both forecasting and scheduling can use one of any number of methods. Methods commonly employed for forecasting include linear regression, time-series, Kalman filters, and neural networks [29]. Methods commonly employed for scheduling include dynamic programming, convex programming, linear programming, and mixed-integer programming [30].

III.A. Forecasting

Linear programming is used for scheduling. Because a one-week window is used, forecasting of future prices is necessary. Several methods, including artificial neural networks (ANN), decision trees [31], and linear regression [22] were investigated for the forecasting. Ridge regression, a form of linear regression was selected. Decision trees were an appealing option because they naturally allow for extrapolation of rules such as those an expert human operator would use. Additionally, they naturally integrate both numerical (eg. system load in MW) or categorical (eg. Is today a holiday or working day?) variables. However, the data is nonstationary across seasons. For example, both the shape and magnitude of the daily load profile is different

depending on if it is summer or winter. Therefore, only a small training interval consisting of the two previous month's data is used for training the forecaster. This corresponds to the problem "large d, small n," where the number of training samples is small compared to the dimensionality of the predictor variables. With insufficient samples compared to predictor variables, the forecaster will be overfit, modeling random noise as well as the general trends in the data. The results in the forecaster modeling the training data well, but performing poorly on other data [31]. However, the predictor variables are highly correlated. Ridge regression is a type of linear regression that includes a penalty term in the cost function, forcing the weights to have similar values, thereby preventing overfitting. An additional benefit of the penalty term is that it improves numerical stability when the predictor matrix is close to singular, as is frequently the case when the variables are correlated [32].

The form of classical linear regression is

$$y_i = \beta \cdot x_{i.} \tag{35}$$

In the above, the forecasted value for the i^{th} sample y_i is a linear function of the i^{th} predictor variable x_i. Generally both the weight β and predictor variable x_i are $p \times 1$ vectors. Commonly, the predictor variable is augmented so that $x_i^{aug} = [1, x_i']'$, allowing the forecaster to take into account a fixed offset between the predictor and predicted variables. The cost function for linear regression is typically the sum of squared errors

$$J = \|y - X\beta\|^2. \tag{36}$$

In the above, X is a $n \times p$ matrix of $[x_1', x_2', \ldots, x_n']'$ and y is a $n \times 1$ vector of $[y_1, y_2 \ldots, y_n]'$. This formulation allows for the weight β corresponding to minimum cost to be calculated analytically using

$$\beta = (X'X)^{-1}X'y. \tag{37}$$

However, if $X'X$ is close to singular, the method suffers from numerical accuracy issues. For the case of ridge regression, the cost function is augmented with a penalty term

$$J = \|y - X\beta\|^2 + \lambda\|\beta\|^2. \tag{38}$$

The new minimum cost corresponds to

$$\beta = (X'X + \lambda I)^{-1}X'y. \tag{39}$$

The additional term λI helps make the inverse more robust. However, it comes at a cost in the form of a bias in the estimation of β. To reduce this issue, it is necessary to select a small value of β using either cross- validation [31] or a ridge trace [32]. In a ridge trace, the optimal weights are plotted with respect to λ. The value of λ corresponding to the point when the weights begin to stabilize is selected, in this case 2.5.

For each sample, a window of one week is used. For hourly pricing data, this corresponds to 168 samples. Separate predictors are trained for each lookahead interval, however the same feature vector is used for every lookahead interval. Only lagged and averaged previous price values are used for forecasting. Adding historical prices and temperature forecasts were considered, but these did not yield improved performance. For predictor variables where the lookahead interval exceeds the lag of the previous price values (meaning that the predictor would be given future data as inputs) the corresponding lagged prices are censored by setting them equal to zero. The predictor variables used are illustrated in Table I. The variables are scaled so that they fall within the range ± 10.

TABLE I. PREDICTOR VARIABLES USED FOR RIDGE REGRESSION.

Feature	Lags	Scaling
Working day indicator {0,1}	0	1
Day of week {1,2,…7}	Previous day, same hour price	1
Hour {0,1,2…23}	0	1/10
Electricity price	1,2,3 22,23,…26 166,167,…170 190,191,…194	1/10
Weekly average electricity price	168	1/1000

III.B. Calculation of Price Thresholds

Because the scheduler only operates on one week at a time, battery lifetime constraints cannot be included directly in the scheduling. Instead, they are addressed by setting a minimum price threshold for discharging and a maximum price threshold for charging.

These thresholds limit the amount of energy throughput experienced by the battery. The thresholds are determined by observation of the output power vs. price of the optimal schedule using perfect information. Based on the data, the thresholds are set at $\mu - 2$, where μ is the mean electricity price, approximately $36/MWh.

IV. CASE STUDY

The New York Independent System Operator (NYISO) market and load data for the Buffalo, NY region from July 2009 to July 2010 is used, illustrated in Fig. 2, along with the problem parameters in Table II [33]. Seventeen sets of training/testing data are used. For each set, a three-week period is used for testing, and the previous two months of data is used for training.

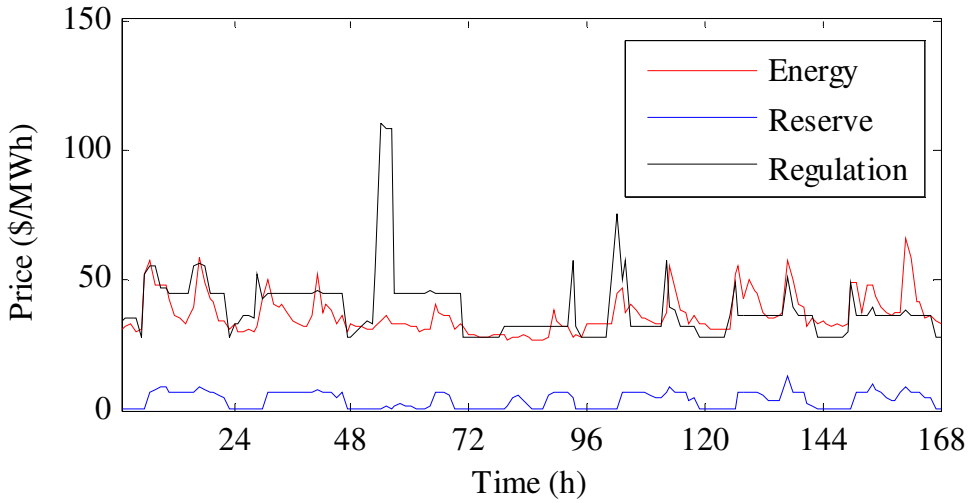

Fig. 2. Pricing data for January 7-28, 2010.

TABLE II. PROBLEM SETUP PARAMETER VALUES

Parameter	Value
Converter power rating	2.5 MW
Converter cost	$150/kW
Siting	$100/kW
Subsidization of battery cost	30%
Fixed yearly O&M cost c'_{fixed}	5% of battery cost
Variable yearly O&M cost	$0/kWh
Battery cost	$315/kWh
Battery lifetime	4500 cycles at 80% DoD
Battery round-trip efficiency	92%
Converter efficiency	97 %
Project lifetime	10 years
Project start year	2021 (10 years from present)
MARR	8 %
Price increase rate	2.8%/year

V. NUMERICAL RESULTS AND DISCUSSION

Based on the scheduler with perfect information, the necessary battery capacity is 5.8 MWh. Fig. 3 shows forecasting results. Table III lists performance results for both the scheduler using perfect information and the RHC scheduler using a one-week forecast. Fig. 4 illustrates the accuracy of forecasting during 2009-2010 using ridge regressors trained on data from two months ahead.

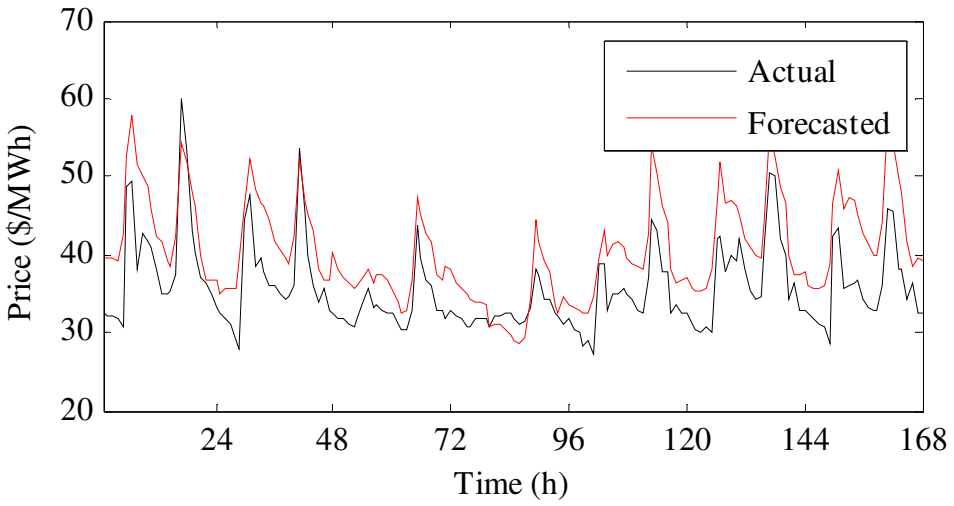

Fig. 3. Energy market forecasting results for 168 hours ahead during the course of one week.

TABLE III. COMPARISON OF PERFORMANCE WITH PERFECT KNOWLEDGE AND FORECASTING

	Perfect Knowledge	**Forecasting**
Weekly Revenue	$8489.04	$7782.60
Throughput	37.5 MWh	36.7 MWh
Lifetime	10 years	10.99 years

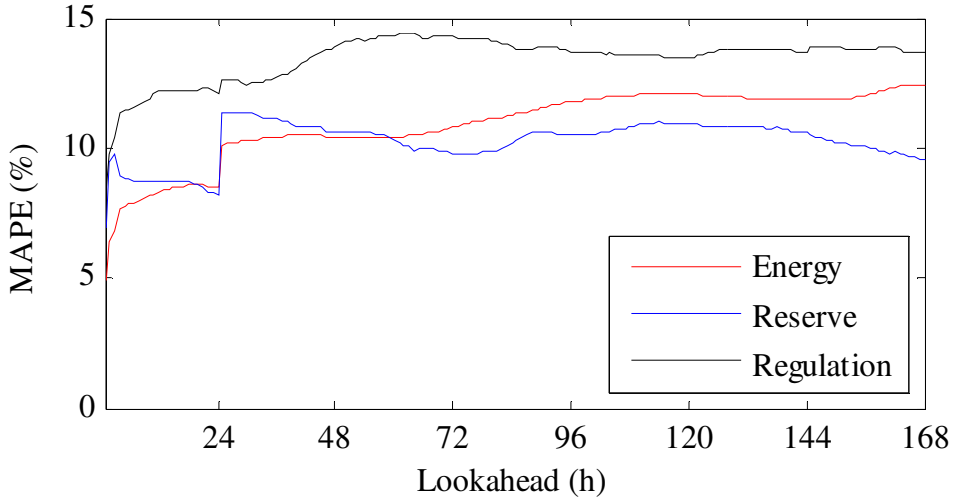

Fig. 4. Forecasting accuracy for the data from September 2009 to September 2010.

Although the forecasting results are actually discrete-time signals (sampled at one-hour intervals) for visual clarity they are plotted as lines. The RHC scheduler obtains 91% of the weekly profits of the scheduler using perfect information. Two factors make the RHC scheduler obtain a high fraction of the ideal profit: First, in scheduling the ESU, it is the relative price difference between low and high periods during the day that determines when the ESU charges and discharges rather than the absolute value of the price. Thus, the high mean absolute percent error (MAPE) that occurs when performing medium-term forecasting (lookahead intervals in excess of one day) caused by steadily increasing error in the mean daily prices does not significantly affect the ideal schedule. Second, most of the ES profits come from providing frequency regulation and spinning reserve services. Because the energy requirements from delivering these services are low, the ESU is scheduled to provide them most of the time, except during periods of low daily prices, when it is scheduled to charge. The price volatility during these charging times is low, so the ESU is very likely to charge at or near the lowest price period each day. Fig. 5 illustrates how both in the case of perfect knowledge and forecasting charging occurs during the early morning

hours, while Fig 6 and Fig. 7. show how the ESU provides regulation and reserve services throughout most of the day.

VI. CONCLUSIONS

This paper illustrates the allocation and scheduling of ES for the purposes of generating profit via a real-time pricing structure. Even with imperfect knowledge it is possible to size an ESU using historical data from the NYISO system and schedule it using a linear forecaster. It is demonstrated that a sparsity-promoting predictor gives good performance by exploiting redundancy in the predictor variables. Taking into account lifetime constraints when designing and scheduling the ESU is a computationally difficult problem, but which can be solved heuristically by linearizing the ESU lifetime Wh vs. DoD curves at two different points; the first reflecting daily SoC variations and the second representing small SoC variations from frequency regulation. The issue of accounting for lifetime constraints when scheduling is handled more simply by using a threshold for the maximum price allowable to charge the ESU. The ESU derives most of its revenue through the reserve and regulation services. The scheduler finds it economical to schedule the ESU to provide both of these services throughput most of the day. Only during the period of the day with the lowest overall prices (the prices for energy, reserve, and regulation services are well correlated) does the ESU not provide these services, and charges in order to account for discharge when called upon for reserve, and losses incurred in providing regulation services. Because electricity price volatility increases as the price increases, the forecast of low price periods is more accurate than high price periods. This results in the real-world performance of the forecaster with the ESU to be much better than the simple MAPE performance criterion indicates. The resulting loss in ESU profitability resulting from forecasting error compared with perfect knowledge is small, under 10%.

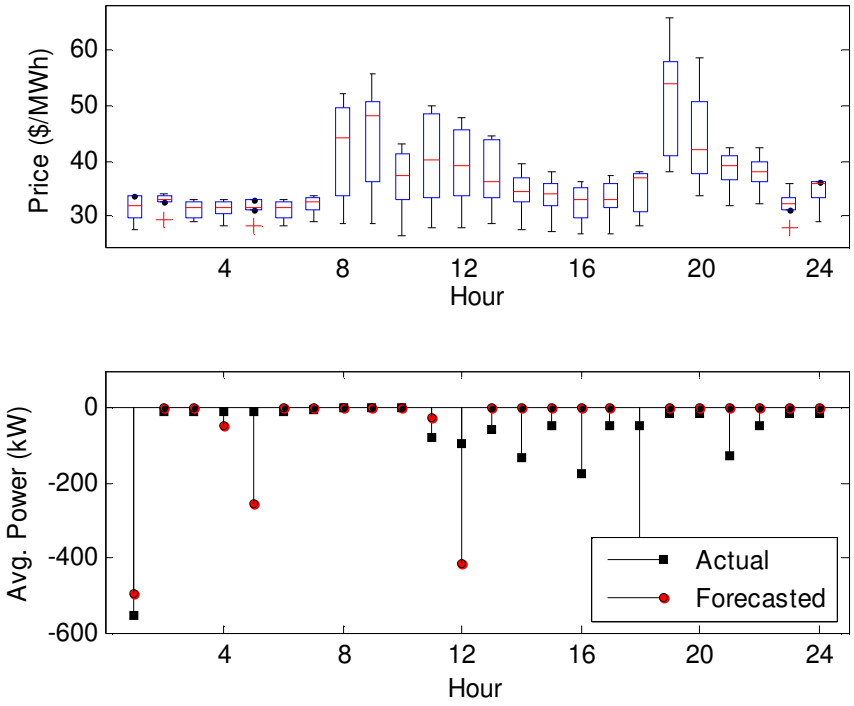

Fig. 5. Scheduled charging power.

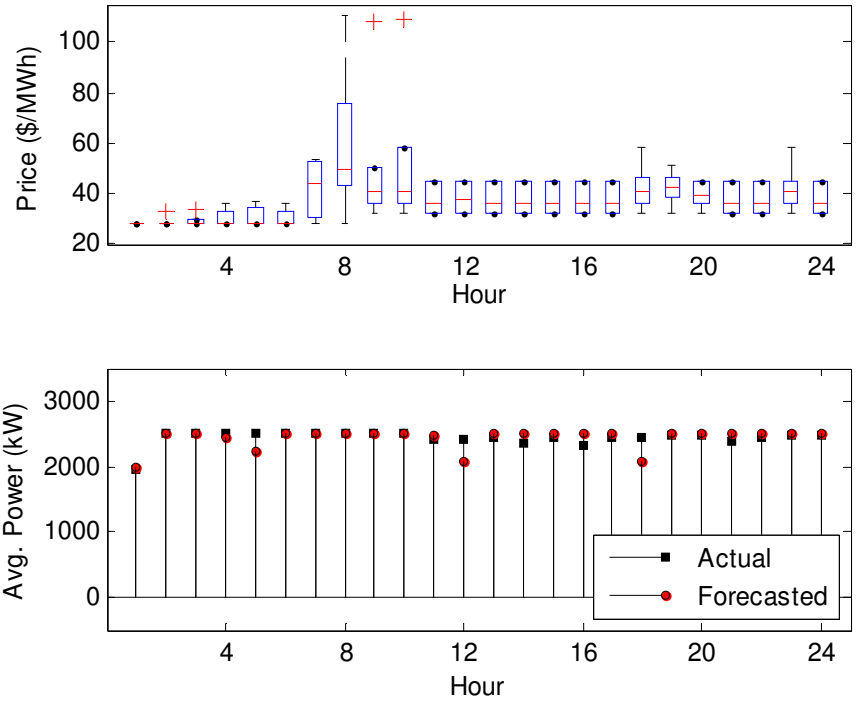

Fig. 6. Scheduled regulation power.

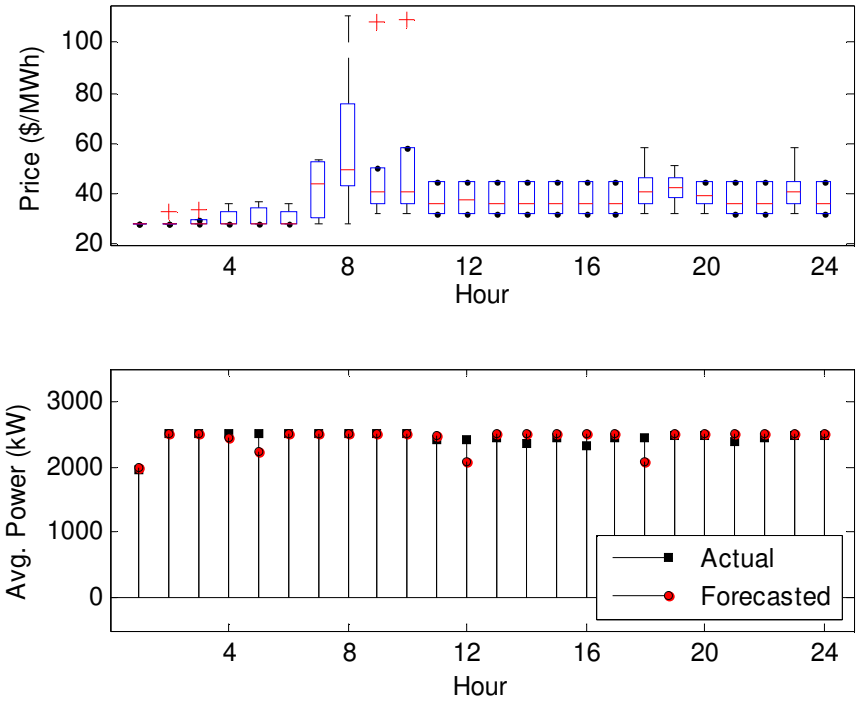

Fig. 7. Scheduled reserve power.

REFERENCES

[1] M. Korpas and A. T. Holen, "Operation planning of hydrogen storage connected to wind power operating in a power market," *Energy Conversion, IEEE Transactions on*, vol. 21, no. 3, pp. 742–749, 2006.

[2] Y. Xu, L. Xie, and C. Singh, "Optimal scheduling and operation of load aggregator with electric energy storage in power markets," in *North American Power Symposium (NAPS),* 2010, pp. 1–7.

[3] P. Mokrian, "Modeling and assessment of electricity market initiatives," Ph.D. Dissertation, Department of Management Science and Engineering, Stanford University, Palo Alto, CA, 2009.

[4] A. M. Tankari, B. Dakyo, and C. Nichita, "Improved sizing method of storage units for hybrid wind-diesel powered system," in *Power Electronics and Motion Control Conference*, 2008, pp. 1911–1917.

[5] Y. Makarov, P. Du, M. C. W. Kintner-Meyer, C. Jin, and H. Illian, "Optimal size of energy storage to accommodate high penetration of renewable resources in WECC system," in *Innovative Smart Grid Technologies (ISGT)*, 2010, pp. 1–5.

[6] P. Faria, Z. Vale, J. Soares, H. Khodr, and B. Canizes, "ANN based day-ahead ancillary services forecast for electricity market simulation," in *MELECON 2010 - 2010 15th IEEE Mediterranean Electrotechnical Conference*, 2010, pp. 1159–1164.

[7] S. Jalal Kazempour and M. P. Moghaddam, "Economic viability of NaS battery plant in a competitive electricity market," in *International Conference on Clean Electrical Power*, 2009, pp. 453–459.

[8] C. Jin, S. Lu, N. Lu, and R. A. Dougal, "Cross-market optimization for hybrid energy storage systems," in *IEEE PES General Meeting*, 2011, pp. 1–6.

[9] P. Wolfs and G. S. Reddy, "A receding predictive horizon approach to the periodic optimization of community battery energy storage systems," in *Universities Power Engineering Conference (AUPEC)*, 2012 22nd Australasian, 2012, pp. 1–6.

[10] S. J. Kazempour, M. P. Moghaddam, and G. R. Yousefi, "Self-scheduling of a price-taker hydro producer in day-ahead energy and ancillary service markets," presented at the *IEEE Canada Electric Power Conference*, 2008, pp. 1–6.

[11] S. J. Kazempour, M. Hosseinpour, and M. P. Moghaddam, "Self-scheduling of a joint hydro and pumped-storage plants in energy, spinning reserve and regulation markets," in *IEEE Power and Energy Society (PES) General Meeting*, Calgary, Canada, 2009, pp. 1–8.

[12] A. Khatamianfar, M. Khalid, A. V. Savkin, and V. G. Agelidis, "Wind power dispatch control with battery energy storage using model predictive control," in *2012 IEEE International Conference on Control Applications (CCA)*, 2012, pp. 733–738.

[13] Tsung-Ying Lee and Nanming Chen, "Determination of optimal contract capacities and optimal sizes of battery energy storage systems for time-of-use rates industrial customers," *IEEE Transactions on Energy Conversion*, vol. 10, no. 3, pp. 562–568, Sep. 1995.

[14] A. Barnes, J. C. Balda, A. Escobar, and S. O. Geurin, "Optimal battery chemistry, capacity selection, charge/discharge schedule, and lifetime of energy storage under time-of-use pricing," in *IEEE PES Innovative Smart Grid Technologies Europe*, Manchester, England, 2011.

[15] S. O. Geurin, "A method for operating large-scale energy storage systems for arbitrage under variable pricing structures," M.S. Thesis, Department of Electrical Engineering, University of Arkansas, Fayetteville, AR, 2011.

[16] D. W. Trowler, "Sizing community energy storage systems to reduce transformer overloading with emphasis on plug-in electric vehicle loads," M.S. Thesis, Department of Electrical Engineering, University of Arkansas, Fayetteville, AR, 2011.

[17] C. R. Vergara, “Parametric interface for Battery Energy Storage Systems providing ancillary services,” in *2012 3rd IEEE PES International Conference and Exhibition on Innovative Smart Grid Technologies (ISGT Europe)*, 2012, pp. 1–7.

[18] M. T. Holmberg, M. Lahtinen, J. McDowall, and T. Larsson, “SVC Light® with energy storage for frequency regulation,” in *IEEE Conference on Innovative Technologies for an Efficient and Reliable Electricity Supply (CITRES)*, 2010, pp. 317–324.

[19] H. Binder, T. Cronin, P. Lunsager, J. F. Manwell, U. Abdulwahid, and I. Baring-Gould, “Lifetime modeling of lead-acid batteries,” Risø National Laboratory, Tech. Rep. Risø-R-1515(EN), Apr. 2005.

[20] L. W. Hruska, “Smart batteries and lithium-ion voltage profiles,” in Battery Conference on Applications and Advances, 1997, pp. 205–210.

[21] IEEE Recommended Practice for the Characterization and Evaluation of Emerging Energy Storage Technologies in Stationary Applications. IEEE Standard 1679-2010, 2010.

[22] “Polynomial curve fitting - MATLAB.” [Online]. Available: http://www.mathworks.com/help/matlab/ref/polyfit.html. [Accessed: 12-Oct-2012].

[23] L. Gaines and R. Cuenca, “Cost of lithium-ion batteries for vehicles,” Center for Transportation Research, Argonne National Laboratory, Tech. Rep. ANL/ESD-42, May 2000.

[24] R. M. Schupbach, “Design of an energy storage unit for fuel-cell and hybrid-electric vehicles,” Ph.D. Dissertation, Department of Electrical Engineering, University of Arkansas, Fayetteville, AR, 2004.

[25] P. A. Nelson, K. G. Gallagher, I. Bloom, and D. W. Dees, “Modeling the performance and cost of lithium-ion batteries for electric-drive vehicles,” Chemical Sciences and Engineering Division, Argonne National Laboratory, Chicago, IL, Tech. Rep. ANL-11/32, Sep. 2011.

[26] F. S. Hillier and G. J. Lieberman, Introduction to Operations Research. McGraw-Hill, 2001.

[27] J. Garcia-Gonzalez, R. M. . de la Muela, L. M. Santos, and A. M. Gonzalez, “Stochastic joint optimization of wind generation and pumped-storage units in an electricity market,” *IEEE Transactions on Power Systems*, vol. 23, no. 2, pp. 460–468, May 2008.

[28] T. K. . Brekken, A. Yokochi, A. von Jouanne, Z. Z. Yen, H. M. Hapke, and D. A. Halamay, “Optimal energy storage sizing and control for wind power applications,” *IEEE Transactions on Sustainable Energy*, vol. 2, no. 1, pp. 69–77, Jan. 2011.

[29] A. Khosravi, S. Nahavandi, and D. Creighton, “Construction of optimal prediction intervals for load forecasting problems,” *IEEE Transactions on Power Systems*, vol. 25, no. 3, pp. 1496–1503, Aug. 2010.

[30] R. Cahalan and J. Joseph, “Fractal statistics of cloud fields,” *Monthly Weather Review*, vol. 117, pp. 261–272, 1989.

[31] R. O. Duda, P. E. Hart, and D. G. Stork, Pattern classification. Wiley, 2001.

[32] “Ridge regression - MATLAB.” [Online]. Available: http://www.mathworks.com/help/stats/ridge.html. [Accessed: 23-Oct-2012].

[33] “NYISO market and operational data.” [Online]. Available: http://www.nyiso.com/public/markets_operations/market_data/pricing_data/index.jsp. [Accessed: 12-Nov-2012].

APPENDIX A: CERTIFICATION OF FIRST AUTHOR

I hereby certify that Arthur K. Barnes is first author of the article this chapter is based on and has completed at least 51% of the work described in the article.

Juan Carlos Balda

Signature _____

Date _____

APPENDIX B: RELEASE FOR USE IN DISSERTATION

Thesis / Dissertation Reuse

The IEEE does not require individuals working on a thesis to obtain a formal reuse license, however, you may print out this statement to be used as a permission grant:

Requirements to be followed when using any portion (e.g., figure, graph, table, or textual material) of an IEEE copyrighted paper in a thesis:

1) In the case of textual material (e.g., using short quotes or referring to the work within these papers) users must give full credit to the original source (author, paper, publication) followed by the IEEE copyright line © 2011 IEEE.

2) In the case of illustrations or tabular material, we require that the copyright line © [Year of original publication] IEEE appear prominently with each reprinted figure and/or table.

3) If a substantial portion of the original paper is to be used, and if you are not the senior author, also obtain the senior author's approval.

Requirements to be followed when using an entire IEEE copyrighted paper in a thesis:

1) The following IEEE copyright/ credit notice should be placed prominently in the references: © [year of original publication] IEEE. Reprinted, with permission, from [author names, paper title, IEEE publication title, and month/year of publication]

2) Only the accepted version of an IEEE copyrighted paper can be used when posting the paper or your thesis on-line.

3) In placing the thesis on the author's university website, please display the following message in a prominent place on the website: In reference to IEEE copyrighted material which is used with permission in this thesis, the IEEE does not endorse any of [university/educational entity's

name goes here]'s products or services. Internal or personal use of this material is permitted. If interested in reprinting/republishing IEEE copyrighted material for advertising or promotional purposes or for creating new collective works for resale or redistribution, please go to http://www.ieee.org/publications_standards/publications/rights/rights_link.html to learn how to obtain a License from RightsLink.

If applicable, University Microfilms and/or ProQuest Library, or the Archives of Canada may supply single copies of the dissertation.

CHAPTER FOUR

PLACEMENT OF ENERGY STORAGE COORDINATED WITH SMART PV INVERTERS

Arthur Barnes, Juan Carlos Balda, Scott O. Geurin, and Andrés Escobar-Mejía

A.K. Barnes, J.C. Balda, A. Escobar Mejía, and S.O. Geurin, "Placement of energy storage coordinated with smart PV inverters," in *IEEE PES Innovative Smart Grid Technologies (ISGT)*, 2012, pp. 1–7.

***Abstract* — Energy storage (ES) is increasing used in electrical transmission and distribution systems because it can perform many functions. These include peak shaving, voltage regulation, frequency regulation, spinning reserve, and aiding integration of renewable generation by mitigating the effects of intermittency. This work focuses on the usage of energy storage for peak shaving and voltage regulation on a distribution system having a high penetration of photovoltaic (PV) generation. The PV stations considered make use of smart PV inverters as proposed by the Electric Power Research Institute (EPRI). These inverters assist the energy storage with voltage regulation. Additionally, the proposed method includes support for varying energy storage unit (ESU) sizes, non-radial distribution systems, and reverse power flow, both real and reactive. The method is applied to the worst-case voltage regulation scenario. The impact of the placement and voltage regulation on the profitability of energy storage is assessed. This is accomplished by adding voltage regulation as a constraint to the problem scheduling energy storage in order to maximize profit. Applying the method shows that the best place to put an ESU is near the**

end of a feeder. Validation of the method shows that it does not impact the ability of ES to be scheduled in order to maximize economic benefits with time-of-use pricing.

Index Terms **— Energy storage, power system optimization, distribution system planning, simulated annealing**

Manuscript received July 20, 2011. This work was supported in part by Grid-Connected Power Electronic Systems (GRAPES), an NSF I/UCRC).

A. K. Barnes is with the Department of Electrical Engineering, University of Arkansas, Fayetteville, AR 72701 USA (phone: 479-575-2715; e-mail: artbarnes@ieee.org).

J. C. Balda is the interim Department Head of the Department of Electrical Engineering, University of Arkansas, Fayetteville, AR 72701 USA (e-mail: jbalda@uark.edu).

A. Escobar Mejia is with the Department of Electrical Engineering, University of Arkansas, Fayetteville, AR 72701 USA (e-mail: axe011@uark.edu).

S. O. Geurin is with the Department of Electrical Engineering, University of Arkansas, Fayetteville, AR 72701 USA (e-mail: sgeurin@uark.edu).

I. NOMENCLATURE

I.A. Placement

N	Number of busses in the system
n	Bus index
c	Total cost of placing energy storage in $
c'	Variable component of ESU cost in $/kW
c_0	Fixed component of ESU cost in $

e_n Binary indicator variable for ESU placement at bus n

S_n^{esu} Rated power of the ESU at bus n in kVA

P_n^{esu} Real power output of the ESU at bus n in kW

Q_n^{esu} Reactive power output of the ESU at bus n in kVAr

S_n^{pv} Rated power of the PV inverter at bus n in kVA

P_n^{pv} Real power output the PV inverter at bus n in kW

Q_n^{pv} Reactive power output the PV inverter at bus n in kVAr

δ_n Weighting used to place ESU at bus n

V_n Voltage magnitude at bus n

u Uncertainty factor

ρ_n Probability of selecting bus n for a move

k Iteration number

T_k Temperature at iteration k

α Learning rate

I.B. Scheduling

E_{rated} Rated energy capacity of battery in kWh

D Depth of discharge (ranges from 0 to 1)

N_f Battery cycles to failure at D

E_f Battery energy throughput to failure in kWh

E_{f0} Battery normalized energy throughput to failure

NPV Net present value

Y Project lifetime in years

y	Year
i	Minimum acceptable return rate
α	Rate of electricity cost increase per year
$\alpha(y)$	Project cash flow at year y in \$
a_0	Initial cash flow in \$
c_0	Initial cost of ESU in \$
a_r	Revenue and maintenance of ESU
c_{om}	Yearly operation & maintenance cost of ESU in \$
c_{conv}	Cost of power conversion system in \$/kW
c_{siting}	Siting cost in \$/kW
r_1^{yearly}	Revenue produced by the ESU at the end of year 1 in \$
c	Yearly cost of operating the ESU in \$
c'	Cost of batteries per kWh in \$
K	Number of seasons considered
k	Season index
M_k	Number of time periods in rate structure during season k
m	Time period
$\Delta t_{k,m}$	Duration of time period m during season k
$c_{k,m}^{elec}$	Cost of electricity at time period m during season k in \$/kWh
c_i	Value of feed-in tariff in \$/kWh
d_k	Number of days in season k
$p_{k,m}$	Net power output of ESU at time period m during season k in kW

$p_{k,m}^{d}$ Discharge power of ESU at time period m during season k in KW

$p_{k,m}^{c}$ Charge power of ESU at time period m during season k in kW

$p_{k,m}^{v}$ Net power required to provide voltage regulation

r_{k}^{daily} Daily revenue of ESU during season k in $

$E_{k,m}$ SoC of ESU at time period m during season k in kWh

η Round-trip efficiency of ESU

II. INTRODUCTION

Energy storage can perform many different functions on both electrical transmission and distribution systems. These include peak shaving, voltage regulation, frequency regulation, spinning reserve, and aiding integration of renewable generation by mitigating the effects of intermittency [1], [2]. Among these functions, this work focuses on the usage of energy storage to provide voltage regulation on a distribution system. The distribution system has a high penetration of PV generation, which has been shown to cause local voltage regulation issues [3-6]. The PV stations make use of smart PV inverters as proposed by EPRI [7]. This allows them to be coordinated in order to help regulate voltage on distribution systems [8], [9]. Based on knowledge from shunt capacitor placement and distributed generation placement, in order to provide voltage regulation in the most cost-effective manner, energy storage must be placed appropriately in the distribution system. When the energy storage is placed and used to provide voltage regulation, this places a constraint on when it can be charged and discharged. This constraint must be taken into account when scheduling the energy storage. Additionally, failure to properly place the energy storage will hinder its ability to assist with voltage regulation.

Most existing work with both energy storage, distributed generation, and shunt capacitor placement focuses mainly on reduction of conductor losses [10-14]. Currently little work exists on placement of energy storage devices. The work of Celli et al and Geth et al focuses on placement of energy storage on a distribution system [15], [16]. The former supports non-radial distribution systems, but does not consider voltage regulation. The latter takes into account voltage regulation, but does not handle non-radial distribution systems. Because of the general and difficult problem formulation, both authors resort to using a genetic algorithms approach to solve the problem. This has the disadvantage that the ESU sizes are constrained to a discrete range of values. The proposed method places energy storage in order to meet voltage regulation requirements in conjunction with smart PV inverters. The method used is simulated annealing to determine placement of energy storage units, with an inner optimal power flow (OPF) determining the necessary power ratings of each ESU for each placement considered. The method has several appealing properties – it does not have the limitations of analytical or dynamic programming methods. These include: the cost function used can include both a fixed and variable component, negative real and reactive power flows are supported, the full, nonlinear set of electrical network equations is supported, and non-radial distribution systems are supported. A disadvantage of the OPF method used is that it works only at a single time step – it is not possible to consider state-of-charge balance in this case. However, for the voltage regulation problem considered this is not necessary, as it is only needed to verify that the battery used has enough capacity to maintain voltage regulation during peak loading conditions.

This paper is divided into the following sections: section II describes the method used. Section III describes the problem considered – an actual feeder. Section IV presents an analysis of the results obtained, and verifies that the placement solution will maintain voltage regulation within

limits during discharging, charging, and standby conditions, as well as satisfying the energy capacity limitations of the battery.

III. PLACEMENT OF THE ENERGY STORAGE UNITS

The placement problem consists of placing a small number of energy storage units at particular busses in a distribution system. Because there is a fixed cost to placing an ESU, similar to shunt capacitors, a smaller number of units is favored [10]. By contrast, a large number of nodes will have smart PV inverters, reflecting the proliferation of rooftop and pole-mounted PV systems. The objective of the placement problem is to minimize the cost of installing the energy storage while meeting voltage regulation constraints. The cost of installing the energy storage is as follows:

$$c = \sum_{n=1}^{N} (c' S_n^{esu} + c_0 e_n). \tag{1}$$

The cost of installing each ESU at bus n consists of a fixed installation cost c_0 plus a component that depends on the capacity of the energy storage unit c'. The effect of this piecewise linear cost function is that it is more cost-effective to have a smaller number of larger energy storage units, as a lesser number of fixed installation costs are incurred. The problem is subject to the following constraints:

$$(P_n^{esu})^2 + (Q_n^{esu})^2 \leq (S_n^{esu})^2, \tag{2}$$

$$0.95V_{rated} \leq V_n \leq 1.05V_{rated}. \tag{3}$$

The first, an inequality constraint, represents the maximum power rating of the ESU power conversion system. Because this is a nonlinear constraint, it is difficult to work with. Observing

that the analysis only takes place during peak load conditions when the energy storage is outputting only real power, this constraint con be eliminated so that

$$P_n^{esu} = S_n^{esu}, \tag{4}$$

$$Q_n^{esu} = 0. \tag{5}$$

The new cost function is now of the form:

$$c = \sum_{n=1}^{M} (c' P_n^{esu} + c_0 e_n), \tag{6}$$

This work uses simulated annealing in conjunction with a set of rule-based placement heuristics that speed up convergence by favoring moves that are better based on knowledge of the system. The simulated annealing approach makes use of the following moves:

(1) *Add*: Add an ESU at a particular bus;

(2) *Delete*: Delete an ESU from a particular bus; and

(3) *Swap*: Move an ESU to a different bus.

Each type of move is selected based on a probability. Given that there are a small number of energy storage units on the distribution system, the *swap* move is favored with a probability of 70%, versus 15% each for the *add* and *delete* moves. Which busses to use for the moves are selected randomly, but with a bias based on rules. These rules make use of prior knowledge of the system, such as how an expert human operator would use when approaching the problem by hand. These rules include:

(1) Place the energy storage at the busses with the lowest voltages

(2) Place the energy storage at busses that are far from the substation (in terms of impedance)

(3) Place the energy storage at busses that are near loads (in terms of impedance).

The placement rules take into account rules 1 and 2 by weighting the busses in terms of three criteria. The particular criterion used for the move is chosen randomly and uniformly. These criteria include:

(1) Bus voltage;

(2) Bus real power demand; and

(3) Bus reactive power demand

The probabilities are selected as follows: First, the weighting δ_n for each bus n is selected based on the criteria used for weighting and whether or not an ESU is present at the bus under consideration, illustrated in Table 1. An uncertainty factor u is then added to the weighting and it is normalized to produce a probability:

$$\rho_n = \frac{(\delta_n + u)}{|\delta_n + u|}. \tag{7}$$

Depending on the move, a bus is selected randomly from the set of empty busses, the set of busses with an ESU present, or both. The trial solution produced by the move is then used as the input to an OPF to see if it is feasible in terms of voltage regulation and what is the resulting cost of placing energy storage. If the solution is not feasible, it is never accepted.

TABLE 1. WEIGHTING SELECTION FOR ESU PLACEMENT

Criteria	**No ESU at bus n**	**ESU at bus n**
Voltage	$\delta_n^{V0} = \frac{(\max V - V_n)}{(\min V - V_n)}$	$\delta_n^{V1} = \frac{(\max V - V_n)}{(\min V - V_n)}$
Real Power	$\delta_n^{P0} = \frac{(P_n - \min P)}{(\max P - P_n)}$	$\delta_n^{P1} = \frac{(P_n - \min P)}{(\max P - P_n)}$
Reactive Power	$\delta_n^{Q0} = \frac{(Q_n - \min Q)}{(\max Q - Q_n)}$	$\delta_n^{Q1} = \frac{(Q_n - \min Q)}{(\max Q - Q_n)}$

Otherwise, the solution is always accepted if it results in a lower cost than the current best cost. If the solution is feasible but the cost is equal to or greater than the current best cost, the solution is accepted with probability

$$e^{-\Delta c/T_k}, \tag{8}$$

where $\Delta c = c^* - c_k$, the difference between the trial solution and current solution. This serves to allow the algorithm to recover from local minima. At each iteration the temperature is reduced according to the cooling rate so

$$T_{k+1} = \alpha T_k. \tag{9}$$

The algorithm stops when the cost function has converged or the maximum number of iterations has been exceeded.

IV. SCHEDULING AND IMPACT ON PROFITABILITY

With the placement of the energy storage units selected, the next step is to evaluate if the use of energy storage for voltage regulation is feasible, and if so, what its impact on the profitability of the energy storage is. The main use of the energy storage is for energy arbitrage. The application of energy storage considered is a commercial customer that purchases electricity using a time-of-use rate. The customer uses the ESU in order to reduce its cost of electricity or generate profit in conjunction with TOU pricing. In order to maximize profit however, it is needed to select the necessary battery capacity, and the charge/discharge schedule. The power rating of the inverter for each ESU is determined in section II. A linear optimization method is used for this.

The objective of the linear optimization method is to determine the optimal capacities and charge/discharge schedule for an ESU, given a battery chemistry and pricing structure. Revenue

from ancillary services is not considered, the constant-Ah battery lifetime model is used [11], and the cost of electricity increases at a fixed rate during the project lifetime. Furthermore, the method makes the assumptions addressed below:

The constant-Ah model specifies that the lifetime of a battery, in terms of Ah or Wh throughput, is roughly independent of the depth-of-discharge [11]. This is accomplished by considering a battery with rated energy capacity E_{rated}. At each measured depth of discharge the battery has the following energy throughput to failure

$$E_f = DN_f. \tag{10}$$

For each depth of discharge the throughput to failure is approximately constant. Dividing E_f by E_{rated} gives the normalized energy throughput to failure

$$E_{f0} = E_{failure}/E_{rated}. \tag{11}$$

Fig. 1 illustrates the constant-Ah model applied for the case of the East Penn 8G8D lead-acid battery [13]. Throughout the range of D, E_f varies by only a small amount.

IV.A. Optimization Objective

Net present value (NPV) is a method for measuring the value of pursuing a project that takes into account the time value of money [14]. It is useful for comparing the benefit of pursuing different project options. The project is assumed to last Y years. The NPV of the project is then given by

$$NPV = \sum_{y=0}^{Y} \frac{a(y)}{(1+i)^y}. \tag{12}$$

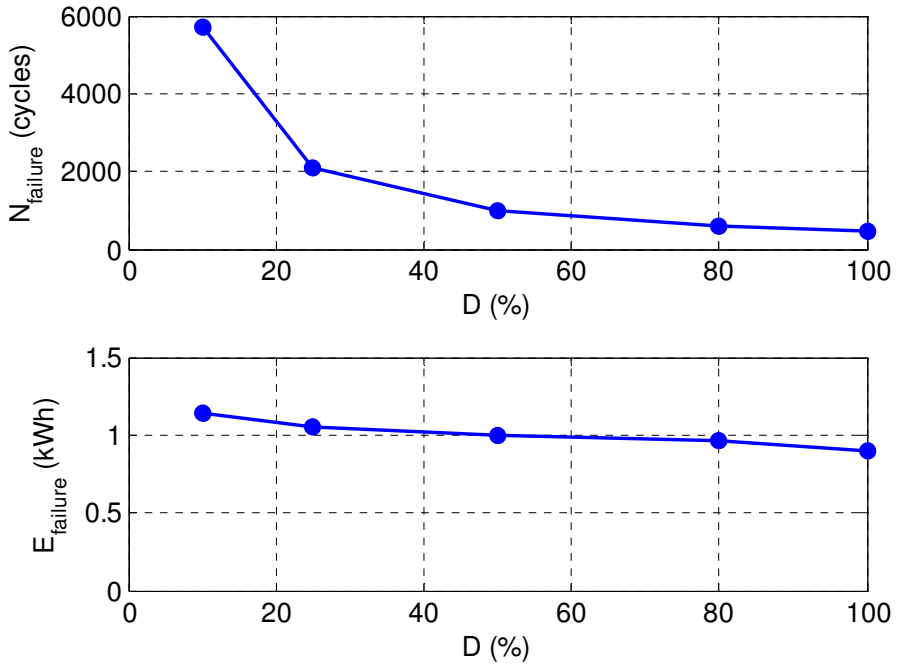

Fig. 1. Cycle life and energy throughput vs. depth of discharge for the East Penn 8G8D lead-acid battery.

Because the rate structure does not change over the project life, if the rate structure increases at rate α,

$$a(y) = (1+\alpha)^{y-1} r_1^{yearly}. \tag{13}$$

Additionally, the denominator of the summation for year 0 is 1. Therefore, the NPV can be broken up for either the case of fixed rate or increasing rate into two terms

$$NPV = a_0 + a_r, \tag{14}$$

where $a_0 = c_0$, the initial cost of the ESU, and

$$a_r = \sum_{y=1}^{Y} \frac{c_{om} + (1+\alpha)^{y-1} r_1^{yearly}}{(1+i)^y}, \tag{15}$$

where c_{om} is the yearly operation and maintenance (O&M) cost of the ESU, and r_1^{yearly} is the revenue produced by the ESU at the end of year one. Separating terms and substituting,

$$NPV = -c_0 + k_r r_1^{yearly} - k_c c_{om} \tag{16}$$

$$k_r = \sum_{y=1}^{Y} \frac{(1+\alpha)^{y-1}}{(1+i)^y} \tag{17}$$

$$k_c = \sum_{y=1}^{Y} \frac{1}{(1+i)^y}. \tag{18}$$

This is used to obtain the following cost function for the optimization problem

$$c = c_0 + k_r r_1 - k_c c_{om} \tag{19}$$

$$c_0 = c_{conv} + c_{siting} + c' E_{rated}\,. \tag{20}$$

Different rate structures are considered depending on the season. In this case, there are $K = 2$ different seasons, one for winter and one for summer pricing. Each price structure has M_k different time periods. The daily profit and variable operating cost for season k is

$$r_k^{daily} = \sum_{m=1}^{M_k} \left(c_i + c_{k,m}^{elec}\right) \Delta t_{k,m} p_{k,m}. \tag{21}$$

The yearly profit is then

$$r_1^{yearly} = \sum_{k=1}^{K} d_k r_k^{daily}. \tag{22}$$

For the purpose of the optimization, the output power is broken up into the discharge power and charging power, respectively, so $p_{k,m} = p_{k,m}^d - p_{k,m}^c$. The charging and discharging powers for each chemistry n are

$$p_{k,m}^{d} = \sum_{n=1}^{N} p_{k,m}^{d}, \tag{23}$$

$$p_{k,m}^{c} = \sum_{n=1}^{N} p_{k,m}^{c}. \tag{24}$$

IV.B. Method Constraints

Taking into account the round-trip efficiency of the battery chemistry using a discrete-time formulation [7], the state of charge (SoC) of each battery is

$$E_{k,m+1} = E_{k,m+1} + \Delta t_{k,m}\left(\eta p_{k,m}^{c} - p_{k,m}^{d}\right). \tag{25}$$

At each time step, the battery SoC $E_{k,m}$ is constrained to be less than the rated capacity of the battery, so

$$0 \leq E_{k,m} \leq E_{rated}. \tag{26}$$

The lifetime of the battery must not be violated

$$Y \sum_{k=1}^{K} d_k \sum_{m=1}^{M} \Delta t_{k,m} p_{k,m}^{d} \leq E_{f0} E_{rated}. \tag{27}$$

The last constraint depends on the requirement for voltage regulation

$$p_{k,m} \geq p_{k,m}^{v}, \tag{28}$$

Representing the power demanded of the energy storage unit to maintain voltage regulation within limits during the current load condition. This can be set up as a linear optimization problem [15].

V. PROBLEM SETUP

The problem considered is an eleven-node distribution feeder in central Arkansas with feeder parameters given below in Table 2 and Table 3. This is illustrated in Fig. 2. The method is validated using the dataset of Celli in order to verify that the method is applicable to non-radial systems, illustrated in Fig. 3 [16]. This dataset uses a trunk feeder which is fed by two substations. In order to make the dataset applicable to the voltage regulation problem here, impedances are increased by a factor of 10. The total voltage difference on the Arkansas feeder is within ±5%, so voltage regulation can be handled using a tap changer. However, if conservative voltage reduction (CVR) is to be used, the requirements for voltage regulation are more stringent [17]. Using energy storage to assist with voltage regulation during CVR is an appealing option, as this occurs during peak load (and therefore peak price) conditions when the energy storage would likely be operating anyways if purely economic scheduling were to be used, as in [18].

TABLE 2. FEEDER BRANCH PROPERTIES

From Branch	To Branch	Resistance (Ω)	Reactance (Ω)
3	4	0.29	0.62
4	5	0.17	0.35
5	6	0.09	0.19
6	7	0.42	0.90
7	8	0.22	0.47
8	9	0.96	0.78
9	10	0.63	0.51
10	11	0.90	0.73

TABLE 3. FEEDER BUS PROPERTIES

Bus	Real Power (kW)	Reactive Power (kVAr)
3	350	200
4	450	200
5	400	250
6	1700	1100
7	2000	1000
8	800	400
9	400	300
10	100	100
11	100	50

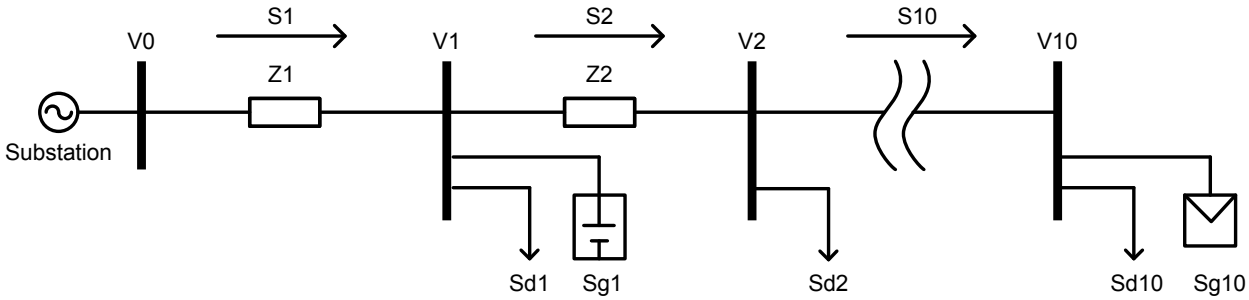

Fig. 2. Eleven-node distribution feeder under study.

The customer uses a three-level time-of-use profile as shown in Fig. 4. This uses separate rates for summer and winter seasons, shown in Table 4 and Table 5, taken from [19]. Fig. 5 shows the optimal charge/discharge schedule of the energy storage without power constraints stemming from voltage regulation. Noting that the ES is discharged during the peak period, CVR is also applied during that time.

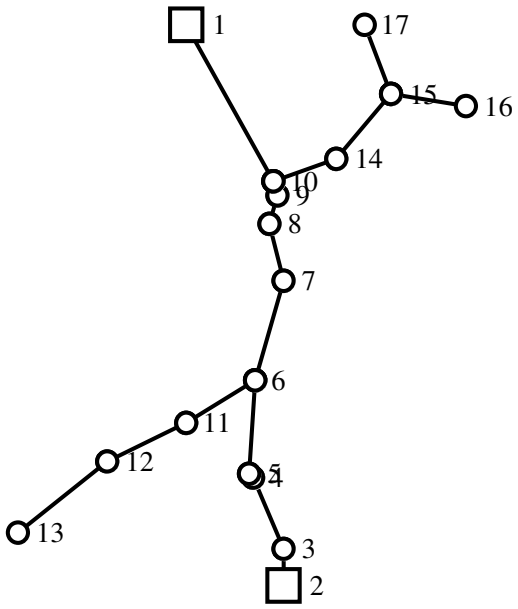

Fig. 3. Distribution system of Celli at al [16].

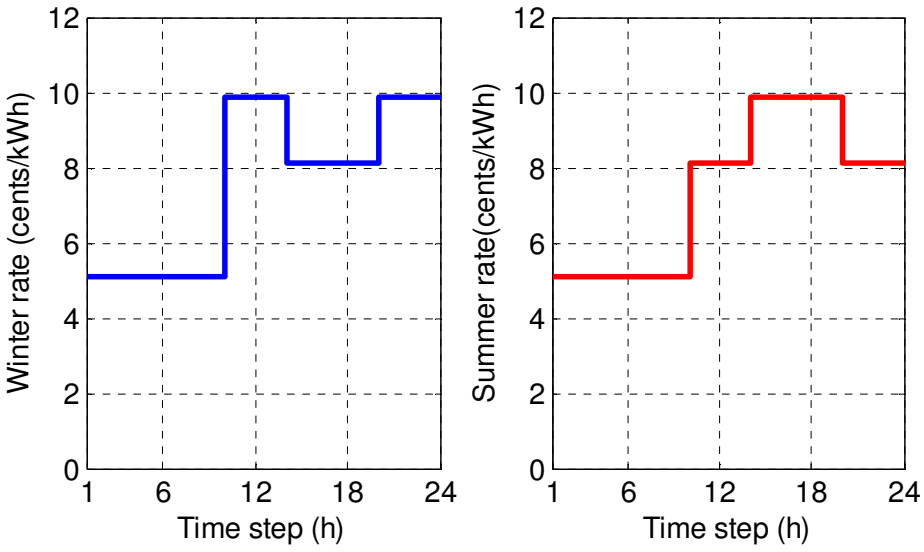

Fig. 4. TOU pricing structure for winter and summer.

TABLE 4. TOU RATE FOR WINTER

Time	Period	Cost (¢/kWh)
7 am to 11 am	On-peak	9.9
11 am to 5 pm	Mid-peak	8.1
5 pm to 9 pm	On-peak	9.9
9 pm to 7 am	Off-peak	5.1

TABLE 5. TOU RATE FOR SUMMER

Time	Period	Cost (¢/kWh)
7 am to 11 am	Mid-peak	8.1
11 am to 5 pm	On-peak	9.9
5 pm to 9 pm	Mid-peak	8.1
9 pm to 7 am	Off-peak	5.1

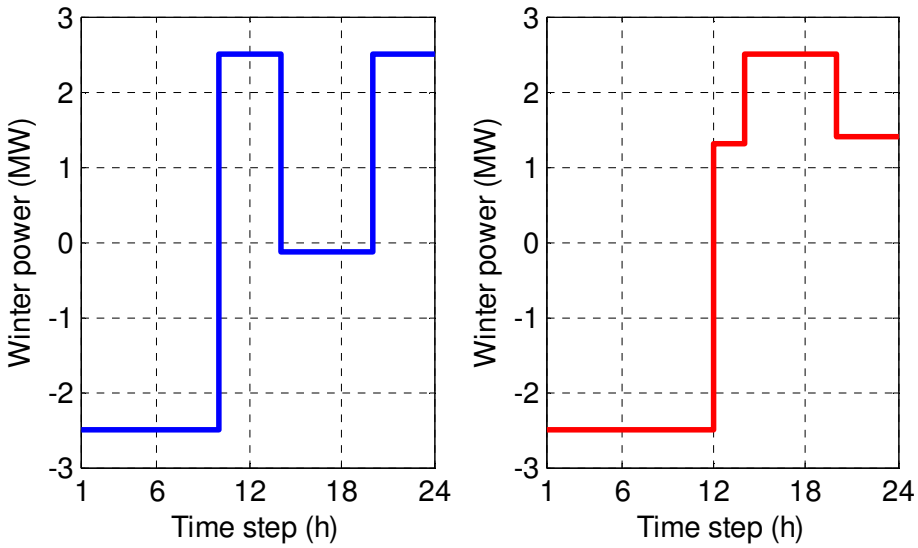

Fig. 5. Optimal economic schedule for energy storage.

TABLE 6. PARAMETERS FOR THE PROBLEM SETUP

Parameter	Value
Converter power rating	2.5 MW
Converter cost	$150/kW
Siting	$100/kW
Subsidization of initial cost	30%
O&M	1%
Converter efficiency	97 %
Design lifetime	20 years
MARR	8 %

VI. NUMERICAL RESULTS AND ANALYSIS

The outcome of the method is to place a single ESU at bus 10 with rated power of 730 kW (with no PV 1.3 MW of ES at bus 9 is needed). Fig. 6 shows how the method improves the voltage profile on the feeder during the worst-case conditions – in this case peak load with CVR applied *and* no real power output from the PV, lowering the voltage at the beginning of the feeder to 1.02 pu. During standby and charging periods, the voltage at the beginning of the feeder is raised to 1.05 pu. For charging, the ESU can charge up to 1.22 MW without violating voltage constraints. This means that the same ESU schedule can be used as when not considering the provision of voltage regulation. For the case of Celli et al's system, the energy storage units are placed at busses 12 and 16, one less than Celli et al. The required power ratings are about 50% greater than those determined by Celli et al.

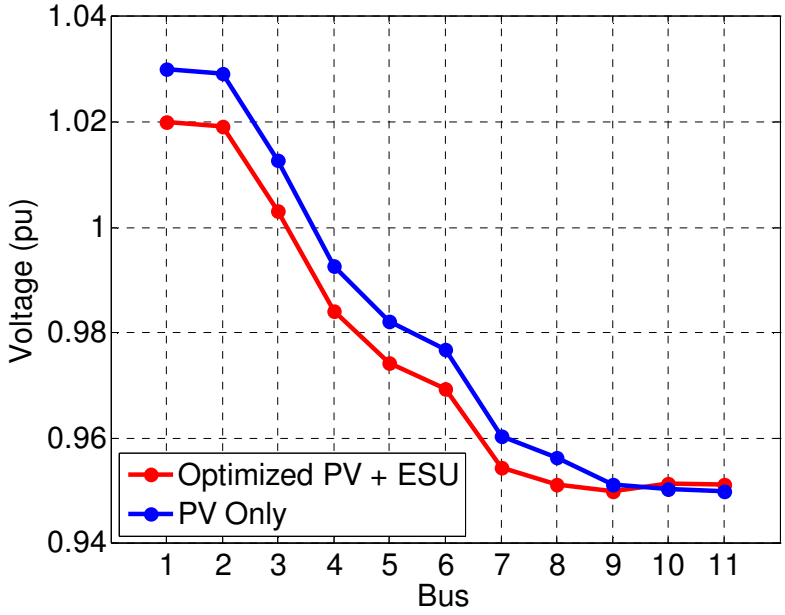

Fig. 6. Improvement of the feeder voltage profile.

VII. CONCLUSIONS

Energy storage in conjunction with smart PV inverters is shown to aid in demand management by allowing increased use of CVR through improving the voltage profile on a feeder. To maintain good voltage regulation on the feeder, busses near the end of the feeder as opposed to busses near load centers are favored for placement of the energy storage. Encouraging for the use of energy storage, using it to maintain a voltage profile on a feeder during peak loading conditions does not require it to deviate from the optimum schedule for economic self-scheduling. Additionally, allowing the use of smart PV inverters reduces the amount of energy storage required in order to maintain voltage regulation on the feeder.

REFERENCES

[1] L. Mears, H. Gotschall, and H. Kamath, "EPRI-DOE handbook of energy storage for transmission and distribution applications," Tech. Rep. 1001834, EPRI, 2003.

[2] S. M. Schoenung and W. Hassenzahl, "Long vs. short-term energy storage: Sensitivity analysis," Tech. Rep. SAND2007-4253, Sandia National Laboratories, 2007.

[3] R. A. Shayani and M. A. G. de Oliveira, "Photovoltaic generation penetration limits in radial distribution systems," *IEEE Trans. Power Syst.*, vol. PP, no. 99, 2010.

[4] W. T. Jewell, R. Ramakumar, and S. R. Hill, "A study of dispersed photovoltaic generation on the PSO system," *IEEE Trans. Energy Convers.*, vol. 3, no. 3, pp. 473-478, 1988.

[5] F. Giraud and Z. M. Salameh, "Analysis of the effects of a passing cloud on a grid-interactive photovoltaic system with battery storage using neural networks," *IEEE Trans. Energy Convers.*, vol. 14, no. 4, pp. 1572-1577, 1999.

[6] Y. Ueda, K. Kurokawa, T. Tanabe, K. Kitamura, and H. Sugihara, "Analysis results of output power loss due to the grid voltage rise in grid-connected photovoltaic power generation systems," *IEEE Trans. Ind. Electron.*, vol. 55, no. 7, pp. 2744-2751, 2008.

[7] B. Seal, "Specification for Smart Inverter Interactions with the Electric Grid Using International Electrotechnical Commission 61850," Standard 1021674, Knoxville, TN: Electric Power Research Institute, 2010.

[8] K. Turitsyn, P. Sulc, S. Backhaus, and M. Chertkov, "Local control of reactive power by distributed photovoltaic generators," in *2010 1st IEEE Int. Conf. Smart Grid Commun. (SmartGridComm)*, pp. 79-84.

[9] J. W. Smith, W. Sunderman, R. Dugan, and B. Seal, "Smart inverter volt/var control functions for high penetration of PV on distribution systems," in *Proc. 2011 IEEE/PES Power Syst. Conf. and Exposition (PSCE)*, pp. 1-6.

[10] H. N. Ng, M. M. A. Salama, and A. Y. Chikhani, "Classification of capacitor allocation techniques," *IEEE Trans. Power Del.*, vol. 15, no. 1, pp. 387-392, 2000.

[11] M. Baran and F. F. Wu, "Optimal sizing of capacitors placed on a radial distribution system," *IEEE Trans. Power Del.*, vol. 4, no. 1, pp. 735-743, 1989.

[12] M. E. Baran and F. F. Wu, "Optimal capacitor placement on radial distribution systems," *IEEE Trans. Power Del.*, vol. 4, no. 1, pp. 725-734, 1989.

[13] R. Niemi and P. D. Lund, "Decentralized electricity system sizing and placement in distribution networks," *Applied Energy*, vol. 87, no. 6, pp. 1865-1869, 2010.

[14] F. Pilo, G. Celli, S. Mocci, and G. G. Soma, "Multi-objective programming for optimal DG integration in active distribution systems," in *Proc. 2010 IEEE Power and Energy Soc. General Meeting*, pp. 1-7.

[15] F. Geth, J. Tant, E. Haesen, J. Driesen, and R. Belmans, "Integration of energy storage in distribution grids," in *2010 Power and Energy Soc. General Meeting*, pp. 1-6.

[16] G. Celli, S. Mocci, F. Pilo, and M. Loddo, "Optimal integration of energy storage in distribution networks," in *Proc. IEEE PowerTech 2009*, pp. 1-7.

[17] C. A. McCarthy and J. Josken, "Applying capacitors to maximize benefits of conservation voltage reduction," in *Proc. 2003 Rural Electr. Power Conf.*, pp. C4-1-C4-5.

[18] S. J. Kazempour, M. Hosseinpour, and M. P. Moghaddam, "Self-scheduling of a joint hydro and pumped-storage plants in energy, spinning reserve and regulation markets," in *Proc. 2009 IEEE Power and Energy Soc. General Meeting*, Calgary, Canada, 2009, pp. 1-8.

[19] "Time-of-Use Prices." [Online]. Available: http://www.ieso.ca/imoweb/siteshared/tou_rates.asp?sid=ic.

APPENDIX A: CERTIFICATION OF FIRST AUTHOR

I hereby certify that Arthur K. Barnes is first author of the article this chapter is based on and has completed at least 51% of the work described in the article.

Juan Carlos Balda

Signature _____

Date _____

APPENDIX B: RELEASE FOR USE IN DISSERTATION

Thesis / Dissertation Reuse

The IEEE does not require individuals working on a thesis to obtain a formal reuse license, however, you may print out this statement to be used as a permission grant:

Requirements to be followed when using any portion (e.g., figure, graph, table, or textual material) of an IEEE copyrighted paper in a thesis:

1) In the case of textual material (e.g., using short quotes or referring to the work within these papers) users must give full credit to the original source (author, paper, publication) followed by the IEEE copyright line © 2011 IEEE.

2) In the case of illustrations or tabular material, we require that the copyright line © [Year of original publication] IEEE appear prominently with each reprinted figure and/or table.

3) If a substantial portion of the original paper is to be used, and if you are not the senior author, also obtain the senior author's approval.

Requirements to be followed when using an entire IEEE copyrighted paper in a thesis:

1) The following IEEE copyright/ credit notice should be placed prominently in the references: © [year of original publication] IEEE. Reprinted, with permission, from [author names, paper title, IEEE publication title, and month/year of publication]

2) Only the accepted version of an IEEE copyrighted paper can be used when posting the paper or your thesis on-line.

3) In placing the thesis on the author's university website, please display the following message in a prominent place on the website: In reference to IEEE copyrighted material which is used with permission in this thesis, the IEEE does not endorse any of [university/educational entity's

name goes here]'s products or services. Internal or personal use of this material is permitted. If interested in reprinting/republishing IEEE copyrighted material for advertising or promotional purposes or for creating new collective works for resale or redistribution, please go to http://www.ieee.org/publications_standards/publications/rights/rights_link.html to learn how to obtain a License from RightsLink.

If applicable, University Microfilms and/or ProQuest Library, or the Archives of Canada may supply single copies of the dissertation.

CHAPTER FIVE

PLACEMENT OF DISTRIBUTED ENERGY STORAGE VIA MULTIDIMENSIONAL SCALING AND CLUSTERING

Arthur Barnes and Juan Carlos Balda

A.K. Barnes and J.C. Balda, "Placement of distributed energy storage via multidimensional scaling and clustering," in *International Conference on Renewable Energy Research and Applications (ICRERA)*, Milwaukee, WI, 2014.

***Abstract* — Energy storage has long been proposed at the distribution level, where it can provide additional benefits via ancillary services. This work studies how to place energy storage units (ESU) on a distribution feeder in the most cost-effective manner while still meeting voltage regulation requirements. The feeder also has photovoltaic (PV) generation, and the PV ability to supply reactive power is considered. The placement of the ESU is performed via a fast heuristic, in which multidimensional scaling (MDS) is used to transform the combinatorial placement problem into a continuous-valued problem by mapping buses to points in a space. In the new space, clustering algorithms can be applied to determine the ESU locations from a set of candidate locations. The method reduces computation time by an order of magnitude, allowing for various distribution feeder configurations to be quickly compared.**

***Keywords*—Energy storage, photovoltaic systems, renewable energy sources, optimization, clustering methods**

The authors are grateful for the financial assistance by the industry members of Grid-Connected Advanced Power Electronics Systems, an NSF I/UCRC.

I. INTRODUCTION

This paper focuses on ESU used principally for providing frequency regulation, but also for supplying reserve power during periods of high demand. The case addressed is a distribution system operator (DSO) that has made the purchase of a fixed amount of energy storage in terms of MWh capacity and "smart" PV inverters. The DSO seeks to determine the best solution in terms of numbers of ESU and "smart" PV units, their power ratings and placements on the system.

The "smart" PV inverter is a concept proposed by EPRI [1] that has the ability to draw or inject reactive power based on a power vs. voltage curve, allowing it to assist with voltage regulation. Because of the "smart" PV functions, it is desirable to integrate them with the ESU at the same time. When determining placement, the scenario of ESU and "smart" PV providing reserve power during peak load conditions is examined. The total load on the distribution feeder as viewed from the distribution substation can be lowered by appropriately placing the ESU and PV to flatten the voltage profile on the feeder, thereby allowing for conservation voltage reduction (CVR) to be applied [2]. CVR refers to lowering the overall voltage on the system, (usually by the substation transformer tap settings), in order to reduce overall load demand by taking advantage of the increasing power vs. voltage curve of the system load. However, dispersing the ESU on a distribution feeder as opposed to placing them at the substation will impact their ability to provide frequency regulation services.

This placement problem is closely related to that of placing distributed generation and shunt capacitors. The existing methods for placing these devices are categorized as: analytical,

numerical optimization, heuristic search, and randomized search. The most common approach is genetic algorithms (GA), a form of randomized search which comes in both pure and hybrid optimal power flow (OPF) forms [3]. In the latter, the GA only selects the ESU locations, while an inner OPF selects their required power ratings, reducing the size of the GA search space and improving convergence time.

The placement method proposed in this work is a heuristic search that takes advantage of the observation that the number of ESU to be placed is small when compared to the total number of buses in the distribution feeder. The placement problem is then converted from a combinatorial problem to a continuous-valued problem by transforming the ESU bus locations into points in a continuous space with MDS. The ESU positions are then calculated with a clustering algorithm in the new space. By contrast, it is assumed that the power ratings of the "smart" PV installations are low as is the case with rooftop installations, and many of them can be placed on the feeder.

Although hierarchical clustering algorithms exist that can operate over a pairwise distance matrix, they suffer from sensitivity to initial conditions. The MDS algorithm allows classical k-means type algorithms to be applied, which are much less sensitive [4]. Additionally, it comes at a low cost in terms of both computational and programming burden, as it can be implemented in two lines in a high-level language with a set of matrix multiplications and eigenvector decomposition.

Clustering for placement reduces computational complexity over both pure and hybrid GA approaches, because it only runs a computationally intensive OPF twice, as opposed to the 10s to 100s of OPF necessary for GA [5]. This enables a distribution feeder designer to quickly evaluate several different ESU/"smart" PV configurations in a hypothetical software application by clicking a toolbar button.

The remaining sections of this paper describe how the method operates, illustrate its application to place ESU on a distribution feeder, evaluate the benefits of the ESU, and compare its performance against an existing GA approach.

II. CALCULATING CANDIDATE LOCATIONS AND POWER INJECTIONS USING AN OPF

The ESU inject power to increase frequency towards 60 Hz (referred to here as up-regulating) or supply power during critical peaks. They also draw power to help reduce frequency towards 60 Hz (referred to here as down-regulating) and charge during off-peak times to account for losses. Thus, while it is desirable to place ESU where they make a large impact on the voltage regulation and power drawn by the feeder during critical peak load reduction and up-regulation, this placement is a hindrance when the ESU are to down-regulate or charge.

The problem objective is to minimize the cost of power delivered from the substation bus during periods of high demand, expressed as

$$\min. \sum_{t=1}^{N_t} C_t P_{1t}\,, \tag{1}$$

where t is the index of the current load/ESU/PV scenario, N_t is the number of scenarios, P_{1t} is the power supplied by the substation bus (bus 1) during the current scenario, and C_t is the relative cost of electricity supplied during the current scenario.

The problem is subject to several constraints, which are discussed in the remainder of this section. It is assumed that the ratio of the total power rating to the total energy capacity of the ESU is fixed at approximately 1:1 [6]. This means that the total energy capacity in MWh of energy storage purchased is equal to the total power rating of all ESU in MVA. Thus,

$$\sum_{n=1}^{N} S_n^{esu} \leq S_{tot}^{esu}, \tag{2}$$

where N is the number of buses, S_n^{esu} is the rated power of the ESU at bus n, and S_{tot}^{esu} is the total rated power of all the ESU in pu. For an optimal solution, the two terms in (2) will be equal. Similarly,

$$\sum_{n=1}^{N} S_n^{pv} \leq S_{tot}^{pv}, \tag{3}$$

where S_n^{pv} is the rated power of the PV inverter at bus n and S_{tot}^{pv} is the total rated power of all the PV inverters in MVA.

The apparent power scaling is a vector whose length is the number of scenarios included in the problem, where each element K_t^{esu} represents the fraction of rated power that each ESU operates at during the corresponding scenario. An equivalent element K_t^{pv} applies for the PV. The power scalings for ESU and PV are not included as decision variables because these quantities are typically determined by a scheduler independent of network constraints; this assumption represents current practice [7]. Similarly, power factors for ESU and PV are also not included.

Rather than having these quantities as decision variables, they are used as inputs to the problem. The power factors are not represented directly, but instead as the angle between voltage and current. For the ESU and PV, these are represented as ϕ_{nt}^{esu} and ϕ_{nt}^{pv}, respectively. The real and reactive powers for the ESU and PV are given by

$$P_{nt}^{esu} = K_t^{esu} S_n^{esu} \cos \phi_t^{esu} \tag{4}$$

$$Q_{nt}^{esu} = K_t^{esu} S_n^{esu} \sin \phi_t^{esu} \quad (5)$$

$$P_{nt}^{pv} = K_t^{pv} S_n^{pv} \cos \phi_t^{pv} \quad (6)$$

$$Q_{nt}^{esu} = K_t^{pv} S_n^{pv} \sin \phi_t^{pv} . \quad (7)$$

The cost of installing the ESU is

$$c = \sum_{n=1}^{N} (c' S_n^{esu} + c_0 u_n), \quad (8)$$

where c is the total cost of placing the ESU in U.S. dollars, c' is the incremental cost of placing an ESU in dollars per pu, c_0 is the fixed installation cost of placing an ESU, and u_n is a binary variable indicating if an ESU is placed at bus n.

These quantities are not used again, except to highlight that the cost of installing each ESU at bus n consists of a fixed installation cost (c_0) plus a component that depends on the capacity of the ESU (c'). The effect of this piecewise linear cost function is that it is more cost-effective to have a smaller number of larger ESU, as less fixed installation cost is incurred. In this study, the PV does not have any such fixed cost, and there is no incentive to aggregate PV installations.

Including a nonlinear cost makes the problem considerably harder, since it now has a mixed-integer nonlinear formulation [3]. In order to circumvent this issue, the OPF formulation is only used to select candidate buses for ESU placement. The placement is solved as a separate problem, using the candidate buses and the necessary power injections as inputs to a clustering algorithm which determines the actual ESU power ratings and locations. The clustering algorithm requires that the number of ESU be selected beforehand. However, as this number is small, it is reasonable to determine its optimal value by an exhaustive iteration over a fixed range from 0 to a maximum number of ESU N_{max}^{esu}.

Using a static load model, which is discussed later in more detail, the power injections into each bus are represented as

$$P_{nt} = P_{nt}^{esu} + P_{nt}^{pv} - P_{nt}^{d} \tag{9}$$

$$Q_{nt} = Q_{nt}^{esu} + Q_{nt}^{pv} - Q_{nt}^{d} \tag{10}$$

$$P_{nt}^{d} = K_t^d P_n^{d0} |V_{nt}|^{\beta_p} \tag{11}$$

$$Q_{nt}^{d} = K_t^d Q_n^{d0} |V_{nt}|^{\beta_q}. \tag{12}$$

In the above, P_{nt} and Q_{nt} are the real and reactive powers supplied by bus n during scenario t. P_{nt}^d and Q_{nt}^d are the load real and reactive powers for bus n. P_n^{d0} and Q_n^{d0} are the rated load real and reactive power demands for bus n. K_t^d is the feeder loading during the current scenario t. V_{nt} is the voltage at bus n during scenario t. The exponents β_p and β_q represent the relationship between voltage and load power, discussed in more detail later. The power flow constraints are represented as

$$P_{nt} = \left(P_{nt}^{esu} + P_{nt}^{pv} - P_{nt}^{d}\right) - \sum_{m=1}^{N} |V_{nt}||V_{mt}| y_{mn} \cos(\theta_{mn} - \delta_{mt} - \delta_{nt}) \tag{13}$$

$$Q_{nt} = \left(P_{nt}^{esu} + P_{nt}^{pv} - P_{nt}^{d}\right) - \sum_{m=1}^{N} |V_{nt}||V_{mt}| y_{mn} \sin(\theta_{mn} - \delta_{mt} - \delta_{nt}) \tag{14}$$

$$S_n^{esu} \leq S_{max}^{esu} \tag{15}$$

$$V_{min} \leq |V_{nt}| \leq V_{max} \tag{16}$$

$$V_{max} = 1.05 V_{base} \tag{17}$$

$$V_{min} = 0.95 V_{base}. \tag{18}$$

In the above, y_{mn} is the magnitude of complex impedance matrix **Y**, while θ_{mn} is the phase of the impedance between buses m and n. The variable δ_{nt} is the phase of the voltage at bus n during scenario t. V_{min} and V_{max} are the minimum and maximum allowable voltage magnitudes on the feeder respectively, while V_{base} is the base voltage.

For this OPF, this exponential load model is used

$$P_{nt}^{d} = K_t^d P_n^{d0} |V_{nt}|^{\beta_p}$$

$$Q_{nt}^{d} = K_t^d Q_n^{d0} |V_{nt}|^{\beta_q}.$$

In the above, P_{nt}^{d} and Q_{nt}^{d} are the load real and reactive power demands. The term $|V_{nt}|$ is the voltage magnitude in pu seen by the load. The terms $\beta_p = 1.38$ and $\beta_q = 3.32$ [8]. Again, P_{nt}^{d0} and Q_{nt}^{d0} are the rated real and reactive power demands of the load at a voltage of 1 pu, while K_t^d is the feeder loading during the current scenario t. In order to calculate the required amount of power injection at each candidate bus, a nonlinear constrained optimizer is used on the problem, in this case `fmincon()` from the MATLAB™ optimization toolbox.

III. SELECTION OF THE ESU LOCATIONS

In this particular problem, the key idea is that it is not desirable to place ESU at buses that are very "close" to one another, which in this context means that the impedance between them is low. To determine how to best combine the candidate locations into a smaller number of well-spaced ESU, the candidate locations are mapped into a continuous space that is easier to work with than the original discrete locations. To accomplish this, dimensionality scaling methods are employed [9], [10]. However, even with the candidate locations mapped into a continuous space, the problem is still combinatorial in nature. Fortunately, the new problem space allows for the use of clustering methods, which represent a "good" suboptimal solution to the problem [4].

III.A. Multidimensional Scaling

The candidate buses are mapped to points in a q-dimensional space using MDS, a dimensionality reduction technique that is commonly used in the social sciences. It works by first calculating pairwise distances between each object (in this case, a bus) in a set (in this case, the M ESU candidate locations). The objects are then mapped to arbitrarily placed points in the q-dimensional space. The classical MDS (CMDS) algorithm is employed. It maps the objects using their pairwise distances onto a q-dimensional space. It does this by applying a pair of transformation matrices in order to convert the pairwise distance matrix **D** into a positive semidefinite matrix **B** of rank q. The matrix **B** is then used to produce matrix **W**, whose columns are the position vectors $\boldsymbol{w}_1, \boldsymbol{w}_2, \ldots, \boldsymbol{w}_M$.

The method is illustrated as follows:

First, the distance matrix **D** is transformed

$$\mathbf{B} = (\mathbf{I}_M - M^{-1}\mathbf{1}_M\mathbf{1}_M^T)\mathbf{A}(\mathbf{I}_M - M^{-1}\mathbf{1}_M\mathbf{1}_M^T). \tag{19}$$

In the above expression,

$$a_{nm} = \frac{1}{2}d_{nm} \tag{20}$$

$$\mathbf{1}_M = [1 \quad 1 \quad \cdots \quad 1]^T, \tag{21}$$

where a_{nm} and d_{nm} denote the elements of in the n^{th} row and m^{th} column of the matrices **A** and **D**, respectively. The term $\mathbf{I}_M$ is a $M \times M$ identity matrix. The q eigenvectors $\boldsymbol{v}_n$ corresponding to the nonzero eigenvalues λ_n of **B** are selected, i.e. those corresponding to

$$\mathbf{B}\boldsymbol{v}_n = \lambda_n\boldsymbol{v}_n, \qquad \lambda_n \neq 0. \tag{22}$$

These are concatenated into a new matrix

$$\mathbf{W} = \left[\boldsymbol{v}_1, \boldsymbol{v}_2, \ldots, \boldsymbol{v}_q\right]^T. \tag{23}$$

Each column $\boldsymbol{w}_n$ of $\mathbf{W}$ represents a point in the new space.

The essence of the method is that if each element of $\mathbf{A}$, a_{nm} is proportional to a distance metric d_{nm} calculated between objects n and m, then the Euclidean distance between columns $\boldsymbol{w}_n$ and $\boldsymbol{w}_m$ of $\mathbf{W}$ is also d_{mn}. Thus, by the definition of an Euclidean distance,

$$d_{nm} = \|\boldsymbol{w}_n - \boldsymbol{w}_m\|_2 . \tag{24}$$

It is important to realize however, that the distances, d_{nm}, *do not necessarily correspond to the distances between two points in an original space*, as is the case with both similarity scores on questionnaires and the impedance between two buses in a distribution feeder.

III.B. Clustering Algorithm

The goal of the clustering algorithm is to group together buses that are candidate locations. To perform the clustering, a number of clusters K (corresponding to the number of ESU to be placed) is selected as an input to the clustering algorithm. The requirements of the clustering algorithm are to assign each bus to a particular ESU and to select the bus that the units will be placed at. Hence, the objective of the clustering algorithm is to minimize the intra-cluster variance

$$J = \sum_{n \in \mathcal{D}_k} \|\boldsymbol{w}_n - \boldsymbol{\mu}_k\|^2 \tag{25}$$

where $\boldsymbol{w}_n$ is a point in cluster k, $\boldsymbol{\mu}_k$ is the centroid (or center of mass) of cluster k, and $\mathcal{D}_k$ is the set of points belonging to cluster k. A last issue is that the amount of ESU power injection at each bus is not identical. This could result in erroneous results if there is a bus with only a small amount of power injection and another bus with a large amount. To account for this, the k-means

algorithm is used [4], but the centroid calculation is modified to use the amount of power injection at each bus as a weight. In the original k-means algorithm, the centroids are calculated as

$$\boldsymbol{\mu}_k = \frac{1}{N_k} \sum_{n \in \mathcal{D}_k} \boldsymbol{w}_n, \tag{26}$$

where N_k is the number of points in cluster k. By contrast, in the modified algorithm, the centroids are calculated as

$$\boldsymbol{\mu}_k = \sum_{n \in \mathcal{D}_k} \gamma_n \boldsymbol{w}_n, \tag{27}$$

where the weighting γ_n is equal to

$$\gamma_i = \frac{S_n^{esu}}{\sum_{n \in \mathcal{D}_k} S_n^{esu}}. \tag{28}$$

To perform placement, the ESU are allocated to the bus nearest to their corresponding centroid. The power injections of each ESU candidate are then assigned to their corresponding ESU, as illustrated in Fig. 1.

IV. CASE STUDY AND NUMERICAL RESULTS

The proposed method is tested on the radial Italian rural distribution feeder given in [11] and illustrated in Fig. 2. There are two substations at buses 1 and 2, the load profile is shown in Fig. 3, and the parameters are listed in Tables I and II.

The total power rating of all the ESU to be placed is set at 1/10th the total feeder real power demand, while the total power rating of the "smart" PV to be placed is 1/40th the total feeder real power demand. Based on the results in [11], the number of ESU to be placed is 2. This is presented in Table III, along with other relevant inputs to the placement problem.

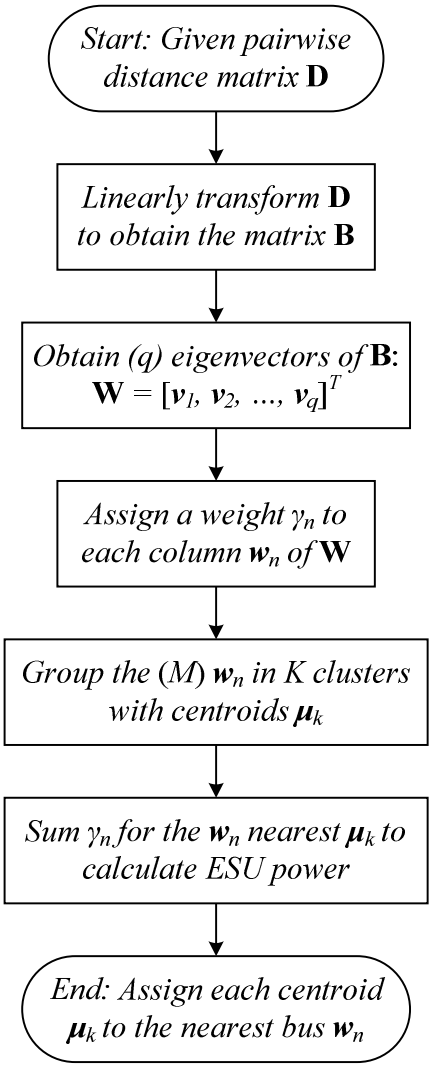

Fig. 1. Flowchart for the CMDS/clustering algorithm.

Five different scenarios were analyzed in placement. In addition to the base case without ESU or PV, a peak evening condition was selected for the objective. The ESU and PV are placed to minimize power demand from the feeder under this condition. As an evening case is used, the PV injects reactive power only. In addition, three other cases are included, which verify if the ESU is able to provide frequency regulation without causing flicker issues, as well as its ability to charge and discharge without violating voltage constraints. These scenarios are presented in Tables IV and V.

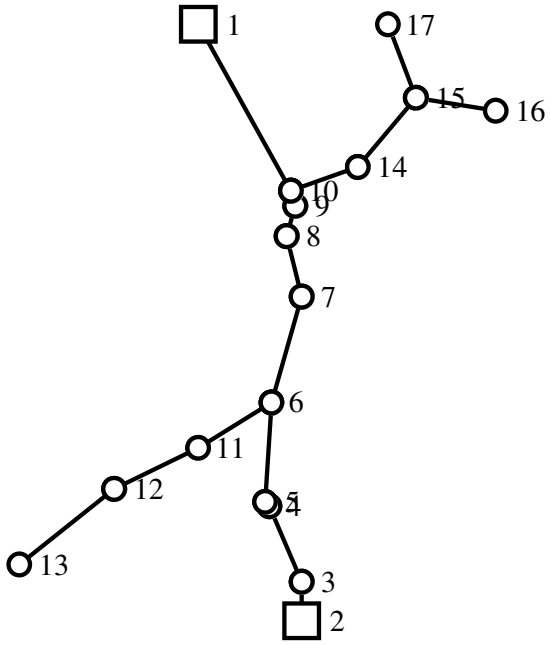

Fig. 2. Configuration of the feeder case study.

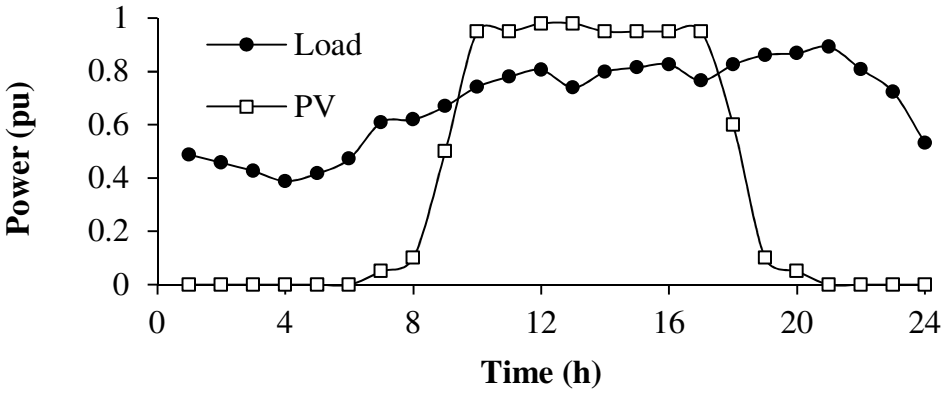

Fig. 3. Feeder average load and PV profile over one day.

TABLE I. BRANCH CONNECTIVITY AND IMPEDANCES

From	To	R	X
1	10	0.00169	0.00073
10	14	0.00676	0.00291
14	15	0.00024	0.00010
15	16	0.00507	0.00218
15	17	0.00566	0.00268
10	9	0.00338	0.00146
9	8	0.00217	0.00094
8	7	0.00048	0.00021
7	6	0.00435	0.00187
6	5	0.00483	0.00208
5	4	0.00580	0.00250
4	3	0.00386	0.00166
3	2	0.00531	0.00229
6	11	0.00435	0.00187
11	12	0.00435	0.00187
12	13	0.00966	0.00416

TABLE II. LOAD POWER AT EACH BUS

Bus Number	Power (kW)	Power Factor
1	0.00	0.00
2	0.00	0.00
3	90.00	0.90
4	100.00	0.90
5	320.00	0.90
6	90.00	0.90
7	83.67	0.90
8	420.00	0.90
9	60.00	0.90
10	90.00	0.90
11	0.00	0.00
12	600.00	0.88
13	50.00	0.71
14	550.00	0.71
15	500.00	0.90
16	400.00	0.90
17	0.00	0.00

TABLE III. CASE STUDY PARAMETERS

Parameter	Expression	Value
Base Voltage	V_{base}	20 kV
Base Power	S_{base}	2 MW
Substation 2 power	P_{2t}, Q_{2t}	$\frac{K_t^d}{6}\sum_{n=1}^{N} P_n^{d0}, \frac{1}{6}\sum_{n=1}^{N} Q_n^{d0}$
Number of ESU	K	2
Total ESU Power	S_{tot}^{esu}	$\frac{1}{10}\sum_{n=1}^{N} P_n^{d0}$
Total PV Power	S_{tot}^{pv}	$\frac{1}{40}\sum_{n=1}^{N} P_n^{d0}$
Minimum Voltage	V_{min}	0.95 pu
Maximum Voltage	V_{min}	1.05 pu
Cost	C_t	$1, \quad t = 1$ $0.1, \quad \text{otherwise}$

TABLE IV. DESCRIPTION OF EVALUATED SCENARIOS

Scenario	Load State	PV State	ESU State
0 (base)	Peak	Off	Off
1 (objective)	Peak	Inject Q	Discharge
2 (up-regulating)	Peak	Off	Discharge
3 (down-regulating)	Peak	Off	Charge
4 (up-regulating)	Off-Peak	Off	Discharge

TABLE V. LOAD, ESU AND PV PARAMETERS FOR EACH SCENARIO

Scenario	K_t^d	K_t^{esu}	ϕ_t^{esu}	K_t^{pv}	ϕ_t^{pv}
0 (base)	1.000	0.0	0	0	0.00
1 (objective)	1.000	1.0	0	1	$\pi/2$
2 (up-regulating)	1.000	1.0	0	0	0.00
3 (down-regulating)	1.000	1.0	π	0	0.00
4 (up-regulating)	0.454	1.0	0	0	0.00

Although the *average* feeder load does not reach 1.0 pu, a 1.0 pu peak load is selected as a worst case. To evaluate whether flicker is an issue, the maximum change in voltage

$$\Delta V = \max_n(|V_{n2}| - |V_{n3}|) \tag{29}$$

at any bus is measured between scenarios 2 (up-regulating) and 3 (down-regulating). Assuming a 4-s period in the regulation signal, any change lower than 1% is considered tolerable according to the worst case for the IEC-868 flicker curve [12], [13]. To evaluate if voltage regulation problems are caused during charging and discharging, scenarios 3 (peak load, up-regulating) and 4 (off-peak load, down-regulating) are studied.

To evaluate the performance improvement against competing methods, the placement problem is also performed with genetic algorithms, following the approach of the original analysis [11]. To more fairly compare against the proposed method, the chromosome encoding is changed so that the number of ESU to be placed is fixed, as illustrated in Fig. 4. Rather than encoding the ESU placement as a binary vector whose number of elements is the number of buses N, it is now encoded as an integer vector whose number of elements is the number of ESU to be placed K. Additionally, the parameters listed in Table VI are applied.

Tables VII-IX present placement results. The genetic algorithm was able to find the optimal placement after the first generation because of the small search space. However, the clustering-based placement is able to complete in under 2 s, over an order of magnitude less than a single

iteration of the genetic algorithm. The results for the different scenarios indicate that the optimal placement of the ESU for reducing peak power does not cause voltage violations under other conditions. However, the ability of the ESU to provide regulation services is impeded, as the worst-case voltage variation will be noticeable.

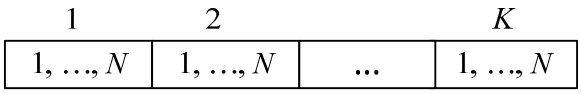

Fig. 4. Chromosome encoding for the genetic algorithm.

TABLE VI. GENETIC ALGORITHM PARAMETERS

Parameter	Value
Fitness function	rank
Selection function	remainder selection
Population replacement	generational
Elite individuals	$\frac{1}{20}\min[\max(10N, 40),100]$ (2-5 depending on sample size)
Mutation function	uniform
Mutation rate	0.01
Crossover type	scattered
Crossover fraction	0.8
Population size	$\max(N, 30)$
Convergence iterations	100
Maximum iterations	200

TABLE VII. CLUSTERING PLACEMENT RESULTS

Parameter	Value
ESU buses	13, 16
ESU power ratings (kW)	127.8, 207.6
PV total power rating (kW)	83.84
Feeder demand without PV and ESU (MW)	3.174
Feeder demand with PV and ESU (MW)	2.898
Reduction in feeder demand (kW)	611.1
Max ΔV between charge and discharge (%)	1.333
Clustering time to complete (s)	2.073

TABLE VIII. GA PLACEMENT RESULTS

Parameter	Value
ESU buses	12, 16
ESU power ratings (kW)	175.3, 160.1
PV total power rating (kW)	83.84
Feeder demand with PV and ESU (MW)	2.985
Reduction in feeder demand (kW)	614.7
Generations to convergence	1
Time to complete	35 s / iteration

TABLE IX. OPF RESULTS FOR CLUSTERING PLACEMENT

Scenario	Feeder Power	Min. Voltage	Max. Voltage
0 (base)	3.1741	0.9500	0.9976
1 (objective)	2.8984	0.9500	0.9928
2 (up-regulating)	2.8027	0.9500	0.9912
3 (down-regulating)	3.5534	0.9500	1.0046
4 (up-regulating)	1.0096	0.9500	0.9639

V. CONCLUSIONS

A placement method for distributed ESU that considers the addition of "smart" PV inverters was proposed. It demonstrated the utility of ESU in reducing peak load, while quantifying the amount of unwanted flicker introduced by performing frequency regulation with the placed ESU. The method employed a novel heuristic involving MDS and clustering that reduced computation time compared to the genetic algorithm methods commonly applied to this class of problems. This reduced computational time makes the method appealing for use in interactive software packages such as distribution analysis applications.

REFERENCES

[1] B. Seal, "Specification for smart inverter interactions with the electric grid using international electrotechnical commission 61850," Electric Power Research Institute, Knoxville, TN, Standard 1021674, Oct. 2010.

[2] C. A. McCarthy and J. Josken, “Applying capacitors to maximize benefits of conservation voltage reduction,” in *Rural Electric Power Conference*, 2003, pp. C4–1–C4–5.

[3] J. C. Carlisle, A. A. El-Keib, D. Boyd, and K. Nolan, “A review of capacitor placement techniques on distribution feeders,” in *Twenty-Ninth Southeastern Symposium on Syst. Theory*, 1997, pp. 359–365.

[4] R. O. Duda, P. E. Hart, and D. G. Stork, Pattern Classification. Wiley, 2001.

[5] A. Alarcon-Rodriguez, E. Haesen, G. Ault, J. Driesen, and R. Belmans, “Multi-objective planning framework for stochastic and controllable distributed energy resources,” *IET Renew. Power Gener.*, vol. 3, no. 2, pp. 227–238, Jun. 2009.

[6] M. T. Holmberg, M. Lahtinen, J. McDowall, and T. Larsson, “SVC Light® with energy storage for frequency regulation,” in *IEEE Conference on Innovative Technologies for an Efficient and Reliable Electricity Supply (CITRES)*, 2010, pp. 317–324.

[7] A. Barnes, J. C. Balda, A. Escobar, and S. O. Geurin, “Optimal battery chemistry, capacity selection, charge/discharge schedule, and lifetime of energy storage under time-of-use pricing,” in *IEEE PES ISGT Europe*, Manchester, England, 2011.

[8] M. E. El-hawary and L. G. Dias, “Incorporation of load models in load-flow studies. form of model effects,” *Proc. IEEE Gener. Transm. Distrib.*, vol. 134, no. 1, pp. 27–30, Jan. 1987.

[9] F. Belmudes, D. Ernst, and L. Wehenkel, “Pseudo-geographical representations of power system buses by multidimensional scaling,” in *Int. Conf. on Intelligent Syst. Appl. to Power Syst.*, 2009, pp. 1–6.

[10] G. Yesuratnam and D. Thukaram, “Congestion management in open access based on relative electrical distances using voltage stability criteria,” *Electr. Power Syst. Res.*, vol. 77, no. 12, pp. 1608–1618, Oct. 2007.

[11] G. Celli, S. Mocci, F. Pilo, and M. Loddo, “Optimal integration of energy storage in distribution networks,” in *IEEE PowerTech, Burcharest*, 2009, pp. 1–7.

[12] R. C. Dugan, M. F. McGranaghan, S. Santoso, and H. W. Beaty, Electrical Power Systems Quality, Third Edition. McGraw Hill Professional, 2012.

[13] N. Lu, M. R. Weimar, Y. V. Makarov, F. J. Rudolph, S. N. Murthy, J. Arseneaux, and C. Loutan, “Evaluation of the flywheel potential for providing regulation service in California,” in *2010 IEEE Power and Energy Society General Meeting*, 2010, pp. 1–6.

APPENDIX A: CERTIFICATION OF FIRST AUTHOR

I hereby certify that Arthur K. Barnes is first author of the article this chapter is based on and has completed at least 51% of the work described in the article.

Juan Carlos Balda

Signature _____

Date _____

APPENDIX B: RELEASE FOR USE IN DISSERTATION

Thesis / Dissertation Reuse

The IEEE does not require individuals working on a thesis to obtain a formal reuse license, however, you may print out this statement to be used as a permission grant:

Requirements to be followed when using any portion (e.g., figure, graph, table, or textual material) of an IEEE copyrighted paper in a thesis:

1) In the case of textual material (e.g., using short quotes or referring to the work within these papers) users must give full credit to the original source (author, paper, publication) followed by the IEEE copyright line © 2011 IEEE.

2) In the case of illustrations or tabular material, we require that the copyright line © [Year of original publication] IEEE appear prominently with each reprinted figure and/or table.

3) If a substantial portion of the original paper is to be used, and if you are not the senior author, also obtain the senior author's approval.

Requirements to be followed when using an entire IEEE copyrighted paper in a thesis:

1) The following IEEE copyright/ credit notice should be placed prominently in the references: © [year of original publication] IEEE. Reprinted, with permission, from [author names, paper title, IEEE publication title, and month/year of publication]

2) Only the accepted version of an IEEE copyrighted paper can be used when posting the paper or your thesis on-line.

3) In placing the thesis on the author's university website, please display the following message in a prominent place on the website: In reference to IEEE copyrighted material which is used with permission in this thesis, the IEEE does not endorse any of [university/educational entity's

name goes here]'s products or services. Internal or personal use of this material is permitted. If interested in reprinting/republishing IEEE copyrighted material for advertising or promotional purposes or for creating new collective works for resale or redistribution, please go to http://www.ieee.org/publications_standards/publications/rights/rights_link.html to learn how to obtain a License from RightsLink.

If applicable, University Microfilms and/or ProQuest Library, or the Archives of Canada may supply single copies of the dissertation.

CHAPTER SIX

VALUE ASSESSMENT OF DISTRIBUTED ENERGY STORAGE VIA MULTIDIMENSIONAL SCALING

Arthur Barnes, Luciano A. Garcia R. and Juan Carlos Balda

A.K. Barnes, L.A. Garcia R., and J.C. Balda, "Value assessment of distributed energy storage via multidimensional scaling," *IEEE Transactions on Power Systems* (to be submitted), December 2014.

Abstract **— The concept of distributed energy storage units (ESU) places ESU at points dispersed on distribution systems, where they can provide additional benefits via ancillary services. In particular, ESU are able to reduce both distribution system line losses and overall load power consumption by injecting both real and reactive power. This work studies cost-effective placement of a fixed amount of ESU in terms of total apparent power rating.**

Selecting the dispersed points on a practical feeder with thousands of buses could be time consuming when using common randomized search methods such as genetic algorithms (GA), requiring hours or days to complete. A fast heuristic search for placing ESU is proposed, in which multidimensional scaling (MDS) is used to transform the combinatorial placement problem into a continuous-valued space. Then, the convex DistFlow formulation is extended to take into account voltage-dependent loads and power electronic interface (PEI) losses. Lastly, static voltage regulation constraints are examined

when ESU economic dispatch does not correlate with feeder load, and flicker constraints are examined when the ESU are providing frequency regulation.

The results demonstrate that although distributed ESU are limited in their ability to provide frequency regulation, they can reduce overall load power consumption and line losses on a distribution system. ESU can complement shunt capacitors deployed in an economic fashion to reduce system power consumption even with a conservative estimate of PEI efficiencies. However, this reduction is low. Additionally, it is envisioned that the ability of ESU to reduce system power consumption will decrease in the future. This decrease is caused by the proliferation of PEI with power factor correction (PFC) functionality in loads. Such PEI make loads operate at constant-power with near-unity power factor. However, technologies such as silicon carbide (SiC) and gallium nitride (GaN) will enable higher PEI efficiencies for ESU. These higher efficiencies enable ESU to still reduce system power consumption even under low reactive power draw and a large number of constant-power loads.

***Keywords*—Energy storage, photovoltaic systems, renewable energy sources, optimization, clustering methods**

The authors are grateful for the financial assistance by the industry members of Grid-Connected Advanced Power Electronics Systems, an NSF I/UCRC.

I. INTRODUCTION

Electrical energy is unique amongst all commodities in that (in traditional markets) it cannot be stored, instead it must immediately be consumed. This results in inefficiencies as power

generation must always be matched to load. The current most cost-effective solution is to construct peaker electricity plants to meet the highest demand during the peak hours of the day. These plants are typically single-cycle gas turbines or natural gas fed internal combustion engines [1]. Because their utilization is low, it is cost-effective to use these for peak generation even though their efficiencies are less than other generation technologies. While this is an economically sound solution with low natural gas prices and plant utilization, expected volatility and price increases in natural gas calls this approach into question [2]. Furthermore, an increased demand is expected for peaking and load-following capabilities brought on by the proliferation of renewable generation. ESU are proposed as an energy-efficient solution to these inherently wasteful generation sources [3], [4].

ESU form an integral part of the concept of future energy systems, an integrated approach to reduce the environmental impacts of supplying energy to a community. Such future energy systems use several enabling technologies, including combined heat-and-power, distributed generation, and renewable energy sources. These are combined with increased sensing, increased communication, and new pricing structures. Future energy systems both empower and provide economic incentives for customers to take part in demand management activities [5]. The presence of distributed generation and energy storage also improves reliability in the case of grid failure via the microgrid concept [6]. These capabilities lead to tangible benefits, such as reducing consumption of and emissions from carbon-based fuels, long-term cost savings for both utilities and customers, and improving system reliability indices.

Because batteries are inherently created of small cells and do not produce either noise or emissions like generators, ESU do not need to be located in large bulk installations. Instead, ESU can be located near loads, which allows for them to provide ancillary services that have been

extensively documented in the literature, such as powering critical customer loads during power outages [7]–[9]. For the purposes of peak shaving, it can be shown that cumulative line losses are minimized by placing the ESU as close to loads as possible (and losses are maximized by placing the ESU as close to generation as possible). This is demonstrated in Appendix A. Placing ESU near customer loads also allows for them to provide reactive power compensation with any surplus power processing capability in the PEI not used to handle real power [10].

This paper takes a slightly different approach than existing work in the topic, which generally focuses on economic assessment of ESU, typically in the context of a net present value analysis [11]. Instead, this work focuses on the benefits and limitations of distributed ESU vs. ESU connected directly to transmission (e.g. at the high-voltage bus of a power substation). To perform this comparison, rather than carrying out an economic analysis, this work implements an engineering study in terms of (i) the total power consumed and (ii) the line losses on the distribution system. While total power consumed by a distribution system is a useful measurement, it is not always the most appropriate one, as not all public utility commissions will allow utilities to receive economic remuneration from reducing customer energy consumption. Typically, distribution system operators are only accountable for their own losses. This analysis makes certain effects clear, notably the impact of voltage-dependent loads and PEI efficiencies on the benefits of distributed ESU.

In order to perform the analysis described above, the case addressed is a distribution system operator (DSO) that has made the purchase of a fixed amount of energy storage in terms of total apparent power rating. The DSO seeks to determine the best solution – how many ESU should be placed, their power ratings, and where they should be placed on the system.

When determining placement, the scenario of the ESU providing peak shaving is examined. The total load on the distribution system can be lowered by appropriately placing the ESU and PV to flatten the voltage profile on the feeder, thereby allowing for conservation voltage reduction (CVR) to be applied [12]. CVR refers to lowering the overall voltage on the system (usually by the substation transformer tap settings) in order to reduce overall load demand by taking advantage of the increasing power vs. voltage curve of the system load. CVR is intrinsic to volt/VAR optimization (VVO), a control strategy in which equipment for voltage regulation and reactive power compensation on a distribution system are coordinated to reduce power consumption. The concept of VVO won success with utilities, allowing them to reduce power consumption with their existing equipment. Both major utility equipment manufacturers and upstarts have responded by developing their own VVO systems, including Cooper Power Systems, PCS Utilidata, ABB, and S&C [13].

This placement problem is closely related to that of placing distributed generation and shunt capacitors. The existing methods for placing these devices are categorized as: analytical [14], [15], numerical optimization (either linear , nonlinear, or mixed-integer nonlinear [16]), heuristic search [17], and randomized search [18], [19].

Recently convex optimization methods have been applied in distribution system engineering [20]–[23]. Convex optimization methods provide a guarantee that the achieve solution x^* will be a global optimum, so that for an objective function $f(x)$ and any feasible solution x, then $f(x^*) \leq f(x)$ [24]. Additionally, convex optimization problems can be formulated using a disciplined convex programming (DCP) ruleset that provides building blocks of legal operations which can be combined to formulate a convex optimization problem in a legible fashion [25]. It can be shown that under certain conditions an ac optimal power flow can be described as a

convex problem. These conditions include if the distribution system is radial or if phase-shifters have been installed on any loops present in the system. The methodology is well established for positive-sequence representations of radial systems, where it has been proved that the convex relation is tight [23].

This paper elaborates on earlier work that proposes a heuristic placement method [26]. Here, certain properties of the method are analyzed. It is shown that for positive-sequence representations of a distribution system, the transformed representation closely approximates the original one. The reduction in benefits resulting from aggregating ESU via the clustering methodology is quantified to first-order. The method is extended to include PEI loss models and applied to two new distribution systems. The results are interpreted to derive conclusions about the benefits of reactive power injection when considering non-ideal, lossy PEIs. Last, the scalability of the methodology is demonstrated by applying it to a large, 2998-bus distribution system model [27].

The proposed placement method falls under the category of heuristic search methods, in that it solves a simpler problem, whose solution is highly correlated with the optimal solution of the original problem. The methodology converts the placement problem from a combinatorial problem to a continuous-valued one by transforming the ESU bus locations into a continuous space with multidimensional scaling (MDS). The ESU positions are calculated with a clustering algorithm in the new space. Clustering for placement reduces computational complexity over both pure and hybrid genetic algorithm (GA) approaches, as it only runs a computationally intensive optimal power flow (OPF) twice, as oCh6pposed to the hundreds or thousands of OPF necessary for randomized search. The resulting long execution time is a hindrance for a distribution system engineer who wants to evaluate several different options for constructing or

upgrading a feeder. By contrast, the proposed method enables the engineer to quickly evaluate several different ESU configurations in a hypothetical software application by clicking a toolbar button.

This paper is arranged as follows. Section II describes the OPF used to select candidate buses to consider for ESU placement. Section III describes the scaling and clustering methods used for selecting ESU locations among the candidate buses. Additionally, it also provides some analytical results on performance of the methodologies. Section IV describes the GA methodology used as a performance benchmark. Section V describes the three case study systems. Section VI presents numerical results from applying both the proposed and benchmark methodologies. Last, section VII discusses conclusions about the benefits and potential applications of the proposed methodology.

II. CALCULATING CANDIDATE LOCATIONS AND POWERS WITH AN OPF

The high-level goal of the placement problem is to install a fixed amount of energy storage and to minimize power consumed by a distribution system under peak load while meeting voltage regulation constraints. The ESU inject power to increase frequency towards 60 Hz (referred to here as up-regulating) or supply power during critical peaks, but also draw power to help reduce frequency towards 60 Hz (referred to here as down-regulating) and charge during off-peak times to account for losses. Thus, while it is desirable to place ESU where they make the largest impact on voltage regulation and power consumed by the distribution system during peak load conditions and up-regulating, this property is a hindrance when the ESU are to down-regulate or charge. This analysis assumes that the ESU are always able to charge during off-peak times, so state-of-charge constraints are not included in the analysis.

II.A. Raw Problem Formulation

The distribution system is modeled using the DistFlow formulation, which allows a purely radial distribution system to be represented as a series of real-valued equations in terms of voltage magnitude squared and power [28], [29]. This formulation eliminates the requirements for a distribution system solver or optimal power flow (OPF) to handle complex numbers or invert large matrices. Fig. 1 illustrates the key variables for a branch k linking the sending bus i and receiving bus j. In this formulation, the voltages are represented as magnitudes squared, so that given the phasor voltage $\boldsymbol{V}_i$, then $W_i = \|\boldsymbol{V}_i\|^2$. The expression $P_k + \jmath Q_k$ is the complex power entering branch k, where script $\jmath$ denotes the imaginary number. The expression $R_k + \jmath X_k$ is the positive-sequence complex impedance of branch k. At bus j, the expression $P_j^{load} + \jmath Q_j^{load}$ is the complex power drawn by the load, while $P_j^{esu} + \jmath Q_j^{esu}$ is the complex power injected by the ESU and $\jmath Q_j^{cap}$ is the complex power injected by the shunt capacitor. The term $\mathcal{C}_j$ represents the set of child branches that connect to the receiving bus j of branch k. In Fig. 1, n such branches are depicted. For the m^{th}child branch, $P_{\mathcal{C}_{km}} + \jmath Q_{\mathcal{C}_{km}}$ is the power flowing into its sending end. All quantities listed are in per-unit. The problem objective is to minimize the power delivered from the substation, bus 1, during peak demand periods; that is

$$\text{minimize } P_{sub} = \sum_{k \in \mathcal{C}_1} P_k + P_1^{load} - P_1^{esu}. \tag{1}$$

The problem is subject to several constraints, which are discussed in the remainder of this section. As this work focuses only on demand reduction rather than economic aspects of the ESU, the total apparent power rating of the ESU is fixed so that

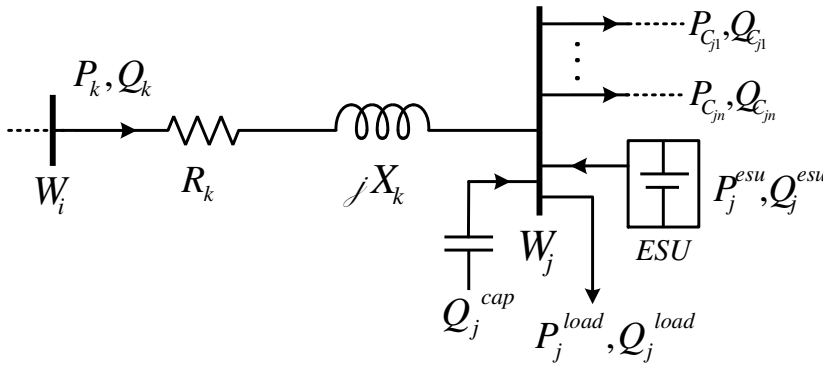

Fig. 1. Illustration of two buses in the DistFlow representation of a distribution system.

$$\sum_{i=1}^{N} S_i^{esu} \leq S_{tot}^{esu}, \tag{2}$$

where N is the number of buses, S_i^{esu} is the rated power of the ESU at bus i, and S_{tot}^{esu} is the total rated power of all the ESU in pu. The ESU PEI at bus i is oversized by a fixed amount given by

$$\kappa = \frac{S_i^{esu}}{P_i^{esu}}. \tag{3}$$

This value κ is the same for each ESU. Similarly, for each ESU

$$Q_i^{esu} = \zeta P_i^{esu} \tag{4}$$

and

$$\zeta = \sqrt{\kappa^2 - 1}. \tag{5}$$

The ESU PEI has the following loss function in terms of the fractional loss $(1 - \eta)$

$$P_i^{loss} = (1 - \eta) S_i^{esu} = (1 - \eta) \kappa P_i^{esu}, \tag{6}$$

where η is the fractional efficiency of the PEI at unity power factor. The power flow constraints for branch k are represented as

$$P_k = R_k \frac{(P_k^2 + Q_k^2)}{W_i} + P_j^{load} - P_j^{esu} + P_j^{loss} + \sum_{l \in \mathcal{C}_j} P_l \tag{7}$$

$$Q_k = X_k \frac{(P_k^2 + Q_k^2)}{W_i} + Q_j^{load} - Q_j^{esu} - Q_j^{cap} + \sum_{l \in \mathcal{C}_j} Q_l \tag{8}$$

$$W_j = W_i - 2(R_k P_k + X_k Q_k) + \frac{(R_k^2 + X_k^2)(P_k^2 + Q_k^2)}{W_i} \tag{9}$$

$$V_{min}^2 \leq W_i \leq V_{max}^2 . \tag{10}$$

In the above, V_{min} and V_{max} are the minimum and maximum allowable voltages in pu, respectively.

A static load model is employed such that

$$P_i^{load} = P_i^{load0}(1 + \alpha \Delta W_i) \tag{11}$$

$$Q_i^{load} = Q_i^{load0}(1 + \beta \Delta W_i). \tag{12}$$

In (11) and (12), $\Delta W_i = W_i - 1$ is the deviation of the squared voltage magnitudes from 1 pu. Note that the above equations are linear in W_i, but are quadratic in $\|\boldsymbol{V_i}\|$. As $\|\boldsymbol{V_i}\|$ remains near 1 pu, this is a reasonable approximation. The terms P_i^{load} and Q_i^{load} are nominal real and reactive powers drawn by the load at bus i, respectively. The terms α and β represent the change in real and reactive power drawn by the load with respect to the voltage at the load bus, respectively. Similar to the case of the load, the capacitors also have voltage dependence so that the injected power is

$$Q_i^{cap} = Q_i^{cap0} W_i, \tag{13}$$

where Q_i^{cap0} is the nominal reactive power of the capacitor in pu.

The cost of placing an ESU on the distribution system is assumed to have both a fixed installation cost in addition to a portion of the cost that is proportional to the apparent power rating of the ESU, as illustrated in Fig. 2. The effect of this piecewise linear cost is that it is more cost-effective to have a smaller number of larger ESU, as less fixed installation cost is incurred.

However, including this in the cost makes the problem considerably more difficult from a computational perspective, as it now a mixed-integer nonlinear problem [29]. In order to circumvent this issue, the OPF formulation is only used to select candidate buses for ESU placement. The placement is solved as a separate problem, using the candidate buses and the necessary power injections as inputs to a clustering algorithm which determines the actual ESU power ratings and locations. The clustering algorithm requires that the number of ESU be selected beforehand. However, as this number is small, it is reasonable to determine its optimal value by an exhaustive iteration over a fixed range from 0 to a maximum number of ESU K_{max}.

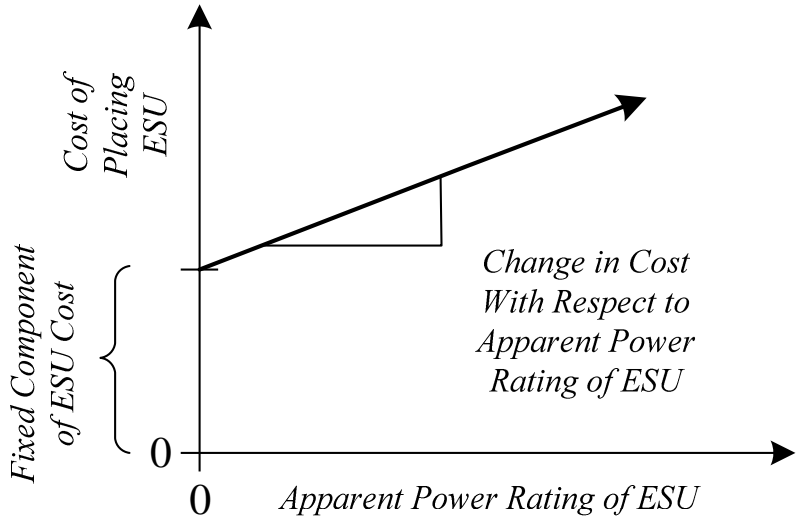

Fig. 2. Nonlinear cost of placing ESU.

II.B. Convex Placement Formulation

For the purposes of solving the optimal power flow (OPF) problem, the CVX package for Matlab is employed, which provides guaranteed convergence provided that the problem can be formulated in terms of disciplined convex programming [25].

In the systems analyzed, there is only one branch originating from the substation bus. Loads at the substation bus are not accounted for when placing ESU (though they are included when calculating the final distribution system power demand). Therefore, the DCP formulation for the problem is

$$\text{minimize } P_1 \tag{14}$$

subject to

$$\sum_{i=1}^{N} P_i^{esu} \leq P_{tot}^{esu} \tag{15}$$

$$P_i^{loss} = (1-\eta)\kappa P_i^{esu} \tag{16}$$

$$P_k = R_k L_k + P_j^{load} - P_j^{esu} + \sum_{l \in \mathcal{C}_j} P_l \tag{17}$$

$$Q_k = X_k L_k + Q_j^{load} - \zeta P_j^{esu} - Q_j^{cap} + \sum_{l \in \mathcal{C}_j} Q_l \tag{18}$$

$$W_j = W_i - 2(R_k P_k + X_k Q_k) + (R_k^2 + X_k^2) L_k \tag{19}$$

$$L_k \geq \frac{P_k^2}{W_i} + \frac{Q_k^2}{W_i} \tag{20}$$

$$V_{min}^2 \leq W_i \leq V_{max}^2 \tag{21}$$

$$P_j^{esu} \leq [1 - \kappa(1-\eta)] P_j^{esu0} \tag{22}$$

$$P_i^{load} \geq P_i^{load0}(1 + \alpha \Delta W_i) \tag{23}$$

$$Q_i^{load} \geq Q_i^{load0}(1 + \beta \Delta W_i) \tag{24}$$

$$Q_i^{cap} \leq Q^{cap0} W_i. \tag{25}$$

In (20), L_k is a helper variable necessary for the convex relaxation, while P_j^{esu0} is the desired ESU output real power without losses [30].

II.C. Scoring and Convex Validation Formulation

To score the reduction in distribution system power consumption gained by applying ESU, it is necessary to consider the total feeder energy consumed over the course of a day. For this analysis, it is assumed that the ESU charge and discharge times are short compared to the daily load variations. Based on this assumption, these calculations are performed using only on- and off-peak load values. All scenarios considered are compared with a base scenario in which the ESU is placed at the substation and used for peak shaving (but not reduction of distribution system losses). The base case accounts for losses within the ESU. The daily energy consumed for the base scenario is

$$E_{base} = T_{dis}\left(P_{sub}^{pk,base} - P_{tot,dis}^{esu}\right) + T_{chg}(P_{sub}^{op,base} - P_{tot,chg}^{esu}) \tag{26}$$

$$\eta T_{chg} = T_{dis}. \tag{27}$$

In (26), E_{base} is the daily energy consumed, while T_{dis} and T_{chg} are the ESU discharge and charge times, respectively. Additionally, $P_{sub}^{pk,base}$ and $P_{sub}^{op,base}$ are powers demanded by the substation during peak and off-peak times, respectively (not including the ESU power). Similarly, $P_{tot,dis}^{esu}$ and $P_{tot,chg}^{esu}$ are the total powers of the ESU during the discharge and charge periods, respectively. The discharge period corresponds exactly with the peak period, while the

charge period corresponds exactly with the off-peak period. For the case of ESU placed, the daily energy consumption is then

$$E = T_{dis}P_{sub}^{pk} + T_{chg}P_{sub}^{op}. \tag{28}$$

In (28), P_{sub}^{pk} and P_{sub}^{op} are the substation peak and off-peak powers assuming that ESU have been placed on the feeder. Again, it is assumed that the ESU will discharge during the peak period and charge during the off-peak period. The reduction in distribution system energy consumption is then $E_{base} - E$, which could be negative if the ESU are not operated in an effective manner.

For the purpose of validation, the OPF is run again with the ESU placed at the buses $i \in \mathcal{E}$ under a number of scenarios. It is assumed the ESU charge at night during off-peak periods and there is always sufficient time to do so. For this reason, the state-of-charge is not included in the validation formulation. Instead, the validation verifies whether or not the ESU will:

1. violate steady-state voltage constraints when charging or discharging, and/or
2. violate flicker limits when providing frequency regulation.

For the purpose of checking steady-state voltage constraints, the distribution system voltage profiles during the scenarios of peak load / ESU discharging and off-peak load / ESU charging are examined. For the case of ESU charging, the problem formulation must be changed slightly so that (22) becomes

$$P_j^{esu} \leq -[1 + (1 - \eta)]P_j^{esu0}. \tag{29}$$

In (29), it is assumed that the ESU always operates at unity power factor while charging.

For the case of flicker, the voltage profiles while the ESU is down-regulating frequency (charging) and up-regulating frequency (discharging) are compared during peak feeder load. The

substation output voltage is calculated during the down-regulating scenario, and held fixed at the same value during the up-regulating scenario.

III. SELECTION OF THE ESU LOCATIONS

In this particular problem, the key idea is that it is not desirable to place ESU at buses that are very "close" to one another, which in this context means that there is a low impedance or voltage drop between them. To determine how to best combine the candidate locations into a smaller number of well-spaced ESU, the candidate ESU locations are mapped into a continuous space that is easier to work with than the original discrete space. To accomplish this, dimensionality scaling methodologies are employed [31]–[33]. However, even with the candidate locations mapped into a continuous space, the problem is still combinatorial in nature. Fortunately, the new problem space allows for the use of clustering methods, which represent a "good" suboptimal solution to the problem, in that they will produce a solution having an objective function value only slightly larger than the one produced by exhaustive search [34].

Although hierarchical clustering algorithms exist that can operate over a pairwise distance matrix, they suffer from sensitivity to initial conditions. The MDS algorithm allows classical k-means type algorithms to be applied, which are much less sensitive [34]. Additionally, MDS comes at a low cost in terms of both computational and programming burden, as it can be implemented in two lines of a high-level language with a set of matrix multiplications and eigenvector decomposition.

III.A. Multidimensional Scaling

The candidate buses are mapped to points in a q-dimensional space using MDS, a dimensionality reduction technique that is commonly used in the social sciences for visualizing

results from survey data [31]. This methodology works by first calculating pairwise distances between each object (in this case, a bus) in a set (in this case, all the N buses in the distribution system model). The objects are then mapped to arbitrarily placed points in the q-dimensional space. The classical MDS (CMDS) algorithm is employed. CMDS maps the objects using their pairwise distances onto the q-dimensional space by applying a pair of transformation matrices to convert the pairwise $N \times N$ distance matrix $\mathbf{D}$ into a positive semidefinite matrix $\mathbf{B}$ of rank q. $\mathbf{B}$ is then used to produce matrix $\mathbf{Y}$, whose columns are the position vectors $\boldsymbol{y}_1, \boldsymbol{y}_2, \dots, \boldsymbol{y}_N$.

The method is illustrated as follows. First, the distance matrix $\mathbf{D}$ is transformed

$$\mathbf{B} = \frac{1}{2}(\mathbf{I}_N - \mathbf{O})\mathbf{D}(\mathbf{I}_N - \mathbf{O}), \tag{30}$$

where I_N is a $N \times N$ identity matrix and $\mathbf{O}$ is another $N \times N$ matrix in which each element $\mathrm{O}_{ij} = N^{-1}$. The q eigenvectors $\boldsymbol{v}_i$ corresponding to the nonzero eigenvalues λ_i of $\mathbf{B}$ are selected, therefore

$$\mathbf{B}\boldsymbol{v}_i = \lambda_i \boldsymbol{v}_i, \qquad \lambda_i \neq 0. \tag{31}$$

These are concatenated into a new matrix

$$\mathbf{Y} = \left[\boldsymbol{v}_1, \boldsymbol{v}_2, \dots, \boldsymbol{v}_q\right]^T. \tag{32}$$

Each column $\boldsymbol{y}_i$ of $\mathbf{Y}$ represents a point in the new space.

The salient property of the method is that if each element of $\mathbf{D}$ corresponds to an Euclidean distance D_{ij} calculated between objects i and j, then the Euclidean distance between columns $\boldsymbol{y}_i$ and $\boldsymbol{y}_j$ of $\mathbf{Y}$ is also

$$D_{ij} = \left\|\boldsymbol{y}_i - \boldsymbol{y}_j\right\|_2. \tag{33}$$

It is important to realize however, that the distances D_{ij} *do not necessarily correspond to the distances between two points in an original space*, as is the case with both similarity scores on questionnaires and the impedance between two buses in a distribution system. Additionally, if D_{ij} does not correspond to a Euclidean distance, then the two sides in (33) will become only approximately equal.

There exists another form of MDS, the nonmetric MDS algorithm, that calculates the $\boldsymbol{y}_i$ using an iterative algorithm. This algorithm attempts to minimize the difference between the original distances and the distances between the $\boldsymbol{y}_i$. The nonmetric algorithm typically yields superior performance when it is desired to map the distances into a low-dimensional space. In the CMDS algorithm, the dimensionality of the resulting space is restricted by discarding the dimensions corresponding to the smallest eigenvalues, but this typically results in lower accuracy than the nonmetric MDS algorithm [31]. Both forms are used in this paper, with the nonmetric form applied to small datasets (less than 100 buses) and the classical form applied to large datasets (more than 100 buses).

The set of pairwise distances **D** used as an input for MDS has certain applicable mathematical properties itself. It can be shown via the bus impedance (Z-bus) matrix method that the set of pairwise distances completely describes the positive-sequence representation of an electrical distribution system. This is demonstrated with the following 4 buses from a radial distribution system illustrated in Fig. 3. The substation bus is indicated by 1, and corresponds to the reference bus in the Z-bus formulation [1].

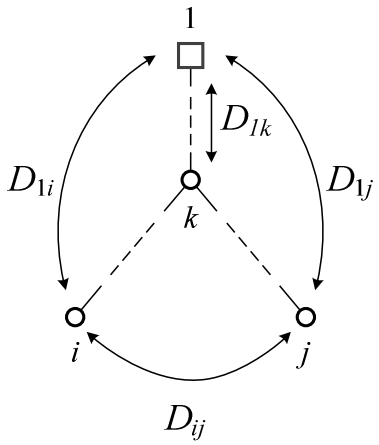

Fig. 3. Four buses from a radial distribution system and the corresponding distances between them.

For a radial system, each element in the (symmetric) Z-bus matrix is defined as follows

$$Z_{ij} = \left.\frac{V_i}{I_j}\right|_{I_j \neq 0,\ I_1,\ldots,I_n = 0}. \tag{34}$$

From Fig. 3, it can be shown that

$$D_{1i} = Z_{ii} \tag{35}$$

$$D_{1j} = Z_{jj} \tag{36}$$

$$Z_{ij} = Z_{kk}. \tag{37}$$

Therefore

$$Z_{kk} = D_{1k} \tag{38}$$

$$2D_{1k} = D_{1i} + D_{1j} - D_{ij} \tag{39}$$

$$2Z_{ij} = Z_{1i} + Z_{1j} - Z_{ij} \tag{40}$$

$$Z_{ij} = \frac{1}{2}\left(D_{1i} + D_{1j} - D_{ij}\right). \tag{41}$$

Although the distance matrix is defined as a real matrix by definition, the above holds true if the notion of distance is somewhat abused and a complex "distance" matrix is created by adding the distance matrices corresponding the real and imaginary portions of the positive-sequence impedance. Therefore, the full Z-bus matrix is defined uniquely in terms of the distance matrix

$$Z_{ij} = \begin{cases} D_{i1}, & i = j \\ \frac{1}{2}\left(D_{1i} + D_{1j} - D_{ij}\right), & i \neq j. \end{cases} \tag{42}$$

It is further shown that (assuming the distances in CMDS space match closely with the distances in the original space) an ESU placement on the line segment connecting two *directly connected* buses in CMDS space will correspond to placing the ESU on the physical line connecting the two buses i and j in the distribution system, as illustrated in Fig. 4. This is demonstrated in the following expressions. First, given that point $\boldsymbol{y}_k$ is on the line segment between points $\boldsymbol{y}_i$ and $\boldsymbol{y}_j$, it can be described as a convex relationship of the two points

$$\boldsymbol{y}_k = \theta \boldsymbol{y}_i + (1-\theta)\boldsymbol{y}_j. \tag{43}$$

Now let the distances between $\boldsymbol{y}_k$ and its neighboring points be

$$D_{ik} = \left\| \boldsymbol{y}_i - \theta \boldsymbol{y}_i - (1-\theta)\boldsymbol{y}_j \right\| \tag{44}$$

$$D_{kj} = \left\| \boldsymbol{y}_j - \theta \boldsymbol{y}_i - (1-\theta)\boldsymbol{y}_j \right\|. \tag{45}$$

The distance between points $\boldsymbol{y}_i$ and $\boldsymbol{y}_j$ can therefore be expressed as

$$D_{ik} + D_{kj} = \left\| \boldsymbol{y}_i - \theta \boldsymbol{y}_i - (1-\theta)\boldsymbol{y}_j \right\| + \left\| \boldsymbol{y}_j - \theta \boldsymbol{y}_i - (1-\theta)\boldsymbol{y}_j \right\|. \tag{46}$$

Rearranging terms,

$$D_{ik} + D_{kj} = \|(1-\theta)\boldsymbol{y}_i - (1-\theta)\boldsymbol{y}_j\| + \|\theta\boldsymbol{y}_j - \theta\boldsymbol{y}_i\|. \quad (47)$$

By the absolute homogeneity property of a norm, and observing that both θ and $1-\theta$ are nonegative

$$D_{ik} + D_{kj} = (1-\theta)\|\boldsymbol{y}_i - \boldsymbol{y}_j\| + \theta\|\boldsymbol{y}_j - \boldsymbol{y}_i\|. \quad (48)$$

Finally,

$$D_{ik} + D_{kj} = \|\boldsymbol{y}_i - \boldsymbol{y}_j\| = D_{ij}. \quad (49)$$

For $\boldsymbol{y}_k$ not located between $\boldsymbol{y}_i$ and $\boldsymbol{y}_j$ the triangle inequality holds, so

$$D_{ik} + D_{kj} \geq D_{ij}. \quad (50)$$

For the practical case of an ESU location (cluster centroid) that is not placed on any line segment corresponding to a physical line, it can be shown that assigning it to the nearest neighbor bus will result in a quality solution under certain conditions. These conditions occur when the sum of the distances in the cluster is much smaller than the distance from the center of the cluster to the tree root (substation). This can be expressed as follows (to first order, neglecting the incremental change in losses or voltage regulation caused by nonlinearities in the distribution system). Consider a single cluster with centroid $\boldsymbol{\mu}$, and let the nearest neighbor bus with respect to $\boldsymbol{\mu}$ be b, at location $\boldsymbol{y}_b$.

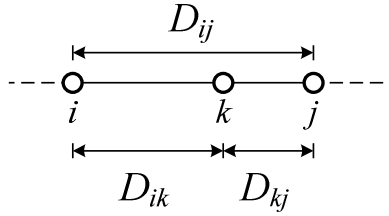

Fig. 4. Relationship of point placement in the CMDS space and position on the physical feeder.

Let $i \in \mathcal{D}$ be the set of buses in that cluster, with locations $\boldsymbol{y}_i$. For all the ESU candidate buses $\{\boldsymbol{y}_i | i \in \mathcal{D}\}$ in that centroid, the benefit of installing storage is

$$J = \sum_{i \in \mathcal{D}} \gamma_i D_{1i}, \tag{51}$$

where γ_i is a weight proportional to the real power injection of that ESU determined by the convex OPF. The γ_i are normalized so their sum in that cluster is one. Assume once again there is a bus k at the endpoint of the shared path from all buses in the cluster. Neglecting D_{kb} an upper bound on the reduced benefit incurred by clustering can therefore be expressed as

$$\Delta J = \sum_{i \in \mathcal{D}} \gamma_i D_{1i} - D_{1k}. \tag{52}$$

Assuming M buses in the cluster, this can be re-expressed in terms of the Z-bus matrix and expanding

$$\Delta J = \sum_{i \in \mathcal{D}} \gamma_i D_{1i} - \sum_{i \in \mathcal{D}} Z_{bi} \tag{53}$$

$$\Delta J = \sum_{i \in \mathcal{D}} \gamma_i D_{1i} - \sum_{i \in \mathcal{D}} \frac{1}{2}(D_{1i} + D_{1j} - D_{ij}) \tag{54}$$

$$\Delta J = \sum_{i \in \mathcal{D}} \gamma_i D_{1i} - \frac{1}{2}\sum_{i \in \mathcal{D}} D_{1i} - \frac{1}{2}\sum_{i \in \mathcal{D}} D_{1b} + \frac{1}{2}\sum_{i \in \mathcal{D}} D_{bi} \tag{55}$$

$$\Delta J = \sum_{i \in \mathcal{D}} \gamma_i D_{1i} - \frac{1}{2}\sum_{i \in \mathcal{D}} D_{1i} - \frac{M}{2} D_{1b} + \frac{1}{2}\sum_{i \in \mathcal{D}} D_{bi}. \tag{56}$$

From the above, it is apparent that when $D_{1b} \gg \frac{1}{M}\sum_{i \in \mathcal{D}} D_{bi}$, the benefit reduction ΔJ will be small. Therefore, when the cluster size is small compared to the distance of the cluster from the substation, then clustering will not significantly affect the solution quality.

III.B. Derivation of Placement Rules

In order to validate the scalability of the placement algorithm, it is necessary to run it on a large (1000+ bus) unbalanced distribution system model. Unfortunately, this precludes the use of the convex OPF formulation described in Section II, as (i) the convex OPF relaxation has only been shown to be tight for a balanced system, and (ii) existing literature has only scaled the OPF up to distribution system models in the low 100s of buses. To circumvent this issue, a simple ad-hoc single-class classifier is designed to select the ESU buses. Because the test systems employed for the OPF (described later in Section IV) are only on the order of the low 10s of buses, insufficient training data exists to design a statistical classifier [34]. To overcome this second issue, a single feature was selected manually, and used as the input for a threshold-based classifier, which selects buses whose feature value is in the top 10^{th} percentile. Three features are considered:

1. the sum of resistive power losses along the path from the substation to each bus (quadratically related to the current at each branch),
2. the sum of voltage drops along the path from the substation to each bus (linearly related to the current at each branch), and
3. the sum of impedance magnitudes along the path from the substation to each bus (independent of the current at each branch).

These features are illustrated in Fig. 5 and Fig. 6, which demonstrate that buses selected for ESU candidates can be predicted with either resistive power losses or voltage drop. In this study, the voltage drop was selected as it is easily extracted from the results from a distribution system analysis tool without additional post-processing.

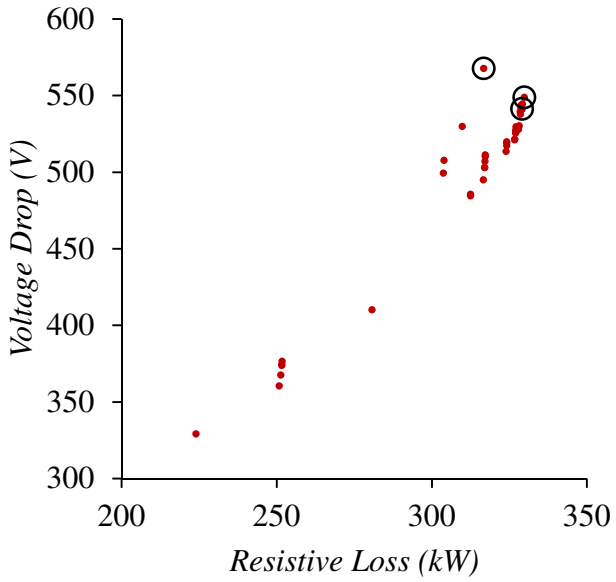

Fig. 5. Plot of voltage drop and resistive loss along the path from the substation to each bus on a 42-bus feeder. Candidate buses for ESU placement (those in the top 10th percentile in terms of injected power) are circled.

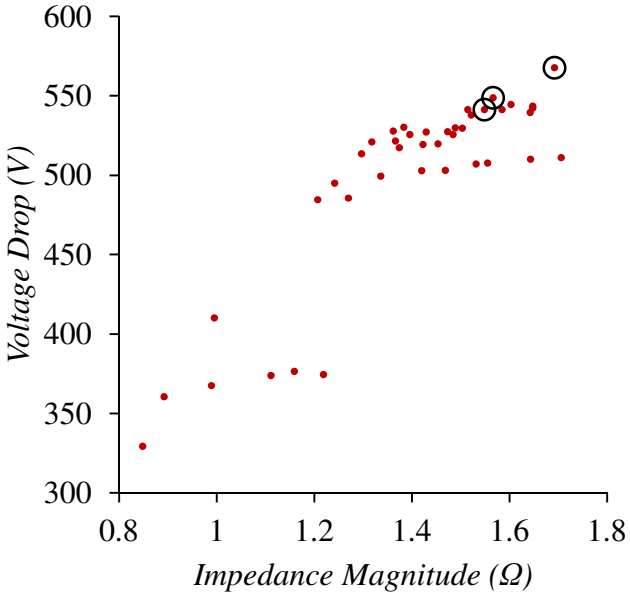

Fig. 6. Plot of voltage drop and impedance magnitude along the path from the substation to each bus on a 42-bus feeder. Candidate buses for ESU placement (those in the top 10th percentile in terms of injected power) are circled.

III.C. Clustering Algorithm

The goal of the clustering algorithm is to group together buses that are candidate locations for placing ESU. A number of clusters K (corresponding to the number of ESU to be placed) is selected as an input to the algorithm. The requirements of the clustering algorithm are to assign each bus to a particular ESU and to select the buses that the ESU will be placed at.

Hence, the objective of the algorithm is to minimize the intra-cluster variance

$$\text{minimize}\, J = \sum_{i \in \mathcal{D}_k} \|\boldsymbol{y}_i - \boldsymbol{\mu}_k\|^2, \tag{57}$$

where $\boldsymbol{y}_i$ is a point in cluster k, $\boldsymbol{\mu}_k$ is the centroid (or center of mass) of cluster k, and $\mathcal{D}_k$ is the set of points belonging to cluster k. Although it is possible for the first criterion to be handled directly in the clustering itself, it is taken into account indirectly by selection of the number of clusters instead. A last issue is that the amount of ESU power injection at each bus is not identical. This could cause skewed results for the case of a bus with only a small amount of power injection counting as much as a bus with a large amount. To account for this, the weighted k-means algorithm is used [34], in which the centroid calculation is modified to use the amount of power injection at each bus as a weight. In the original k-means algorithm, the centroids are calculated as

$$\boldsymbol{\mu}_k = \frac{1}{N_k} \sum_{i \in \mathcal{D}_k} \boldsymbol{y}_i, \tag{58}$$

where N_k is the number of points in cluster k. By contrast, in the weighted algorithm, the centroids are calculated as

$$\boldsymbol{\mu}_k = \sum_{i \in \mathcal{D}_k} \gamma_i \boldsymbol{y}_i, \tag{59}$$

where the weighting γ_i is equal to

$$\gamma_i = \frac{P_i^{esu}}{\sum_{j \in \mathcal{D}_k} P_j^{esu}}. \tag{60}$$

To perform placement, the ESU are allocated to the bus closest to their centroid. The power injections of each ESU candidate are then assigned to their corresponding ESU, shown in Fig. 7.

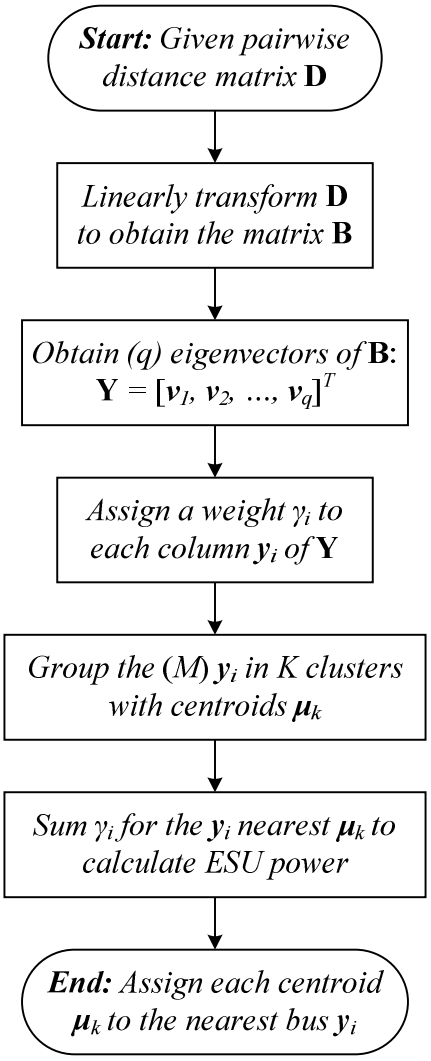

Fig. 7. Flowchart for the CMDS/clustering algorithm.

IV. VALIDATION AGAINST GA

Although a variety of methods have been investigated for placement of ESU, distributed generation, and shunt capacitors, GA and similar randomized search methods are very commonly employed [35], [36]. To provide a benchmark against which the proposed methodology can be compared, the GA approach described in [19] is also implemented.

The problem formulation is somewhat different here, however. The placement OPF in this study is a convex problem taken over a single time interval, compared to the quadratic multi-step problem taken in [19]. Furthermore, in this study the total number of ESU and total power rating of the ESU are both fixed inputs to the problem. To account for this, the GA parameters are changed, as described in Table I. In this work the function `ga()` from the Matlab™ optimization toolbox is used.

TABLE I. GA PARAMETERS

Parameter	Value
Fitness function	rank
Selection function	Remainder selection
Population replacement	generational
Elite individuals	$\frac{1}{20}\min[\max(10 \cdot N, 40), 100]$ (2…5 indivduals depending on sample size)
Mutation function	uniform
Mutation rate	0.01
Crossover type	scattered
Crossover fraction	0.8
Population size	$\max(N, 30)$
Convergence iterations	100
Maximum iterations	200

To summarize:

1) Encoding

The GA uses the encoding in Fig. 8, in which each chromosome is composed of K alleles. Each allele is a positive integer than can take on the values $1, \dots, N$. If the number of ESU to be placed K is small compared to the total number of buses, then the total search space is significantly reduced: $N^K \ll 2^N$, and the valid search space $\binom{N}{K}$ is even further reduced, eliminating many OPF evaluations.

2) Population

The algorithm operates with a constant population size. The number of individuals in the population is the maximum of either the number of buses N or 30, whichever is larger. Based on empirical studies, 30 individuals is the minimum number necessary to ensure sufficient population diversity, increasing the likelihood that the search space is sufficiently explored [37].

3) Fitness function

The rank fitness function is used, in which each individual is ranked according to its cost function. The individual with the k^{th} lowest cost function is accorded the fitness value $1/\sqrt{k}$.

4) Selection function

The algorithm uses the remainder selection method to choose which individuals will produce children for the next generation. In the remainder selection method, the number of times each individual is selected for reproduction depends on its fitness. First, the individual is selected a deterministic number of times based on the integer part of its fitness. The remainder of the individuals selected for reproduction is done randomly, in which the likelihood of their selection is weighted by the fractional portion of their fitness.

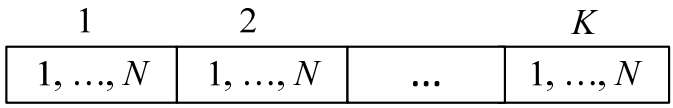

Fig. 8. Chromosome encoding for the GA.

5) Population replacement method

The algorithm uses the generational replacement method, in which all individuals are replaced after the *elite*, *mutation*, and *crossover* operations are performed.

6) Elite reproduction

A small number of individuals with high fitness are likely to yield solutions whose cost is either the global optimum or only slightly greater. These individuals are cloned in addition to producing children through the *mutation* and *crossover* operations. The exact number of individuals selected is $\frac{1}{20}\min[\max(10 \cdot N, 40), 100]$, which amounts to 2-5 individuals, depending on the number of buses in the distribution system.

7) Crossover reproduction and crossover fraction

The scattered crossover function is employed. In this method, a uniform random binary vector of length K is generated for each child produced by *crossover*. The child alleles with a "0" in their position receive alleles from the first parent, while those with a "1" in their position receive alleles from the second parent. The number of children produced by *crossover* is 80% of the population of the next generation (excluding those produced by the *elite* operation).

8) Mutation function and rate

The uniform mutation function with rate of 0.01 is selected. The uniform mutation function operates on the remaining 20% of the next generation (excluding those produced by the *elite* operation). It works by altering the chromosomes in the next generation by randomly selecting 1% of the alleles, then randomly assigning those alleles a number in the range $1, \ldots, N$.

9) Maximum generations and termination generations

The GA terminates if the highest fitness in the population does not improve after 100 generations have passed, or if 200 generations have passed, regardless of any change in the fitness functions of the population.

V. CASE STUDIES

The proposed method is tested on three test cases. These are: a 17-bus positive-sequence distribution system model (TC17) [38], a 42-bus positive-sequence distribution system model (TC42) [30], and a 2998-bus unbalanced three-phase distribution system model (TC2998) [27]. The latter system is produced by the Electric Power Research Institute (EPRI), and referred to as ckt5 in its literature.

V.A. Parameters for Calculating Performance Improvement and Validation

In TC17 and TC42, the total real power rating of the ESU to be placed is 12.5% of the total feeder real power demand (excepting loads placed directly at the substation bus). For TC2998, the total power rating of the ESU is equal to the sum of load powers at the load buses in the bottom 10^{th} percentile. Additionally, TC2998 is not used to measure power reduction on the distribution system gained by the placement of ESU; it serves only to demonstrate the scalability of the algorithm. Table II describes the parameters used for the cases employed in both scoring and validation. Cases BP, BO, DP and CO are used for scoring. Cases R+O and R−P are the scenarios when validating that the ESU will not violate steady-state voltage regulation limits, though all scenarios analyzed are also included.

TABLE II. DESCRIPTION OF SCORING AND VALIDATION CASES

Scenario	Load	ESU	Regulator
BP (Base Peak)	Peak	Off	Optimum
BO (Base Off-peak)	Off-Peak	Off	Optimum
DP (Objective; Discharge Peak)	Peak	Discharge	Optimum
CO (Objective; Charge Off-peak)	Off-Peak	Charge	Optimum
R+O (Up-regulating)	Off-Peak	Discharge	Optimum
R+P (Up-regulating)	Peak	Discharge	Optimum
R−P (Down-regulating)	Peak	Charge	Same as (3)

TABLE III. CASE STUDY PARAMETERS FOR TC17 AND TC42

Parameter	Symbol	Value
Number of ESU	K	2
Total ESU Real Power	P_{tot}^{esu}	$\frac{1}{8}\sum_{n=1}^{N} P_n^{d0}$
ESU Oversizing for Nominal Reactive Power Injection	k_1	15%
Nominal ESU Losses	a_1	3.68%
Nominal Real Power CVR Factor	α_1	0.7
Nominal Reactive Power CVR Factor	β_1	2.0
Minimum Voltage	V_{min}	0.95 pu
Maximum Voltage	V_{max}	1.05 pu

TABLE IV. CASE STUDY PARAMETERS FOR TC2998

Parameter	Symbol	Value
Number of ESU	K	2
Buses Selected for ESU Candidates	$\mathcal{E}$	Buses with voltage in the bottom 10th percentile
ESU Candidate Bus Power	P_i^{esu}	P_i^{load}

Unless otherwise specified, the parameters in Table III are used for both TC17 and TC42. For TC2998, the relevant parameters are listed in Table IV, but the EPRI feeder model is not modified.

V.B. Parameters for TC17

The feeder TC17 is a 12.5 kV system originally used in a voltage harmonic mitigation study [38]. It is presented here with some modifications. A one-line diagram of the distribution system is presented in Fig. 9. Table V – Table VIII list general, line, and load parameters for the system, respectively.

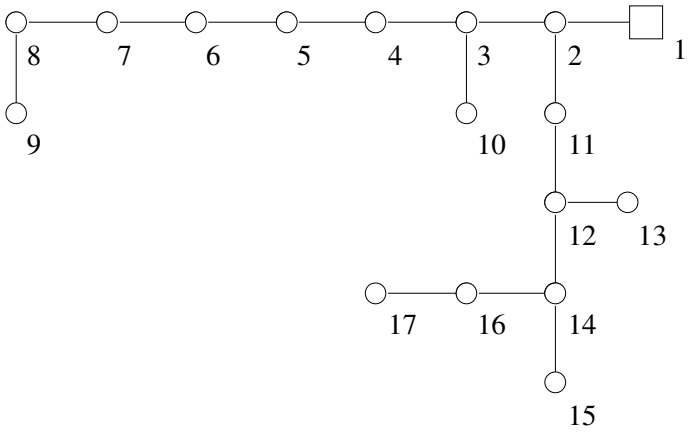

Fig. 9. One-line diagram of TC17. Substation is located at bus 1.

TABLE V. GENERAL PARAMETERS FOR TC17

Parameter	Symbol	Value
Base Voltage	V_b	12.5 kV
Base Power	S_b	10 MVA

TABLE VI. LINE PARAMETERS FOR TC17

From Bus	To Bus	R (pu)	X (pu)	From Bus	To Bus	R (pu)	X (pu)
1	2	0.00810	0.07107	3	10	0.01706	0.02209
2	3	0.00431	0.01204	2	11	0.02910	0.03768
3	4	0.00610	0.01677	11	12	0.02222	0.02888
4	5	0.00316	0.00882	12	13	0.04803	0.06218
5	6	0.00896	0.02502	12	14	0.03985	0.05160
6	7	0.00295	0.00824	14	15	0.02910	0.03768
7	8	0.01720	0.02120	14	16	0.03727	0.04593
8	9	0.04070	0.03053	16	17	0.02208	0.02720

TABLE VII. LOAD PARAMETERS FOR TC17

Bus No.	P (pu)	Q (pu)	Bus No.	P (pu)	Q (pu)
1	0.00	0.00	10	0.05	0.031
2	0.00	0.00	11	0.10	0.062
3	0.02	0.012	12	0.03	0.019
4	0.04	0.025	13	0.02	0.012
5	0.15	0.093	14	0.08	0.05
6	0.30	0.226	15	0.05	0.031
7	0.08	0.050	16	0.10	0.062
8	0.02	0.012	17	0.02	0.012
9	0.10	0.062			

TABLE VIII. SHUNT CAPACITOR BANK PARAMETERS FOR TC17

Bus No.	Nameplate Capacity (kVAR)
5	3150
14	1350

V.C. Parameters for TC42

The feeder TC42 is a 12.35 kV system originally used in a study on centralized control for loss reduction and voltage rise mitigation with "smart" PV [30]. A one-line diagram of the distribution system is presented in Fig. 10. Table IX - Table XII list general, line, and load parameters for the system, respectively.

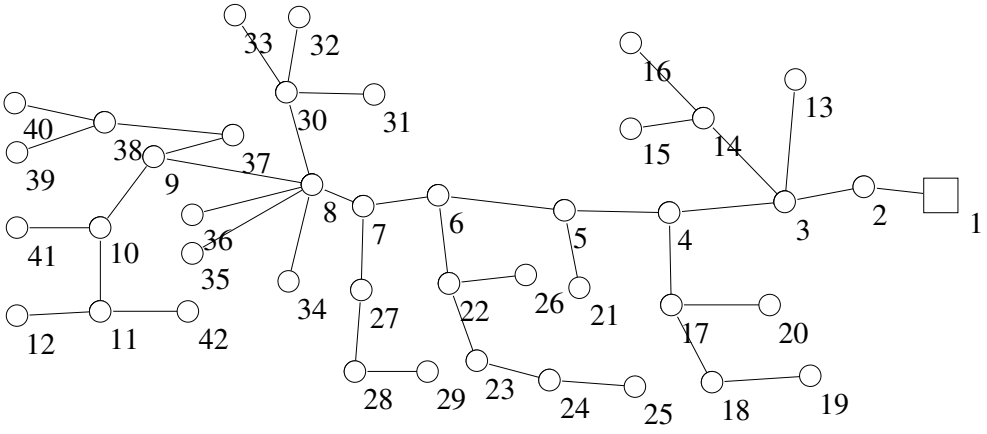

Fig. 10. One-line diagram of TC42. Substation is located at bus 1.

TABLE IX. GENERAL PARAMETERS FOR TC42

Parameter	Symbol	Value
Base Voltage	V_b	12.35 kV
Base Power	S_b	45 MVA

TABLE X. LINE PARAMETERS FOR TC42

From Bus	To Bus	R (Ω)	X (Ω)	From Bus	To Bus	R (Ω)	X (Ω)
1	2	0.259	0.808	9	10	0.015	0.015
2	3	0.031	0.031	9	42	0.153	0.046
3	4	0.046	0.092	10	11	0.107	0.076
3	14	0.092	0.031	11	12	0.076	0.046
3	15	0.214	0.046	15	18	0.046	0.015
4	20	0.336	0.061	15	16	0.107	0.015
4	5	0.107	0.183	20	21	0.122	0.092
5	26	0.061	0.015	20	25	0.214	0.046
5	6	0.015	0.031	21	22	0.198	0.046
6	27	0.168	0.061	27	31	0.046	0.015
6	7	0.031	0.046	27	28	0.107	0.031
7	32	0.076	0.015	28	29	0.107	0.031
7	8	0.015	0.015	29	30	0.061	0.015
8	40	0.046	0.015	32	33	0.046	0.015
8	39	0.244	0.046	33	34	0.031	0.000
8	41	0.107	0.031	35	36	0.076	0.015
8	35	0.076	0.015	35	37	0.076	0.046
8	9	0.031	0.031	35	38	0.107	0.015

TABLE XI. LOAD PARAMETERS FOR TC42

Bus No.	Peak MVA	Bus No.	Peak MVA
1	30.0	31	0.07
11	0.67	32	0.13
12	0.45	33	0.27
14	0.89	34	0.20
16	0.07	36	0.27
18	0.67	38	0.45
21	0.45	39	1.34
22	2.23	40	0.13
25	0.45	41	0.67
26	0.20	42	0.13
28	0.13	44	0.45
29	0.13	45	0.20
30	0.20	46	0.45

TABLE XII. SHUNT CAPACITOR BANK PARAMETERS FOR TC42

Bus No.	Nameplate Capacity (kVAR)
1	6000
3	1200
37	1800
47	1800

V.D. Parameters for TC2998

The feeder TC2998 is a 12.35 kV system model developed by EPRI for distribution system studies [27]. The model is too large to include in this document, but EPRI makes it freely available for download. The model was developed in EPRI's open-source software package for distribution system analysis, OpenDSS [39]. For this study, only phase A of the system is analyzed. A heat map of the voltage magnitudes on the system is visualized in Fig. 11.

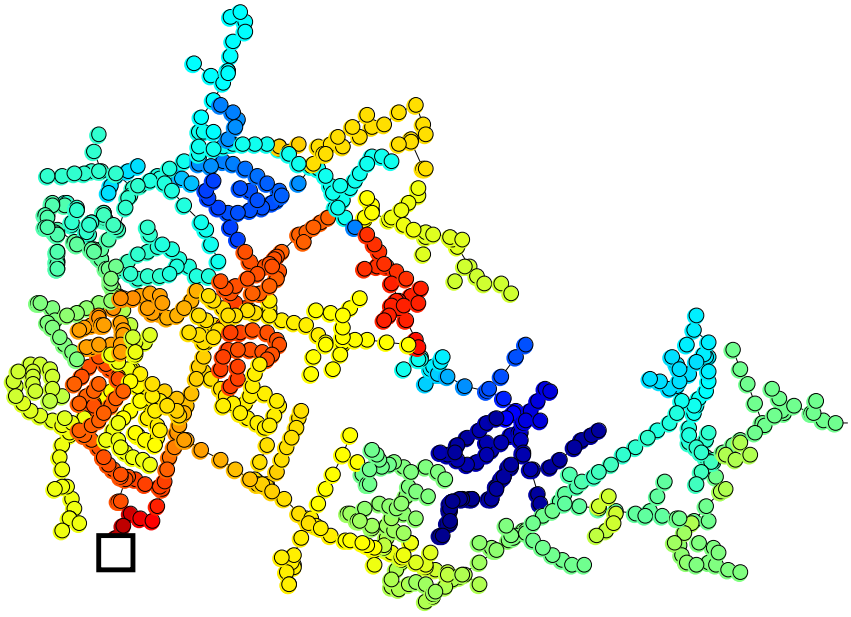

Fig. 11. Bus voltages for phase A of ckt5. Substation is designated with a white square. Voltage magnitudes range from 0.9716 pu (dark blue) to 1.0165 pu (dark red).

VI. NUMERICAL RESULTS

For TC42, the mapping of the nonmetric MDS is illustrated. For both TC17 and TC42, the performance of ESU placement using nonmetric MDS is presented, and compared with the placement using GA. For TC2998, a placement using CMDS is presented along with the computation time to produce that placement.

VI.A. Results for Performance Improvement and Validation on TC17 and TC42

The mapping of TC42 in the CMDS space is presented in Fig. 12 and Fig. 13. It is important to note that these figures do not merely scale the length of the lines proportionately to their impedances. Instead, the straight-line distance between any two buses approximates the impedance along the physical lines joining them.

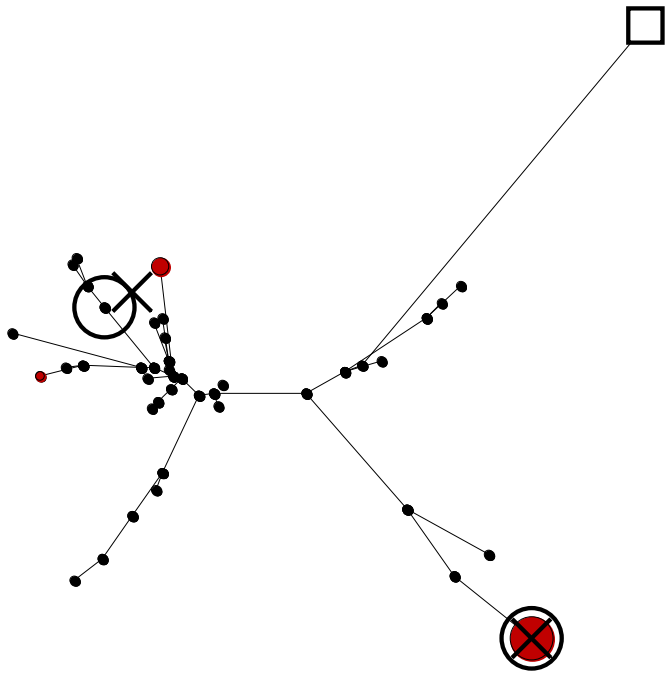

Fig. 12. Representation of TC42 in the MDS space. Substation is denoted by white square, ESU candidates by red circles with power injection proportional to the area, cluster centers by ×'s, and ESU locations by black circles.

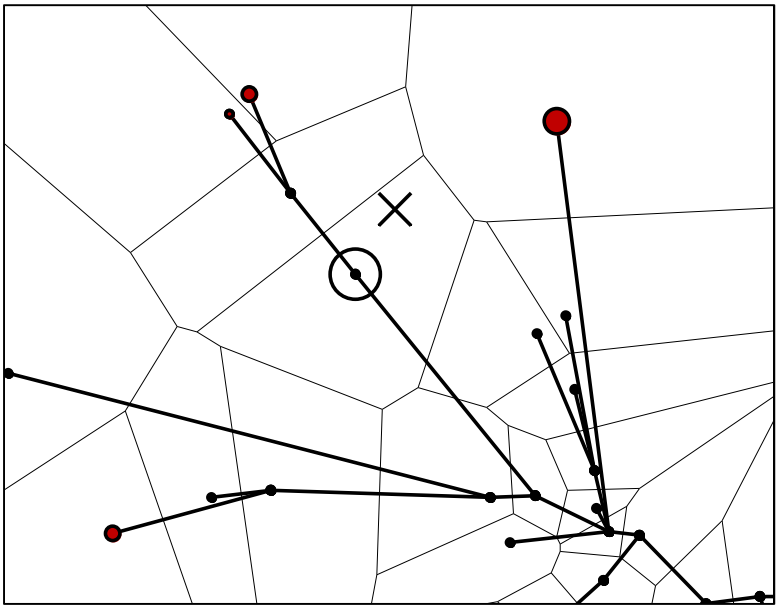

Fig. 13. Voronoi diagram of a portion of TC42 illustrating the region of the MDS space closest to each bus.

Fig. 13 illustrates a Voronoi diagram of a close-up of the feeder representation [34]. In a Voronoi diagram, the space is divided into regions consisting of all points that are closer to one seed (in this case, a bus) than any other. The figure demonstrates how the final bus to place an ESU is selected, by choosing the bus that falls within the same space as the cluster centroid corresponding to that ESU.

Fig. 14 and Fig. 15 illustrate the relationship between the all unique distances between buses in the feeders and in the nonlinear MDS approximations. In both case studies, the original and approximated distances are highly correlated, using Pearson's correlation coefficient, as Table XIII confirms [40].

Table XIV presents the energy savings gained by using the ESU. With a CVR factor representative of current distribution feeders, oversizing the ESU to inject reactive power will yield modest energy savings, even when considering PEI losses.

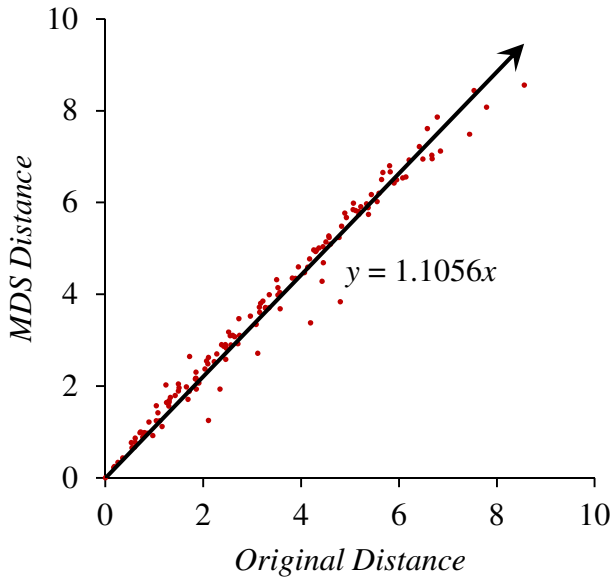

Fig. 14. Best-fit plot between original and predicted distances for TC17.

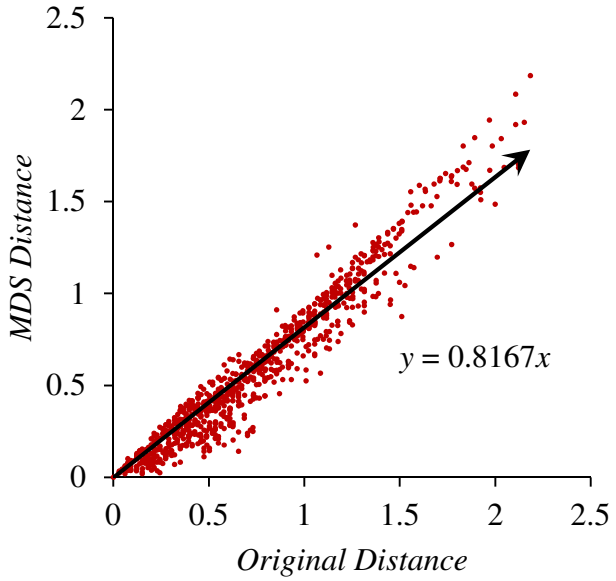

Fig. 15. Best-fit plot between original and predicted distances for TC42.

TABLE XIII. VERIFICATION OF MDS PERFORMANCE, STEADY-STATE VOLTAGE REGULATION AND FLICKER CONSTRAINTS

Test Case	Correlation Cofficient	Min. Voltage (pu)	Max. Voltage (pu)	Max. Flicker (%)
TC17	0.9896	0.9000	0.9555	2.1414
TC42	0.9693	0.9000	0.9236	0.8126

TABLE XIV. CHANGE IN FEEDER POWER UNDER CONSIDERED SCENARIOS

Real Power CVR Factor α	**Reactive Power CVR Factor β**	**ESU Oversizing k (%)**	**ESU Loss a (%)**	**Change in Power (%)**	
				TC17	**TC42**
α_1	β_1	k_1	a_1	−0.4561	−1.4418
α_1	β_1	0	a_1	−0.3139	−1.3547
0	0	k_1	a_1	+1.7380	+0.4370
α_1	β_1	k_1	a_0	+1.0442	+0.0286

However, if loads become constant power (caused by the move to loads with more PEI) then injecting reactive power via the ESU will actually increase losses. Similarly, if a PEI with sufficiently high losses is used for the ESU, then they will also increase losses when used to inject reactive power.

Table XV and Fig. 16 compare performance for both the MDS and GA placement methods. The table indicated that there was not a significant difference in performance between the two classes of methods for the case studies with the parameters listed in Table III. It is likely that the GA placement time could be reduced by an order of magnitude by reducing the number of generations required to establish convergence from 100 to 10. However, even with this reduction in time, the GA would still require about two orders of magnitude more time to complete than the MDS/clustering methodology. Fig. 16. compares the solution quality (in terms of peak feeder substation demand) for MDS, GA, and ESU placed at the beginning of the feeder adjacent to the substation (bus 2). In the figure, the ESU penetration is increased relative to the other analyses such that the total real power rating of the ESU is 50% of the total feeder real power demand (excepting loads connected directly to the substation). Although the installation cost of such a large amount of storage is prohibitive, this serves to increase the reduction in feeder power caused by ESU placement, making the difference in performance between the placement

methods more noticeable. The figure illustrates that although the GA method produces a higher quality solution, the difference in performance is low compared to the baseline placement near the substation. It is further worth noting that distribution feeder parameters are typically not known exactly. In particular, customer loads are estimated based on distribution transformer power ratings, substation power measurements, and historical metering data [41].

VI.B. Results for Verifying Scalability on TC2998

The projection of the CMDS transformation of TC2998 into two dimensions is illustrated in Fig. 17. Buses that appear to be adjacent (in the first two dimensions) on the three major arms of the feeder are actually well separated in the other dimensions not visualized. As described in Section III, the bottom 10^{th} percentile of buses (in terms of voltage magnitude) are selected as candidates for ESU placement. Given that this corresponds to only 302 points, the number of dimensions for each point must be restricted to ensure that the clusters remain well-separated. For this feeder, the ten dimensions corresponding to the ten largest eigenvalues were selected, which is sufficient to achieve a correlation coefficient of 0.9067.

TABLE XV. COMPARISON OF CMDS/CLUSTERING AND GA RESULTS

	TC17	**TC42**
MDS/Clustering Time To Complete (s)	5.4585	11.2086
GA Time to Complete (s)	4410.48 (1.2251 h)	14442.7 (4.0119 h)
MDS/Clustering ESU Buses	{9, 16}	{19, 37}
GA ESU Buses	{9, 16}	{12, 19}
MDS/Clustering Objective (MW)	9.7616	37.3589
GA Objective (MW)	9.7616	37.3591

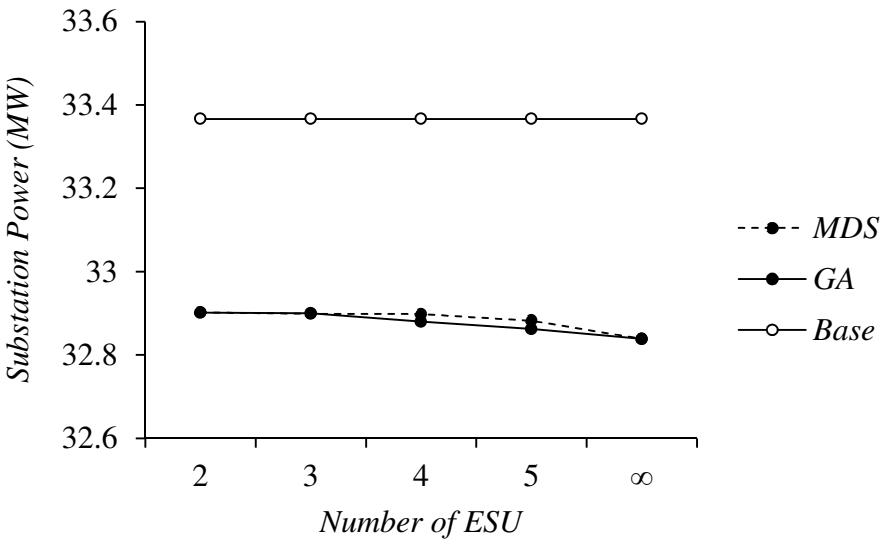

Fig. 16. Comparison of peak feeder demand for MDS, GA, and substation ESU placement on TC42.

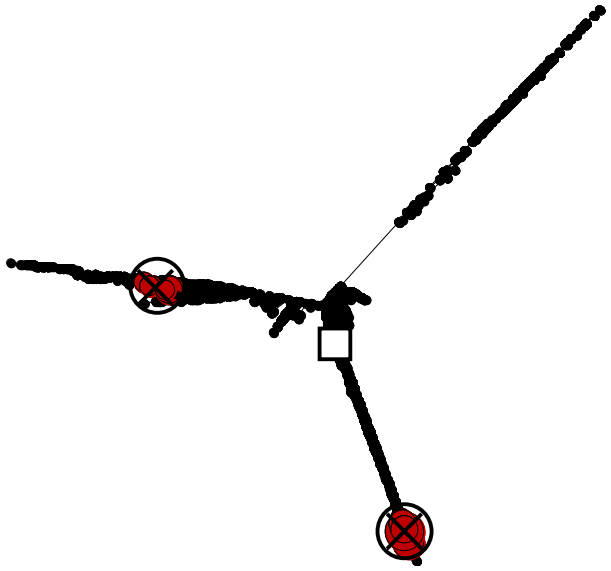

Fig. 17. ESU candidate locations (red), centroids (black x's), and final ESU buses (black circles) in the CMDS space for TC2998.

Fig. 18 illustrates the relationship between the original and CMDS distances for 500 randomly selected (with repetition) pairs of buses. The random subset of buses was selected for

visualization purposes; plotting all $\binom{2998}{2}$ combinations would not permit individual points to be distinguished. The candidate buses and selected buses for ESU placement (illustrated in the CMDS space in Fig. 17) are visualized in physical coordinates in Fig. 19. Without including the time to build the pairwise distance matrix, the placement takes 51.35 s on a system with an Intel Core i3 Processor and 8 GB RAM. Building the pairwise distance matrix takes significantly longer, though the implementation for doing so is not optimized and requires dynamically building shortest paths from the substation to each bus. A more efficient implementation that statically allocates memory would reduce this bottleneck significantly. The results of the placement are summarized in Table XVI.

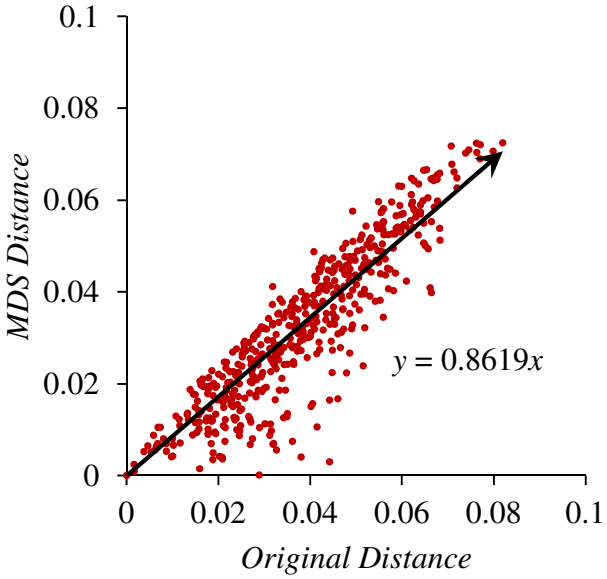

Fig. 18. Best-fit plot between original and predicted distances for TC2998.

VII. CONCLUSIONS

A placement method is described for ESU on a distribution system that reduces computation time compared to an existing GA approach while still providing a high quality solution. The method employs a novel heuristic search involving MDS and clustering.

Fig. 19. ESU candidate locations (red) and final buses (black circles) for TC2998. Marker area is proportional to ESU power injection.

TABLE XVI. SUMMARY OF RESULTS FOR TC2998

Parameter	Value
Number of ESU Candidate Buses	302
Correlation Between Original and CMDS Pairwise Distances	0.9067
MDS/Clustering Time To Complete Without Building Pairwise Distance Matrix	51.35 s

The method is applied to reach certain qualitative conclusions about the utility of dispersed ESU on a distribution system, while producing a solution with computation time on the order of seconds, compared to several hours required for GA. This faster solution time is of value to the distribution engineer who needs to quickly compare several different project options. Furthermore, given that distribution system loads are not known exactly, it is not guaranteed that the GA solution will indeed be of higher quality on the physical system.

Distributed ESU employed for peak shaving can indeed reduce distribution system power consumption, though distributed ESU may be limited in their ability to provide frequency regulation. Additionally, the capability of such ESU to reduce power consumption will decrease as loads move to having a constant-power characteristic. It is predicted that this decrease will occur as loads increasingly adopt PEI with PFC. This decrease will likely reduce the incentive for ESU to provide reactive power injection. However, increased efficiency of the PEI in ESU brought on by new semiconductor technologies such as SiC or GaN could enable ESU to still provide benefit. It is envisioned that future work could extend the method to placement of other types of shunt-connected distribution system equipment (such as distributed generation and shunt capacitors) and add support for unbalanced power flow. This would expand the applicability of the method to both current and future distribution systems.

REFERENCES

[1] D.P. Kothari and I.J. Nagrath, *Modern Power System Analysis*. New Delhi: Tata McGraw-Hill, 2003.

[2] Z. Li, "Natural gas for generation: a solution or a problem?," *IEEE Power and Energy Magazine*, vol. 3, no. 4, pp. 16–21, July 2005.

[3] S. Tewari and N. Mohan, "Value of NAS energy storage toward integrating wind: Results from the wind to battery project," *IEEE Transactions on Power Systems*, vol. 28, no. 1, pp. 532–541, 2013.

[4] H. Daneshi and A. Srivastava, "Security-constrained unit commitment with wind generation and compressed air energy storage," *IET Generation, Transmission Distribution*, vol. 6, no. 2, pp. 167–175, February 2012.

[5] M. Rahimiyan, L. Baringo, and A. Conejo, "Energy management of a cluster of interconnected price-responsive demands," *IEEE Transactions on Power Systems*, vol. 29, no. 2, pp. 645–655, March 2014.

[6] X. Xu, J. Mitra, T. Wang, and L. Mu, "Evaluation of operational reliability of a microgrid using a short-term outage model," *IEEE Transactions on Power Systems*, vol. 29, no. 5, pp. 2238–2247, September 2014.

[7] L. Mears, H. Gotschall, and H. Kamath, "EPRI-DOE handbook of energy storage for transmission and distribution applications," EPRI, Tech. Rep. 1001834, December 2003.

[8] S.O. Geurin, A.K. Barnes, and J.C. Balda, "Smart grid applications of selected energy storage technologies," in *IEEE PES Innovative Smart Grid Technologies (ISGT)*, 2012, pp. 1–8.

[9] J. Eyer and G. Corey, "Energy storage for the electricity grid: Benefits and market potential assessment guide," Sandia National Laboratories, Tech. Rep. SAND2010-0815, 2010.

[10] S. Gill, I. Kockar, and G.W. Ault, "Dynamic optimal power flow for active distribution networks," *IEEE Transactions on Power Systems*, vol. 29, no. 1, pp. 121–131, January 2014.

[11] G. Carpinelli, G. Celli, S. Mocci, F. Mottola, F. Pilo, and D. Proto, "Optimal integration of distributed energy storage devices in smart grids," *IEEE Transactions on Smart Grid*, vol. 4, no. 2, pp. 985–995, June 2013.

[12] C.A. McCarthy and J. Josken, "Applying capacitors to maximize benefits of conservation voltage reduction," in *Rural Electric Power Conference*, 2003, pp. C4–1– C4–5.

[13] K.P. Schneider and T.F. Weaver, "A method for evaluating volt-VAR optimization field demonstrations," *IEEE Transactions on Smart Grid*, vol. 5, no. 4, pp. 1696–1703, July 2014.

[14] Caisheng Wang and M.H. Nehrir, "Analytical approaches for optimal placement of distributed generation sources in power systems," *IEEE Transactions on Power Systems*, vol. 19, no. 4, pp. 2068– 2076, November 2004.

[15] S. Elsaiah, M. Benidris, and J. Mitra, "Analytical approach for placement and sizing of distributed generation on distribution systems," *IET Generation, Transmission Distribution*, vol. 8, no. 6, pp. 1039–1049, June 2014.

[16] R.S.A. Abri, E.F. El-Saadany, and Y.M. Atwa, "Distributed generation placement and sizing method to improve the voltage stability margin in a distribution system," in

International Conference on Electric Power and Energy Conversion Systems (EPECS), 2011, pp. 1–7.

[17] P.S. Georgilakis and N.D. Hatziargyriou, "Optimal distributed generation placement in power distribution networks: models, methods, and future research," *IEEE Transactions on Power Systems*, vol. 28, no. 3, pp. 3420–3428, August 2013.

[18] M.F. Shaaban, Y.M. Atwa, and E.F. El-Saadany, "DG allocation for benefit maximization in distribution networks," *IEEE Transactions on Power Systems*, vol. 28, no. 2, pp. 639–649, May 2013.

[19] G. Carpinelli, G. Celli, S. Mocci, F. Mottola, F. Pilo, and D. Proto, "Optimal Integration of Distributed Energy Storage Devices in Smart Grids," *IEEE Transactions on Smart Grid*, vol. 4, no. 2, pp. 985–995, June 2013.

[20] M. Farivar and S.H. Low, "Branch flow model: Relaxations and convexification; Part I," *IEEE Transactions on Power Systems*, vol. Early Access Online, 2013.

[21] M. Farivar and S.H. Low, "Branch flow model: Relaxations and convexification; Part II," *IEEE Transactions on Power Systems*, vol. Early Access Online, 2013.

[22] E. Dall'Anese, H. Zhu, and G.B. Giannakis, "Distributed optimal power flow for smart microgrids," *IEEE Transactions on Smart Grid*, vol. 4, no. 3, pp. 1464–1475, September 2013.

[23] J. Lavaei, D. Tse, and B. Zhang, "Geometry of power flows and optimization in distribution networks," *IEEE Transactions on Power Systems*, vol. 29, no. 2, pp. 572–583, March 2014.

[24] S. Boyd and L. Vandenberghe, *Convex Optimization*. Cambridge University Press, 2009.

[25] M. Grant, S. Boyd, and Y. Ye, "CVX: Matlab software for disciplined convex programming," 2008. [Online]. Available: http://cvxr.com/cvx/download/. [Accessed: 19-Sep-2014].

[26] A.K. Barnes and J.C. Balda, "Placement of distributed energy storage via multidimensional scaling and clustering," in *International Conference on Renewable Energy Research and Applications (ICRERA)*, Milwaukee, WI, 2014.

[27] EPRI, "Summary of EPRI test circuits." [Online]. Available: http://svn.code.sf.net/p/electricdss/code/trunk/Distrib/EPRITestCircuits/. [Accessed: 10-Nov-2013].

[28] M. Baran and F.F. Wu, "Optimal sizing of capacitors placed on a radial distribution system," *IEEE Transactions on Power Delivery*, vol. 4, no. 1, pp. 735–743, January 1989.

[29] M.E. Baran and F.F. Wu, "Optimal capacitor placement on radial distribution systems," *IEEE Transactions on Power Delivery*, vol. 4, no. 1, pp. 725–734, January 1989.

[30] M. Farivar, C.R. Clarke, S.H. Low, and K.M. Chandy, “Inverter VAR control for distribution systems with renewables,” in *SmartGridComm*, 2011, pp. 457–462.

[31] G.A.F. Seber, *Multivariate observations*. Wiley, 1984.

[32] F. Belmudes, D. Ernst, and L. Wehenkel, “Pseudo-geographical representations of power system buses by multidimensional scaling,” in *International Conference on Intelligent System Applications to Power Systems*, 2009, pp. 1–6.

[33] G. Yesuratnam and D. Thukaram, “Congestion management in open access based on relative electrical distances using voltage stability criteria,” *Electric Power Systems Research*, vol. 77, no. 12, pp. 1608–1618, October 2007.

[34] R.O. Duda, P.E. Hart, and D.G. Stork, *Pattern Classification*. Wiley, 2001.

[35] J.C. Carlisle, A.A. El-Keib, D. Boyd, and K. Nolan, “A review of capacitor placement techniques on distribution feeders,” in *Southeastern Symposium on System Theory*, 1997, pp. 359–365.

[36] K. Abookazemi, M.Y. Hassan, and M.S. Majid, “A review on optimal placement methods of distribution generation sources,” in *IEEE International Conference on Power and Energy (PECon)*, 2010, pp. 712–716.

[37] A.D. Alarcón-Rodríguez, “A multi-objective planning framework for analysing the integration of distributed energy resources,” M.S. Thesis, University of Strathclyde, Glasgow, 2009.

[38] W.M. Grady, M.J. Samotyj, and A.H. Noyola, “The application of network objective functions for actively minimizing the impact of voltage harmonics in power systems,” *IEEE Transactions on Power Delivery*, vol. 7, no. 3, pp. 1379–1386, July 1992.

[39] R.C. Dugan, “Reference Guide: The Open Distribution System Simulator (OpenDSS),” Jun-2013. [Online]. Available: http://svn.code.sf.net/p/electricdss/code/trunk/Distrib/Doc/OpenDSSManual.pdf. [Accessed: 11-Sep-2014].

[40] G. Casella and R.L. Berger, *Statistical Inference*, 2nd edition. Australia ; Pacific Grove, CA: Cengage Learning, 2001.

[41] H.L. Willis, *Power Distribution Planning Reference Book*. CRC Press, 2004.

Appendix A: Certification of First Author

I hereby certify that Arthur K. Barnes is first author of the article this chapter is based on and has completed at least 51% of the work described in the article.

Juan Carlos Balda

Signature _____

Date _____

APPENDIX. A: OPTIMALITY OF ESU AT LOAD

It is shown via a simplified case as follows that the optimal location for an ESU performing peak shaving is at the load. In this case a three-bus dc system is considered, shown in Fig. A1, and voltage drop is assumed to be negligible. A load is connected to a generator along a line whose total resistance is R. During peak times, the load draws current I_p, and during off-peak times, it draws current I_o.

An ESU is connected to the line at a fraction θ of the distance from the generator to the load. The ESU charges and discharges with current magnitude I_b. It is assumed that the variation of the load current during periods of ESU charging and discharging is negligible. This is illustrated in Fig. A2.

Neglecting the periods when the ESU is not operating, the energy losses L due to resistive losses and ESU losses are

$$L = \theta R T_d \left(I_p - I_b\right)^2 + \theta R \eta^{-1} T_d (I_o + I_b)^2 + T_d (1-\eta) I_b + (1-\theta) R T_d I_p + (1-\theta) R \eta^{-1} T_d I_o \quad \text{(A1)}$$

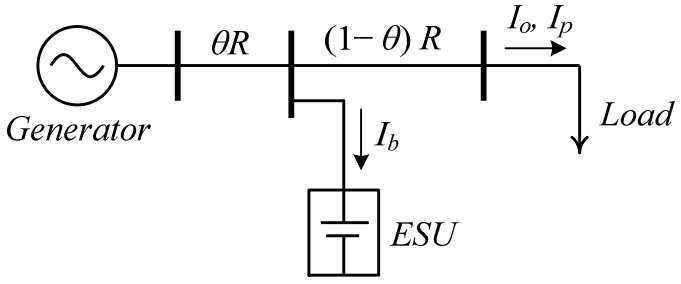

Fig. A1. Simplified case for calculation of optimal ESU location.

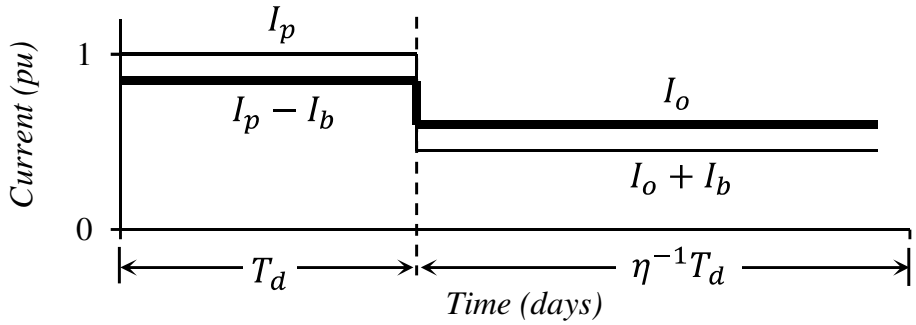

Fig. A2. Two-level load profile for calculation of the optimal ESU location.

In the above, T_d is the ESU discharge duration and η is the ESU efficiency. The optimal battery current I_b is solved for by taking the derivative of L, setting it equal to 0, and solving for I_b

$$\frac{\partial L}{\partial I_b} = -2\theta R T_d\left(I_p - I_b\right) + 2\theta R\eta^{-1}T_d(I_o + I_b) + T_d(1-\eta). \tag{A2}$$

It is verified that this is indeed an optimum by checking that the second derivative is positive

$$\frac{\partial^2 L}{\partial I_b^2} = 2\theta R T_d + 2\theta R\eta^{-1}T_d. \tag{A3}$$

The optimal I_b^* is

$$I_b^* = \frac{I_p - \eta^{-1}I_o - (1-\eta)/(2\theta R)}{\eta^{-1}+1}. \tag{A4}$$

As the efficiency η approaches 1, I_b^* approaches half the difference between I_p and I_o. This has the effect of smoothing out the overall current over the course of a day as much as possible. To locate the optimal location θ of the ESU, the derivative of the ESU losses with respect to θ are taken

$$\frac{\partial L}{\partial I_b} = \left[R T_d\left(I_p - I_b^*\right)^2 + R\eta^{-1}T_d(I_o + I_b^*)^2\right] - \left[R T_d I_p + R\eta^{-1}T_d I_o\right]. \tag{A5}$$

In the above, it is apparent that this derivative is the difference between the losses for optimal I_b (I_b^*) and zero I_b (0). By the definition of an optimum, the derivative is less than or equal to zero. Additionally, it is noted that the derivative is constant. For functions with a constant derivative, the minimum will occur at an constraint boundary, in this case, the value $\theta = 1$. Therefore, it follows that for an ESU performing arbitrage, the optimal location to reduce losses is at the load bus.

APPENDIX B: RELEASE FOR USE IN DISSERTATION

Thesis / Dissertation Reuse

The IEEE does not require individuals working on a thesis to obtain a formal reuse license, however, you may print out this statement to be used as a permission grant:

Requirements to be followed when using any portion (e.g., figure, graph, table, or textual material) of an IEEE copyrighted paper in a thesis:

1) In the case of textual material (e.g., using short quotes or referring to the work within these papers) users must give full credit to the original source (author, paper, publication) followed by the IEEE copyright line © 2011 IEEE.

2) In the case of illustrations or tabular material, we require that the copyright line © [Year of original publication] IEEE appear prominently with each reprinted figure and/or table.

3) If a substantial portion of the original paper is to be used, and if you are not the senior author, also obtain the senior author's approval.

Requirements to be followed when using an entire IEEE copyrighted paper in a thesis:

1) The following IEEE copyright/ credit notice should be placed prominently in the references: © [year of original publication] IEEE. Reprinted, with permission, from [author names, paper title, IEEE publication title, and month/year of publication]

2) Only the accepted version of an IEEE copyrighted paper can be used when posting the paper or your thesis on-line.

3) In placing the thesis on the author's university website, please display the following message in a prominent place on the website: In reference to IEEE copyrighted material which is used with permission in this thesis, the IEEE does not endorse any of [university/educational entity's

name goes here]'s products or services. Internal or personal use of this material is permitted. If interested in reprinting/republishing IEEE copyrighted material for advertising or promotional purposes or for creating new collective works for resale or redistribution, please go to http://www.ieee.org/publications_standards/publications/rights/rights_link.html to learn how to obtain a License from RightsLink.

If applicable, University Microfilms and/or ProQuest Library, or the Archives of Canada may supply single copies of the dissertation.

CHAPTER SEVEN

SELECTION OF CONVERTER TOPOLOGIES FOR DISTRIBUTED ENERGY RESOURCES

Arthur Barnes, Juan Carlos Balda and Corris M. Stewart

A.K. Barnes, J.C. Balda, and C.M. Stewart, "Selection of converter topologies for distributed energy resources," in *IEEE Applied Power Electronics Conference and Exposition (APEC)*, 2012, pp. 1418–1423.

Abstract **— Distributed energy resources (DER) are becoming increasingly common on the electrical grid. Depending on the operating conditions of the DER, which depend on the application, different topologies need to be selected in order to achieve the maximum efficiency of each DER. Complicating the selection is the fact that operating conditions vary over time. For example, the voltage and current drawn from a PV panel varies over the course of a day. To calculate the overall efficiency, the efficiency of a topology at each operating point and the amount of time spent at that operating point must be considered. This work extends existing analytical methods for loss calculations by taking this into account. The specific DER applications considered are a three-phase ultracapacitor energy storage unit (UC-ESU), battery energy storage unit (B-ESU), and photovoltaic array (PV). This work determines for each application if an inverter-only (single-stage) or an inverter plus boost converter (double-stage) topology is more efficient. The results show that a single-stage topology is better for the B-ESU and PV, while the double-stage topology is better for the UC-ESU. The method is applicable to other DER types, including wind turbines, micro-hydro generators, variable-speed gensets, and microturbines.**

I. NOMENCLATURE

P	Real power injected by ESU into grid
Q	Real power injected by ESU into grid
S_{rated}	Rated ESU power
E_{ll}	Inverter output line-line voltage magnitude
ϕ	Inverter output voltage phase
V_{ll}	Grid line-line voltage magnitude
X	Equivalent impedance of output filter
V_{dc}	Equivalent impedance of output filter
f_{sw}	Switching frequency
P_{loss}	Total converter losses

I.A. Inverter Loss Calculations

m_a	Inverter modulation index
pf	Inverter power factor
I_o	Inverter output current
P_{CT1}	Inverter conduction losses for a single IGBT
P_{CD1}	Inverter conduction losses for a single diode
P_{swT1}	Inverter switching losses for a single IGBT
P_{swD1}	Inverter switching losses for a single diode (negligible, not used)
$P_{loss,inv}$	Total inverter power losses

I.B. Boost Converter Loss Calculations

V_{in}	Boost converter input voltage
L	Boost converter inductance

D Boost converter duty cycle

I_L Boost converter inductor current

ΔI_L Boost converter inductor current ripple

I_{Ton} Boost converter IGBT turn-on current

I_{Toff} Boost converter IGBT turn-off current

I_{Tav} Boost converter IGBT average current

I_{Trms} Boost converter IGBT rms current

I_{Dav} Boost converter diode average current

I_{Drms} Boost converter diode rms current

$P_{CT1,dc}$ Boost converter conduction losses for a single IGBT

$P_{CD1,dc}$ Boost converter conduction losses for a single diode

$P_{swT1,dc}$ Boost converter switching losses for a single IGBT

$P_{swD1,dc}$ Boost converter switching losses for a single diode (negligible, not used)

$P_{loss,dc}$ Total converter losses

I.C. Device Parameters

V_{ce0} IGBT zero-current voltage drop

r_c IGBT on-state resistance

V_{d0} Diode zero-current forward voltage drop

r_d Diode on-state forward resistance

V_{dcnom} IGBT dc-bus voltage under nominal conditions

I_{cnom} IGBT conduction current under nominal conditions

E_{on} IGBT turn-on switching loss under nominal conditions

E_{off} IGBT turn-off switching loss under nominal conditions

I.D. Ultracapacitor Calculations

C Ultracapacitor capacitance

V_c Ultracapacitor voltage

J Ultracapacitor energy

II. INTRODUCTION

Distributed generation and energy storage, collectively referred to as DER, are two enabling technologies for future distribution systems. These allow for both increased penetration of renewable sources as well as the relocation of generation assets closer to load centers, reducing energy consumption, system losses, and enhancing system reliability in the presence of contingencies [1], [2]. Many DER are dc in nature. These include: batteries, ultracapacitors, photovoltaic cells, and permanent magnet generators (dc link). The latter see applications in wind turbines, micro hydro generators, and small fossil-fuel generators based on reciprocating engines and microturbines [1], [3–5]. Permanent magnet generators are used because of their high efficiencies [6]. Additionally, by using a converter the prime mover speed is independent of the output electrical frequency. This allows for increased efficiency under a wide range of operating conditions [7].

Many different converter topologies have been developed to connect DER to the grid [8–11], though most converters use the single and double-stage inverter topologies [12], [13]. The former connects a three-phase inverter directly to the DER, while the latter connects it via a boost converter. These are depicted in Fig. 1.

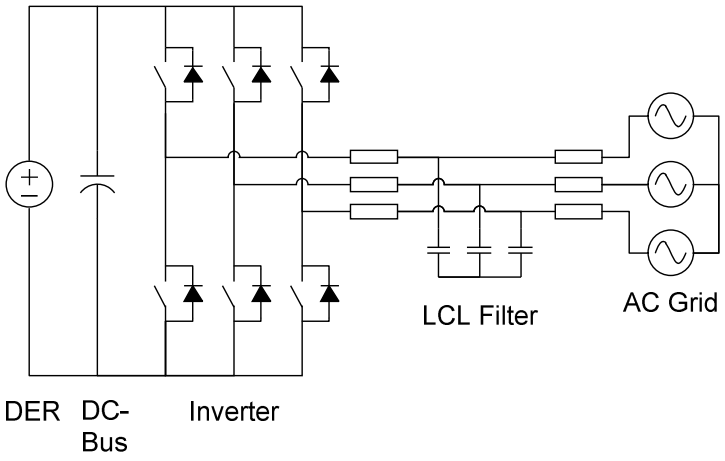

(a) Single-stage inverter.

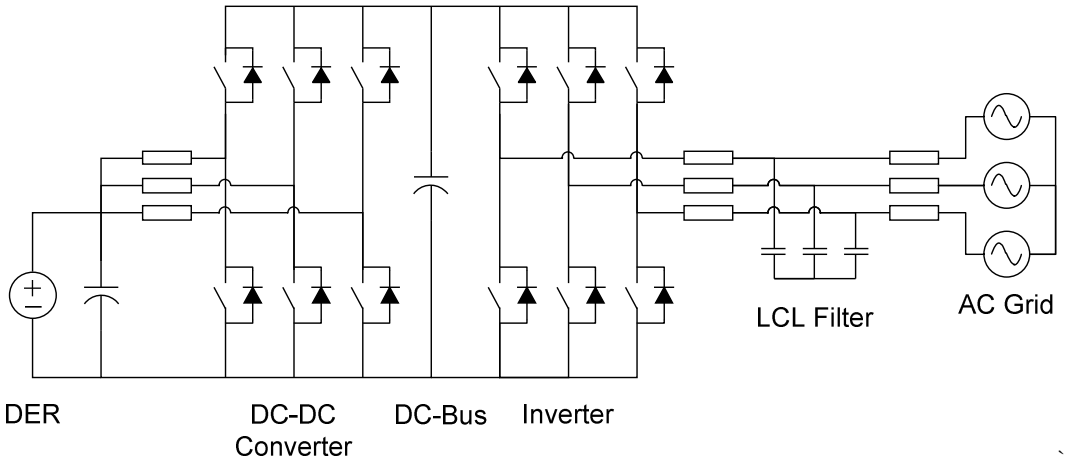

(b) Double-stage inverter.

Fig. 1. Single and double-stage inverter topologies.

Goals when selecting a topology include: increasing efficiency, reducing output current and voltage harmonics, decreasing size, and reducing cost [10], [11], [14]. Although the two topologies have the same harmonic content and similar size, which one is more efficient varies depending on the operating conditions [12].

The work in [15] compares dc-dc converter topologies for connecting an ultracapacitor bank to the dc-bus of a hybrid electric vehicle. Similarly, [12] compares the efficiency of single vs. double-stage topologies at different dc input voltages. More recently, [14], [16] compare dc-dc converter and transformer-less inverter topologies for PV, respectively. Their method uses datasheet parameters for the switching devices as inputs to analytical expressions for converter losses. The work of [17] compares the two topologies for the case of PV connecting to single-phase ac considering the effect of 120 Hz voltage ripple on the MPPT efficiency of a PV array. However, converter efficiencies are approximated as constant, and experimental results are limited to several points over a single day. This work extends the method of [12], [14], [16] to calculate the overall efficiencies of the two topologies for three-phase DER with varying operating conditions, in this case B-ESU, UC-ESU, and PV.

Section II describes the selection of the parameters of the distributed energy resources, based on the desired output power and voltage, the analytical methods used to calculate losses, and the extension to sources with varying input voltages. Section III shows efficiency curves for varying input voltages, and lists overall efficiencies. Section IV presents conclusions about the proposed method guiding the selection of a particular topology for a particular application.

III. BACKGROUND AND EVALUATION METHOD

In order to calculate the converter efficiency, the required dc-bus voltage of the converter is first selected based on the ac grid voltage, the impedance of the inverter output filter, and the desired reactive power output. This work focuses on a DER that interfaces to either a low-voltage or medium-voltage three-phase ac grid through a transformer. The filter impedance is approximated as a series inductance that is a fixed percentage of the inverter base impedance [18]. The DER is designed to assist with local voltage regulation or reactive power

compensation. This is accomplished through the injection of reactive power by the inverter. It is assumed that the operating range of the inverter is a circle in the PQ-space as shown in Fig. 2.

III.A. Output Voltage Selection

The dc-bus voltage must be high enough for it to accomplish this task. The DER is modeled as a voltage source in series with an inductor, as shown in Fig. 3. From [1] the real and reactive powers through an inductor are approximately

$$P \approx \frac{E_{ll} V_{ll}}{X} \phi \tag{1}$$

$$Q \approx \frac{V_{ll}}{X} (E_{ll} - V_{ll}), \tag{2}$$

where P and Q are the real and reactive powers, respectively, E_{ll} and V_{ll} are the inverter and grid voltages, respectively, and ϕ is the phase of the inverter voltage. For the case of the double-stage topology, appropriate values for the dc-bus voltage and transformer turns are selected so it is able to inject rated reactive power into the grid. For the case of the single-stage topology, a sufficient transformer turns ratio is selected so the DER can inject rated reactive power when the input voltage is at its minimum.

Analytical expressions are used to calculate the losses at each operating point for the three-phase inverter and boost converter. The operating point is defined by the dc voltage and current of the DER and the power factor of the inverter. Depending on the type of DER, either a parameter sweep is used to plot efficiency over the range of operating conditions, or the overall efficiency is calculated using recorded data over time for the DER.

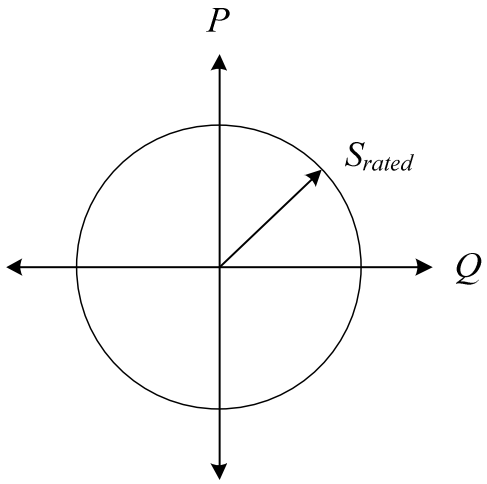

Fig. 2. Operating area of a grid- connected inverter in PQ-space.

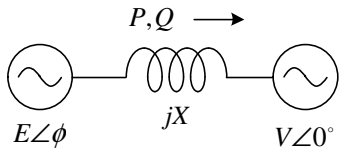

Fig. 3. Inverter model.

III.B. Loss Calculations

The method described in [19] is used to calculate the losses for three-phase inverter and dc-dc converter. The losses are divided into IGBT conduction losses, freewheeling diode conduction losses, and IGBT switching losses. The diode switching losses are assumed to be small and neglected. The formulas used are

$$P_{CT1} = V_{ce0} I_o \left(\frac{1}{2\pi} + \frac{m_a pf}{8}\right) + r_c I_o^2 \left(\frac{1}{8} + \frac{m_a pf}{3\pi}\right) \tag{3}$$

$$P_{CD1} = V_{d0} I_o \left(\frac{1}{2\pi} - \frac{m_a pf}{8}\right) + r_d I_o^2 \left(\frac{1}{8} - \frac{m_a pf}{3\pi}\right) \tag{4}$$

$$P_{swT1} = \frac{f_{sw}}{\pi}\left(E_{on} + E_{off}\right) \cdot \left(\frac{V_{dc}}{V_{cnom}} \cdot \frac{I_o}{I_{cnom}}\right) \tag{5}$$

for the losses in each device in the inverter. It is assumed that switching losses are linearly related to the conduction current, so that the switching losses can be calculated using the average switch current over a half cycle. Additionally, it is assumed that the switching losses are linearly related to the dc-link voltage. The total inverter losses are

$$P_{loss,inv} = 6(P_{CT1} + P_{CD1} + P_{swT1}). \tag{6}$$

The operating parameters for the dc-dc converter are

$$I_L = \frac{P}{3V_{in}} \tag{7}$$

$$D = 1 - \frac{V_{in}}{V_{dc}} \tag{8}$$

$$\Delta I_L = \frac{D}{L} \cdot \frac{V_{in}}{V_{dc}} \tag{9}$$

$$I_{Ton} = I_L - \Delta I_L/2 \tag{10}$$

$$I_{Toff} = I_L + \Delta I_L/2 \tag{11}$$

$$I_{Tav} = DI_L \tag{12}$$

$$I_{Trms}^2 = DI_L^2 \tag{13}$$

$$I_{Dav} = (1 - D)I_L \tag{14}$$

$$I_{Drms}^2 = (1 - D)I_L^2. \tag{15}$$

Note that for the purpose of calculating the dc-dc converter losses, the inverter losses are neglected, so the input power of the dc-dc converter is set equal to the output power. The losses for each switch of the dc-dc converter are

$$P_{CT1,dc} = V_{ce0} I_{Tav} + r_c I_{Trms}^2 \tag{16}$$

$$P_{CD1,dc} = V_{D0} I_{Dav} + r_D I_{Drms}^2 \tag{17}$$

$$P_{swT1,dc} = f_{sw} \left(E_{on} \cdot \frac{I_{Ton}}{I_{cnom}} + E_{off} \cdot \frac{I_{Toff}}{I_{cnom}} \right) \cdot \frac{V_{dc}}{V_{dcnom}}. \tag{18}$$

Because the dc-dc converter uses a three-phase interleaved design, the total losses for the dc-dc converter are

$$P_{loss,c} = 3\left(P_{CT1,dc} + P_{CD1,dc} + P_{swT1,dc}\right). \tag{19}$$

In order to calculate overall losses, several steps are performed: First, a minimum input voltage is selected, and the DER output transformer is designed based on this. Second, the efficiency with respect to input voltage is plotted for each DER/topology combination. If the efficiencies for the two types do not cross as illustrated in Fig. 4, then one topology is always more efficient and no further analysis need be performed.

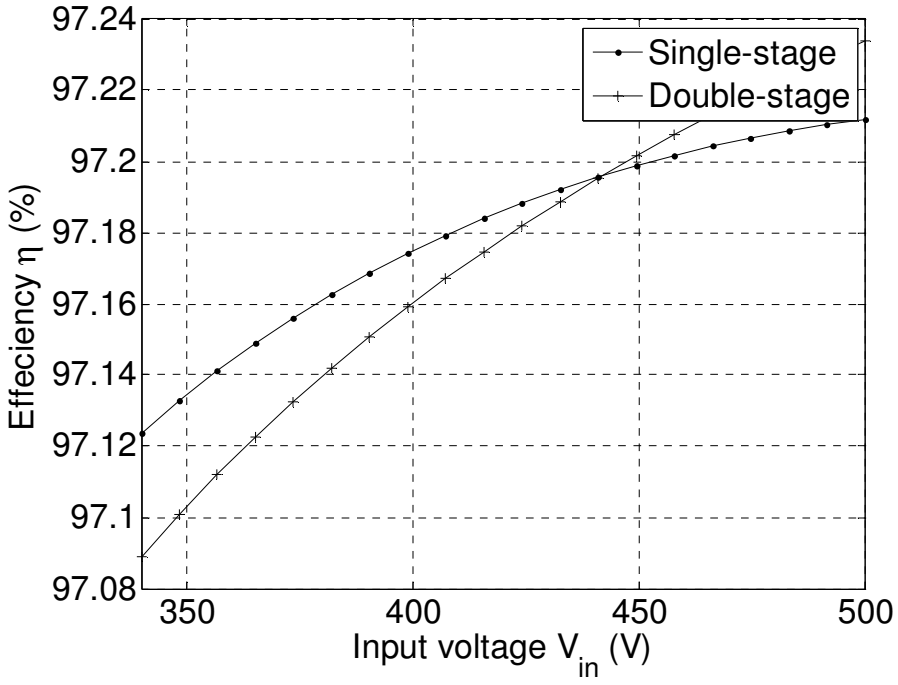

Fig. 4. Efficiency of generic DER with 340 V minimum input and power factor of 0.8.

This is the case for the UC-ESU and B-ESU, as illustrated in Section IV. The case of the PV is more difficult because there is not a natural input voltage range as with the other two types. Instead, there is a tradeoff in selecting the minimum input voltage, which in this case is the minimum maximum-power-point-tracking (MPPT) voltage. For the case of the single-stage converter, decreasing the MPPT voltage results in more energy extracted from the photovoltaic panels, but a less efficient converter design. The best configuration represents an optimal tradeoff between the two criteria.

IV. PROBLEM SETUP

The devices used for the experiment are the ABB 5SNS 0300U120100 1200 V/300 A three-phase IGBT integrated power modules (IPM) [20]. Two modules are used; one for the output inverter and one for the three-phase interleaved dc-dc converter. The on-resistances are estimated from the plot of collector-emitter voltage vs. collector current using the manufacturer's recommended gate-emitter voltage. These and other parameters are illustrated in Table I.

For this case, it is assumed that the BESS uses a 100 kVA inverter and connects to 208Vac line-line. The module uses an LCL filter that can be modeled as a series reactance of approximately 10% [18].

TABLE I. SEMICONDUCTOR DEVICE PARAMETERS USED FOR ABB 5SNS 0300U120100 1200 V/300 A IPM

Parameter	Symbol	Value
IGBT zero-current voltage drop	V_{ce0}	1.34 V
IGBT on-state resistance	R_{ce}	1.217 mΩ
IGBT conduction current under nominal conditions	I_{cnom}	300 A
IGBT dc-bus voltage under nominal conditions	V_{dcnom}	600 V
IGBT turn-on switching loss under nominal conditions	E_{on}	28 mJ
IGBT turn-off switching loss under nominal conditions	E_{off}	34 mJ
Diode zero-current forward voltage drop	V_{D0}	1.5 V
Diode on-state forward resistance	R_D	1.429 mΩ

The exact value of the reactance is 43 mΩ. Using the expression for reactive power, the 10% reactance can be substituted into (2). For a 208Vac grid this yields a required inverter output voltage of 230 V, or $1.1V_{ll}$.

The methods used in the previous section yield efficiencies for several different inverter configurations. The double-stage inverter uses a 500 V dc bus and is connected to 208Vac. For the case of the single-stage transformer the output ac voltage is selected using (2), the minimum dc-bus voltage the inverter will operate at, and the relationship for line-line output voltage vs. dc-bus voltage

$$E_{ll} = 0.612 m_a V_{dc}. \tag{20}$$

Based on the results of Subsection (A), for the case of the maximum output voltage where $m_a = 1$ at the minimum dc-bus voltage $V_{dc,min}$,

$$V_{ll} \leq \frac{0.612}{1.1} V_{dc,min}. \tag{21}$$

If the condition of (21) is met, then the inverter will always be able to supply rated reactive power. This is used to find the required output ac voltage based on the minimum input voltage from the energy source.

For the case of the UC-ESU, it is assumed that the ultracapacitor is discharged at 25% state-of-charge, or half of rated voltage. This is taken from the formula for energy in a capacitor.

$$J = \frac{1}{2} C V_c^2. \tag{22}$$

It is assumed that the UC-ESU uses 4 125 V modules in a series configuration, for a total rated voltage of 500 V [21].

For the case of the B-ESU, the maximum battery voltage is the voltage at the end of charging, which is also set at 500 V. The nominal battery voltage is 440 V. The minimum battery voltage is the voltage during discharge, at which point the state-of-charge has fallen to 80%. This minimum voltage is 370 V. These battery voltages are calculated based on the standby voltages and terminal voltages recorded during charge/discharge curves for individual Li-Ion cells during a series of battery characterization experiments [22].

V. NUMERICAL RESULTS FOR EFFICIENCY CURVES

Fig. 4 compares the efficiency of the single and double-stage converters when the voltage for a generic DER is in the range of 330–500 V. In this case the more efficient topology depends on if the input voltage is greater than 440 V. However, for DER with a minimum input voltage higher than approximately 340 V, the single-stage topology is always more efficient, and for DER with a minimum voltage lower than approximately 340 V, the double-stage topology is always more efficient. Fig. 5 shows that the double-stage topology is always more efficient for the UC-ESU, which has a minimum input voltage of 250 V. Fig. 6 and Fig. 7 illustrate that the single-stage topology is always more efficient for the B-ESU, though only by a small fraction.

The case of PV is more complicated. Fig. 8 shows PV data taken at the Florida Solar Energy Center over one week [23]. Input current is roughly proportional to the output power, while input voltage remains fairly constant except at low power levels. During operation, current is uniformly distributed between 0–175 A, while voltage is normally distributed around 450 V. The tight voltage range suggests that the single-stage topology is more efficient.

Fig. 9 compares the average output power of the two topologies on the dataset using different minimum MPPT voltages. As expected, the single-stage is slightly more efficient given an appropriate choice of the minimum MPPT voltage.

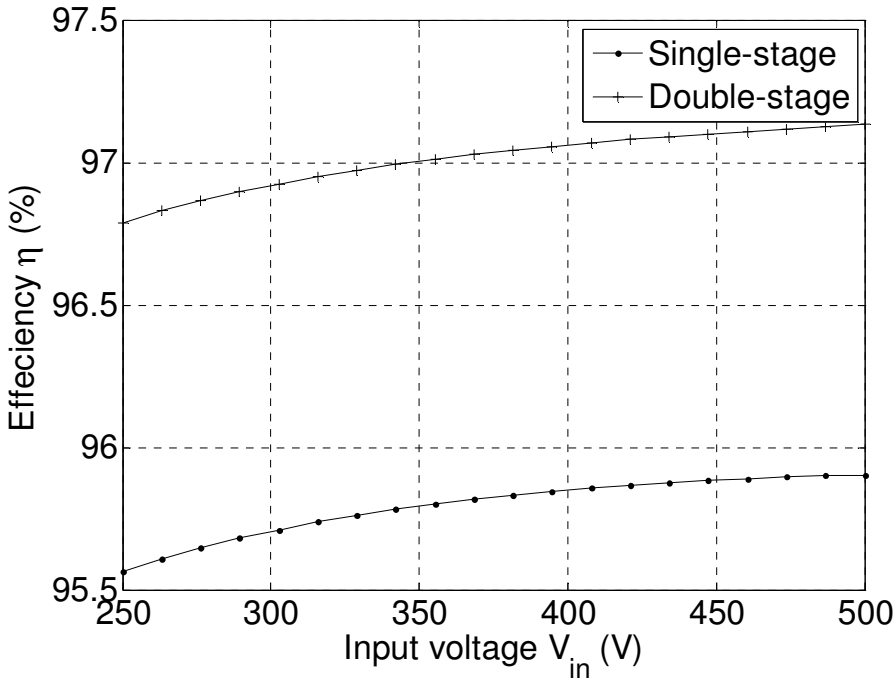

Fig. 5. Efficiency of UC-ESU injecting rated real power.

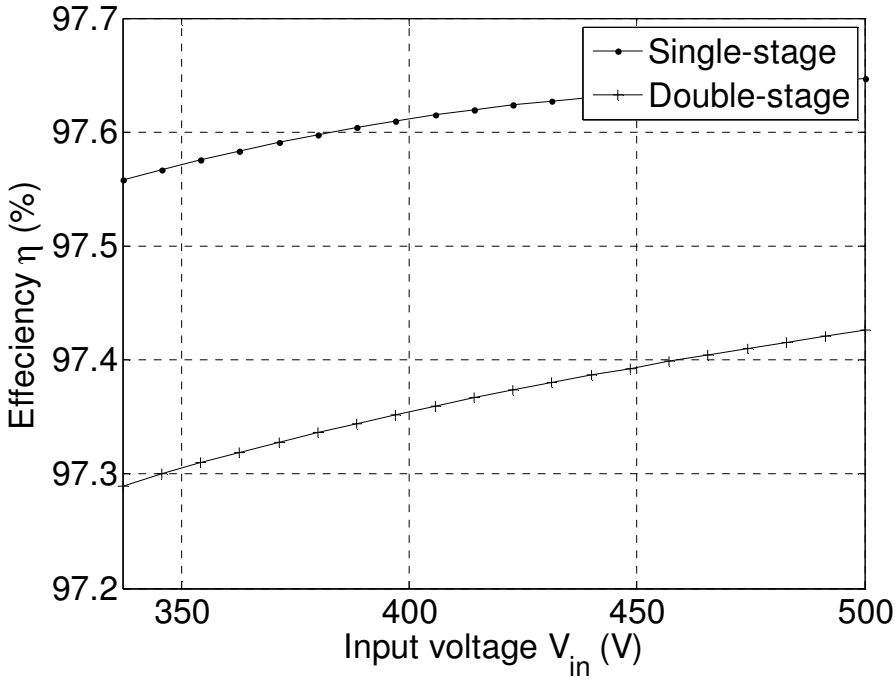

Fig. 6. Efficiency of B-ESU injecting rated real power.

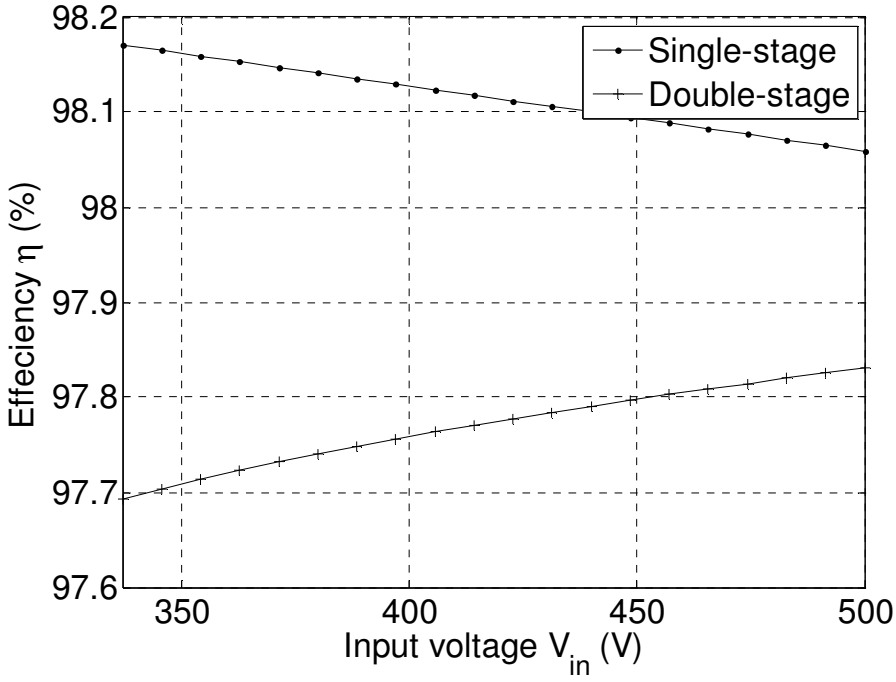

Fig. 7. Efficiency of B-ESU injecting rated reactive power.

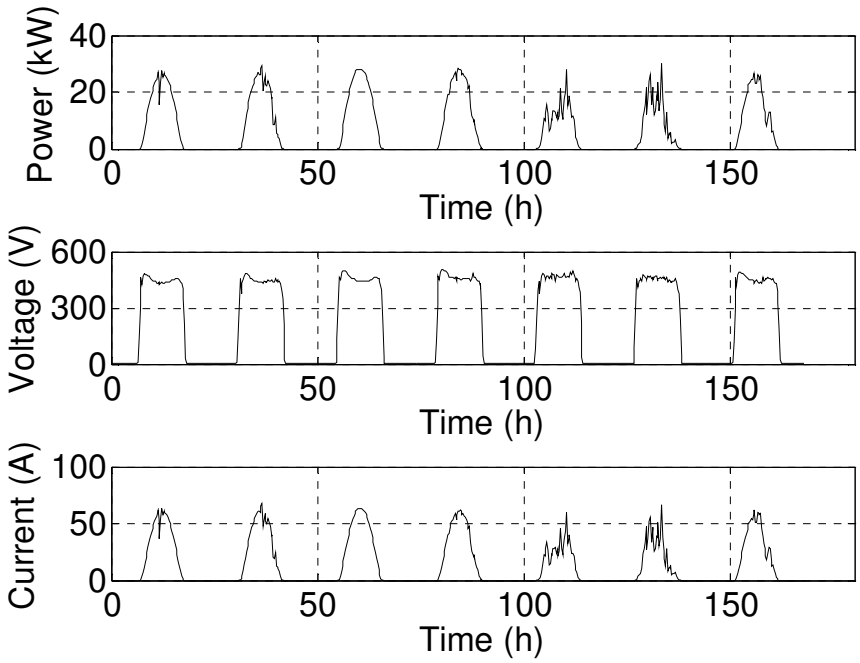

Fig. 8. Measured PV power, voltage, and current over a week.

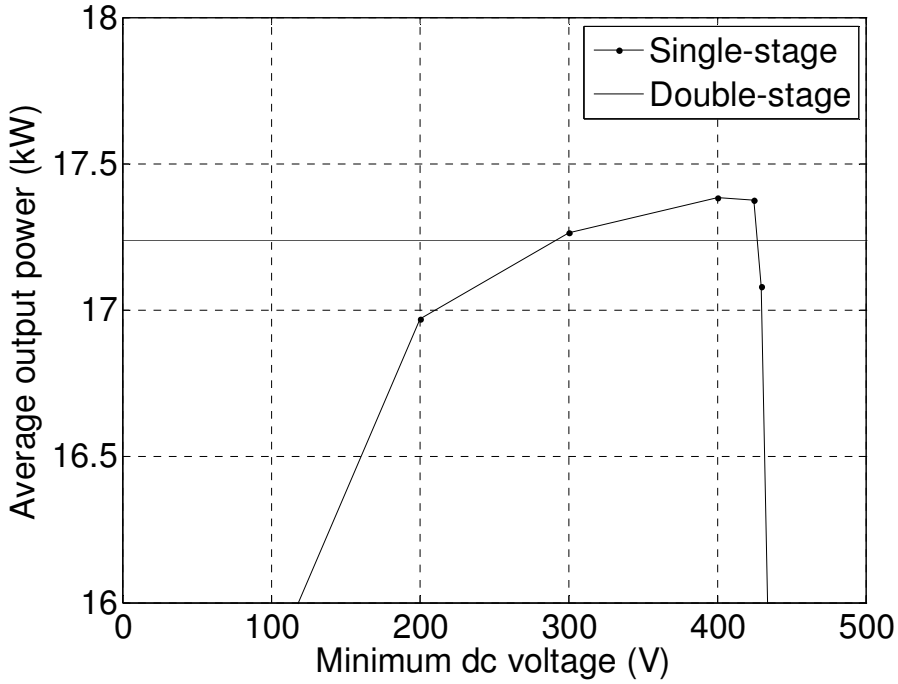

Fig. 9. PV average power output of single vs. double-stage inverters.

VI. CONCLUSIONS

Previous work shows that a double-stage topology has higher efficiency than a single-stage one if the input voltage is low. However, the case of a varying input voltage has not been previously addressed. Here, the method is applied for DER with varying input voltages: UC-ESU, B-ESU, and PV. For the UC-ESU, the double-stage is more efficient. Conversely, for the B-ESU the single-stage is slightly more efficient. Given that the amount of devices used for single-stage B-ESU is reduced and the control complexity remains unchanged compared to the double-stage, it is the preferred choice for this application. However, the results show that for applications where it is desirable to add battery energy storage to another DER type, for example a hybrid PV inverter or microturbine, there is only a small efficiency penalty incurred by using the double-stage. Thus, for applications with multiple sources, the double-stage is preferred. The optimal choice of the minimum MPPT voltage for the PV results in the single-stage topology

yielding better efficiency. Given suitable assumptions or recorded data, the method can be applied to other DER, such as wind turbines, micro-hydro, variable-speed gensets, and microturbines.

REFERENCES

[1] F. Blaabjerg, Z. Chen, and S. B. Kjaer, "Power electronics as efficient interface of renewable energy sources," *International Power Electronics and Motion Control Conference (IPEMC)*, 2004, vol. 3, pp. 1731-1739 Vol.3.

[2] M. Prodanovic and T. C. Green, "High-quality power generation through distributed control of a power park microgrid," *IEEE Transactions on Industrial Electronics*, vol. 53, no. 5, pp. 1471-1482, Oct. 2006.

[3] H. B. Puttgen, P. R. MacGregor, and F. C. Lambert, "Distributed generation: Semantic hype or the dawn of a new era?," *IEEE Power and Energy Magazine*, vol. 1, no. 1, pp. 22-29, Feb. 2003.

[4] S. P. Adhau, "A comparative study of micro hydro power schemes promoting self sustained rural areas," *International Conference on Sustainable Power Generation and Supply (SUPERGEN)*, 2009, pp. 1-6.

[5] M. Mohibullah, A. M. Radzi, and M. I. . Hakim, "Basic design aspects of micro hydro power plant and its potential development in Malaysia," *Power and Energy Conference (PECon)*, 2004, pp. 220- 223.

[6] Tze-Fun Chan and L. L. Lai, "Permanent-magnent machines for distributed power generation: a review," *IEEE Power Engineering Society General Meeting*, 2007, pp. 1-6.

[7] L. M. Tolbert et al., "Electronic power conversion system for an advanced mobile generator set," *IEEE Industry Applications Conference*, 2001, vol. 3, pp. 1763-1768 vol.3.

[8] M. Calais, J. Myrzik, T. Spooner, and V. G. Agelidis, "Inverters for single-phase grid connected photovoltaic systems – an overview," *Power Electronics Specialists Conference*, 2002, vol. 4, pp. 1995-2000.

[9] F. Blaabjerg, Z. Chen, and S. B. Kjaer, "Power electronics as efficient interface in dispersed power generation systems," *IEEE Transactions on Power Electronics*, vol. 19, no. 5, pp. 1184-1194, Sep. 2004.

[10] H. Al-Nasseri and M. A. Redfern, "Solid-state converter topologies for interfacing dc sources with utility power systems," *Universities Power Engineering Conference*, 2004, vol. 2, pp. 629-633.

[11] S. B. Kjaer, J. K. Pedersen, and F. Blaabjerg, "A review of single-phase grid-connected inverters for photovoltaic modules," *IEEE Transactions on Industry Applications*, vol. 41, no. 5, pp. 1292-1306, Oct. 2005.

[12] S. Ponnaluri, G. O. Linhofer, J. K. Steinke, and P. K. Steimer, "Comparison of single and two stage topologies for interface of BESS or fuel cell system using the ABB standard power electronics building blocks," *European Conference on Power Electronics and Applications*, 2005.

[13] B. D. Min et al., "A novel grid-connected PV PCS with new high efficiency converter," *International Conference on Power Electronics*, 2007, pp. 478-482.

[14] W. T. Franke, N. Oestreich, and F. W. Fuchs, "Comparison of transformerless converter topologies for photovoltaic application concerning efficiency and mechanical volume," *IEEE International Symposium on Industrial Electronics (ISIE)*, 2010, pp. 724-729.

[15] R. M. Schupbach and J. C. Balda, "Comparing dc-dc converters for power management in hybrid electric vehicles," *IEEE International Electric Machines and Drives Conference (IEMDC)*, 2003, vol. 3, pp. 1369-1374.

[16] G. Graditi, D. Colonnese, and N. Femia, "Efficiency and reliability comparison of dc-dc converters for single phase grid connected photovoltaic inverters," *International Symposium on Power Electronics Electrical Drives Automation and Motion (SPEEDAM)*, 2010, pp. 140-147.

[17] Tsai-Fu Wu, Chih-Hao Chang, Li-Chiun Lin, and Chia-Ling Kuo, "Power loss comparison of single and two-stage grid-connected photovoltaic systems," *IEEE Transactions on Energy Conversion*, vol. 26, no. 2, pp. 707-715, Jun. 2011.

[18] M. Liserre, F. Blaabjerg, and S. Hansen, "Design and control of an LCL-filter-based three-phase active rectifier," *IEEE Transactions on Industry Applications*, vol. 41, no. 5, pp. 1281-1291, 2005.

[19] D. Graovac and M. Pürschel, "IGBT power losses calculation using the data-sheet parameters," Infineon, Appl. Note, V1.1, 2009.

[20] ABB, "IGBT module LoPak5 SPT 5SNS 0300U120100," Datasheet Doc. No. 5SYA1528-02, Jul. 2003.

[21] Maxwell, "125 V heavy transportation modules," Datasheet 1014696.3.

[22] L. W. Hruska, “Smart batteries and lithium ion voltage profiles,” *Battery Conference on Applications and Advances*, 1997, pp. 205-210.

[23] “Inverter Testing for PV Systems.” [Online]. Available: http://www.fsec.ucf.edu/en/research/photovoltaics/inverter/index.htm. [Accessed: 14-Nov-2011].

APPENDIX A: CERTIFICATION OF FIRST AUTHOR

I hereby certify that Arthur K. Barnes is first author of the article this chapter is based on and has completed at least 51% of the work described in the article.

Juan Carlos Balda

Signature _____

Date _____

APPENDIX B: RELEASE FOR USE IN DISSERTATION

Thesis / Dissertation Reuse

The IEEE does not require individuals working on a thesis to obtain a formal reuse license, however, you may print out this statement to be used as a permission grant:

Requirements to be followed when using any portion (e.g., figure, graph, table, or textual material) of an IEEE copyrighted paper in a thesis:

1) In the case of textual material (e.g., using short quotes or referring to the work within these papers) users must give full credit to the original source (author, paper, publication) followed by the IEEE copyright line © 2011 IEEE.

2) In the case of illustrations or tabular material, we require that the copyright line © [Year of original publication] IEEE appear prominently with each reprinted figure and/or table.

3) If a substantial portion of the original paper is to be used, and if you are not the senior author, also obtain the senior author's approval.

Requirements to be followed when using an entire IEEE copyrighted paper in a thesis:

1) The following IEEE copyright/ credit notice should be placed prominently in the references: © [year of original publication] IEEE. Reprinted, with permission, from [author names, paper title, IEEE publication title, and month/year of publication]

2) Only the accepted version of an IEEE copyrighted paper can be used when posting the paper or your thesis on-line.

3) In placing the thesis on the author's university website, please display the following message in a prominent place on the website: In reference to IEEE copyrighted material which is used with permission in this thesis, the IEEE does not endorse any of [university/educational entity's

name goes here]'s products or services. Internal or personal use of this material is permitted. If interested in reprinting/republishing IEEE copyrighted material for advertising or promotional purposes or for creating new collective works for resale or redistribution, please go to http://www.ieee.org/publications_standards/publications/rights/rights_link.html to learn how to obtain a License from RightsLink.

If applicable, University Microfilms and/or ProQuest Library, or the Archives of Canada may supply single copies of the dissertation.

CHAPTER EIGHT

MODELLING PV CLOUDING EFFECTS USING A SEMI-MARKOV PROCESS WITH APPLICATION TO ENERGY STORAGE

Arthur Barnes, Juan Carlos Balda and Jonathan K. Hayes

NOTICE: this is the author's version of a work that was accepted for publication in *19th IFAC World Congress, August 24-29, 2014, Cape Town, South Africa*. Changes resulting from the publishing process, such as peer review, editing, corrections, structural formatting, and other quality control mechanisms may not be reflected in this document. Changes may have been made to this work since it was submitted for publication. The definitive version was published in:

A.K. Barnes, , "Modeling PV clouding effects using a semi-Markov process with application to energy storage," in *International Federation of Automatic Control World Congress (IFAC)*, Cape Town, South Africa, 2014.

***Abstract* — Cloud-induced intermittency of photovoltaic (PV) generation forces equipment on the electrical grid to cycle excessively, preventing PV from being considered as a reliable or dispatchable source of power. Energy storage units (ESU) are proposed to turn PV power dispatchable. In order to use an ESU most effectively, it must be controlled appropriately by considering cloud-induced effects. To this end, the cloud structure is modeled as a random sequence inferred from clouding data. The proposed model is valid for centralized PV installations and serves to develop not only a control methodology to coordinate an ESU with existing grid equipment but also as a sizing criterion for an ESU.**

The above methodology is demonstrated on both clouding data collected from a rooftop PV installation that includes a pyranometer.

I. INTRODUCTION

Improvements in the manufacturing process of PV generation are lowering costs and leading to increased grid penetration. However, the power output of PV inverters varies sharply because of changing cloud cover that may cause transitions from rated power to less than half of rated power within minutes [1]. This may cause over- or under-voltages on distribution systems [2], [3] in addition to reducing the maintenance interval of voltage regulating equipment such as substation load tap-changers (LTC) or in-line voltage regulators [4].

Energy storage has long been proposed as a solution; however, it is necessary to either model or predict cloud-induced intermittency to develop a more-efficient ESU control strategy [5]–[8]. Frequency-domain methods have been previously applied to characterize PV power [9]. Unfortunately, the resulting frequency-domain signal has units without physical significance [10]. Despite these methods being useful for observing qualitative features of PV power intermittency, they not suitable for sizing ESU which requires knowledge of the peak energy amount charged to or discharged from a battery.

Methods for control of the ESU include deterministic scheduling, stochastic scheduling, rule-based control, feedback control, and feedforward control [4]–[7], [11], with deterministic scheduling employed most commonly. Prediction of PV power is necessary for ESU control methods based on deterministic scheduling [11], and has received significant attention in recent years. Current methods are divided into two major groups [12]. The first group consists of those methods using numerical weather prediction to estimate hourly averaged power with look-ahead intervals on the order of one or more days [13]. The second group of methods uses sky imagers,

geographically distributed sensor arrays, or satellite imagery to track cloud position over time [14]–[16]. This yields power predictions on the order of a few hours ahead [17]. The time resolution for both methods are too coarse for predicting cloud-induced power variations, which occurs in seconds [15].

The contributions of this work are a random-sequence model for cloud-induced intermittency in a single PV installation, and its application to develop an efficient rule-based ESU control strategy. The model is applicable to large, central PV installations that form 38% of installed PV generation [18]. Unlike frequency-domain methods, the model outputs have physical units. The control strategy requires neither sky imaging data nor remote irradiance measurements, unlike existing methods. Additionally, both the model and rule-based controller operate over time scales on the order of seconds, suitable for modelling and mitigating the effects of cloud-induced intermittency. The model is also useful for generating simulated test data, similar to the case of wind generation, where either the Weibull distribution or time-series models are used.

This paper is organized as follows: the PV data collection is described in Section II; the data processing is explained in Section III; the data analysis and development of statistical distributions are addressed in Section IV; the reward process used to develop a control policy is described in Section V; the results of the methodology applied to a case study are presented in Section VI; and lastly, the conclusions on the work performed as well as directions for future work are given in Section VII.

II. PV DATA ACQUISITION

Irradiance is captured with an irradiance sensor (Apogee SP-125 5V amplified pyronameter [19] in conjunction with a LabVIEW-based data acquisition system (National Instruments USB-6259) using a custom program. The pyranometer is installed at the University of Arkansas (UA)

in Fayetteville (AR) on the top of the John A. White Engineering Hall roof next to a pair of 225 W PV panels as shown in Fig. 1. It was installed on the same plane as the panels, facing South with tilt angle of 66º from horizontal. The PV data are available on the web at http://energy.uark.edu/pv.

An unanswered question for PV generation systems is that of sample rate selection. Notably, very wide ranges of sample rates abound, including 3 seconds [20] to 1 hour [20]. The authors sought to select a sample rate that preserved the salient characteristics of cloud-induced intermittency. The system supports sample rates of up to 25 Hz with the sample rate selected on the theoretical frequency content of the irradiance sensor output voltage and inspection of recorded data.

Fig. 1. Experimental setup at UA.

The 25 Hz maximum sample rate of the data acquisition system was determined to be sufficient, and data was initially collected at this rate. However, this sample rate results in prohibitively large amounts of data over long periods of time.

Moreover, it is only necessary in this application to detect the presence of large changes in irradiance, those where the irradiance changes by 70% of the maximum irradiance value or more [21]. Visual inspection revealed that the time duration between peaks in the irradiance profile meeting this criteria was usually 2.5 s or more. Hence, the selected final sample rate selection is 1 Hz.

III. PV DATA PROCESSING

Erroneous values corrupted by noise and nonlinear effects in the sensor are unfortunately captured by the data acquisition system. Hence, the data must be processed to remove these erroneous values that occur at low irradianceas well as to capture statistics on clouding. This processing classifies data as *clear* or *shaded*, using the algorithm described in Fig 2.

Convergence is established within 3 iterations, so a convergence check was not implemented. The algorithm works by alternately estimating the clear-sky irradiance profile using a second-order curve fit and classifying the data as *clear* or *shaded*. Note that for PV systems with tracking, the irradiance profile will be flattened near mid-day [22], so a higher-order curve fit will be necessary. Each value is divided by the clear-sky irradiance profile at the corresponding time. The resulting values are clustered using k-means clustering with two centroids [23]. Each subsequent clustering results in a more refined estimate of the clear-sky irradiance profile. Fig. 3 shows the classification results.

The processing accomplishes two goals: First, the data are classified as either *clear* or *shaded*, allowing for statistics to be taken on cloud cover.

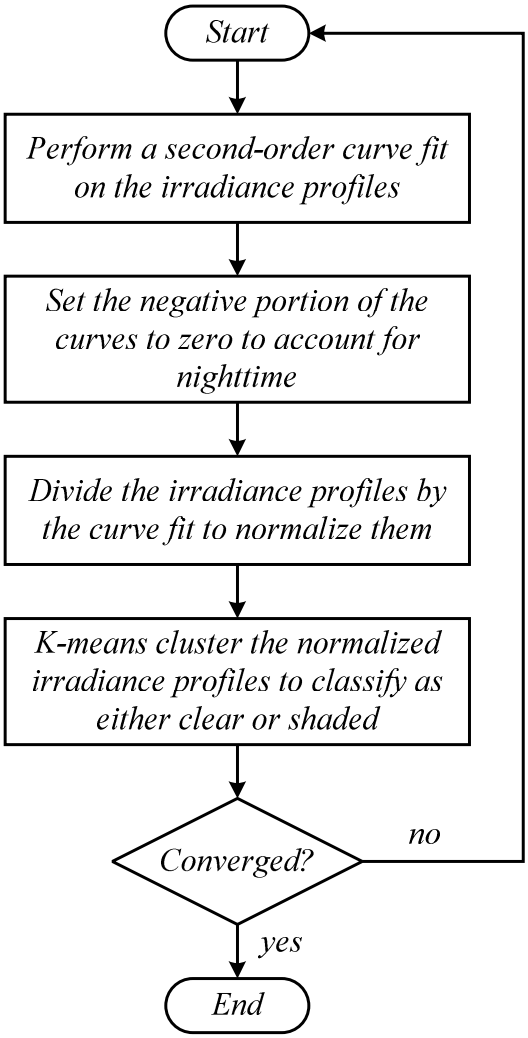

Fig. 2. Flowchart for the classification algorithm.

Second, it mitigates corrupted data by removing erroneous samples and interpolating between the remaining good data. For the case of the pyranometer, two factors were observed to corrupt data. First, accuracy at high solar angles of incidence is poor as the output drops off. Second, oscillation is present at those high angles of incidence, illustrated around 6 am and 7 pm (19 h) in Fig. 3, which compares the measured and corrected data To overcome these issues, the corrupted samples are removed and a weighted sum of the predicted and measured irradiance is used to estimate the true irradiance.

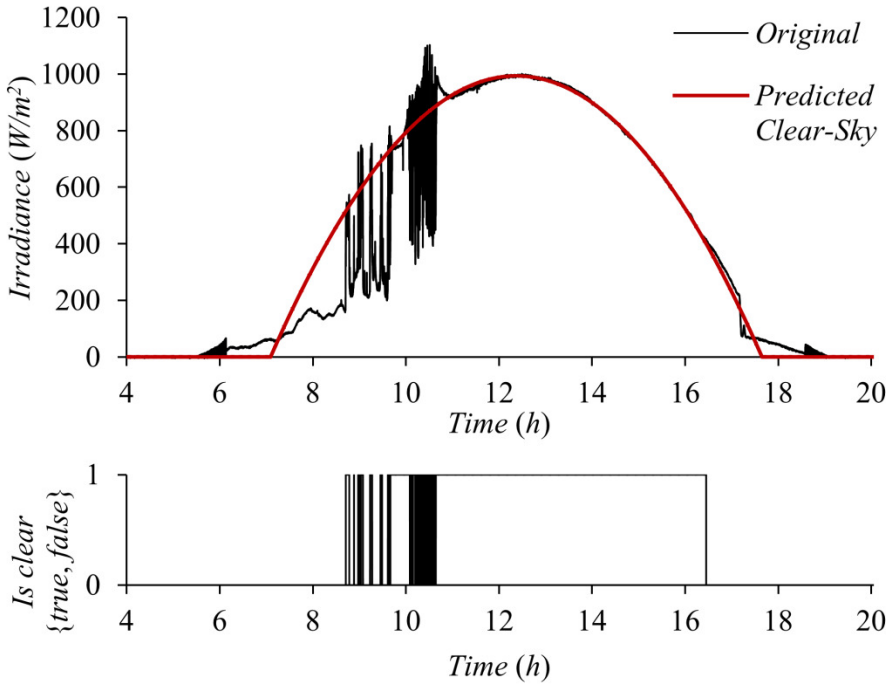

Fig. 3. Classified irradiance data for a partly cloudy day (Aug 27, 2011). The original irradiance profile and predicted clear-sky irradiance profile are in the top graphs, while the classification results (whether or not it is clear or shaded) are in the bottom graph.

IV. EXPLORATORY DATA ANALYSIS AND STATISTICAL INFERENCE OF CLOUD DURATIONS

In order to characterize and forecast the PV output, it is assumed that the *clear* and *shaded* durations follow statistical distributions. Based on existing work in climate science [24], cumulus clouds have a fractal structure, so the distribution of the cloud size x, and thus the duration of shading t, follow a power law distribution

$$f(x) = Ax^b, \tag{1}$$

where A and b are distribution parameters. Through exploratory data analysis, it is inferred that the *clear* and *shaded* distributions follow a generalized Pareto distribution of the form

$$f(t|k,\sigma,\theta) = \frac{1}{\sigma}\left[1 + k\frac{(t-\theta)}{\sigma}\right]^{-1-\frac{1}{k}}, \quad (2)$$

where k, σ, θ are parameters of the distribution. Although the duration of *clear* conditions is truncated based on the length of a day, the effect of truncation is neglected. Two separate distributions are inferred for the duration of *clear* and *shaded* events, respectively. Quantile-quantile (QQ) plots are used to evaluate how the fitted distributions handle outliers, illustrated in Fig. 4. In these figures, the inverse cumulative distribution functions (CDF) of the inferred distributions are plotted against the observed values for *clear* and *shaded* durations. The better the inferred distribution fits the data, the more the plotted points fall on the line $y = x$. The inferred distributions fit the data well with the exception that the distribution of *shaded* durations is more long-tailed than the observed data, and quantization occurs at small time scales.

V. APPLICABILITY OF CLOUDING DISTRIBUTIONS TO ESU

The characterization of the distribution of the *clear* and *shaded* durations, as well as the likelihood that the PV installation will be *clear* or *shaded* at a given time in the future are necessary to develop an ESU control strategy or sizing criterion.

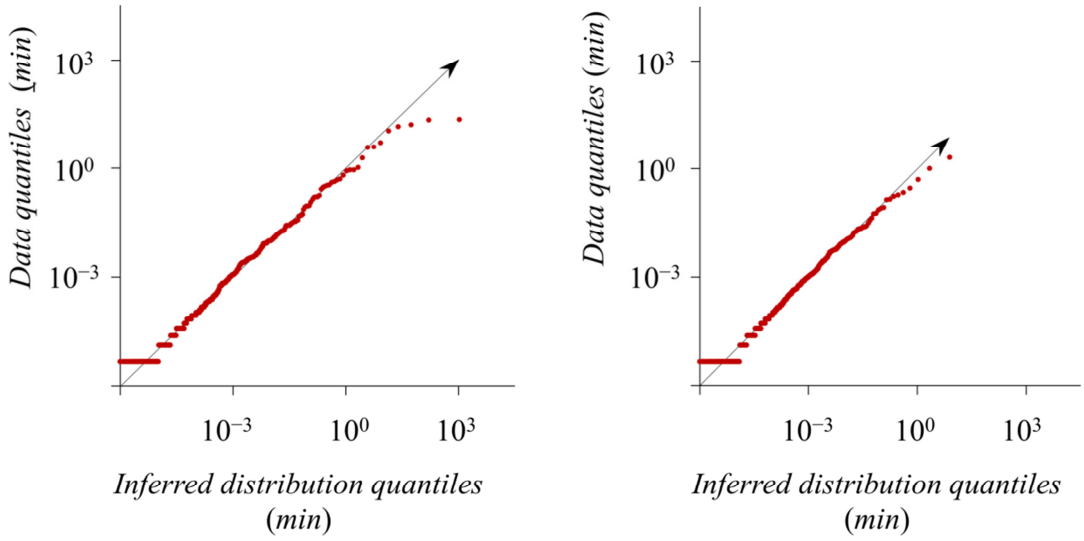

Fig. 4. QQ plots of shaded durations comparing the distribution against data.

The state of the PV installation is modelled as a time series $s_1, s_2, \ldots s_N$, where each at sample n, the state s_n is either 1, denoting *clear*, or 2, denoting *shaded.* Section 4 revealed that s_n is dependent not just on s_{n-1}, but also on the total duration that the sensor has been *clear* or *shaded*, thereby violating the Markov property [23]. This is apparent because the distributions of the *clear* and *shaded* events are not exponential, which is required for the Markov property to hold [23]. Next, it is shown that the distributions of *clear* and *shaded* times can still be used to model the shading as a discrete-time semi-Markov process [25].

V.A. Semi-Markov Discrete-Time Process Model

A Markov process has a set of states and a state-transition probability matrix indicating the likelihood p_{ij} of transitioning from state i to state j at sample n [26]–[28]. The semi-Markov discrete-time process (SMDTP) is a generalization of the Markov process that waits for a random hold time before each transition. Therefore, each element p_{ij} of the SMDTP state-transition probability matrix has a corresponding hold time distribution $h_{ij}(m)$. When a SMDTP has

transitioned to state i, it randomly selects the next state j based on the p_{ij}. In the discrete-time case addressed here, the selection is based on $h_{ij}(m)$, the number of samples m to wait before transitioning to state j.

Irradiance is modelled by a two-state model in which virtual state transitions are forbidden (that is, transitions from a state to itself), illustrated in Fig. 5. This results in a simpler representation of the system, as the state-transition probability matrix is simply a two-by-two identity matrix. The SMDTP can be executed via the algorithm described in Fig. 6 in order to generate simulated data.

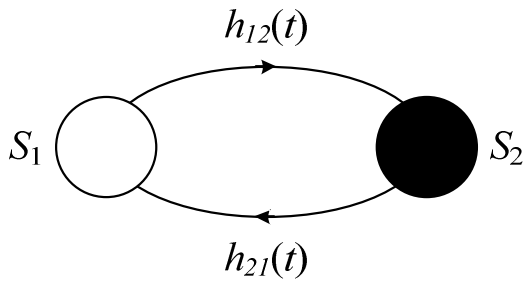

Fig. 5. Graphical illustration of the SMDTP model.

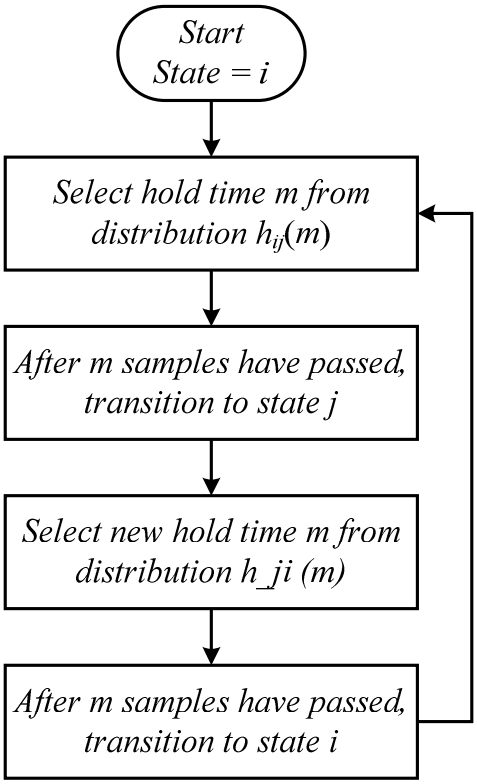

Fig. 6. Simulation of the SMDTP.

For forecasting, the quantities of interest are the interval transition probabilities, giving the likelihood that the PV is *clear* or *shaded* at sample n given that it transitioned to be *clear* or *shaded* at sample 0. The interval transition probability $\phi_{ij}(n)$ is the probability that the process is in state i at sample n, given that it entered state j at sample 0; in particular

$$\phi_{12}(n) = \sum_{n=0}^{N} \sum_{m=1}^{n} h_{12}(m)\phi_{22}(n-m). \tag{3}$$

$$\phi_{21}(n) = \sum_{n=0}^{N} \sum_{m=1}^{n} h_{21}(m)\phi_{11}(n-m). \tag{4}$$

Again, the term $h_{ij}(m)$ is the probability that the process will transition into state i at sample m given that it entered state j at sample 0. Because these calculations rely on a series of multiply-

accumulate operations which are performed quickly by modern computers, they are easily computed numerically using the following initial conditions

$$\Phi(0) = \begin{bmatrix} 1 & 0 \\ 0 & 1 \end{bmatrix} \tag{5}$$

and the definition of a probability mass function

$$\phi_{11}(n) + \phi_{21}(n) = 1 \tag{6}$$

$$\phi_{12}(n) + \phi_{22}(n) = 1, \tag{7}$$

where (5) reflects the fact that at sample 0 the state of the process is known as it has just been observed.

The interval transition probabilities allow for performing forecasting by taking the state with the highest likelihood. For example, if a process transitioned from *clear* to *shaded* at sample 0, it will most likely remain shaded for 50 seconds until $\phi_{21}(n)$ exceeds 0.5, as illustrated by Fig. 7. This figure illustrates the evolution of the interval transition probabilities over time assuming that the system started in *clear* (state 1, red lines), or *shaded* (state 2, black lines).

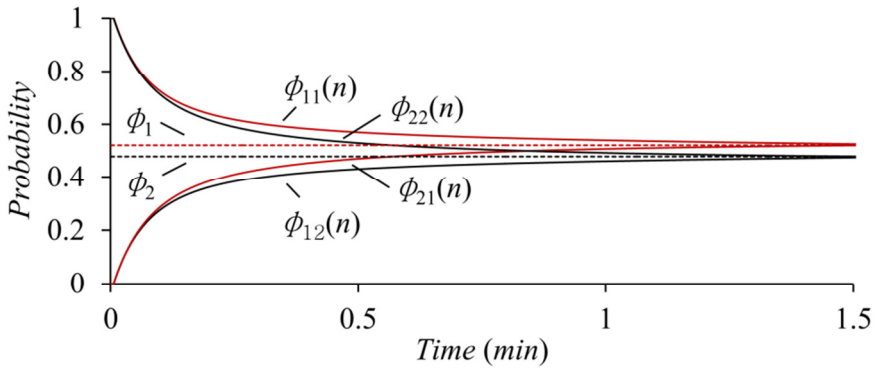

Fig. 7. Interval transition probabilities $\phi_{ij}(n)$ converging to the steady-state probabilities ϕ_i. The probabilities $\phi_1 + \phi_2 = 1$.

As time increases, the uncertainty in the interval transition probabilities increases and they converge to their steady-state values, the marginal likelihood of the system being either *clear* or *shaded.*

V.B. Voltage Variations Caused by PV Intermittency

The variations in voltage caused by intermittency of PV generation on the feeder are calculated as follows. It is assumed that the feeder can be modelled as a voltage source behind an equivalent series impedance [2], illustrated in Fig. 8. Using the notation in [29], the voltage magnitude as function of real and reactive power injections is

$$V_{pv}^2 = V_\infty^2 + 2(RP + XQ) - \frac{Z^2}{V_{pv}^2}(P^2 + Q^2) \tag{8}$$

$$P = P_{pv} + P_{esu} - P_{load} \tag{9}$$

$$Q = -Q_{load}. \tag{10}$$

In Fig 8., R and X are the resistive and reactive portions of the line impedance while P and Q are the real and reactive powers flowing into the PV bus at the end of the line. The real power is broken up into the PV real power injection P_{pv}, ESU real power injection P_{esu}, and load real power draw P_{load}.

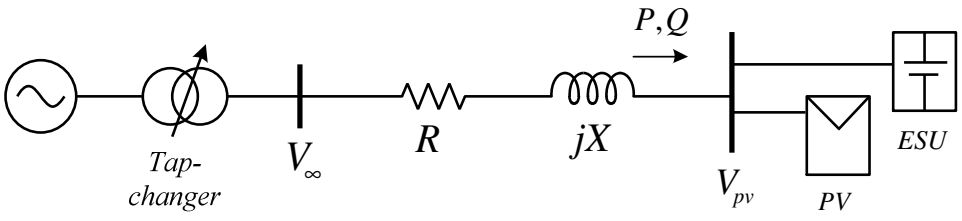

Fig. 8. Equivalent feeder model with transformer LTC, PV generation and ESU.

The reactive power consists only of the load reactive power draw Q_{load}. For notational convenience, V_∞, V_{pv} and Z are defined as the magnitudes of the infinite bus voltage, PV installation bus voltage, and equivalent series impedance.

The change in voltage magnitude with respect to real power injection is

$$J = \frac{\partial V_{pv}}{\partial P} = \frac{-2V_{pv}^2 + 2Z^2P}{4V_{pv}^2 + (2RP - 2V_\infty^2)V_{pv}}. \tag{11}$$

It is assumed that the substation LTC has T taps allowing for a total variation of $\pm\Delta V$ V from nominal. Assuming voltage sensing at the PV bus, the amount of voltage variation required for the LTC to cycle is therefore $\pm 2\Delta V/T$ V. This corresponds to a change in power of

$$P_{tap} = \pm 2\Delta V/(TJ). \tag{12}$$

V.C. Real-Time ESU Control Strategy

The high-level ESU control strategy is illustrated in Fig. 9. This strategy is implemented in a high-level controller that forms a portion of the controller hierarchy illustrated in Fig. 10. Details of the concept of a control hierarchy for grid-connected power electronic converters are provided in [30]. The high-level rule-based controller will provide power setpoints to an open-loop controller, which calculates the necessary currents in direct-quadrature (d-q) space to produce the desired real and reactive power setpoints. This in turn is passed to a closed-loop current controller, which calculates the necessary inverter voltage references in d-q space to produce the desired real and reactive current setpoints. Last, a pulse-width modulation (PWM) block converts the voltage references into a set of PWM signals that are output to the gate drivers for the power stage.

The ESU includes a classifier operating in real time that detects when the PV generation it is smoothing is in in a *clear* or *shaded* state. If the PV is in a *clear* state, then the ESU will follow the power setpoint mandated by an economic self-scheduler, as illustrated in Fig. 10. When the PV transitions to a *shaded* state, the effect of the controller to produce a power reference to the ESU, such that the aggregate output power of the PV/ESU combination will track the clear-sky predicted power for a time period d. After this time, the rule-based controller will timeout, and the ESU high-level control will revert back to economic self-scheduling.

Although the classification of the PV as *clear* or *shaded* and the ESU rule-based controller will operate in real-time, it must be noted that the distribution properties of the *clear* and *shaded* states will not. It is envisioned that these will be updated in a batch fashion at night, when the ESU has reverted to pure economic self-scheduling.

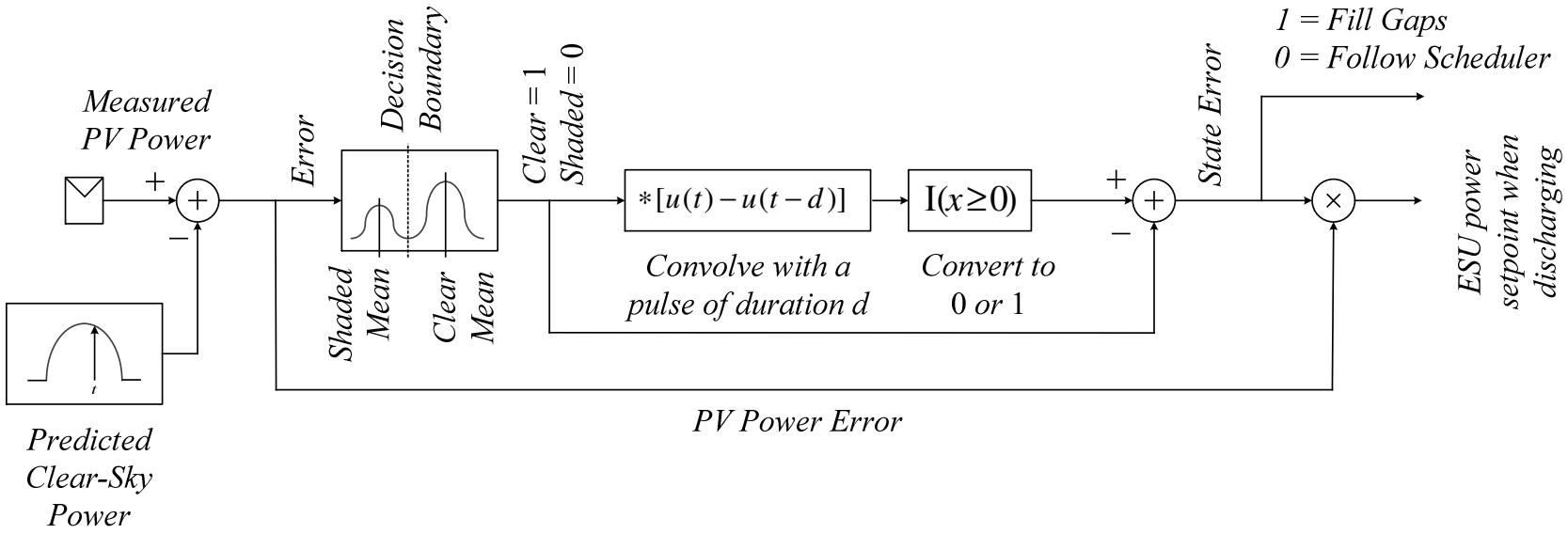

Fig. 9. Proposed rule-based controller for an ESU smoothing PV. $u(\cdot)$ denotes the unit step function, t is the current time, and d is the maximum shading duration over which the ESU will supply power.

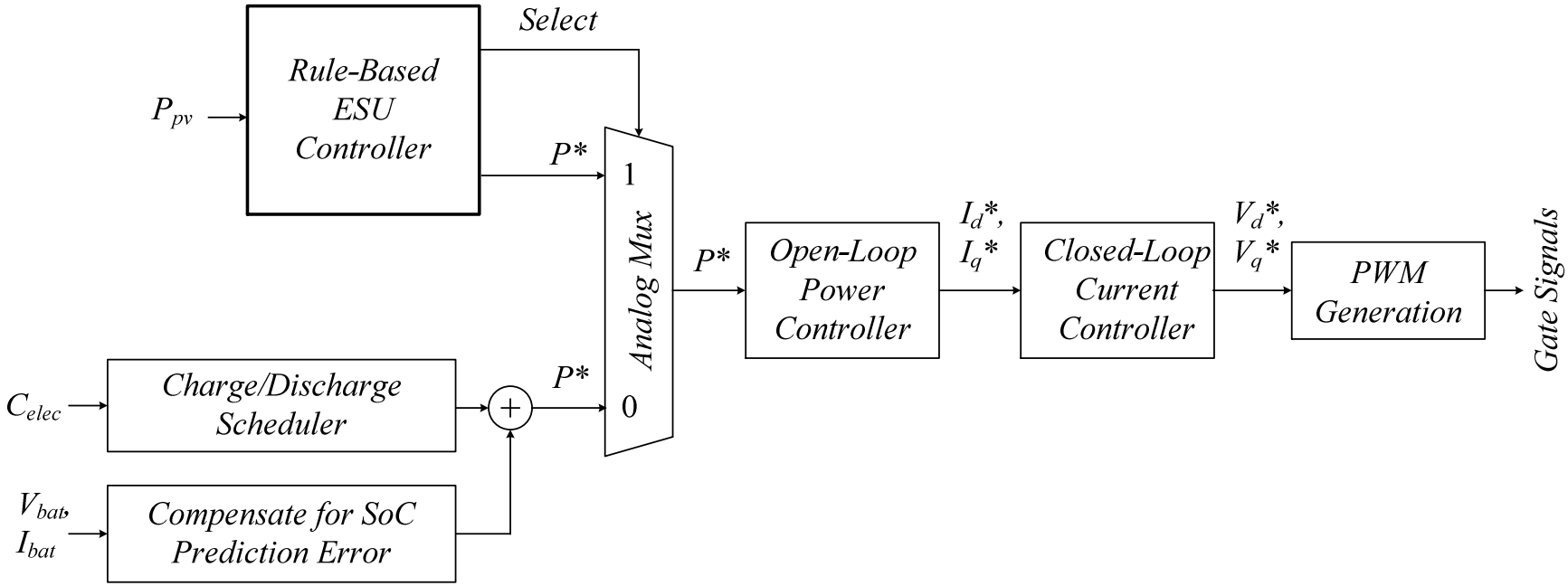

Fig. 10. Location of the proposed rule-based controller in the controller hierarchy. C_{elec} denotes cost of electricity. V_{bat} and I_{bat} denote measured battery voltage and current, respectively. P_{pv} denotes measured PV power. P^*denotes ESU real power reference. *Select* is {0,1} digital signal selecting desired input of an analog multiplexer (mux). I_d^* and I_q^* denote ESU PEI direct and quadrature reference currents, respectively. V_d^* and V_q^* denote ESU direct and quadrature voltages, respectively.

V.D. Reward Model

Two reward processes are used to calculate both the number of LTC tap-changes and the ESU battery throughput. These two quantities are considered the rewards to be determined, though they are actually costs. Similar to the case of the interval transition probabilities, the reward processes are calculated recursively as follows

$$v_1(n) = {}^{>}y_1(n) + r_1(n) + \sum_{m=1}^{n} h_{12}(n)\, v_2(n-m) \tag{13}$$

$$v_2(n) = {}^{>}y_2(n) + r_2(n) + \sum_{m=1}^{n} h_{21}(n)\, v_1(n-m) \tag{14}$$

$${}^{>}y_1(n) = y_1(n,1) \sum_{m=n+1}^{\infty} h_{12}(m) \tag{15}$$

$${}^{>}y_2(n) = y_2(n,1) \sum_{m=n+1}^{\infty} h_{21}(m) \tag{16}$$

$$r_1(n) = \sum_{m=1}^{n} h_{12}(n)\, y_1(n,1) \tag{17}$$

$$r_2(n) = \sum_{m=1}^{n} h_{21}(n)\, y_2(n,1) \tag{18}$$

$$y_i(m,1) = \sum_{l=0}^{m-1} y_{i,x}(l) \tag{19}$$

$$y_{i,tc}(l) = \begin{cases} 1, & l = n_{sw} \\ 0, & otherwise \end{cases} \tag{20}$$

$$y_{i,esu}(l) = \begin{cases} \Delta E_{esu}, & i = 2 \; and \; l \leq n_{sw} \\ 0, & otherwise \end{cases} \tag{21}$$

These assume zero initial rewards, so $v_i(0) = 0$. The significances of the terms are as follows: $v_i(n)$ is the expected reward of the process at sample n given that the process entered state i at sample 0. The term ${}^{>}y_i(n)$ is the expected reward conditioned on the event that the process transitions to another state after sample n. The term $r_i(n)$ is the expected reward that the process earns in state i, conditioned on the event that the process transitions to another state before sample n. The last terms in (13) and (14) are the expected rewards earned over samples $n - m$ to n conditioned on the event that the process transitions to another state before sample n. The term $y_i(m,1)$ represents the cumulative reward accrued over m samples. The term $y_{i,x}(l)$ is the reward rate at l samples after having transitioned into state i. In this case the reward is actually a cost. Two reward rates are considered. The rate, $y_{i,tc}(l)$ is the number of tap-changes that occur, while $y_{i,esu}(l)$ is the battery throughput (measured in MWh). These assume that a tap-change will occur when a timeout period equal to n_{sw} samples has elapsed after the process has changed states. During those n_{sw} samples, the ESU will either supply or draw a fixed amount of power to regulate voltage. Battery throughput in can be applied to predict the lifetime of ESU under a given usage scenario. This is valid if the battery usage characteristics allow the

assumption of battery degradation that is linear with respect to throughput [31]. Only discharge power is considered in calculating battery throughput, so this quantity is independent of battery efficiency. The two costs are used to select the timeout period that minimizes the ESU throughput while maintaining the expected number of tap-changes per day within the allowable maximum.

VI. METHODOLOGY RESULTS

The objective is to assess the necessary amount of energy storage and develop a control strategy to avoid excessive cycling of a LTC. The selected strategy is for the ESU to fill in dips in power until a timeout counter expires. The SMDTP is used to select the timeout parameter. For this analysis, one-minute data taken on May 1, 2013 from the 15 kW Fayetteville (AR) Public Library PV installation is studied. The inferred parameters for the *clear* and *shaded* durations are illustrated in Table I. These parameters are applied to study the 2 MW PV installation illustrated in Fig. 8. It is envisioned that this case study corresponds to a large industrial building such as a factory or warehouse with rooftop PV. Typical of large industrial installations, the building will operate with three shifts, so daily load variations are negligible and do not contribute to operating of the LTC [32].

This analysis uses the feeder parameters from [2] and the additional parameters specified in Table II. Both the ESU and PV are approximated as ideal ac current sources (assuming only small changes in V_{pv} in Fig. 8. Based on the desired lifetime of the transformer/LTC, the ESU control strategy must limit the number of tap changes per day to

$$O_{day} = \frac{N_{life}}{365 \times Y_{life}} = \frac{3 \times 10^5}{365 \times 40} = 20. \tag{22}$$

Given the feeder parameters, a load-flow analysis indicates a 1.27% voltage rise per MW. For an LTC with the parameters in Table II, the power change for a tap-change is $P_{tap} = (2\Delta V)/(TJ) = (2 \cdot 0.01)/(32 \cdot 0.0127) = 489$ kW. Based on previous work in cloud intermittency, a typical cloud will result in the power output decreasing to 30% of clear-sky conditions [21]. Thus, the minimum necessary clear-sky output power in kW need for the PV to induce a tap-change during clouding is

$$\check{P}_{pv} = P_{tap}/\alpha = 489/0.7 = 689. \tag{23}$$

Based on the collected data, the duration during the studied day that the 2 MW PV generation can cause a tap-change $\check{t}_{pv}$ and the average change in PV power during clouding $\Delta\bar{P}_{pv}$ are calculated and given in Table III. These figures are used to calculate the battery capacity.

By sweeping the ESU timeout, the corresponding ESU throughput at 20 tap-changes per day is 2.625 MWh, using a zero-order approximation of ESU power (ESU power is approximated by the average power in the reward calculations). However, the actual discharge durations are at most equal to the selected ESU timeout corresponding to 20 minutes. Fig. 11 illustrates the number of tap-changes and the battery throughput over the course of a day with the selected control parameters. Fig. 12 shows a snapshot of the ESU charge/discharge schedule as the ESU compensates for cloud-induced intermittency.

TABLE I. DISTRIBUTIONS OF CLEAR AND SHADED DURATIONS

		K	σ	θ
Irradiance Sensor	*Clear*	1.798	3.808×10^{-3}	10^{-4}
	shaded	1.206	3.452×10^{-3}	10^{-4}
PV Power	*Clear*	0.367	0.231	10^{-4}
	shaded	0.056	0.0631	10^{-4}

TABLE II. STUDY PARAMETERS

Component	Parameter	Expression	Value
PV	Rated power	$\hat{P}_{pv}$	2 MW
Transformer	Desired lifetime	Y_{life}	40 years
LTC	Lifetime operations	O_{life}	3×10^5
	Regulation range	ΔV	10%
	LTC steps	T	32
PV	Cloud-induced power reduction	α	70%

TABLE III. STUDY RESULTS

Component	Parameter	Expression	Value
Feeder	Change in net power required to induce a tap-change	P_{tap}	489 kW
PV	Minimum PV output power for a tap-change to occur during clouding	$\check{P}_{pv}$	698 kW
	Time during studied day that $P_{pv} \geq \check{P}_{pv}$	$\check{t}_{pv}$	11.6 h
	Average PV power while $P_{pv} \geq \check{P}_{pv}$	$\bar{P}_{pv}$	1.5 MW
	Average change in power during clouding while $P_{pv} \geq \check{P}_{pv}$	$\Delta\bar{P}_{pv}$	1.05 MW
ESU	ESU timeout	t_{sw}	20 minutes
	Average ESU output power while $P_{pv} \geq \check{P}_{pv}$	$\bar{P}_{esu}$	525 kW
	Daily ESU energy throughput	E_{day}	2.625 MWh

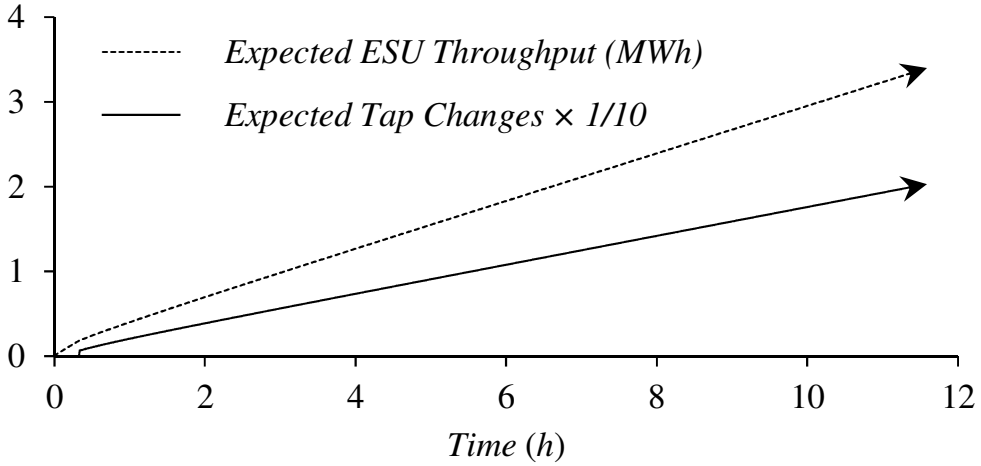

Fig. 11. Expected number of tap-changing operations and ESU throughput vs. time.

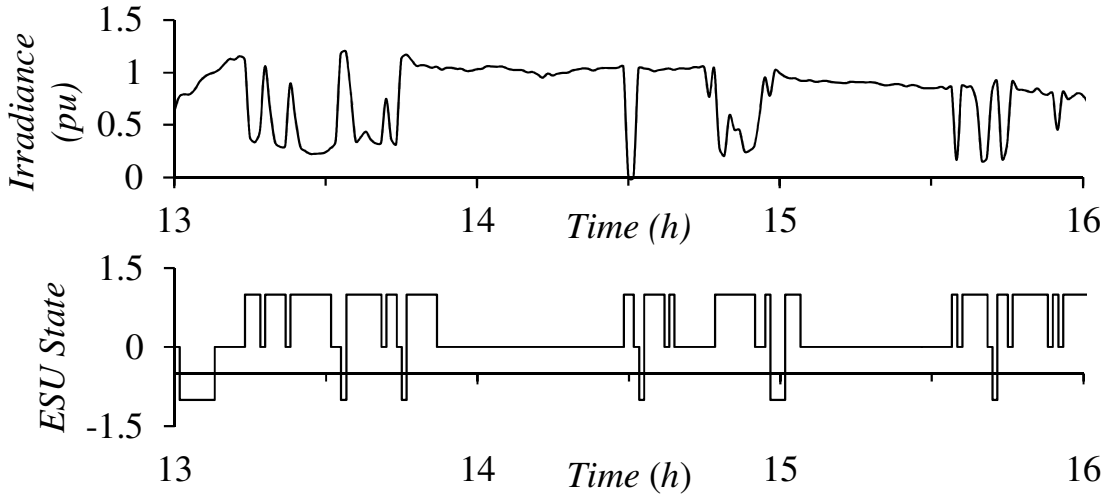

Fig. 12. Irradiance vs. time and ESU state vs. time. A value of +1 indicates discharging, –1 indicates charging, and 0 indicates standby.

VII. CONCLUSIONS

A SMDTP model was proposed to fit observed clouding data. The model was most useful for selecting a control strategy offline because the conditional probabilities of *clear* and *shaded* future states converge to their steady-state values rapidly, though conditioning on weather data offers the potential for improved performance. It was applied to calculate the expected number of tap-changes and battery throughput for an ESU coordinated with a transformer LTC in order to

select a control strategy and battery capacity. The results demonstrate how the proposed method allows for LTC maintenance intervals to be met while minimizing battery utilization in an ESU.

REFERENCES

[1] C. A. Hill, M. C. Such, D. Chen, J. Gonzalez, and W. M. Grady, "Battery energy storage for enabling integration of distributed solar power generation," *IEEE Trans. Smart Grid*, vol. 3, no. 2, pp. 850–857, Jun. 2012.

[2] R. A. Shayani and M. A. G. de Oliveira, "Photovoltaic generation penetration limits in radial distribution systems," *IEEE Trans. Power Syst.*, vol. 26, no. 3, pp. 1625–1631, Aug. 2011.

[3] A. K. Barnes, J. C. Balda, A. Escobar Mejía, and S. O. Geurin, "Placement of energy storage coordinated with smart PV inverters," in *IEEE PES Innovative Smart Grid Technologies (ISGT)*, 2012, pp. 1–7.

[4] X. Liu, A. Aichhorn, L. Liu, and H. Li, "Coordinated control of distributed energy storage system with tap changer transformers for voltage rise mitigation under high photovoltaic penetration," *IEEE Trans. Smart Grid*, vol. 3, no. 2, pp. 897–906, Jun. 2012.

[5] R.-H. Liang and J.-H. Liao, "A fuzzy-optimization approach for generation scheduling with wind and solar energy systems," *IEEE Trans. Power Syst.*, vol. 22, no. 4, pp. 1665–1674, Nov. 2007.

[6] W. A. Omran, M. Kazerani, and M. M. A. Salama, "Investigation of methods for reduction of power fluctuations generated from large grid-connected photovoltaic systems," *IEEE Trans. Energy Convers.*, vol. 26, no. 1, pp. 318–327, Mar. 2011.

[7] S. X. Chen, H. B. Gooi, and M. Q. Wang, "Sizing of energy storage for microgrids," *IEEE Trans. Smart Grid*, vol. 3, no. 1, pp. 142–151, Mar. 2012.

[8] J. Song, V. Krishnamurthy, A. Kwasinski, and R. Sharma, "Development of a Markov-chain-based energy storage model for power supply availability of photovoltaic generation plants," *IEEE Trans. Sustain. Energy*, vol. PP, no. 99, pp. 1 –10, 2012.

[9] W. T. Vetterling, *Numerical Recipes Example Book (C)*. Cambridge University Press, 1992.

[10] F. J. Taylor and J. Mellott, *Hands-On Digital Signal Processing*. McGraw-Hill Professional Publishing, 1998.

[11] M. Korpas and A. T. Holen, “Operation planning of hydrogen storage connected to wind power operating in a power market,” *Energy Conversion, IEEE Transactions on*, vol. 21, no. 3, pp. 742–749, 2006.

[12] E. Lorenz, J. Hurka, D. Heinemann, and H. G. Beyer, “Irradiance forecasting for the power prediction of grid-connected photovoltaic systems,” *IEEE J. Sel. Topics Appl. Earth Observ.*, vol. 2, no. 1, pp. 2 –10, Mar. 2009.

[13] A. Anvari Moghaddam and A. R. Seifi, “Study of forecasting renewable energies in smart grids using linear predictive filters and neural networks,” *IET Renew. Power Gener.*, vol. 5, no. 6, pp. 470 –480, Nov. 2011.

[14] J. Bing, O. Bartholomy, and P. Krishnani, “Validation of solar PV power forecasting methods for high penetration grid integration,” in *IEEE Power and Energy Society General Meeting*, 2012, pp. 1–6.

[15] K. Stefferud, J. Kleissl, and J. Schoene, “Solar forecasting and variability analyses using sky camera cloud detection & motion vectors,” in *IEEE Power and Energy Society General Meeting*, 2012, pp. 1– 6.

[16] V. P. A. Lonij, V. T. Jayadevan, A. E. Brooks, J. J. Rodriguez, K. Koch, M. Leuthold, and A. D. Cronin, “Forecasts of PV power output using power measurements of 80 residential PV installs,” in *38th IEEE Photovoltaic Specialists Conference (PVSC)*, 2012, pp. 003300 – 003305.

[17] E. Rikos, S. Tselepis, C. Hoyer-Klick, and M. Schroedter-Homscheidt, “Stability and Power Quality Issues in Microgrids Under Weather Disturbances,” *IEEE J. Sel. Topics Appl Earth Observ*, vol. 1, no. 3, pp. 170–179, Sep. 2008.

[18] L. Sherwood, “U.S. solar market trends 2011,” Interstate Renewable Energy Council, 2012.

[19] Apogee Instruments, “Pyranometer SP-212 & 215,” 2011. [Online]. Available: http://www.apogeeinstruments.com/manuals/SP-212_215manual.pdf. [Accessed: 21-Jul-2011].

[20] NREL, “NREL: Measurement and Instrumentation Data Center (MIDC) Home Page,” 2011. [Online]. Available: http://www.nrel.gov/midc/. [Accessed: 30-Nov-2011].

[21] W. M. Grady and L. Libby, “A cloud shadow model and tracker suitable for studying the impact of high-penetration PV on power systems,” in *IEEE Energytech*, 2012, pp. 1–6.

[22] S. Seme, G. Štumberger, and J. Voršič, “Maximum Efficiency Trajectories of a Two-Axis Sun Tracking System Determined Considering Tracking System Consumption,” *IEEE Transactions on Power Electronics*, vol. 26, no. 4, pp. 1280–1290, Apr. 2011.

[23] R. O. Duda, P. E. Hart, and D. G. Stork, *Pattern Classification*. Wiley, 2001.

[24] R. Neggers, H. Jonker, and A. Siebesma, "Size statistics of cumulus cloud populations in large-eddy simulations," *Journal of the Atmospheric Sciences*, vol. 60, no. 8, pp. 1060–1074, 2003.

[25] R. A. Howard, *Dynamic Probabilistic Systems: Markov Models*. Mineola, NY: Dover Publications, Incorporated, 2007.

[26] W. Feller, *An Introduction to Probability: Theory and its Applications*, 3rd ed. Wiley India Pvt. Limited, 2008.

[27] A. Papoulis and S. U. Pillai, *Probability, Random Variables, and Stochastic Processes*. Tata McGraw-Hill, 2002.

[28] S. N. Sharma, "A Kushner approach for small random perturbations of the Duffing-Van der Pol system," *Automatica*, vol. 45, no. 4, pp. 1097–1099, Apr. 2009.

[29] M. Baran and F. F. Wu, "Optimal sizing of capacitors placed on a radial distribution system," *IEEE Trans. Power Del.*, vol. 4, no. 1, pp. 735–743, 1989.

[30] M. G. Molina and P. E. Mercado, "Control Design and Simulation of DSTATCOM with Energy Storage for Power Quality Improvements," in *Transmission Distribution Conference and Exposition: Latin America, 2006. TDC '06. IEEE/PES*, 2006, pp. 1–7.

[31] A. K. Barnes, J. C. Balda, S. O. Geurin, and A. Escobar Mejía, "Optimal battery chemistry, capacity selection, charge/discharge schedule, and lifetime of energy storage under time-of-use pricing," in *IEEE PES Innovative Smart Grid Technologies Europe (ISGT-EU)*, 2011, pp. 1–7.

[32] M. Starke, N. Alkadi, and O. Ma, "Assessment of Industrial Load for Demand Response across U.S. Regions of the Western Interconnect," Oak Ridge National Laboratory, Report ORNL/TM-2013/407, 2013.

APPENDIX A: CERTIFICATION OF FIRST AUTHOR

I hereby certify that Arthur K. Barnes is first author of the article this chapter is based on and has completed at least 51% of the work described in the article.

Juan Carlos Balda

Signature _____

Date _____

APPENDIX B: COPYRIGHT AGREEMENT

ThB12.4

INTERNATIONAL FEDERATION OF AUTOMATIC CONTROL IFAC
TRANSFER OF COPYRIGHT AGREEMENT

PLEASE PROVIDE US WITH THE FOLLOWING INFORMATION, REVIEW OUR POLICIES AND THE PUBLISHING AGREEMENT, AND INDICATE YOUR ACCEPTANCE OF THE TERMS.

Title of Meeting	19th IFAC World Congress, August 24-29, 2014, Cape Town, South Africa
Article entitled	Modeling PV Clouding Effects Using a Semi-Markov Process with Application to Energy Storage
Complete list of authors	Arthur Barnes, Juan Carlos Balda

YOUR STATUS

- ☑ I am one author signing on behalf of all co-authors of the manuscript
- ☐ The article is a 'work made for hire' and I am signing as an authorised representative of the employing company
- ☐ All authors are US Government employees and there is no copyright to transfer, but I affirm the author warranties
- ☐ All authors are employees of the UK, Canadian or Australian Government claiming Crown Copyright, but I affirm the author warranties

Signed **Arthur Barnes**	Name Printed **Arthur Barnes**
Date **March 25, 2014**	Job title and company (if employer representative)

THE PUBLISHING AGREEMENT

Assignment of publishing rights

I hereby assign to The International Federation of Automatic Control (IFAC) the copyright in the manuscript identified above (government authors not electing to transfer agree to assign a non-exclusive licence) and any supplemental tables, illustrations or other information submitted therewith that are intended for publication as part of or as a supplement to the manuscript (the "Article") in all forms and media (whether now known or hereafter developed), throughout the world, in all languages, for the full term of copyright, effective when and if the article is accepted for publication. This transfer includes the right to provide the Article in electronic and online forms and systems.

Retention of Rights for Scholarly Purposes

I understand that I retain or am hereby granted (without the need to obtain further permission) rights to use certain versions of the Article for certain scholarly purposes, as described and defined below ("Retained Rights"), and that no rights in patents, trademarks or other intellectual property rights are transferred to the IFAC.

The Retained Rights include the right to use all versions of the Article, for Personal Use, Internal Institutional Use, and for Scholarly Posting. Such posting is limited to noncommercial use.

All papers accepted for IFAC Proceedings will be hosted on-line on IFAC-PapersOnLine website and are considered for subsequent publication in the IFAC journals and in other IFAC-affiliated journals. If the signing author has not been informed in writing wit hin three months of the closing date of the conference that the paper is being so considered, he and his co-authors are free to submit the paper elsewhere, providing that full acknowledgement is given in any subsequent publication to the original IFAC Proceedings and to the conference.

Requests from Third Parties

Requests for all uses not included above, including the authorization of third parties to reproduce or otherwise use all of part of the article (including figures and tables), should be referred to IFAC by writing to the IFAC Secretariat (secr@ifac.co.at).

Author Warranties/Ethics and Disclosure

I affirm the Author Warranties noted below, and confirm that I have reviewed and complied with the relevant Instructions to Authors, the Ethics in Publishing policy, and Conflicts of Interest disclosure. For further information see the IFAC web site, http://www.ifac-control.org

Author warranties

- The article I have submitted to the conference for review is original, has been written by the stated authors and has not been published elsewhere.

- The article is not currently being considered for publication by any other conference/journal and will not be submitted for such review while under review by this conference. •
- The article contains no libelous or other unlawful statements and does not contain any materials that violate any personal or proprietary rights of any other person or entity.
- I have obtained written permission from copyright owners for any excerpts from copyrighted works that are included and have credited the sources in my article.
- If the article was prepared jointly with other authors, I have informed the co-author(s) of the terms of this publishing agreement and that I am signing on their behalf as their agent, and I am authorized to do so.

Funding agency requirements and other policies
I have also been made aware of the conference's policies (Special Subject Repository) with respect to funding agency requirements such as the NIH 'PublicAccess' policy, and the rapid publication 'ArticlesInPress' service. See www.ifac-control.org for details.

IFAC-PapersOnLine Hosting
IFAC may choose to publish an abstract, portions of the paper or the entire paper prior to presentation at the meeting. By signing this copyright form, you are granting IFAC the permission to host the paper on the IFAC-PapersOnLine website.

DEFINITIONS

Accepted Authors Manuscript ("AAM")
Author's version of the manuscript of a paper that has been accepted for publication and which may include any author-incorporated changes suggested through the peer review process. AAMs should not include however other publisher value added contributions such as formatting, pagination, and copy-editing, and should include the Appropriate Bibliographic Citation and a link to the final publication (generally through the relevant DOI).

Appropriate Bibliographic Citation
Authors posting Accepted Authors Manuscript online may later add a citation for the Published Conference Article indicating that the paper was subsequently published, and may mention the conference title provided they add the following text at the beginning of the document: "NOTICE: this is the author's version of a work that was accepted for publication in <Conference title>. Changes resulting from the publishing process, such as peer review, editing, corrections, structural formatting, and other quality control mechanisms may not be reflected in this document. Changes may have been made to this work since it was submitted for publication. A definitive version was subsequently published in PUBLICATION, [VOL#, ISSUE#, (DATE)] DOI#"

Commercial Purposes
The use or posting of articles for commercial gain including the posting by companies or their employee-authored works for use by customers of

such companies (e.g. pharmaceutical companies and physician-prescribers); commercial exploitation such as directly associating advertising with such postings; the charging of fees for document delivery or access; or the systematic distribution to others via e-mail lists or list servers (to parties other than known colleagues), whether for a fee or for free.

Internal Institutional Use
Use by the author's institution for classroom teaching at the institution (including distribution of copies, paper or electronic, and use in course-packs and courseware programs) and posting on secure Intranet sites for scholarly purposes.

Personal Use
Use by an author in the author's classroom teaching (including distribution of copies, paper or electronic), distribution of copies to research colleagues for their personal use, use in a subsequent compilation of the author's works, inclusion in a thesis or dissertation, preparation of other derivative works such as extending the article to book-length form, or otherwise using or re-using portions or excerpts in other works (with full acknowledgment of the original publication of the article).

Pre-print
Author's own write-up of research results and analysis that has not been refereed, nor had any other value added to it by a publisher (such as formatting, copy editing, and the like).

Published Conference Article ("PCA")
The definitive final record of published research that appears or will appear in the c onference proceedings and embodies all value adding publisher activities including formatting, pagination and copy-editing.

Scholarly Posting
Postings on open Web sites operated by the author or the author's institution for scholarly purposes, or (in connection with Pre-prints) pre-print servers, provided there is no Commercial Purpose involved. Deposit in or posting to Special Subject Repositories (such as PubMed Central) is permitted only under specific agreements and only consistent with Elsevier's policies concerning such repositories. If the author wishes to refer to the proceedings in connection with such posting, the Appropriate Bibliographic Citation should be used.

US Government employees
• If all co-authors are US Government employees there is no copyright to transfer. Please sign the form, to confirm the author warranties.

Crown Copyright
• UK Government employee authors may elect to transfer copyright.
• UK Government employees wishing to claim Crown Copyright should mark the appropriate box overleaf and sign the form to affirm the
author warranties.
• The work of Canadian or Australian Government employees is automatically subject to Crown Copyright. Please mark the appropriate box

and sign the form to affirm the author warranties.

Special Subject Repositories
Certain repositories such as PubMed Central ("PMC") are authorized under special arrangement with Elsevier to process and post certain articles such as those funded by the National Institutes of Health under its Public Access policy (see elsevier.com for more detail on our policy).

Articles accepted for publication in an IFAC Conference and possibly subsequently in an Elsevier journal from authors who have indicated that the underlying research reported in their articles was supported by an NIH grant will be sent by Elsevier to PMC for public access posting 12 months after final publication. The version of the article provided by Elsevier will include peer-review comments incorporated by the author into the article. Because the NIH 'Public Access' policy is voluntary, authors may elect not to deposit such articles in PMC. If you wish to 'opt out' and not deposit to PMC, you may indicate this by sending an e-mail to NIHauthorrequest@elsevier.com.

CHAPTER NINE

A SEMI-MARKOV MODEL FOR CONTROL OF ENERGY STORAGE IN UTILITY GRIDS AND MICROGRIDS WITH PV GENERATION

Arthur Barnes and Juan Carlos Balda

A.K. Barnes and J.C. Balda, "A semi-Markov model for control of energy storage in utility grids and microgrids with PV generation," *IEEE Transactions on Sustainable Energy* (in review), August 2014.

Abstract **— Photovoltaic (PV) penetration levels in the power grid have significantly increased during the last years. However, issues such as cloud-induced intermittency in PV generation forces equipment on the electrical grid to cycle excessively, preventing PV from being considered as a reliable or dispatchable source of power, particularly by utilities.**

In this paper a model of PV clouding is proposed for a centralized PV generation installation. The cloud structure is modeled as a random sequence inferred from measured solar data. Unlike existing models of PV power, the proposed model has a wide range of applications across both small and large timescales. These applications include simulating PV power, short-term forecasting of PV power, design of rule-based controllers for energy storage units (ESU), and stochastic scheduling of ESU in conjunction with other resources. The model is applied to study two cases of coordinating ESU with PV generation. In the first case, the model serves to design a coordination scheme for a hybrid battery-ultracapacitor (UC) ESU where the UC serves to extend the lifetime of a lead-acid battery.

In the second case, the model allows probabilistic scheduling in a standalone PV/diesel/battery ESU microgrid.

Index Terms **— Coordinated control, energy storage sizing, high penetration PV, microgrids, power distribution, statistical modeling, semi-Markov process, smart grids, solar intermittency, solar radiation.**

I. INTRODUCTION

Advances in the manufacturing process of solar panels are lowering costs and leading to increased grid penetrations. However, the power output of PV inverters varies sharply because of changing cloud cover that may cause transitions from rated power to less than half of rated power within minutes [1]. This may cause over- or under-voltages on distribution systems [2], [3] in addition to reducing the maintenance interval of voltage regulating equipment such as substation load tap-changers (LTC) or in-line voltage regulators [4]. These adverse issues raise concern among electric utility operation personnel.

At the same time, the concept of the microgrid is gaining traction. Microgrids are standalone electrical grids or portions of a larger utility grid that can operate in a self-sustaining islanded mode. They typically include local generation, ESU and controllable loads with coordinated control [5]. Microgrids that interact with a larger grid use the local generation, ESU and controllable loads to appear as a single controllable load or generator. While connected, they can provide services to the larger grid such as energy arbitrage, demand management, or reactive power compensation. These capabilities provide for reduced power consumption from the larger grid while improving reliability and power quality to the customers within the microgrid. Examples of microgrids include a college campus or military base. For a microgrid with

renewable generation such as PV, it is necessary to make it dispatchable by coordinating it with the ESU and local fossil-fuel generation [6]. This is a requirement for a standalone microgrid to establish power balance, or for a microgrid reducing demand (or supplying power) to a larger grid to be able to guarantee that scheduled load reduction (or supplied power) is provided. This latter requirement holds true not only for PV installations within microgrids, but also for large PV installations that are permanently grid connected, either utility- or customer-owned.

Energy storage has long been proposed as a solution to compensate for power fluctuations commonly found in renewable resources such solar and wind; however, it is necessary to either model or predict cloud-induced intermittency to develop a more-efficient ESU control strategy for mitigating PV intermittency [7]–[10]. Frequency-domain methods have been previously applied to characterize PV power [11]. Unfortunately, the resulting frequency-domain signal has units without physical significance [12]. Despite these methods being useful for observing qualitative features of PV power intermittency, they are not suitable for designing ESU which requires knowledge of the peak energy amount charged to or discharged from a battery.

Methods for controlling an ESU can be broadly classified into deterministic scheduling, stochastic scheduling, rule-based control, feedback control, and feedforward control [7]–[9], [13], [14], with deterministic scheduling most commonly employed. Prediction of PV power is necessary for ESU control methods based on deterministic scheduling [14], and has received significant attention in recent years. Current methods are divided into two major groups [15]. The first group consists of those methods using numerical weather prediction to estimate hourly averaged power with look-ahead intervals on the order of one or more days [16]. The second group of methods uses sky imagers, geographically distributed sensor arrays, or satellite imagery to track cloud position over time [17]–[19]. This yields power predictions on the order of a few

hours ahead [20]. The time resolution for both methods are too coarse for predicting cloud-induced power variations, which occur in seconds [18].

This paper extends work on a semi-Markov discrete-time random process model (SMDTRP) for PV clouding [21]. The SMDTRP is proposed for generating simulated PV power data, short-term forecasting of PV power, and parameter selection for rule-based controllers to coordinate ESU and tap-changers for mitigating PV-induced voltage variability. This paper introduces how to calculate the probability mass function (PMF) and cumulative distribution function (CDF) of the energy produced by PV over a time interval. Two new applications of the SMDTRP are presented: controller parameter selection for a hybrid battery-UC ESU, and stochastic scheduling in standalone PV/diesel/battery-ESU microgrids. The latter makes use of the CDF calculations presented in the scheduling algorithm.

The hybrid battery-UC ESU was first proposed for automotive applications, where the UC served to supply peak powers that would otherwise require a larger battery pack than energy demand alone dictated [22]. It has since been studied for grid-connected applications [1]. However, in the case of grid-connected ESU applied to smooth PV output power to make it dispatchable, the UC is instead applied to reduce battery cycling. This enables the use of cheaper technologies (e.g. lead-acid instead of lithium-ion) with lower cycle life, while still having the ESU meet battery lifetime requirements in terms of years. The SMDTRP is applied in this case to calculate the expected battery lifetime for a given parameter value in a rule-based ESU controller.

In the case of hybrid standalone microgrids, stochastic scheduling allows for uncertainty to be taken into account, reducing fuel consumption vs. deterministic methods [24]. This paper illustrates how knowledge of the CDF of PV energy over a time interval allows stochastic

scheduling methods to be applied, thereby accounting for uncertainty in the PV energy [25]. A rule-based controller is applied to calculate average generator and battery power over each scheduling interval, which allows stochastic dynamic programming to be applied by overcoming the limitation of a quantized state space.

The paper is organized as follows: the PV data collection is described in section II; the data processing and classification is explained in section III; the development of statistical distributions are addressed in section IV; the semi-Markov process is described in section V; case studies of the SMDTRP's utility are presented in section VI; and lastly, the conclusions on the work performed are given in section VII.

II. PV DATA ACQUISITION

Irradiance is captured with an irradiance sensor (Apogee SP-125 5V amplified pyranometer) [26] in conjunction with a LabVIEW-based data acquisition system (National Instruments USB-6259) using a custom program. The pyranometer is installed at the University of Arkansas (UA) in Fayetteville (AR) on the top of the John A. White Engineering Hall roof next to a pair of 225W PV panels as shown in Fig. 1. It was installed on the same plane as the panels, facing South with tilt angle of 66º from horizontal. For the analysis, 10 days of data with a sample rate of 1 Hz are captured during August and September 2011, which are available on the web [27].

III. PROCESSING AND CLASSIFICATION OF PV DATA

Erroneous values corrupted by noise and nonlinear effects in the sensor are unfortunately captured by the data acquisition system. Hence, the data must be processed to remove these erroneous values that occur at low irradiance as well as to capture statistics on clouding. This processing classifies data as *clear* or *shaded*, based on the clear-sky irradiance profile and a

model of clouding effects. The estimated clear-sky irradiance $r_e(n)$ at sample n is calculated using a graphical tool developed in Matlab™, illustrated in Fig. 2. Given a set of time values $t(n) \in [0, 23]$ h and irradiance values $r(n)$ W/m^2, the tool lets the user select the peak irradiance R_d and time of sunrise t_{0d} for each day d. This is applied to normalize the irradiance $r(n)$ to calculate the normalized irradiance $r_n(n)$. Given the set of $\mathcal{N}_d$ samples corresponding to day d, the normalized irradiance and time values are

$$r_n(n) = \frac{1}{R_d} r(n) \quad n \in \mathcal{N}_d \tag{1}$$

$$t_n(n) = t(n) - t_{0d}. \tag{2}$$

A set of normalized points are selected with the tool corresponding to periods of clear sky. A second-order $r_e(n)$curve fits $r_n(n)$ based on the coefficients a_0, a_1, a_2. To account for nighttime it is saturated at 0:

$$r_e(n) = \min[a_2 t^2(n) + a_1 t(n) + a_0, 0]. \tag{3}$$

In removing the deterministic component of irradiance related to the clear-sky irradiance profile, the probabilistic SMDTRP is free to only model clouding effects, reducing the chance for overfitting [28].

As illustrated in Fig. 3, the error distribution can be modeled by the weighted sum of a pair of normal distributions, each distribution corresponding to either *clear* or *shaded* states. To classify the points as *clear* or *shaded*, a Bayes classifier is applied to the normalized error $d_n(n)$, which is calculated as

$$d_n(n) = \frac{r_n(n) - r_e(n)}{r_e(n)}. \tag{4}$$

For each data point $d_n(n)$, the probability of it belonging to state i is given by the weighted normal distribution

$$p_i[d_n(n)] = P_i \frac{1}{\sigma_i\sqrt{2\pi}} e^{-\frac{(d_n(n)-\mu_i)^2}{2\sigma_i^2}}. \quad (5)$$

In the above, P_i is the prior probability of either the *clear* or *shaded* state, μ_i is the mean error of each state, and σ_i is the standard deviation for the error of each state. In this case, the standard deviation is assumed to be the same for both states so that $\sigma_i = \sigma$. This assumption helps ensure convergence of the expectation-maximization algorithm used for parameter inference. The inferred parameters for the data analyzed are presented in Table I.

Note that for PV installations with tracking, the irradiance profile will be flattened near mid-day [29], so a higher-order curve fit will be necessary. The classification results and how the curve is saturated at 0 to account for nighttime are illustrated in Fig. 4. The processing accomplishes two goals: First, the data are classified as either *clear* or *shaded*, allowing for statistics to be taken on cloud cover. Second, it mitigates corrupted data by removing erroneous samples and interpolating between the remaining good data. For the case of the pyranometer, two factors were observed to corrupt data. First, accuracy at high solar angles of incidence is poor as the output drops off. Second, oscillation is present at those high angles of incidence, illustrated around 6 am and 7 pm (19 h) in Fig. 4, which compares the measured and corrected data. To overcome these issues, the corrupted samples are removed and a weighted sum of the predicted and measured irradiance is used to estimate the true irradiance.

Fig. 1. Close-up of the sensor location adjacent to rooftop PV panels at UA.

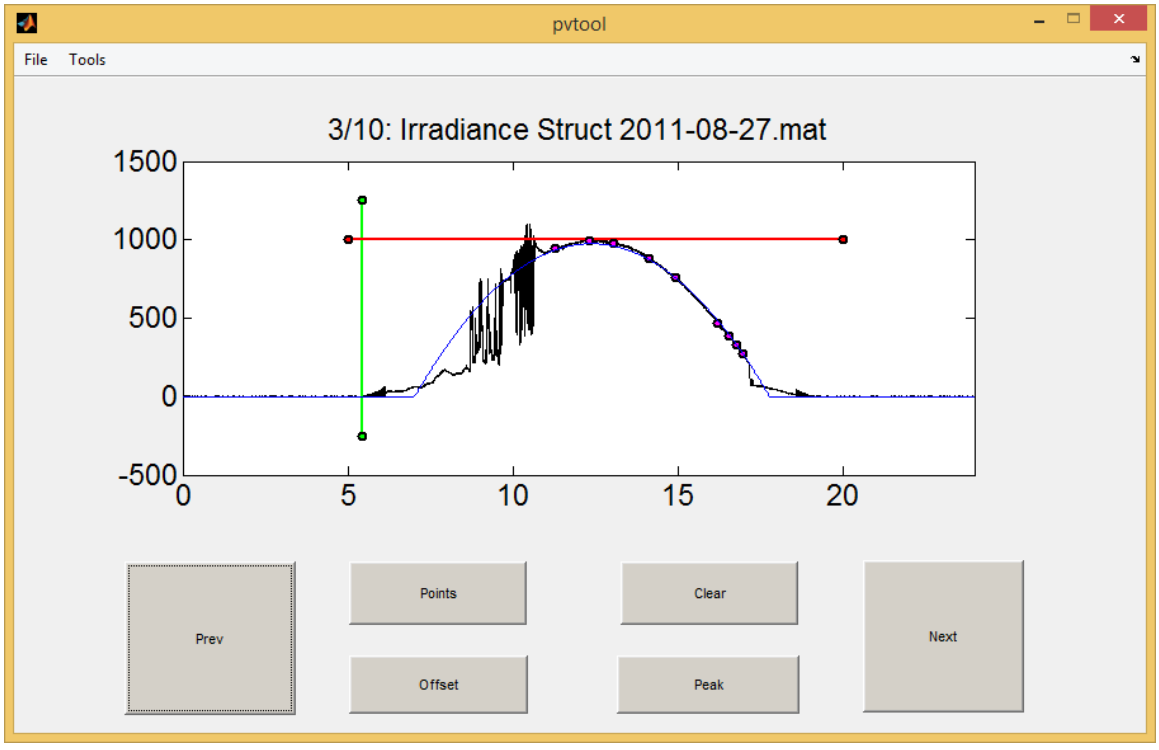

Fig. 2. Screenshot of the Matlab™ tool for fitting the clear-sky irradiance profile from measured data.

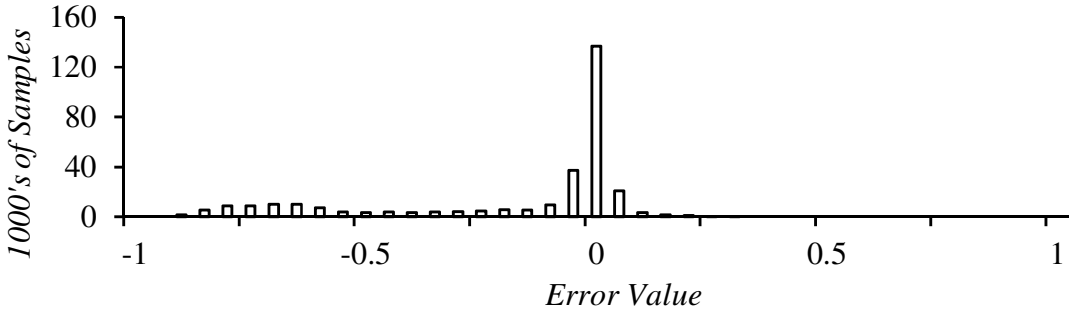

(a)

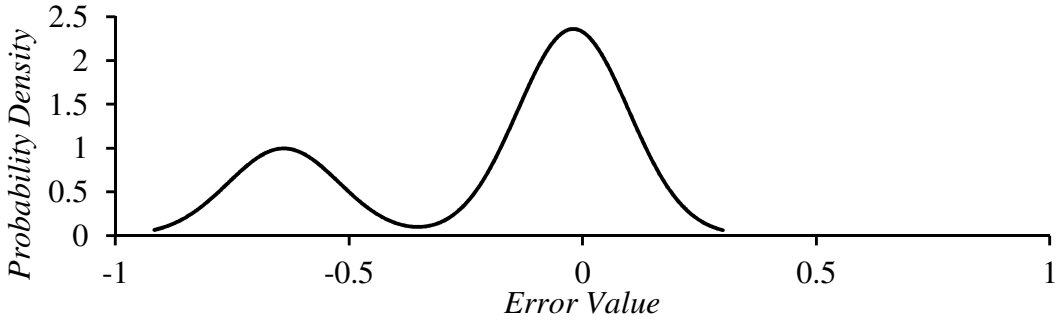

(b)

Fig. 3. Histogram of normalized error (a) and inferred probability distribution of mixture-of-Gaussian model (b).

TABLE I. PARAMETERS FOR ERROR DISTRIBUTION

Parameter	Var.	Value
Prior probability of *clear* state	P_1	0.7032
Prior probability of *shaded* state	P_2	0.2968
Mean of *clear* state	μ_1	–0.0201
Mean of *shaded* state	μ_2	–0.6398
Variance	σ^2	0.0141

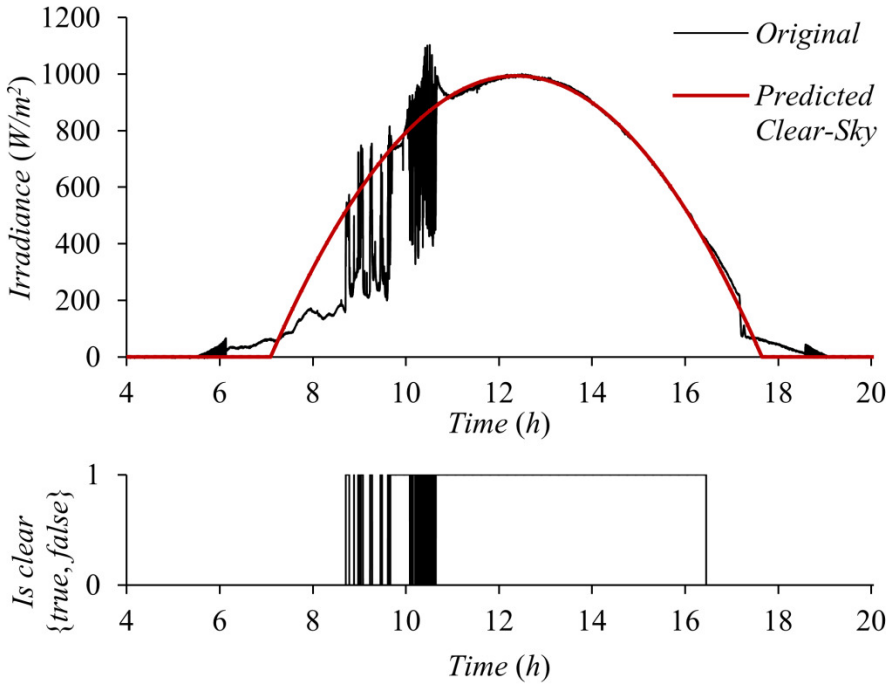

Fig. 4. Classified irradiance data for a partly cloudy day (Aug 27, 2011). The original irradiance profile and predicted clear-sky irradiance profile are in the top graphs, while the classification results (whether or not it is clear or shaded) are in the bottom.

IV. STATISTICAL INFERENCE OF CLOUD DURATIONS

In order to characterize and forecast the PV output, it is assumed that the *clear* and *shaded* durations follow statistical distributions. Based on existing work in climate science [30], cumulus clouds have a fractal structure, so the distribution of the cloud and thus the duration of shading, roughly follow a power law distribution. Through exploratory data analysis, it is inferred that distribution of the *clear* and *shaded* durations T follow a generalized Pareto distribution of the form

$$f\left(T\middle|k_p,\sigma_p,\theta_p\right)=\frac{1}{\sigma_p}\left[1+k\frac{\left(t-\theta_p\right)}{\sigma_p}\right]^{-1-\frac{1}{k_p}} \tag{6}$$

where k_p, σ_p, θ_p are parameters of the distribution [31]. Although the duration of *clear* conditions is truncated based on the length of a day, the effect of truncation is neglected. Two separate distributions are inferred for the duration of *clear* and *shaded* events, respectively.

To validate the inferred parameters, they are compared against data recorded over 4 years from a 15 kW PV array located at the Fayetteville, AR public library. The data consists of the power injected into the ac grid sampled at 1 min intervals. The data are divided into 4 weather classes – *sunny, partly cloudy, cloudy,* and *overcast*. Individual days can be divided into multiple weather classes. The weather classes are selected via a Matlab™ GUI by visual inspection, illustrated in Fig. 5. *Sunny* conditions contain only a few periods of clouding. *Partly cloudy* conditions include frequent clouding, but the clear-sky envelope is readily visible. During *cloudy* conditions, the power is above 30% of rated, but the envelope is not visible. *Overcast* conditions are those when the power falls below 30% for most of the period. The clear-sky irradiance profile is based on a quadratic fit of manually selected points. The relative frequency of weather classes is illustrated in Fig. 6, while Fig. 7 illustrates the statistical variation in the average energy (in W-min) per region. The number of regions for each weather class is selected based on making an accurate estimation of the mean irradiance for that type. The number of required samples is calculated for each weather class. The initial estimate n' of the number of samples is calculated based on the z-value $z_{\alpha/2}$ for a confidence level $1-\alpha$ given the variance estimate $\hat{\sigma}$ and confidence interval half-width HW. The t-value $t_{\alpha/2}$ given n' and α is used to produce a refined estimate n. For this case, the confidence interval is $\pm 5\%$ of the sample mean with a 90% confidence level. The calculations follow:

$$n' = \left(\frac{z_{\alpha/2}\hat{\sigma}}{HW} \right)^2 \tag{7}$$

$$n = \left(\frac{t_{\alpha/2}\hat{\sigma}}{HW} \right)^2 . \tag{8}$$

The number of samples calculated and the actual number of samples n_a are listed Table II. The actual number of samples used exceeds the calculated number because the granularity for selecting data is in units of days, not regions.

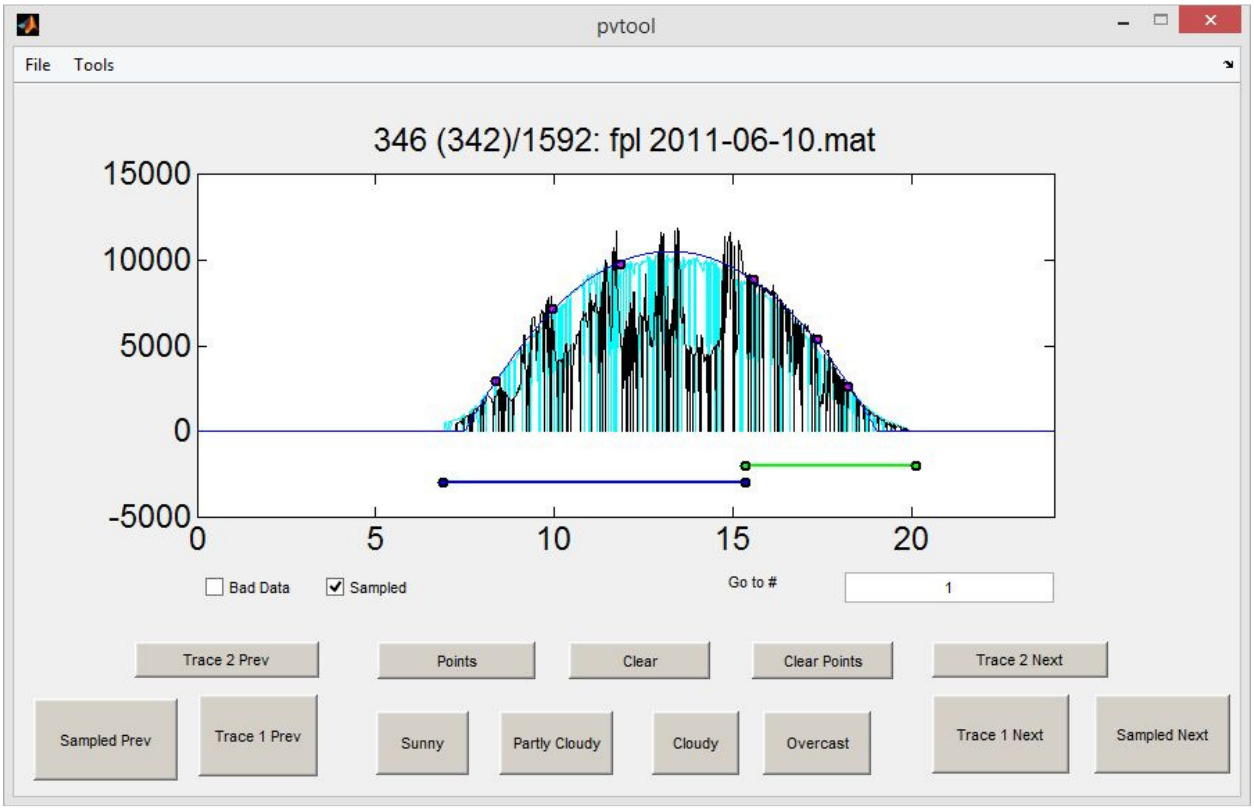

Fig. 5. Illustration of selecting partly cloudy regions (green) and cloudy regions (blue), user-selected points for curve fit (magenta), and curve fit (blue line). Black PV profile is current day, cyan PV profile is a reference day used to assist with selecting points.

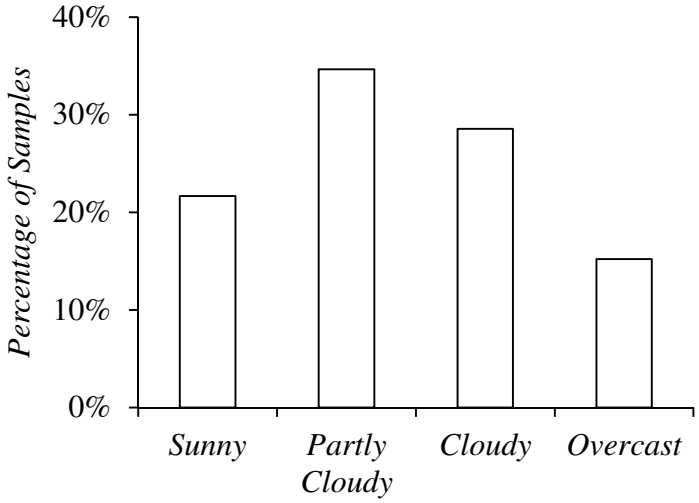

Fig. 6. Relative frequency of weather classes.

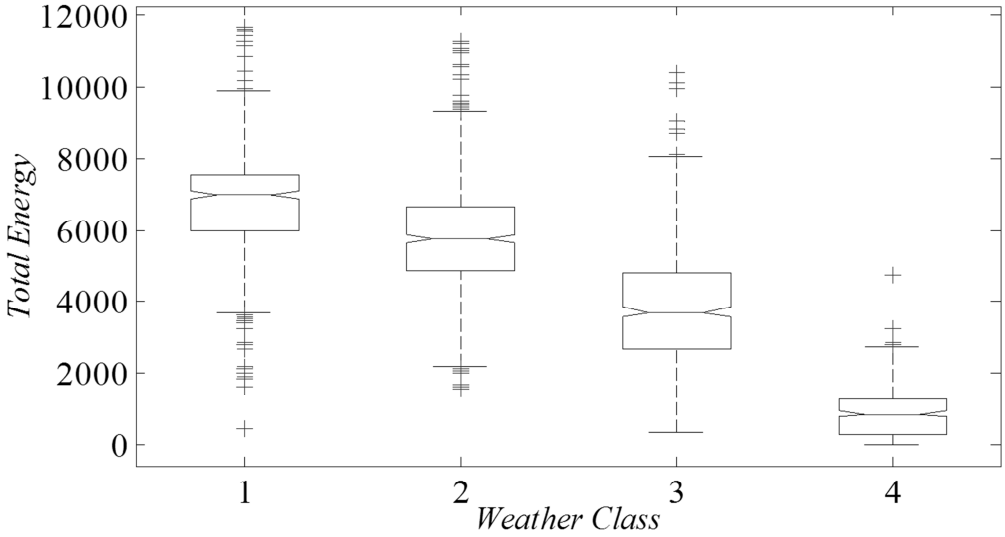

Fig. 7. Box plot of weather classes.

TABLE II. REQUIRED NUMBER OF SAMPLES FOR THE DESIRED CONFIDENCE INTERVALS AND LEVEL

	Sunny	**Partly Cloudy**	**Cloudy**	**Overcast**
n'	59.0433	78.6652	201.414	712.606
n	61	81	204	715
n_a	117	169	235	305

The inferred distribution parameters for the irradiance sensor are presented in Table III. Fig. 8. Illustrates that the quantiles of the inferred distribution with these parameters closely matches those of the data. Additionally, in Table IV the inferred distribution parameters are compared with those for the Fayetteville public library. The main difference lies in the scale parameter, σ_p, which measures how quickly the distribution decays. Depending on the weather type, the expected duration of *clear* periods will vary, in addition to the expected duration of the *shaded* periods themselves. Days of the *sunny* weather class will have long *clear* periods, but the average durations of these periods decreases with cloudier weather.

TABLE III. DISTRIBUTIONS OF CLEAR AND SHADED DURATIONS FOR THE IRRADIANCE SENSOR

State	Parameter	Var.	Value
Clear	Pareto parameters	K_p	1.798
		σ_p	3.808×10^{-3}
		θ_p	0
	Steady-state interval transition probability	ϕ_i	0.59
Shaded	Pareto parameters	K_p	1.206
		σ_p	3.452×10^{-3}
		θ_p	0
	Steady-state interval transition probability	ϕ_i	0.41

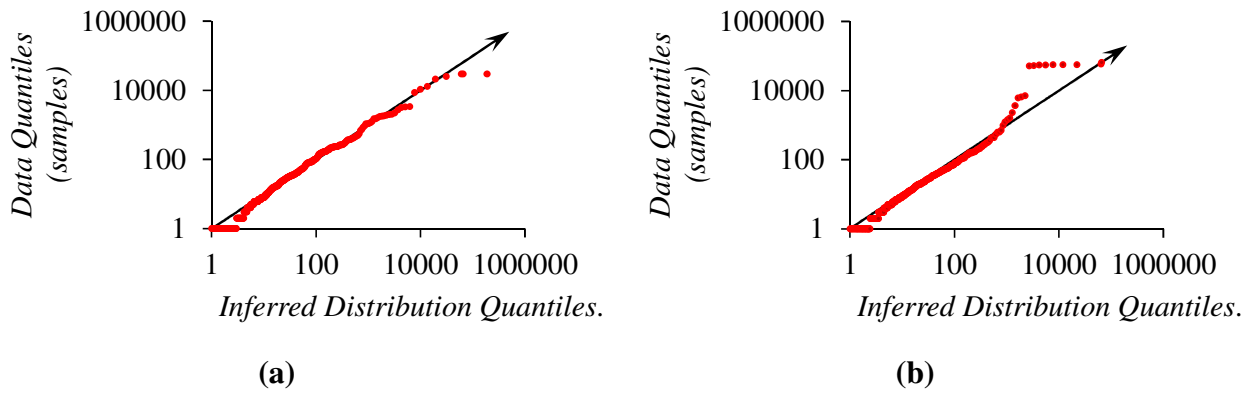

Fig. 8. Quantile-quantile plots comparing the actual and inferred distributions for (a) *clear* durations and (b) *shaded* durations.

TABLE IV. DISTRIBUTIONS OF CLEAR AND SHADED DURATIONS FOR THE FAYETTEVILLE PUBLIC LIBRARY

	K_p	K_p	σ_p	σ_p
	Clear	Shaded	Clear	Shaded
Sunny	0.5438	0.2471	77.2261	2.3671
Partly Cloudy	0.4219	0.1490	6.1137	1.8031
Cloudy	0.5780	0.7733	4.0321	3.1630
Overcast	0.8142	2.4682	5.0093	6.0078
Downsampled Irradiance	0.9575	1.3545	2.7097	2.0609

V. MODELING AS A SEMI-MARKOV PROCESS

Although knowing the distribution of the *clear* and *shaded* durations is not useful in itself, it is applied to create a random process model that has broad applications. The state of the PV installation is modelled as a time series $s(0), s(1), \ldots, s(N-1)$, where at each sample n, the state $s(n)$ is either 1, denoting *clear*, or 2, denoting *shaded.* Section IV revealed that $s(n)$ is dependent not just on $s(n-1)$, but also on the total duration that the sensor has been *clear* or

shaded, thereby violating the Markov property [28]. This is apparent because the distributions of the *clear* and *shaded* durations are not geometric, which is required for the Markov property to hold [28]. However, it is shown next that the distributions of *clear* and *shaded* times can still be used to model the shading as a discrete-time semi-Markov process [32].

A Markov process has a set of states and a state-transition probability matrix indicating the likelihood p_{ij} of transitioning from state i to state j at sample n [33]–[35]. The semi-Markov discrete-time process (SMDTRP) is a generalization of the Markov process that waits for a random hold time before each transition. Therefore, each element p_{ij} of the SMDTRP state-transition probability matrix has a corresponding hold-time distribution $h_{ij}(m)$, the probability that the process will transition into state j at sample m given that it entered state i at sample 0.

Irradiance is modelled by a two-state model in which virtual state transitions are forbidden (that is, transitions from a state to itself), illustrated in Fig. 9. This results in a simpler representation of the system, as the state-transition probability matrix is simply a two-by-two identity matrix. In order to generate simulated data, the SMDTRP is executed via the algorithm described in Fig. 10.

V.A. Interval Transition Probabilities

For forecasting, the quantities of interest are the interval transition probabilities, giving the likelihood that the PV is *clear* or *shaded* at sample n given that it transitioned to be *clear* or *shaded* at sample 0. The interval transition probability $\phi_{ij}(n)$ is the probability that the process is in state i at sample n, given that it entered state j at sample 0; in particular

$$\phi_{12}(n) = \sum_{n=0}^{N} \sum_{m=1}^{n} h_{12}(m)\phi_{22}(n-m) \tag{9}$$

$$\phi_{21}(n) = \sum_{n=0}^{N} \sum_{m=1}^{n} h_{21}(m)\phi_{11}(n-m).$$

Because these calculations rely on a series of multiply-accumulate operations which are performed quickly by modern computers [12], they are easily computed numerically using the following initial conditions

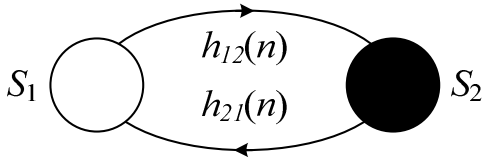

Fig. 9. Graphical illustration of the SMDTRP model states and transitions.

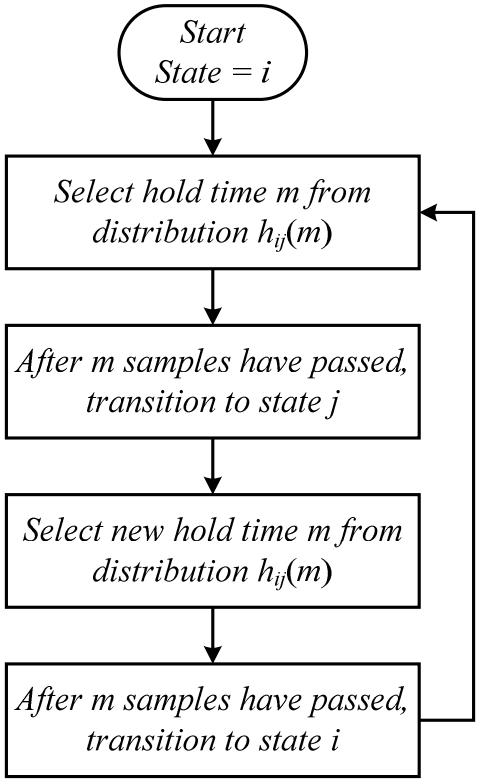

Fig. 10. Flow chart for generating simulated clouding data with the SMDTRP.

$$\Phi(0) = \begin{bmatrix} 1 & 0 \\ 0 & 1 \end{bmatrix} \tag{10}$$

and the definition of a PMF

$$\begin{aligned} \phi_{11}(n) + \phi_{21}(n) &= 1 \\ \phi_{12}(n) + \phi_{22}(n) &= 1, \end{aligned} \tag{11}$$

where (8) reflects the fact that at sample 0 the state of the process is known with no uncertainty.

The interval transition probabilities allow for performing forecasting by taking the state with the highest likelihood. For example, if a process transitioned from *clear* to *shaded* at sample 0, it will most likely remain shaded for 50 seconds until $\phi_{21}(n)$ exceeds 0.5, as illustrated by Fig. 11. This figure illustrates the evolution of the interval transition probabilities over time assuming that the system started in *clear* (state 1, red lines), or *shaded* (state 2, black lines). As time increases, the uncertainty in the interval transition probabilities increases and they converge to their steady-state values ϕ_1 and ϕ_2, the marginal likelihoods of the system being either *clear* or *shaded.* These values are defined as

$$\phi_i = \frac{\tau_i}{\tau_i + \tau_j}. \tag{12}$$

In the above, τ_i is the expected hold time for state i calculated as

$$\tau_i = \sum_{m=1}^{n} m h_{ij}(m). \tag{13}$$

V.B. Reward Model

The SMDTRP can be employed to calculate the expected performance or cost of a rule-based controller applied to a system with PV via reward processes (where the rewards could also be costs). Similar to the case of the interval transition probabilities, the reward processes are calculated recursively as follows

$$v_1(n) = {}^{>}y_1(n) + r_1(n) + \sum_{m=1}^{n} h_{21}(n)\, v_2(n-m)$$

$$v_2(n) = {}^{>}y_2(n) + r_2(n) + \sum_{m=1}^{n} h_{12}(n)\, v_1(n-m) \tag{14}$$

$${}^{>}y_1(n) = y_1(n,1) \sum_{m=n+1}^{\infty} h_{12}(m)$$

$${}^{>}y_2(n) = y_2(n,1) \sum_{m=n+1}^{\infty} h_{21}(m) \tag{15}$$

$$r_1(n) = \sum_{m=1}^{n} h_{12}(n)\, y_1(n,1)$$

$$r_2(n) = \sum_{m=1}^{n} h_{21}(n)\, y_2(n,1) \tag{16}$$

$$y_i(m,1) = \sum_{l=0}^{m-1} y_i(l). \tag{17}$$

These assume zero initial rewards, so $v_i(0) = 0$. The significances of the terms are as follows: $v_i(n)$ is the expected reward of the process at sample n given that the process entered state i at sample 0. The term ${}^{>}y_i(n)$ is the reward contribution when the process transitions to another state after sample n. The term $r_i(n)$ is the expected reward contribution when the process transitions to another state before sample n. The last terms in (12) are the expected rewards earned over samples $n - m$ to n conditioned on the event that the process transitions to another state before sample n. The term $y_i(m,1)$ represents the cumulative reward accrued over m samples. The term $y_i(l)$ is the reward rate at l samples after having transitioned into state i.

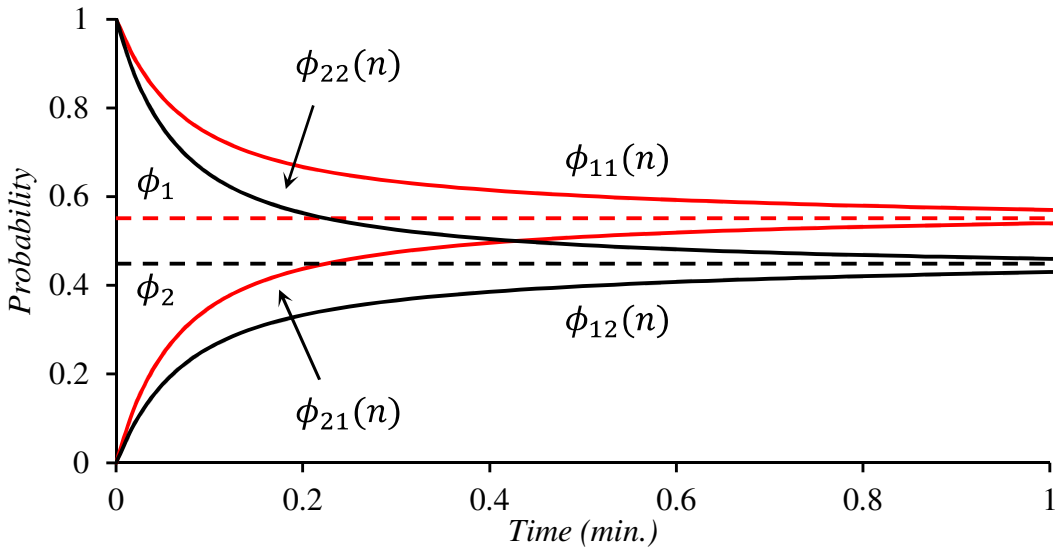

Fig. 11. Interval transition probabilities $\boldsymbol{\phi_{ij}(n)}$ converging to the steady-state values $\boldsymbol{\phi_i}$. The probabilities $\boldsymbol{\phi_1 + \phi_2 = 1}$.

V.C. State Occupancy Distributions

The SMDTRP is also helpful for calculating the distribution of state occupancies in a given time interval. This is useful in order to derive the PMF of energy produced by a PV installation over the course of multiple samples. Given that the process entered state i at sample 0, the probability of k occurences of state j in the interval $0,1,2,\dots,n$ is $w_{ij}(k|n)$.

For the process modeled here, the discrete probability distributions are as follows

$$w_{11}(k|n) = \sum_{m=1}^{n} h_{12}(m)\mathrm{w}_{21}(k|n-m) + \delta(k)\,{>}\,w_1(n)$$
$$w_{12}(k|n) = \sum_{m=1}^{n} h_{12}(m)\mathrm{w}_{22}(k-m|n-m) + \delta(k)\,{>}\,w_2(n) \quad (18)$$

$$w_{21}(k|n) = \sum_{m=1}^{n} h_{21}(m)\mathrm{w}_{11}(k-m|n-m) + \delta(k)\,{>}\,w_1(n) \quad (19)$$

$$w_{22}(k|n) = \sum_{m=1}^{n} h_{21}(m)\mathrm{w}_{11}(k|n-m) + \delta(k)\,{}^{>}w_2(n).$$

In the above $\delta(k)$ is the Kroneker delta function, and

$${}^{>}w_i(n) = \sum_{m=n+1}^{\infty} h_{ij}(m). \tag{20}$$

The state occupancy probability distributions are used to derive the CDF of the state occupancies, $W_{ij}(k|n)$. Only the CDF of the clear states need be calculated, which follow

$$\begin{aligned} W_{11}(k|n) &= \begin{cases} \sum_{m=1}^{n} h_{12}(m)\mathrm{W}_{21}(k|n-m), & k < n+1 \\ 1, & k \geq n+1 \end{cases} \\ W_{21}(k|n) &= \begin{cases} \sum_{m=1}^{n} h_{21}(m)\mathrm{W}_{11}(k|n-m), & k < n \\ 1, & k \geq n. \end{cases} \end{aligned} \tag{21}$$

VI. APPLICABILITY TO ENERGY STORAGE

Two case studies are presented to demonstrate applications of the reward processes and state occupancies. These make use of the distribution parameters listed in Table III.

VI.A. Battery–UC Coordination in a Hybrid ESU

Consider a distribution grid with a PV installation and a hybrid ESU having lead-acid batteries and UC as illustrated in Fig. 12. Other battery chemistries could have been considered. The main control objective is to provide constant power out of the combination PV installation/ESU into the grid source while maximizing the lifetime of the battery. The equivalent grid source is representing the aggregation of the distribution system loads and the infinite bus. The hybrid battery-UC ESU operates by filling in power dips from cloud shading.

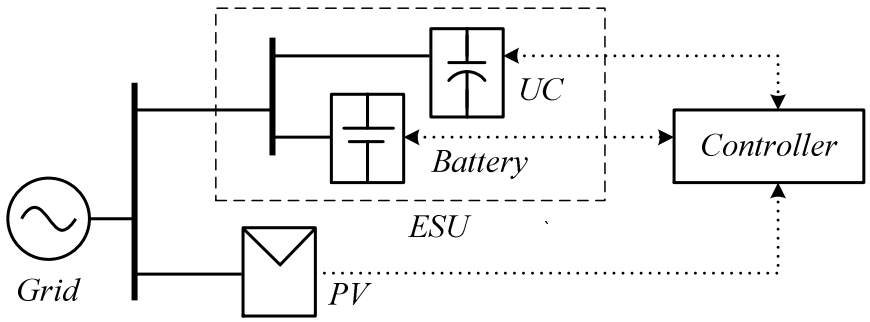

Fig. 12. One-line diagram of the hybrid battery UC ESU for smoothing PV.

The UC is used to extend the lifetime of the ESU's lead-acid battery by filling in small gaps up until a timeout n_d, after which the battery will fill in the power. This case only covers the selection of the timeout period, as the decision of when to charge batteries or start additional generation depends on other factors besides the PV generation. It is assumed that the lifetime of the lead-acid battery is fixed in terms of Wh throughput [36]. The lifetime of the lead-acid battery in terms of total Wh throughput is

$$E_f = \hat{E} D N_f(D). \tag{22}$$

The average power over the course of the day is

$$\bar{P}_v = \frac{2}{\pi} \hat{P}_v. \tag{23}$$

Therefore, when the ESU supplies power the change in energy per sample is

$$\Delta E = \frac{\bar{P}_v}{3600\ \text{s}}. \tag{24}$$

The reward (cost) is

$$y_i(l) = \begin{cases} \Delta E, & i = 2 \text{ and } l > n_d \\ 0, & otherwise. \end{cases} \tag{25}$$

The battery lifetime is therefore

$$Y = \frac{1}{24 \cdot 365} \cdot \frac{E_f}{\phi_1 v_1(n_d) + \phi_2 v_2(n_d)}. \tag{26}$$

The desired lifetime for the lead-acid battery is 2 years. Table V presents the parameters used in the analysis. Table VI presents the results from the parameter selection, showing how the UC allows the battery to meet the design lifetime, while Fig. 13 illustrates the tradeoff between battery lifetime and UC capacity.

VI.B. Scheduling in a Standalone Hybrid Microgrid

The CDF of the state occupancies is applied to a standalone microgrid consisting of a diesel generator, PV generator, battery-ESU and loads, shown in Fig. 14. The surplus PV power can be curtailed, but the load power cannot be controlled. Using a given clear-sky PV power profile in conjunction with the PV clouding model, stochastic dynamic programming [37] is applied to schedule the generator and battery at each hour over the course of one week with the parameters listed in Table VII. The random variable in this case is the PV energy produced during one period, which is linearly related to the number of *clear* state occupancies during that hour. The distribution of PV energy during one hour is therefore the same as *clear* state occupancy distribution over the 3600 samples in that hour.

Because the computational complexity of dynamic programming increases quadratically with the number of states, the number of possible energy levels of the battery is quantized. The levels are indexed by $x_e = 0, \dots, n_e - 1$. Similarly, the number of clear state occupancies is approximated with n_r unique values, and state occupancy index $x_r = 0, \dots, n_r - 1$. the number of occupancies is bx_r where b is a positive integer.

The total number of states is then $n_e n_r$, while the state index is

$$x = n_r x_e + x_r. \tag{27}$$

The actual values the battery energy can take are

TABLE V. PARAMETERS FOR THE HYBRID BATTERY-UC ESU

Component	Parameter	Var.	Value
PV	Rated power	$\hat{P}_v$	500 kW
Battery	Rated energy	$\hat{E}$	250 kWh
	Depth of discharge	D	0.5
	Number of cycles	$N_f(D)$	1000

TABLE VI. RESULTS FOR THE HYBRID BATTERY-UC ESU

Parameter	Var.	Value
Timeout period	n_d	300 s
Lifetime	Y	2.17 years

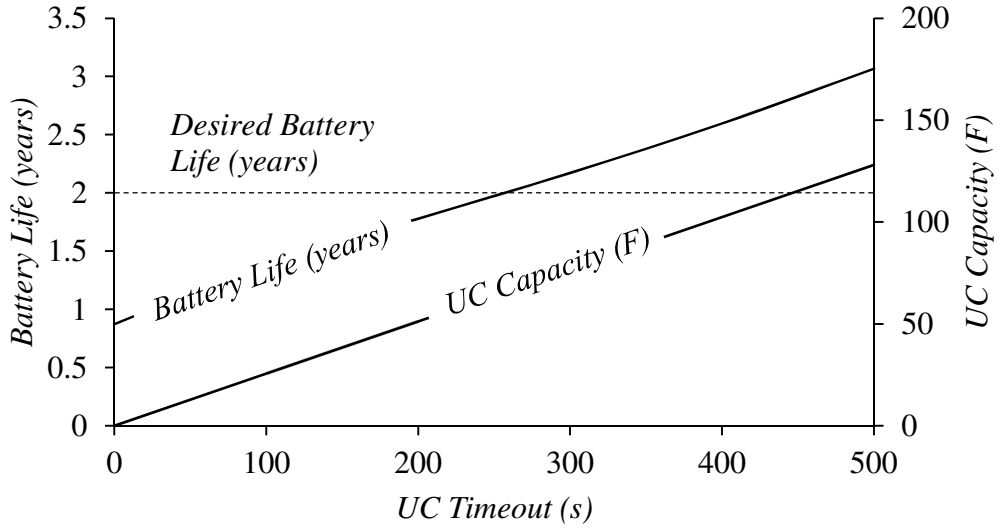

Fig. 13. Tradeoff between lead-acid battery life and required UC capacity.

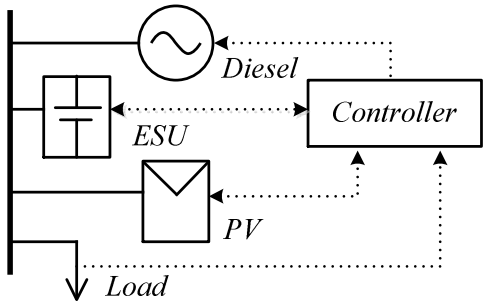

Fig. 14. One-line diagram of the standalone PV/diesel/battery-ESU microgrid.

TABLE VII. MICROGRID PARAMETERS

Component	Parameter	Var.	Value
PV	Rated power	P_{vmax}	10 kW
Load	Maximum power	P_{dmax}	10 kW
Generator	Rated power	P_{gmax}	15 kW
	Standby fuel use	f_{g0}	0.08 liters/kW rated
	Variable fuel use	f_{g1}	0.25 liters/kW
Battery	Rated power	P_{bmax}	10 kW
	Maximum energy	E_{max}	12 kWh
	Minimum energy	E_{min}	6 kWh
	Initial energy	E_0	8 kWh
	Efficiency	η	0.85
Scheduler	Number of samples	N	168
	Number of battery energy states	n_e	5
	Number of clear occupancy states	n_r	5

$$E(x) = \hat{E}\frac{\lfloor x/n_r \rfloor}{n_e - 1}, \tag{28}$$

where $\lfloor \cdot \rfloor$ denotes the floor operator. Similarly, the fraction of samples occupied by a particular state is

$$\rho(x) = \frac{x \bmod n_r}{n_r - 1}, \tag{29}$$

where mod is the modulus operator. The quantized state occupancy distributions over an interval of 3600 s (1 h) are

$$\begin{aligned} f_{11}(x_r) &= \begin{cases} \mathrm{W}_{11}(bx_r|n), & x = 1 \\ W_{11}(bx|n) - W_{11}(b(x-1)|n), & x > 1 \end{cases} \\ f_{21}(x_r) &= \begin{cases} \mathrm{W}_{21}(bx_r|n), & x = 1 \\ W_{21}(bx_r|n) - W_{21}(b(x_r-1)|n), & x > 1. \end{cases} \end{aligned} \tag{30}$$

The likelihood of each quantized state is

$$Pr(x) = \phi_1 f_{11}(x \bmod n_r) + \phi_2 f_{21}(x \bmod n_r). \tag{31}$$

The algorithm requires knowing the *average* battery power at each time step, given the battery energy at the current and next time step. The change in stored energy in the battery between any two states x_1 and x_2 is

$$\Delta E(x_1, x_2) = E(x_2) - E(x_1). \tag{32}$$

Given the round-trip efficiency for the battery η, the power flowing out of the battery is

$$P_b(x_1, x_2) = \begin{cases} -\Delta E(x_1, x_2), & \Delta E(x_1, x_2) \leq 0 \\ -\dfrac{\Delta E(x_1, x_2)}{\eta}, & \Delta E(x_1, x_2) > 0 \end{cases} \tag{33}$$

The battery energy and power are applied to calculate the cost of each possible decision at each time step. At a particular time step, given the actual load power p_d and average available PV output power p_v, the average diesel generator power p_g is

$$p_g = \max[p_d - p_v \rho(x_1) - P_b(x_1, x_2), 0]. \tag{34}$$

Implicit in (32) is the assumption that the PV output power can be curtailed to overcome a power surplus.

Depending on the net load, it may be more efficient to operate the generator and battery in either a load-following or cycle-charging strategy at each time step [38]. In a load-following strategy, the battery stored energy changes only monotonically, either storing surplus PV energy or releasing the stored PV energy to supply load. The generator serves to balance power. Cycle-charging exploits the property that a generator is most efficient when it operates at full power. In this strategy, the generator is at full power for the beginning fraction d of the time step ΔT to both charge the battery and supply load. During the remainder of the time step, the generator turns off and the load is supplied exclusively by the battery and PV. An example profile and the relevant quantities are illustrated in Fig. 15.

The particular generator and PV power setpoints p_g, p_{b1}, p_{b2} are determined via a rule-based controller. The rules are derived by exploiting knowledge that the fuel consumption is a monotonic function of the generator duty cycle d, and therefore the optimal setpoints occur when constraints such as generator power rating or power balance are exactly met.

At each time step, the fuel use of the generator when operating in load-following or cycle-charging mode is compared, and the more efficient strategy is selected.

The power setpoints for the load-following strategy follow.

The corresponding fuel use is f_a, which is a function of the generator's power setpoint and fuel use coefficients f_{g0}, f_{g1}

$$p_{b1} = p_{b2} = P_b(x_1, x_2) \tag{35}$$

$$p_g = \max[p_{net}, 0] \tag{36}$$

$$f_a = f_{g0} + f_{g1} p_{g1}. \tag{37}$$

The cycle-charging strategy is more complex. Let

$$p_{dv} = p_d - p_v \rho(x_1). \tag{38}$$

Which setpoints are selected depends on the case the particular scheduling point falls under. These follow:

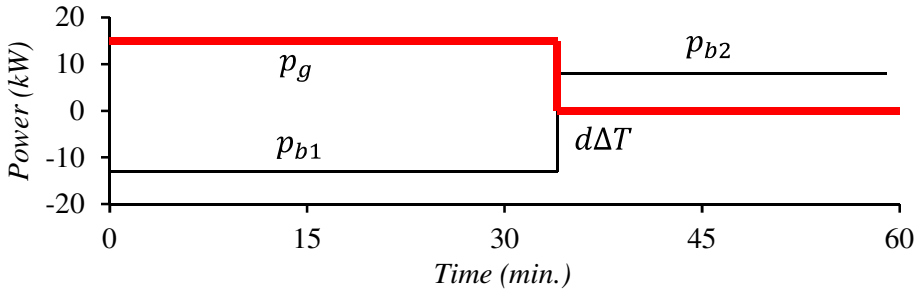

Fig. 15. Example of generator and battery powers for the cycle-charging case.

1) Positive load ($\boldsymbol{p_{dv} \geq 0}$)

The charging power p_c and discharge (supplied) power p_s for the battery are

$$p_c = P_{gmax} - p_{dv} \tag{39}$$

$$p_s = p_{dv} \tag{40}$$

while the duty cycle d is

$$d = \max\left[\frac{\Delta T p_s + \Delta E(x_1, x_2)}{\Delta T p_s + \eta \Delta T p_c}, 0\right]. \tag{41}$$

The setpoints are therefore

$$p_{b1} = -p_c,\ p_{b2} = p_d \tag{42}$$

$$p_g = P_{gmax}. \tag{43}$$

2) Negative load ($\boldsymbol{p_{dv} < 0}$ ***and*** $\boldsymbol{-\Delta T p_{dv} \leq \Delta E(x_1, x_2)}$)

Under both portions of the time step the battery is charging, while the generator only runs during the first portion

$$p_g = \min(P_{bmax}, P_{gmax} - p_{dv}) \tag{44}$$

$$d = \frac{\Delta E(x_1, x_2) + \eta \Delta T p_{dv}}{\eta \Delta T p_g} \tag{45}$$

$$p_{b1} = p_g - p_{dv}, p_{b2} = -p_{dv}. \tag{46}$$

3) Negative load ($\boldsymbol{p_{dv} < 0}$ ***but*** $\boldsymbol{-\Delta T p_{dv} > \Delta E(x_1, x_2)}$)

Under both portions of the time step the battery is charging. The generator is not run and the PV power is curtailed

$$p_g = \min(P_{bmax}, P_{gmax} - p_{dv}) \tag{47}$$

(48)

$$d = 0$$

$$p_{b1} = p_{b_2} = -\frac{\Delta E(x_1, x_2)}{\eta \Delta T}. \tag{49}$$

The fuel use for cycle-charging is

$$f_b = d(f_{g0} + f_{g1} p_g). \tag{50}$$

The ultimate cost of a decision is

$$R'(n, k_1, k_2) = \min(f_a, f_b). \tag{51}$$

Certain elements of the raw decision cost matrix R' are set to infinity to prohibit certain decisions from being taken. The following restricts the battery power to the range $[-P_{bmax}, +P_{bmax}]$, and the starting/ending battery stored energies to the initial energy E_0

$$R(n, x_1, x_2) = \begin{cases} \infty, & \begin{matrix} |P_b(x_1, x_2)| > P_{bmax} \\ n = 1 \; and \; E(x_1) \neq E_0 \\ n = N \; and \; E(x_2) \neq E_0 \end{matrix} \\ R'(n, x_1, x_2), & otherwise. \end{cases} \tag{52}$$

The last step of the scheduling algorithm is to apply value iteration to calculate the cumulative minimum cost $F(n, x)$ for each sample n and state x along the backwards path from the terminal states. The cumulative minimum costs at the final sample $N - 1$ are

$$F(N-1, x_1) = \min_{x_2} Pr(x_2) R(N, x_1, x_2). \tag{53}$$

The cumulative minimum costs at other sample are

$$F(n, x_1) = \min_{x_2} Pr(x_2) \begin{bmatrix} R(N, x_1, x_2) \\ +F(n+1, x_2) \end{bmatrix}. \tag{54}$$

The decision $D(n,x)$ matrix specifies the next state to progress to at each sample n, given the current state x. It is calculated as follows

$$D'(n,x_1) = \arg\min_{x_2} Pr(k_2)R(n,x_1,x_2) \tag{55}$$

$$D(n,x_1) = \begin{cases} D'(n,x_1) & D'(n,x_1) < \infty \\ 0 & otherwise. \end{cases} \tag{56}$$

The resulting states as a function of time $x(n)$ and stored energy as a function of time $E_n(n)$ can be extracted via

$$x(1) = \{x: E(x) = E_0\} \tag{57}$$

$$x(n) = D(n-1, x(n-1)). \tag{58}$$

$$E_n(1) = E_0 \tag{59}$$

$$E_n(n) = E\big(x(n)\big). \tag{60}$$

By applying (39)-(54) and averaging over $Pr(x)$, the battery and generator powers can be recovered.

To evaluate the performance of the performance of the method, it is compared against the baseline of a rule-based scheduler. The rule-based scheduler is roughly based on the scheduler employed in the HOMER software, with the main distinction being that the security constraints for generation dispatch were relaxed to make its results more comparable to those produced by dynamic programming.

The algorithm for the rule-based scheduler is illustrated in Fig. 16. The rule-based scheduler operates in a hysteresis fashion. If there is a surplus of energy from the PV, it will charge the ESU while shutting down the diesel generator. If the PV cannot supply the load power, but the

ESU has sufficient energy to do so, the scheduler will discharge the ESU while still shutting down the diesel generator. If PV cannot supply the load nor does the ESU have sufficient energy to do so, the diesel generator is run to both supply load and charge the ESU.

Unlike the dynamic programming scheduler, the rule-based scheduler will not calculate the expected fuel usage. To overcome this, a set of simulations were run to estimate the expected fuel usage. The number of simulations n_{sim} was set to 10,000 in order to achieve an estimate $\bar{f_a}$ within an interval W of 0.25 liters for 99% confidence. The interval is calculated as follows given that the fuel usage for each simulation is f_{ak} and the variance estimate is $\hat{\sigma}$.

$$\bar{f_a} = \frac{1}{n_{sim}} \sum_{k=1}^{n_{sim}} f_{ak} \tag{61}$$

$$\hat{\sigma} = \frac{1}{n_{sim} - 1} \left[\sum_{k=1}^{n_{sim}} \left(f_{ak} - \bar{f_a} \right)^2 \right]^{\frac{1}{2}} \tag{62}$$

$$W = \left(\bar{f_a} + \frac{t_{\alpha/2} \hat{\sigma}}{\sqrt{n_{sim}}} \right) - \left(\bar{f_a} + \frac{t_{\alpha/2} \hat{\sigma}}{\sqrt{n_{sim}}} \right) = \frac{2 t_{\alpha/2} \hat{\sigma}}{\sqrt{n_{sim}}}. \tag{63}$$

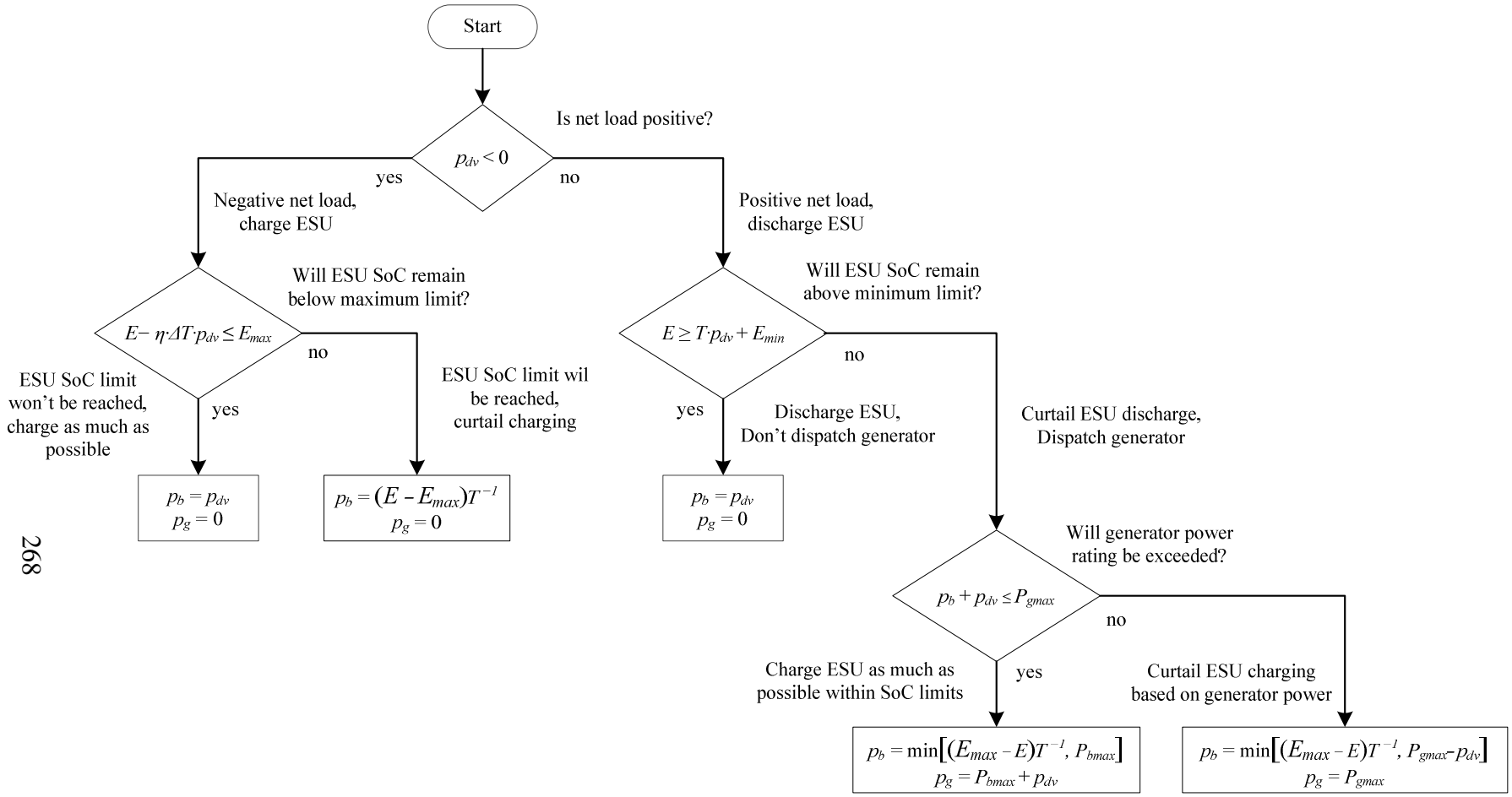

Fig. 16. Flowchart for the rule-based scheduler.

Given the method described and the component parameters listed in Table VII, the schedule is calculated. Examples of random schedules for the dynamic programming and rule-based schedulers are listed in Fig. 17 and Fig. 18. The expectation of the total fuel consumption of the microgrid over the time period studied is 147.4 liters with dynamic programming, while the estimated expected fuel consumption with rule-based scheduling is 156.3 liters.

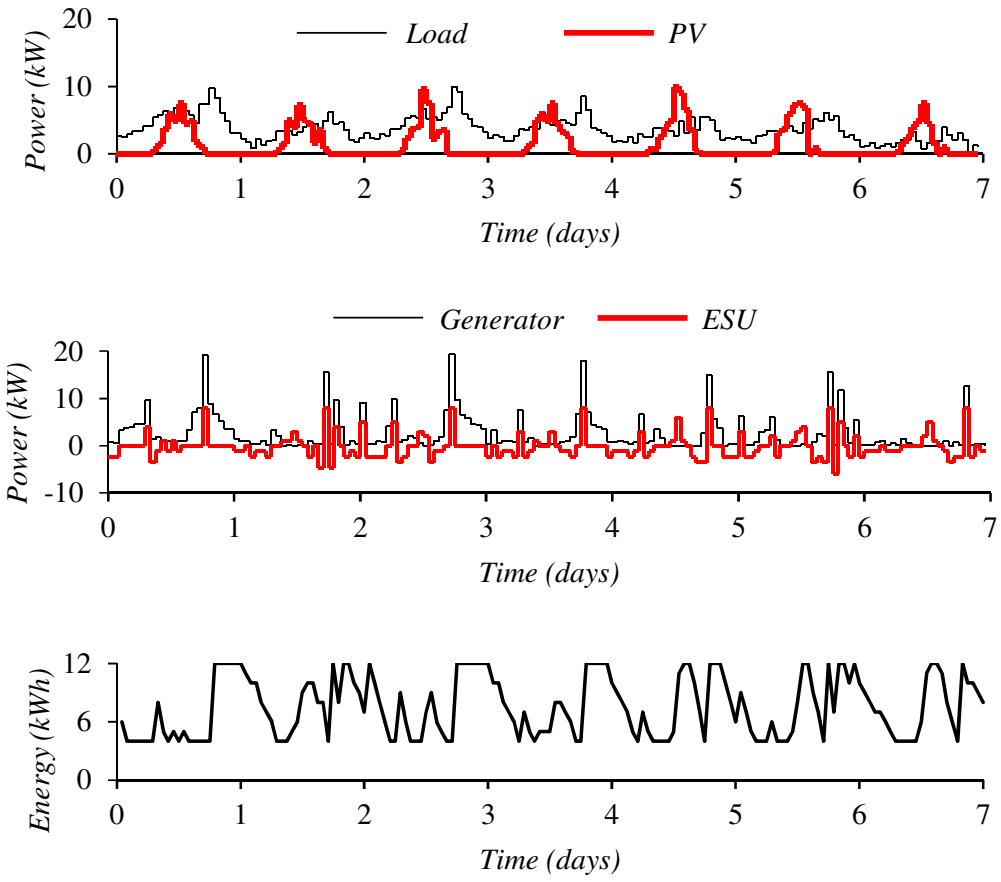

Fig. 17. Scheduled powers and energy for the hybrid standalone microgrid under a random scenario with the stochastic dynamic programming scheduler.

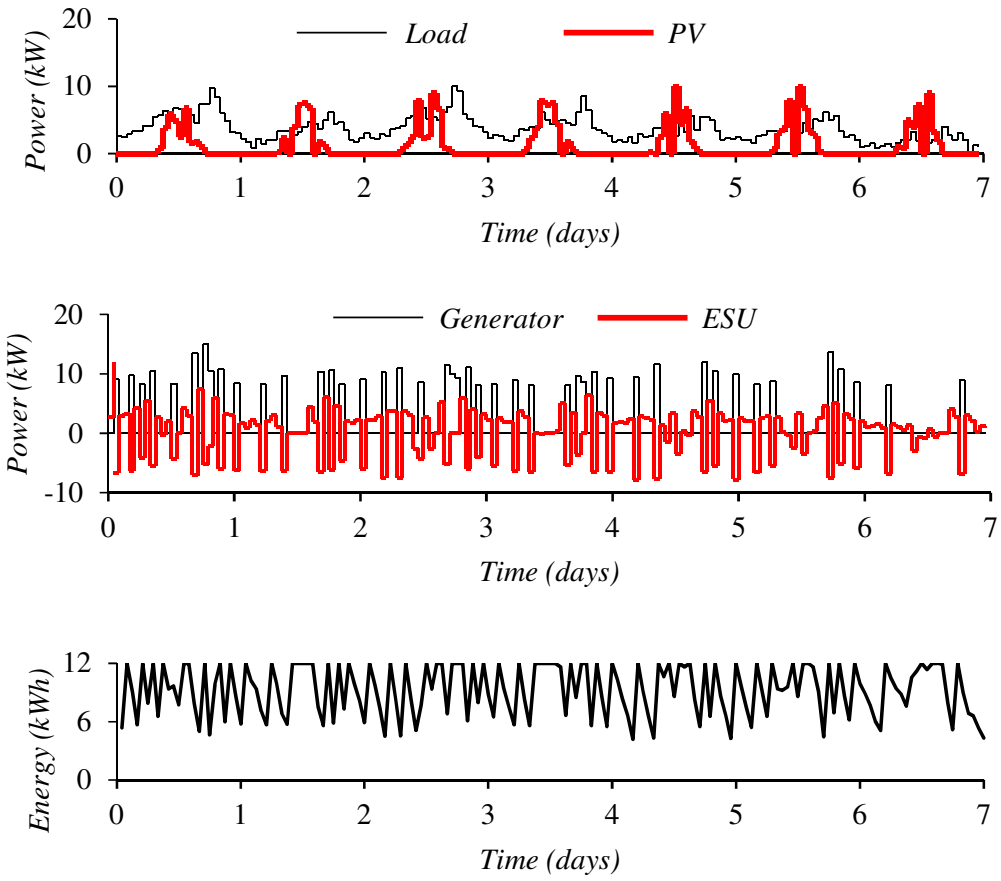

Fig. 18. Scheduled powers and energy for the hybrid standalone microgrid under a random scenario with the rule-based scheduler.

VII. CONCLUSIONS AND FUTURE WORK

A SMDTRP model to fit observed clouding data was proposed in this paper. Previously proposed models based on frequency-domain analysis are only suitable for qualitative study, while the proposed model yields results with physical significance.

Moreover, the same model can be applied to solve a wide variety of problems, including: generating simulated PV data, short-term forecasting of PV power in the absence of sky imaging data, day-ahead forecasting of PV energy, parameter selection for rule-based controllers operating over short time scales, and day-ahead stochastic scheduling for PV hybrid systems. Future work will explore generalizing the model to multiple spatially dispersed PV installations,

multiple weather conditions (e.g. clear, partially cloudy, overcast) or seasons, and the effect of spatial smoothing present on a single large PV installation that covers a large contiguous area.

VIII. ACKNOWLEDGMENT

The authors gratefully acknowledge the contributions of J. K. Hayes for his work in performing the data collection and A. Escobar Mejía for his assistance with editorial issues.

REFERENCES

[1] C. A. Hill, M. C. Such, D. Chen, J. Gonzalez, and W. M. Grady, "Battery energy storage for enabling integration of distributed solar power generation," *IEEE Trans. Smart Grid*, vol. 3, no. 2, pp. 850–857, Jun. 2012.

[2] A. Hoke, R. Butler, J. Hambrick, and B. Kroposki, "Steady-state analysis of maximum photovoltaic penetration levels on typical distribution feeders," *IEEE Trans. Sustain. Energy*, vol. 4, no. 2, pp. 350–357, Apr. 2013.

[3] J. von Appen, T. Stetz, M. Braun, and A. Schmiegel, "Local voltage control strategies for pv storage systems in distribution grids," *IEEE Trans. Smart Grid*, vol. 5, no. 2, pp. 1002–1009, Mar. 2014.

[4] P. Wang, D. H. Liang, J. Yi, P. F. Lyons, P. J. Davison, and P. C. Taylor, "Integrating electrical energy storage into coordinated voltage control schemes for distribution networks," *IEEE Trans. Smart Grid*, vol. 5, no. 2, pp. 1018–1032, Mar. 2014.

[5] M. M. . Abdelaziz, H. E. Farag, and E. F. El-Saadany, "Optimum droop parameter settings of islanded microgrids with renewable energy resources," *IEEE Trans. Sustain. Energy*, vol. 5, no. 2, pp. 434–445, Apr. 2014.

[6] Y. Zhang, N. Gatsis, and G. B. Giannakis, "Robust energy management for microgrids with high-penetration renewables," *IEEE Trans. Sustain. Energy*, vol. 4, no. 4, pp. 944–953, Oct. 2013.

[7] R.-H. Liang and J.-H. Liao, "A fuzzy-optimization approach for generation scheduling with wind and solar energy systems," *IEEE Trans. Power Syst.*, vol. 22, no. 4, pp. 1665–1674, Nov. 2007.

[8] W. A. Omran, M. Kazerani, and M. M. A. Salama, "Investigation of methods for reduction of power fluctuations generated from large grid-connected photovoltaic systems," *IEEE Trans. Energy Convers.*, vol. 26, no. 1, pp. 318–327, Mar. 2011.

[9] S. X. Chen, H. B. Gooi, and M. Q. Wang, "Sizing of energy storage for microgrids," in *Proc. IEEE Trans. Smart Grid*, vol. 3, no. 1, pp. 142–151, Mar. 2012.

[10] J. Song, V. Krishnamurthy, A. Kwasinski, and R. Sharma, "Development of a Markov-chain-based energy storage model for power supply availability of photovoltaic generation plants," *IEEE Trans. Sustain. Energy*, vol. PP, no. 99, pp. 1 –10, 2012.

[11] W. T. Vetterling, Numerical Recipes Example Book (C). Cambridge University Press, 1992.

[12] F. J. Taylor and J. Mellott, Hands-On Digital Signal Processing. McGraw-Hill Professional Publishing, 1998.

[13] X. Liu, A. Aichhorn, L. Liu, and H. Li, "Coordinated control of distributed energy storage system with tap changer transformers for voltage rise mitigation under high photovoltaic penetration," *IEEE Trans. Smart Grid*, vol. 3, no. 2, pp. 897–906, Jun. 2012.

[14] M. Korpas and A. T. Holen, "Operation planning of hydrogen storage connected to wind power operating in a power market," *IEEE Trans. Energy Convers.*, vol. 21, no. 3, pp. 742–749, 2006.

[15] E. Lorenz, J. Hurka, D. Heinemann, and H. G. Beyer, "Irradiance forecasting for the power prediction of grid-connected photovoltaic systems," *IEEE J. Sel. Top. Appl. Earth Obs.*, vol. 2, no. 1, pp. 2 –10, Mar. 2009.

[16] A. Anvari Moghaddam and A. R. Seifi, "Study of forecasting renewable energies in smart grids using linear predictive filters and neural networks," *IET Renew. Power Gener.*, vol. 5, no. 6, pp. 470 –480, Nov. 2011.

[17] J. Bing, O. Bartholomy, and P. Krishnani, "Validation of solar PV power forecasting methods for high penetration grid integration," in *Proc. IEEE PES GM*, 2012, pp. 1–6.

[18] K. Stefferud, J. Kleissl, and J. Schoene, "Solar forecasting and variability analyses using sky camera cloud detection & motion vectors," in *Proc. IEEE PES GM*, 2012, pp. 1– 6.

[19] V. P. A. Lonij, V. T. Jayadevan, A. E. Brooks, J. J. Rodriguez, K. Koch, M. Leuthold, and A. D. Cronin, "Forecasts of PV power output using power measurements of 80 residential PV installs," in *Proc. IEEE Photovoltaic Specialists Conference (PVSC)*, 2012, pp. 003300 –003305.

[20] E. Rikos, S. Tselepis, C. Hoyer-Klick, and M. Schroedter-Homscheidt, “Stability and power quality issues in microgrids under weather disturbances,” *IEEE J. Sel. Top. Appl. Earth Obs.*, vol. 1, no. 3, pp. 170–179, Sep. 2008.

[21] A. Barnes, J. Carlos, and J. Hayes, “Modeling pv clouding effects using a semi-Markov process with application to energy storage,” in Proc. *International Federation of Automatic Control World Congress*, Cape Town, South Africa, 2014, to be published.

[22] R. M. Schupbach, J. C. Balda, M. Zolot, and B. Kramer, “Design methodology of a combined battery-ultracapacitor energy storage unit for vehicle power management,” in *Proc. IEEE PESC*, 2003, vol. 1, pp. 88–93 vol.1.

[23] Q. Xie, Y. Kim, Y. Wang, J. Kim, N. Chang, and M. Pedram, “Principles and efficient implementation of charge replacement in hybrid electrical energy storage systems,” *IEEE Trans. Power Electron.*, vol. 29, no. 11, pp. 6110–6123, Nov. 2014.

[24] L. Guo, W. Liu, B. Jiao, B. Hong, and C. Wang, “Multi-objective stochastic optimal planning method for stand-alone microgrid system,” *IET Gener. Transm. Distrib.*, vol. 8, no. 7, pp. 1263–1273, Jul. 2014.

[25] P. Mokrian, “Modeling and assessment of electricity market initiatives,” Ph.D. Dissertation, Department of Management Science and Engineering, Stanford University, Palo Alto, CA, 2009.

[26] Apogee Instruments, “Pyranometer SP-212 & 215,” 2011. [Online]. Available: http://www.apogeeinstruments.com/manuals/SP-212_215manual.pdf. [Accessed: 21-Jul-2011].

[27] SSEES Research Group: PV Data. [Online]. Available: http://energy.uark.edu/pv/.

[28] R. O. Duda, P. E. Hart, and D. G. Stork, Pattern classification. Wiley, 2001.

[29] S. Seme, G. Štumberger, and J. Voršič, “Maximum efficiency trajectories of a two-axis sun tracking system determined considering tracking system consumption,” *IEEE Trans. Power Electron.*, vol. 26, no. 4, pp. 1280–1290, Apr. 2011.

[30] R. Neggers, H. Jonker, and A. Siebesma, “Size statistics of cumulus cloud populations in large-eddy simulations,” *J. Atmospheric Sci.*, vol. 60, no. 8, pp. 1060–1074, 2003.

[31] G. Casella and R. L. Berger, Statistical Inference, 2nd edition. Australia ; Pacific Grove, CA: Cengage Learning, 2001.

[32] R. A. Howard, Dynamic Probabilistic Systems: Markov Models. Mineola, NY: Dover Publications, Incorporated, 2007.

[33] W. Feller, An Introduction to Probability: Theory and its Applications, 3rd ed. Wiley India Pvt. Limited, 2008.

[34] A. Papoulis and S. U. Pillai, Probability, Random Variables, and Stochastic Processes. Tata McGraw-Hill, 2002.

[35] S. N. Sharma, "A Kushner approach for small random perturbations of the Duffing-Van der Pol system," *Automatica*, vol. 45, no. 4, pp. 1097–1099, Apr. 2009.

[36] A. Barnes, J. C. Balda, A. Escobar, and S. O. Geurin, "Optimal battery chemistry, capacity selection, charge/discharge schedule, and lifetime of energy storage under time-of-use pricing," in *Proc. IEEE PES ISGT Europe*, Manchester, England, 2011.

[37] L. Zhang and Y. Li, "Optimal energy management of wind-battery hybrid power system with two-scale dynamic programming," *IEEE Trans. Sustain. Energy*, vol. 4, no. 3, pp. 765–773, Jul. 2013.

[38] A. Srivastava, A. Kumar, and N. N. Schulz, "Impact of distributed generations with energy storage devices on the electric grid," *IEEE Syst. J.*, vol. 6, no. 1, pp. 110–117, Mar. 2012.

APPENDIX A: CERTIFICATION OF FIRST AUTHOR

I hereby certify that Arthur K. Barnes is first author of the article this chapter is based on and has completed at least 51% of the work described in the article.

Juan Carlos Balda

Signature _____

Date _____

APPENDIX B: RELEASE FOR USE IN DISSERTATION

Thesis / Dissertation Reuse

The IEEE does not require individuals working on a thesis to obtain a formal reuse license, however, you may print out this statement to be used as a permission grant:

Requirements to be followed when using any portion (e.g., figure, graph, table, or textual material) of an IEEE copyrighted paper in a thesis:

1) In the case of textual material (e.g., using short quotes or referring to the work within these papers) users must give full credit to the original source (author, paper, publication) followed by the IEEE copyright line © 2011 IEEE.

2) In the case of illustrations or tabular material, we require that the copyright line © [Year of original publication] IEEE appear prominently with each reprinted figure and/or table.

3) If a substantial portion of the original paper is to be used, and if you are not the senior author, also obtain the senior author's approval.

Requirements to be followed when using an entire IEEE copyrighted paper in a thesis:

1) The following IEEE copyright/ credit notice should be placed prominently in the references: © [year of original publication] IEEE. Reprinted, with permission, from [author names, paper title, IEEE publication title, and month/year of publication]

2) Only the accepted version of an IEEE copyrighted paper can be used when posting the paper or your thesis on-line.

3) In placing the thesis on the author's university website, please display the following message in a prominent place on the website: In reference to IEEE copyrighted material which is used with permission in this thesis, the IEEE does not endorse any of [university/educational entity's

name goes here]'s products or services. Internal or personal use of this material is permitted. If interested in reprinting/republishing IEEE copyrighted material for advertising or promotional purposes or for creating new collective works for resale or redistribution, please go to http://www.ieee.org/publications_standards/publications/rights/rights_link.html to learn how to obtain a License from RightsLink.

If applicable, University Microfilms and/or ProQuest Library, or the Archives of Canada may supply single copies of the dissertation.

CHAPTER TEN

CONCLUSIONS AND RECOMMENDATIONS FOR FUTURE WORK

I. INTRODUCTION

This chapter wraps up the study of integration of energy storage units (ESU) in future energy systems. First, a summary of the conclusions drawn throughout this dissertation is presented. Second, suggestions for future work based on either the methodologies or problem formulations used in this work are listed. Last, final remarks are given on the development of tools for integration of distributed ESU.

II. CONCLUSIONS

Conclusions are presented in terms of area of work.

II.A. Storage Capacity Selection and Scheduling of ESU

An 11-year design lifetime provided the highest net present value (NPV) for an ESU performing energy arbitrage under a time-of-use (TOU) pricing structure, as illustrated in Chapter 2, Fig. 10 [1]. The analysis of Chapter 2 showed that the optimal lifetime occurs because it is necessary to oversize the battery (in terms of storage capacity) in order to meet battery lifetime requirements. The increased initial cost due to oversizing reduced the NPV of the ESU, making it less profitable. The 11-year lifetime resulted in only a small amount of oversizing required.

The same analysis also showed that the battery technology yielding the highest NPV was not necessarily the cheapest in terms of cost per unit of energy capacity. The methodology selected the lithium-ion (Li-ion) battery technology, which is costly in terms of energy capacity. However, the NPV of the ESU was not as sensitive to cost per unit of energy capacity as it was

to round-trip efficiency and cost per total lifetime energy output. As Li-ion is competitive in terms of these metrics, it was recommended for this application.

The energy capacity required for an ESU providing ancillary services is far less than an ESU providing arbitrage. An ESU need supply only 1 hour of output at rated power when providing ancillary services. In contrast, it would need to supply 6 to 8 hours of output at rated power when providing arbitrage [2], [3]. This makes ancillary services a much more appealing use for ESU. Additionally, allowing for an ESU to participate in both regulation and spinning reserve markets (without significant penalties for the ESU running out of power when called upon to provide either regulation or reserve services) increases its value significantly. In Chapter 3 it was demonstrated how lifetime constraints for a Li-ion battery can be taken into account when providing ancillary services by linearizing its lifetime curve at two different points, one for discharge periods of an hour or more, and another for short discharges less than one hour [4].

Chapter 3 also introduced the use of ridge regression for price prediction of ancillary services. It demonstrated that this form of regression can overcome issues related to the price predictor variables being highly correlated. Additionally, it was shown as follows that profitability of an ESU was relatively insensitive to forecaster accuracy. First, it was only necessary to predict the change in price within a period of about one day accurately. Price prediction errors that are roughly constant over the course of a week do not impact the scheduling of the ESU. Second, the ESU was applied mostly to provide spinning reserve and regulation services throughout most of the day, charging during nighttime periods of low price. The ESU was rarely called upon to provide power in the energy market. The periods of low price during which the ESU charges had low variability, and were therefore easily predicted.

II.B. Placement and Power Rating of ESU

The ESU placement problem is computationally difficult because it has a nonconvex, mixed-integer formulation. However, it was still possible to produce desirable suboptimal solutions with low computation time (but whose solution cost was not significantly higher than the global optimum). Both a randomized and a heuristic methodology were investigated for ESU placement.

In Chapter 4, the results of the randomized methodology (simulated annealing) illustrated that for a small system it was possible to produce a desirable solution in reasonable time by using certain heuristics [5]. These heuristics sped up the search process by favoring certain buses for ESU placement that were more likely to be desirable based on a priori knowledge of the problem. The methodology demonstrated that for applications where ESU assisted CVR, locations near the end of the feeder were favored for placement, rather than near load centers. The results of the methodology showed that "smart" PV inverters with appropriate control could assist ESU in maintaining a desired voltage profile and reducing losses, rather than increasing voltage variation on a distribution system. Last, the methodology verified that employing ESU to assist with voltage regulation during CVR would not interfere with optimal economic scheduling of ESU used for energy arbitrage.

The heuristic methodology of Chapter 4 exploited the property that candidate buses for ESU placement tend to be in well-separated groups. An alternative representation of the problem (obtained by applying multidimensional scaling (MDS)) was used in Chapter 5. In the alternative problem representation, the methodology combined candidate buses (via k-means clustering) for ESU placement that were close to each other (in terms of impedance between the two buses) [6]. The motivation behind this heuristic was related to the observation that there was a fixed component in the cost of placing each ESU. Furthermore, if one large ESU was placed instead of

multiple small units, the decrease in benefit for loss reduction or voltage regulation was low. Therefore, it was economically favorable to aggregate candidate buses for ESU placement into a small number of large ESU. This heuristic methodology was shown to reduce computation time by an order of magnitude when compared with genetic algorithms, a popular type of optimizer for this class of problem. Moreover, the methodology was also shown to be easy to implement, requiring only a set of matrix multiplications, eigenvector decomposition, and k-means clustering, all of which are common numerical methods.

The methodology of Chapter 5 was applied to demonstrate the feasibility of distributed ESU by verifying that the ESU were able to assist with CVR and peak loss reduction on the feeder. Furthermore, it confirmed the ability of the ESU to charge and discharge under worst-case conditions without violating steady-state voltage constraints on the feeder. However, the methodology also showed that the ESU exceeded tolerable limits for flicker when providing frequency regulation on the grid. This observation suggested that the substation might be the most appropriate location to place ESU used primarily for frequency regulation. However, this choice would not allow them to be used for CVR and loss reduction.

A follow-up study described in Chapter 6 investigated properties of the MDS and clustering [7], demonstrating that MDS provided the ability to completely represent a positive-sequence model of a distribution system without data loss. Additionally, the reduction in ESU benefits resulting from clustering were quantified to first-order. The scalability of the MDS/clustering was demonstrated by applying it to a large (1699 customer) feeder, selecting candidate buses via a classifier [8]. The MDS/clustering methodology was applied to investigate additional properties related to distributed power electronics, in this case, studying the use of an oversized power electronic interface (PEI) for the ESU to inject reactive power. The results demonstrated

that for practical CVR factors and inverter losses, the ESU could indeed reduce feeder power consumption via reactive power injection. However, the amount of savings was sensitive to both the amount of inverter losses and the CVR factor. The savings would become negative as loads approached constant-power or as the inverter losses increased beyond a certain threshold.

II.C. PEI Topology Selection

Chapter 7 addressed the PEI topology selection problem. It demonstrated that if the dc-bus voltage of a battery was fairly constant, better efficiency was obtained by using a single-stage topology. This is illustrated in Chapter 7, Fig. 6. For the case of a battery-ESU, the input (battery) voltage did not vary by a large amount. For a Li-ion battery this would be about ±15% from nominal voltage [9]. Based on this limited input voltage range, the single-stage topology was recommended. However, the performance penalty incurred by the addition of a dc-dc converter (in the double-stage topology) was small. Additionally, the double-stage topology was more efficient for ultracapacitor-based ESU, as illustrated in Chapter 7, Fig. 5. Moreover, for ESU integrated with distributed generation, hybrid ESU with multiple storage technologies, or battery-ESU with multiple battery strings, the total parts count was reduced with a double stage topology (as opposed to multiple single-stage converters for each power source, storage technology, or battery string). In these aforementioned applications, the double-stage PEI could be the preferred topology.

II.D. Modeling of Cloud-Induced PV Intermittency

Chapter 8 demonstrated that the SMDTRP model was an effective alternative to statistical, frequency-domain, and wavelet-based approaches for characterizing and modeling cloud-induced PV intermittency [10]. It was shown that the methodology could be applied to produce results whose values were in terms of physical units, a notable advantage over frequency-domain

methodologies, whose utility mainly lied in qualitative analysis. It was further demonstrated that the methodology allowed for a single model to be applied to a wide class of problems across a wide range of time scales. These problem classes included: short term simulation of cloud-induced PV intermittency, short-term forecasting of PV intermittency, optimal probabilistic ESU controller design, and probabilistic microgrid scheduling. The methodology demonstrated how to control an ESU to reduce cycling of a tap-changer, allowing it to reach a 20-year lifetime. Additionally, it demonstrated how to control the UC in a hybrid battery-UC ESU, allowing a lead-acid battery to reach a 2-year design lifetime. Last, scheduling for a microgrid was demonstrated and applied to calculate the expectation of the microgrid fuel usage [11].

III. RECOMMENDATIONS FOR FUTURE WORK

This section presents possible follow-up work related to the research presented in this dissertation.

III.A. Storage Capacity Selection and Scheduling of ESU

The first suggestion for future work is the consideration of providing emergency power in the time-of-use (TOU) sizing problem. Given that the ESU will be placed at a customer site, a possible primary use for it is provision of uninterruptible power supply (UPS) capability. In conjunction with this capability, supplying power during periods of very high load is also important. This could either be accomplished through critical peak pricing or direct dispatch via the electric utility. However, calling upon the ESU to provide critical peak loads must not interfere with its ability to provide UPS functionality.

Several improvements are possible when using ESU with real-time pricing. The first is to improve the accuracy of forecasting ancillary service prices. Several solutions are available that could assist this. The first is to obtain a more detailed model of how the ancillary service market

structure works and use this to design a more parsimonious forecaster. The second is to include energy price as a forecaster input. From the plots of the prices, it is apparent that there is a nonlinear relationship between the price of energy and the price of ancillary services [4]. When the price of energy is high, the price of ancillary services is also high. However, when the price of energy is very low, the price of ancillary services will still rise. This is because during these periods the demand and price for energy will incentivize peaking and load-following plants to go offline. The increasing price of ancillary services during this period incentivizes such plants to remain online in order to meet grid stability margins [12]. Because this is a nonlinear relationship, either a transformation of the predictor variables or a nonlinear predictor is required.

Another area of work relates to the observation that distributed ESU would likely be owned by electric utilities. Given that major benefits of distributed ESU include providing continuously variable active and reactive powers for either frequency regulation or volt-VAR optimization (VVO), it is desirable that ESU be operated by electric utilities. It is suggested that the ESU provide system services, and hence are paid for by all customers in a system[13]. Thus, these utilities would charge customers for UPS services provided by the ESU, while primarily using the ESU for frequency regulation or VVO. This observation also suggests that the value of ESU be evaluated by considering them in the context of a generation scheduling problem, such as those carried out by power pools when evaluating bids for generation or consumption of electric energy. It is also important to consider the increasing trend in electrical energy management to deal with the problem in a stochastic formulation, thereby allowing for uncertainty to be taken into account. This formulation is possible for either the pricing-based or generation scheduling-based problem formulations, and offers the promise of a higher-quality solution.

III.B. Placement and Power Rating of ESU

The application of convex optimization methods to power system analysis is a fertile area for research related to the placement of ESU [14], [15]. Currently, the state-of-the art in distribution system analysis applies convex optimization to systems whose size is on the low hundreds of buses. There has recently been work to demonstrate that the scalability of the problem can be improved by decomposing it into a set of parallel subproblems, allowing the use of distributed grid computing [16].

Another relevant issue is that of unbalanced distribution system analysis. Current research has only shown that the convex relaxation is tight for a positive sequence representation of a balanced distribution system [14], [17]. Further work is necessary to show that such relaxations will be tight for an unbalanced system, or to develop a set of reasonable approximations or conditions necessary to do so. A last area of research is to apply more sophisticated methodologies than clustering for determining the ESU locations. The method applied, k-means clustering, lacks mathematical rigor, and it is difficult to make generalized statements about the quality of the solution it produces [18]. Future work could explore other clustering methods, or alternatives to clustering.

III.C. PEI Topology Selection for ESU

Follow-up work in power electronic interface (PEI) topology selection could take into account additional real-world constraints. One such constraint is that medium-frequency ac transformers are only commonly available with certain turns ratios. Other turns ratios will require custom-built transformers at additional costs and lead times. Future analysis could verify whether these constraints will cause practical battery-ESU implementations to favor a two-stage topology over a single-stage one. Other future studies could address experimental validation of

the results. This would require the construction of a pair of three-phase inverters, one for the inverter front-end, and one to act as the three-phase interleaved boost converter. In order to operate at a range of power factors it would be necessary for the inverter to operate grid-paralleled. A controllable, bidirectional dc power supply could be used in order to vary the input dc voltage.

III.D. Modeling Of Cloud-Induced PV Intermittency

Several follow-up topics could be explored in the modeling of cloud-induced photovoltaic (PV) intermittency. A first topic is the inclusion of a more detailed clear-sky irradiance model, which may improve classification accuracy, particularly near sunrise and sunset. Such a model requires estimating parameters of transcendental functions. Moreover, it may require additional measurements such as:

1. the global horizontal irradiance (GHI), measured with a horizontally oriented pyranometer of solar reference cell,
2. the diffuse horizontal irradiance (DNI), measured with a pyrheliometer on a sun tracker, and
3. the diffuse horizontal irradiance (DHI), measured with a pyranometer and shadow ball/ring on a sun tracker [19], [20].

A second topic to address is the effects of spatial smoothing on cloud-induced intermittency. The analyses in this dissertation focused on point irradiance measurements and power measurements from a small (15 kW) PV array. Larger arrays will have more spatial smoothing; the analyses presented will therefore establish an upper bound on the amount of intermittency. Other studies have investigated how spatial smoothing affects intermittency in terms of statistics that measure intermittency across a range of time scales [21], [22]. It is desirable to establish a

relationship between array size and variation in parameters of the generalized Pareto distribution used for modeling intermittency.

Another possibility to address spatial smoothing is to increase the number of states in the semi-Markov discrete-time random process (SMDTRP) model to account for multiple PV installations. This new model would represent the correlation between shading events at different installations via the hold times. However, this could pose a problem for parameter inference, as the number of states increases exponentially with the number of PV installations.

A third possibility for future work is to include support for multiple weather conditions, for example, inferring separate model parameters for clear, partly cloudy, and overcast days. Existing work has followed this approach for other models of PV power [23], [24]. This approach will require additional data collection in order to ensure (i) that there is sufficient data to estimate the probabilities of each class of weather condition, and (ii) that there are enough days recorded of each weather condition to accurately estimate the hold time parameters.

A last possibility is physical implementation of some of the case studies for the SMDTRP model. Fig. 1 and Fig. 2 illustrate a proposed rule-based controller for an ESU smoothing PV power based on the hierarchical control structure described in [25]. In Fig. 1, $u(\cdot)$ denotes the unit step function, t is the current time, and d is the maximum shading duration over which the ESU will supply power. In Fig. 2, C_{elec} is the cost of electricity. The terms V_{bat} and I_{bat} are the measured battery voltage and current, respectively. The term P_{pv} is the measured PV power and P^* is the ESU real power reference. *Select* is a $\{0,1\}$ digital signal that selects the desired input of an analog multiplexer (mux). The terms I_d^* and I_q^* are the ESU PEI direct and quadrature reference currents, respectively. The terms V_d^* and V_q^* are the ESU direct and quadrature voltages, respectively.

Fig. 3 illustrates a proposed implementation of a microgrid control architecture for scheduling PV with other energy resources. The proposed architecture uses an industrial or rackmount PC with an Intel Core i5 or Core i7 processor, and running either Windows Server or Linux. The microgrid scheduler is implemented in a compiled language such as C, C++ or C#, and acts as a server to which client programs (representing devices on the microgrid) will communicate with over TCP/IP on a wired Ethernet network. The client programs will run on embedded ARM-based Linux single-board computers (SBC). Examples of commercially available units are the BeagleBone and Raspberry Pi. Higher-level control functionality is implemented on the SBC. The SBC in turn communicate with lower-level control, implemented on a digital signal processor (DSP) or microcontroller such as the TI TMS320F28335 Delfino. This communication takes place over a logic-level serial communications interface (SCI).

Other communications architectures are available that avoid the need for the Linux SBC and would therefore reduce cost. An example of another architecture implements the scheduler in LabVIEW. The scheduler would communicate with microgrid resources via dedicated analog and digital lines on a data acquisition card. An intermediate architecture option could omit the SBC and have the central controller communicate directly with the DSP via a controller area network (CAN) bus. However, these approaches lose flexibility on both the software and hardware sides. For example, in the latter case, the scheduling software needs to interact with other resources over a low-level CAN interface as opposed to a high-level TCP/IP interface. Additionally, the microgrid resources will no longer have the ability to perform local control or data logging via the SBC.

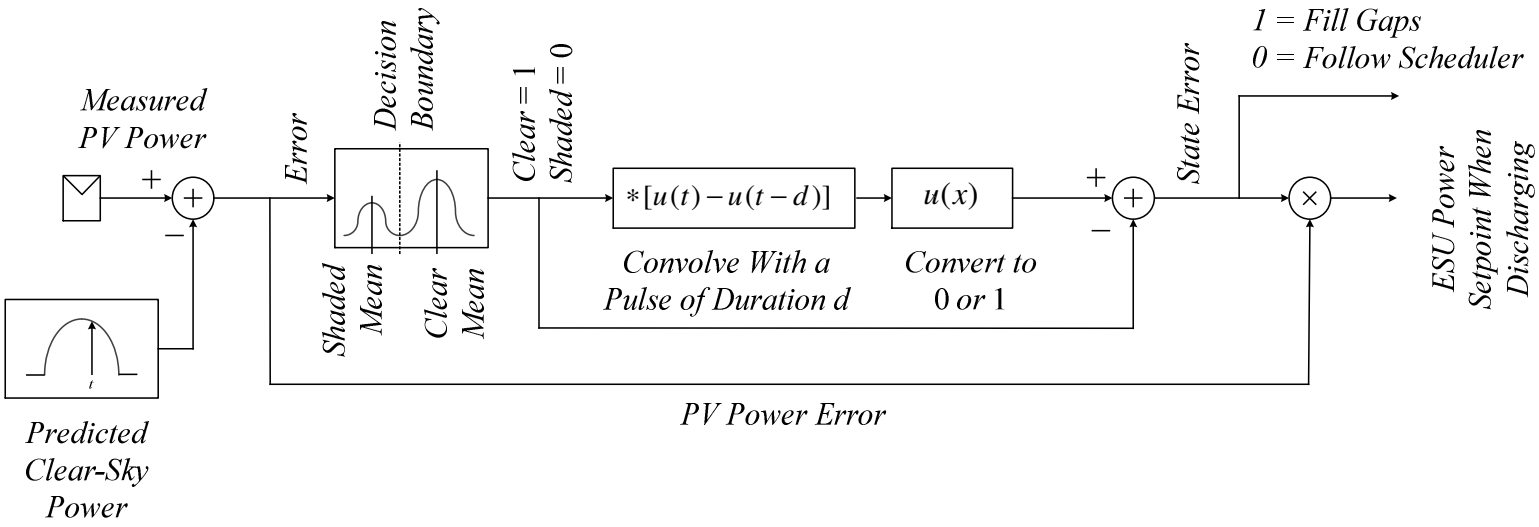

Fig. 1. Proposed rule-based controller for an ESU smoothing PV.

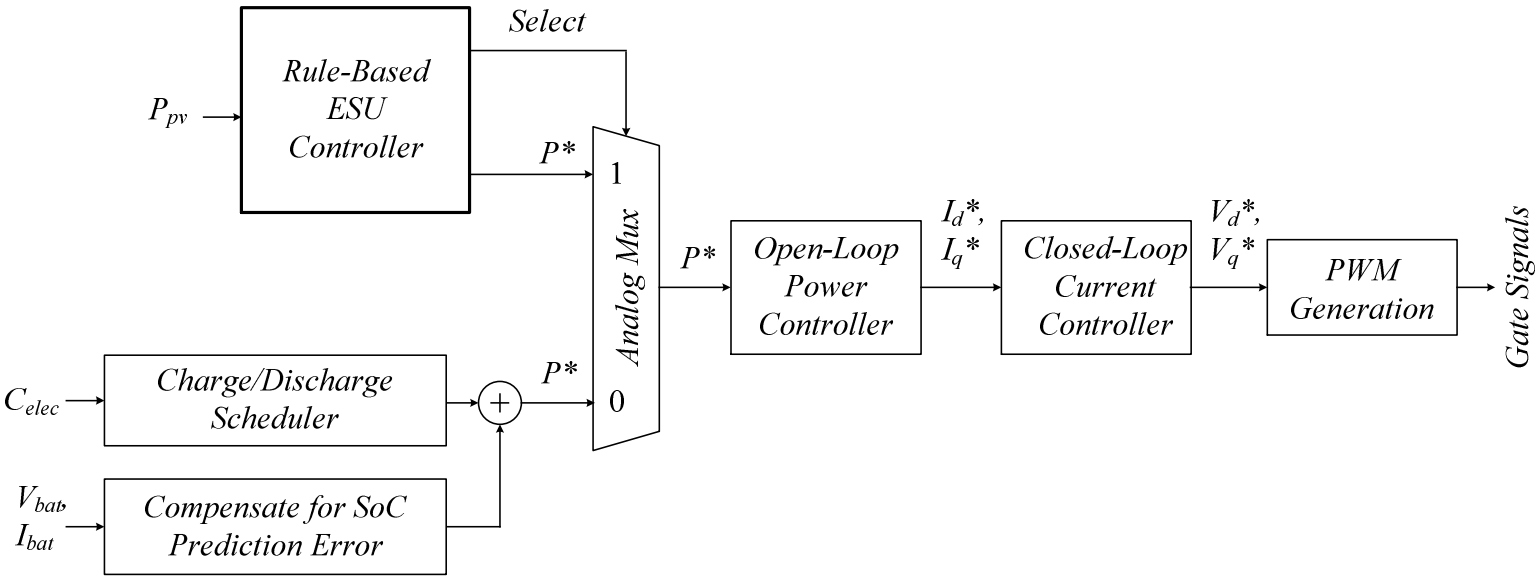

Fig. 2. Location of the proposed rule-based controller in the controller hierarchy.

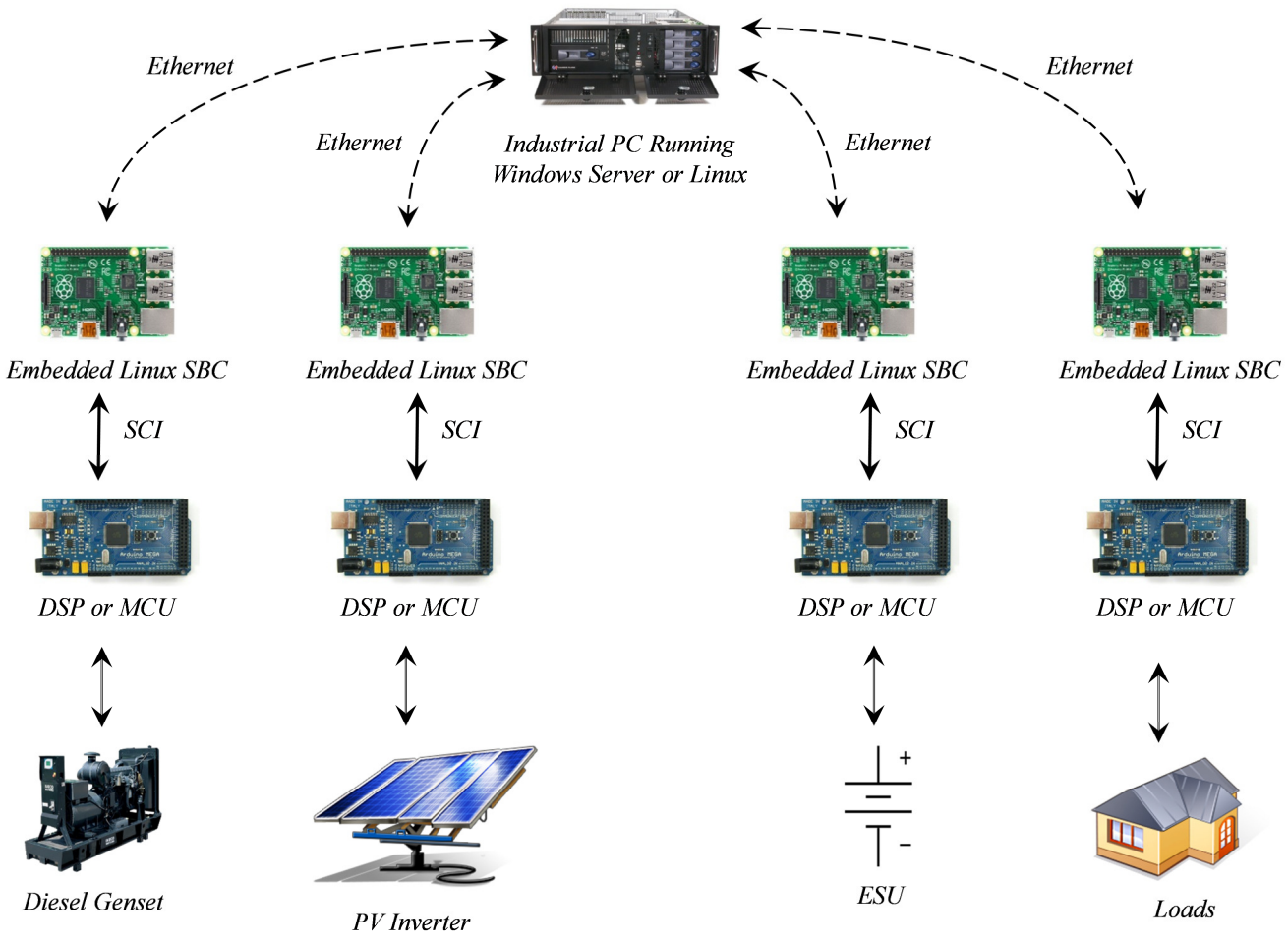

Fig. 3. Proposed hardware implementation of probabilistic microgrid scheduling [26]–[30].

IV. FINAL REMARKS

Energy storage is becoming a tool in the toolbox of the electrical system designer, and will be used by both electric utilities and their customers alike. ESU offer capabilities making them valuable both in the context of transmission and distribution systems. In transmission systems this includes peak load shaving, frequency regulation, and provision of spinning reserve, in addition to other services. In distribution systems, this includes assistance with CVR/VVO and reactive power compensation, in addition to other capabilities. ESU also offer functionality in the context of renewables integration, such as reducing intermittency issues caused by installing a large PV plant on a weak grid. This could include making the PV dispatchable in the context of generation scheduling, or providing power smoothing to reduce power/voltage fluctuations. ESU are most helpful in conjunction with renewable generation when installed in a microgrid. In this case, ESU achieve power balance when operating in standalone mode.

ESU have a number of properties making them different from conventional equipment on distribution systems. This requires the development of new methodologies for analysis and design of distribution systems including ESU. The unique characteristics of energy storage that must be included are: energy constraints, bidirectional power flow, and lifetime constraints.

This dissertation developed methodologies for integration of ESU that are suitable for inclusion in interactive distribution analysis software tools. It is hoped that the contributions here will help pave the way to more sophisticated software tools that offer the distribution system engineer greater degrees of automation, speed, and robustness.

REFERENCES

[1] A.K. Barnes, J.C. Balda, S.O. Geurin, and A. Escobar Mejía, "Optimal battery chemistry, capacity selection, charge/discharge schedule, and lifetime of energy storage under time-of-use pricing," in *IEEE PES Innovative Smart Grid Technologies Europe (ISGT-EU)*, 2011, pp. 1–7.

[2] S. Jalal Kazempour and M.P. Moghaddam, "Economic viability of NaS battery plant in a competitive electricity market," in *International Conference on Clean Electrical Power*, 2009, pp. 453–459.

[3] G. Carpinelli, G. Celli, S. Mocci, F. Mottola, F. Pilo, and D. Proto, "Optimal integration of distributed energy storage devices in smart grids," *IEEE Transactions on Smart Grid*, vol. 4, no. 2, pp. 985–995, June 2013.

[4] A.K. Barnes and J.C. Balda, "Sizing and economic assessment of energy storage with real-time pricing and ancillary services," in *IEEE International Symposium on Power Electronics for Distributed Generation Systems (PEDG)*, Fayetteville, AR, 2013, pp. 1–7.

[5] A.K. Barnes, J.C. Balda, A. Escobar Mejía, and S.O. Geurin, "Placement of energy storage coordinated with smart PV inverters," in *IEEE PES Innovative Smart Grid Technologies (ISGT)*, 2012, pp. 1–7.

[6] A.K. Barnes and J.C. Balda, "Placement of distributed energy storage via multidimensional scaling and clustering," in *International Conference on Renewable Energy Research and Applications (ICRERA)*, Milwaukee, WI, 2014.

[25] A.K. Barnes, "Value assessment of distributed energy storage via multidimensional scaling," *IEEE Transactions on Power Systems* (in review), October 2014.

[8] EPRI, "Summary of EPRI test circuits." [Online]. Available: http://svn.code.sf.net/p/electricdss/code/trunk/Distrib/EPRITestCircuits/. [Accessed: 10-Nov-2013].

[9] A.K. Barnes, J.C. Balda, and C.M. Stewart, "Selection of converter topologies for distributed energy resources," in *IEEE Applied Power Electronics Conference and Exposition (APEC)*, 2012, pp. 1418–1423.

[10] A.K. Barnes, J.C. Balda, and J.K. Hayes, "Modeling PV clouding effects using a semi-Markov process with application to energy storage," in *International Federation of Automatic Control World Congress (IFAC)*, Cape Town, South Africa, 2014.

[29] A.K. Barnes, J.C. Balda, and A. Escobar Mejía, "A semi-Markov model for control of energy storage in utility grids and microgrids with PV generation," *IEEE Transactions on Sustainable Energy* (in review), August 2014.

[12] D.P. Kothari and I.J. Nagrath, *Modern Power System Analysis*. New Delhi: Tata McGraw-Hill, 2003.

[13] S.O. Geurin, A.K. Barnes, and J.C. Balda, "Smart grid applications of selected energy storage technologies," in *IEEE PES Innovative Smart Grid Technologies (ISGT)*, 2012, pp. 1–8.

[14] M. Farivar, C.R. Clarke, S.H. Low, and K.M. Chandy, "Inverter VAR control for distribution systems with renewables," in *SmartGridComm*, 2011, pp. 457–462.

[15] M. Grant, S. Boyd, and Y. Ye, "CVX: Matlab software for disciplined convex programming," 2008. [Online]. Available: http://cvxr.com/cvx/download/. [Accessed: 19-Sep-2014].

[16] S. Bolognani and S. Zampieri, "A distributed control strategy for reactive power compensation in smart microgrids," *IEEE Transactions on Automatic Control*, vol. 58, no. 11, pp. 2818–2833, 2013.

[17] J. Lavaei, D. Tse, and B. Zhang, "Geometry of power flows and optimization in distribution networks," *IEEE Transactions on Power Systems*, vol. 29, no. 2, pp. 572–583, March 2014.

[18] R.O. Duda, P.E. Hart, and D.G. Stork, *Pattern Classification*. Wiley, 2001.

[19] M.J. Reno, C.W. Hansen, and J.S. Stein, "Global horizontal irradiance clear sky models: Implementation and analysis," Sandia National Laboratories, Report SAND2012-2389, March 2012.

[20] Ammonit, "Ammonit Solar Monitoring Systems," *Ammonit Solar Monitoring Systems*, 2013. [Online]. Available: http://www.iem.com.br/images/upload/1373463893Ammonit_SolarMeasurementSystems.pdf. [Accessed: 17-Sep-2014].

[21] M. Lave, J. Stein, A. Ellis, C. Hansen, E. Nakashima, and Y. Miyamoto, "Ota City: Characterizing output variability from 553 homes with residential PV systems on a distribution feeder," Sandia National Laboratories, Report SAND2011-9011, 2011.

[22] M. Lave, J. Kleissl, and J.S. Stein, "A wavelet-based variability model (WVM) for solar PV power plants," *IEEE Transactions on Sustainable Energy*, vol. 4, no. 2, pp. 501–509, April 2013.

[23] M. Nijhuis, B.G. Rawn, and M. Gibescu, "Classification technique to quantify the significance of partly cloudy conditions for reserve requirements due to photovoltaic plants," in *IEEE PowerTech*, 2011, pp. 1–7.

[24] J. Shi, W.-J. Lee, Y. Liu, Y. Yang, and P. Wang, “Forecasting power output of photovoltaic systems based on weather classification and support vector machines,” *IEEE Trans. Ind. Appl.*, vol. 48, no. 3, pp. 1064–1069, June 2012.

[25] M.G. Molina and P.E. Mercado, “Control design and simulation of DSTATCOM with energy storage for power quality improvements,” in *IEEE PES Transmission Distribution Conference and Exposition: Latin America (TDC-LA)*, 2006, pp. 1–7.

[26] D. Lippincott, “Chassis Plans 3U rackmount computer chassis,” *Wikimedia Commons*, 29-Oct-2007. [Online]. Available: http://commons.wikimedia.org/wiki/File:Chassis-Plans-3U.jpg. [Accessed: 25-Sep-2014].

[27] Lucasbosch, “Top face of the Raspberry Pi model B+,” *Wikimedia Commons*, 24-Jul-2014. [Online]. Available: http://commons.wikimedia.org/wiki/File:Raspberry_Pi_B%2B_top.jpg. [Accessed: 16-Sep-2014].

[28] D. Mellis, “Arduino Mega,” *Wikimedia Commons*, 12-Jul-2010. [Online]. Available: http://commons.wikimedia.org/wiki/File:Arduino_Mega.jpg. [Accessed: 25-Sep-2014].

[29] T. Dukov, “Русский: Генератор производства Iveco Motors серии Cursor (Genset Diesel),” *Wikimedia Commons*, 17-Feb-2012. [Online]. Available: http://commons.wikimedia.org/wiki/File:Diesel_genset_iveco_motors.png. [Accessed: 16-Sep-2014].

[30] J. FH, “Symbol of battery power source,” *Wikimedia Commons*, 22-Sep-2007. [Online]. Available: http://commons.wikimedia.org/wiki/File:Battery_symbol2.svg. [Accessed: 16-Sep-2014].